NBS MEASUREMENT SERVICES: SPECTRAL REFLECTANCE

Victor R. Weidner

Jack J. Hsia

Center for Radiation Research
National Measurement Laboratory
National Bureau of Standards
Gaithersburg, MD 20899

U.S. DEPARTMENT OF COMMERCE, Malcolm Baldrige, Secretary
NATIONAL BUREAU OF STANDARDS, Ernest Ambler, Director
Issued July 1987

PREFACE

The calibration and related measurement services of the National Bureau of Standards are intended to assist the makers and users of precision measuring instruments in achieving the highest possible levels of accuracy, quality, and productivity. NBS offers over 300 different calibration, special test, and measurement assurance services. These services allow customers to directly link their measurement systems to measurement systems and standards maintained by NBS. These services are offered to the public and private organizations alike. They are described in NBS Special Publication (SP) 250, NBS Calibration Services Users Guide.

The Users Guide is being supplemented by a number of special publications (designated as the "SP 250 Series") that provide a detailed description of the important features of specific NBS calibration services. These documents provide a description of the: (1) specifications for the service; (2) design philosophy and theory; (3) NBS measurement system; (4) NBS operational procedures; (5) assessment of measurement uncertainty including random and systematic errors and an error budget; and (6) internal quality control procedures used by NBS. These documents will present more detail than can be given in an NBS calibration report, or than is generally allowed in articles in scientific journals. In the past NBS has published such information in a variety of ways. This series will help make this type of information more readily available to the user.

This document (SP 250-8), NBS Measurement Services: Spectral Reflectance, by V. R. Weidner and J. J. Hsia, is the eighth to be published in this new series of special publications. It describes the instrumentation, standards, and techniques used in the measurement of spectral reflectance over the ultraviolet, visible, and near-infrared spectral ranges, from 220 to 2500 nm (see test number 38060S in the SP 250 Users Guide). Inquiries concerning the technical content of this document or the specifications for these services should be directed to the authors or one of the technical contacts cited in SP 250.

The Center for Radiation Research (CRR) is in the process of publishing 21 documents in this SP 250 series, covering all of the calibration services offered by CRR. A complete listing of these documents can be found inside the back cover.

NBS would welcome suggestions on how publications such as these might be made more useful. Suggestions are also welcome concerning the need for new calibration services, special tests, and measurement assurance programs.

George A. Uriano
Director
Measurement Services

Chris E. Kuyatt
Director
Center for Radiation Research

Library of Congress Catalog Card Number: 87-619843

National Bureau of Standards Special Publication 250-8
Natl. Bur. Stand. (U.S.), Spec. Publ. 250-8, 142 pages (July 1987)
CODEN: XNBSAV

Commercial products—materials and instruments—are identified in this document for the sole purpose of adequately describing experimental or test procedures. In no event does such identification imply recommendation or endorsement by the National Bureau of Standards of a particular product; nor does it imply that a named material or instrument is necessarily the best available for the purpose it serves.

U.S. GOVERNMENT PRINTING OFFICE
WASHINGTON: 1987

For sale by the Superintendent of Documents, U.S. Government Printing Office, Washington, DC 20402-9325

TABLE OF CONTENTS

	Page
ABSTRACT	iv
I. Measurement Philosophy, Available Standards, and Services	1
A. Measurement Philosophy	1
B. Available Standards	1
C. Description of Services	1
II. Reference Spectrophotometer for Spectral Reflectance	4
A. Description of Instrumentation	4
1. Basic Instrument	4
2. 6°/Hemispherical-Reflectance Accessory	6
3. Specular-Reflectance Accessory	6
4. 45°/0°-Reflectance-Factor Accessory	10
B. Instrument Calibration and Internal Quality Control	10
1. Wavelength Calibration.	12
2. Linearity of the Photometric Scale	12
3. Stray Radiant Power	14
4. Instrument Sensitivity Function	14
5. Detector Stability	15
C. Establishment of the Reflectance Scales and Calibration of Master Standards and Uncertainties	15
1. 6°/Hemispherical Reflectance	15
2. Specular (Regular) Reflectance	18
3. 45°/0° Reflectance Factor	19
D. Measurement Procedures for Test Samples	20
1. 6°/Hemispherical Reflectance	20
2. Specular (Regular) Reflectance	20
3. 45°/0° Reflectance Factor	20
E. Safety	21
III. Transfer Spectrophotometer for Spectral Reflectance	21
A. Description of the Instrument	21
B. Instrument Calibration	23
1. Wavelength	23
2. Linearity	23
3. Stray Radiation	23
C. Calibration of Standards	23
D. Operational Procedures and Uncertainties	27
E. Calibration Report of Test	28
F. Safety	28
References	30

ABSTRACT

This documentation describes the instrumentation, standards, and techniques used in the measurement of spectral reflectance over the ultraviolet, visible, and near infrared spectral ranges. The documentation is divided into three parts. Part I describes the guiding philosophy for maintaining reference and transfer spectrophotometers for spectral reflectance measurements, and standards and services that are available. Part II describes the NBS high accuracy reference spectrophotometer including specially developed accessory reflectometers. This instrument provides the basis for the development of absolute NBS standards of diffuse and specular reflectance. Part III describes the NBS transfer spectrophotometer, a high precision commercial spectrophotometer used for calibrating Standard Reference Materials (SRMs) such as diffuse reflectance and specular reflectance standards. The transfer instrument relies on master standards that are periodically calibrated on the high accuracy reference spectrophotometer described in Part II. The transfer instrument is also used for performing special measurements on samples submitted by other laboratories in industry and government. References containing details and equations are reproduced in the appendices.

Key Words: diffuse reflectance; spectrophotometers; spectrophotometry; spectral reflectance; specular reflectance

Table of Contents (continued)

LIST OF TABLES

Page

1. Available NBS Standard Reference Materials for Spectral Reflectance and Wavelength Standards 2
2. Emission lines and absorption bands used to calibrate the reference spectrophotometer wavelength scale 13
3. Summary of Estimated Uncertainties of Spectral Reflectance Values for NBS Reference Spectrophotometer 17
4. Emission lines and absorption bands used to calibrate the transfer spectrophotometer wavelength scale 24
5. Linearity check of the photometric scale of the transfer spectrophotometer at 770 nm for the PMT and PbS Detectors 25
6. Stray radiation measurements on the transfer spectrophotometer. . . 26
7. Summary of Estimated Uncertainties of Spectral Reflectance Values for NBS Transfer Spectrophotometer 29

TABLE OF CONTENTS (cont'd)

Appendix A: A Report of Calibration
Appendix B: Development of an NBS Reference Spectrophotometer for Diffuse Transmittance and Reflectance
Appendix C: NBS Specular Reflectometer - Spectrometer
Appendix D: NBS-45^0/Normal Reflectometer for Absolute Reflectance Factors
Appendix E: Establish a Scale of Directional - Hemispherical Reflectance Factor I: The Van den Akker Method
Appendix F: Reflection Properties of Pressed Polytetrafluoroethylene Powder
Appendix G: Laboratory Intercomparison Study of Pressed Polytetrafluoroethylene Powder Reflectance Standards

I. Philosophy, Available Standards and Measurement Services

A. Measurement Philosophy

Spectral reflectance measurements provide information on the properties of many materials. NBS strives to provide the best possible standards for diffuse and specular reflectance as well as special services and a research program to support the national requirements for these mesurements. For this purpose NBS maintains a primary reference laboratory for spectral reflectance with specialized instrumentation and trained personnel. This primary laboratory is responsible for realizing the absolute scales of diffuse and specular reflectance. The instrumentation for realizing these reflectance scales consists of a high-accuracy reference spectrophotometer with several special reflectometer accessories. The reference spectrophotometer is devoted to the highest accuracy measurements such as those required for maintaining master standards. In support of the primary reference instrumentation, a high precision commercial spectrophotometer with a reflectometer accessory is maintained as a transfer instrument. The transfer instrument is calibrated with master standards from the primary laboratory.

Standards calibrated by the transfer instrument under commonly used spectral and geometrical conditions are issued as Standard Reference Materials (SRMs). Special calibrations and tests are supplemental services to the public.

B. Available Standard Reference Materials

The reflectance and wavelength standards listed in Table 1 are available as SRMs as of 1986. They can be obtained from the Office of Standard Reference Materials, Room B311, Chemistry Building, National Bureau of Standards, Gaithersburg, MD 20899.

C. Description of Services (SP250, Item 38060S, Old Number 7.8A)*

NBS provides the following three types of spectral reflectance measurements:

1. 6°/hemispherical spectral reflectance [1] - the ratio of the total reflected radiant flux to that reflected by a perfectly reflecting diffuser (same as to that of the incident flux), the angle of incidence being 6° from normal and the reflected flux being collected hemispherically.

2. Specular (regular) spectral reflectance [1] - the ratio of the reflected radiant flux to the incident flux, the reflection being without diffusion in accordance with the laws of optical reflection as in a mirror.

*NBS Special Publication 250, NBS Calibration Services User Guide, 1986-1988 Edition.

TABLE OF CONTENTS (cont'd)

Page

LIST OF FIGURES

Fig. 1	Pictorial diagram of spectrophotometer optical system	5
Fig. 2	Diffuse reflectance integrating sphere showing detector position	7
Fig. 3	Exit aperture optics and beam switch	8
Fig. 4	Specular reflectance accessory	9
Fig. 5	Schematic of the 45°/0° reflectance accessory	11
Fig. 6	The auxiliary sphere system for determination of an absolute reflectance scale.	16

Table 1

Available NBS Standard Reference Materials* for Spectral Reflectance and Wavelength Standards

Specular Reflectance Standards

SRM No.	Description
2003d	First surface aluminum mirror, 5.1 cm diameter, wavelength range: 250 - 2500 nm.
2011	First surface gold mirror, 5.1 cm diameter, wavelength range: 600 - 2500 nm.
2023	Second surface aluminum mirror, 5.1 x 5.1 cm, wavelength range: 250 - 2500 nm.

Diffuse Reflectance Standards

SRM No.	Description
2015	Opal glass, 2.5 x 5 x 0.64 cm, wavelength range: 400 - 750 nm.
2016	Opal glass, 10 x 10 x 0.64 cm, wavelength range: 400 - 750 nm.
2019b	White ceramic tile, 5.1 x 5.1 cm, wavelength range: 350 - 2500 nm.
2021	Black porcelain enamel tile, 5.1 x 5.1 cm. wavelength range: 280 - 2500 nm.

Wavelength Standards

SRM No.	Description
2034	Holmium oxide solution (transmittance only), wavelength rnage: 240 to 640 nm.
1920	Rare-Earth mixture (reflectance only) wavelength range: 740 to 2000 nm.
2009	Didymium glass mounted in a cuvette holder, (transmittance only) wavelength range: 400 to 750 nm.
2010	Didymium glass, 5.1 x 5.1 cm, (transmittance only) wavelength range: 400 to 750 nm.

*NBS Special Publication 260 "NBS Standard Reference Materials Catalog 1986-87" p. 100,101, June 1986.

3. 45°/0° spectral reflectance factor [1] - the ratio of the radiant flux reflected in the directions bounded by a given cone with the apex at a point of the surface under test to that reflected in the same directions by a perfect reflecting diffuser identically irradiated, the angle of incidence being 45° from normal and the angle of viewing being at the normal direction.

Spectral reflectance measurements on submitted samples are available at cost. Preliminary discussion with NBS staff is required before submission. When high accuracy or a special geometry are needed, the reference instrument is used. The transfer instrument provides most of the measurements unless they can only be done on the reference instrument specular-reflectance and 45°/0°-reflectance factor accessories.

The reference spectrophotometer can provide the following conditions for reflectance measurements:

- 6°/hemispherical reflectance with specular component included, from 220 to 2500 nm. Sample sizes of 5 cm to approximately 30 cm (round or square) can be accommodated.

- Specular (regular) reflectance, from 250 to 2500 nm. The samples can be measured for sample beam incidence angles ranging from 5° to approximately 80°. Measurements are made with the sample beam polarized both horizonally and vertically. The average of these two measurements is the sample reflectance for an unpolarized beam. The samples can range in size from 50 mm to approximately 108 mm (round or square). Second surface mirrors, with the first surface to second surface thickness greater than 2 mm, can only be measured at near normal incidence.

- 45°/0° reflectance factor, from 380-770 nm. This wavelength range can be extended into the ultraviolet and near infrared by calibrating the system as described in reference 5. Measurements are made with the sample beam polarized both horizontally and vertically. The average of these two measurements is the reflectance for an unpolarized beam. The samples can range in size from 50 mm to 108 mm (round or square).

The transfer spectrophotometer can provide the following conditions for reflectance measurements:

- 6°/hemispherical reflectance. This geometry includes the specular and diffuse reflectance of the sample to give the total hemispherical reflectance.

- 0°/hemispherical reflectance. This geometry measures the diffuse reflectance with the specular component of the reflected sample beam excluded from the measurement.

- Specular reflectance of mirrors for 6° incidence only.

For the transfer spectrophotometer, the spectral reflectance data are referenced to absolute scales of reflectance through the use of transfer

standards. The wavelength range is 220 to 2500 nm for diffuse reflectance measurements and the range is 250 to 2500 nm for specular measurements.

The uncertainties associated with the various types of reflectance measurements performed by means of the transfer spectrophotometer depend on wavelength range, sample parameters, and various other instrumental considerations. Discussions of these uncertainties are included in Part III.

Colorimetric terms can be computed from 10 nm interval reflectance data for CIE Standard Illuminants [2] A, C, and D_{65}.

The minimum sample size for the transfer spectrophotometer is approximately 2.5 cm (round or square). The maximum size is approximately 15 cm.

II. Reference Spectrophotometer for Spectral Reflectance

A. Description of Instrumentation

The instrument has been described in detail in previous publications [3,4,5,6], which are included as Appendices B,C,D,E. A brief description of the instrumentation is given in this section.

1. Basic Instrument [3]

The spectrophotometer (Figure 1) consists of the source optics, a monochromator, power supplies, control and data acquisition systems, and specialized reflectance accessories.

The instrument is equipped with three sources: (1) a 150 watt xenon arc lamp for the ultraviolet spectrum below 325 nm; (2) a 100 watt tungsten strip lamp for the visible spectrum; and (3) a 500 watt tungsten lamp for the visible and near infrared. These sources are powered by regulated DC power supplies. An off-axis parabolic mirror collects and collimates the radiation from the source. Polarizers or a chopper for infrared measurements can be placed in this collimated beam. The polarization condition of the horizontally or vertically polarized beam is not altered by the optical components before entering the reflectance accessories.

Another off-axis parabolic mirror refocuses the collimated beam at the entrance slit of a quartz Ebert prism predisperser. The beam passes from the predisperser through the entrance slit of a 1-meter focal length Czerny-Turner monochromator with an effective aperture of f/8.7. Two gratings are used with the monochromator, depending on the spectral range. The grating used for the near ultraviolet and visible spectral range is blazed to give a maximum efficiency at 500 nm; the near infrared grating is blazed for a maximum efficiency at 1250 nm. Both gratings are 150 grooves/mm and with a linear despersion of 6.66 nm/mm. A triangular bandpass can be set selectively to 2, 5, 10, or 20 nm with equal entrance and exit slit widths. The wavelength drive can be operated manually or driven by a computer-controlled stepper motor.

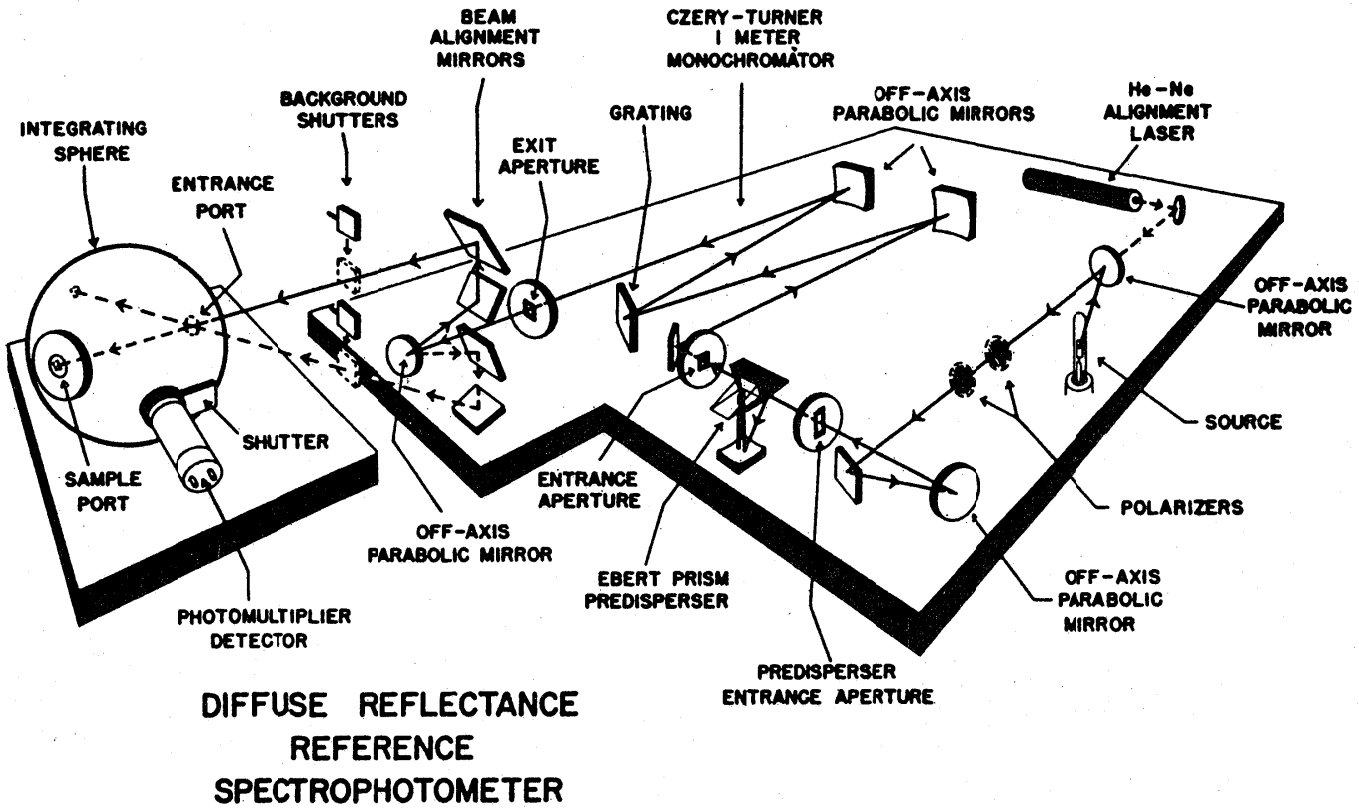

Figure 1. Pictorial diagram of spectrophotometer optical system.

A dedicated microcomputer with interface boards is used to control the instrument, acquire data, and perform data reduction.

2. 6°/Hemispherical-Reflectance Accessory

6°/Hemispherical reflectance measurements are made with a 30 cm diameter integrating sphere. The design of this sphere is illustrated in Figure 2. The sphere has a 3.8 cm diameter beam entrance port, a 5 cm diameter detector port, and a 5 cm diameter sample port. The sample port is attached to the sphere 6° from the tangent. The sphere is coated with pressed polytetrafluoroethylene (PTFE) powder. The detector is located 90° from the other two ports. There is a shutter between the detector and the detector port to protect the detector when the room lights are turned on and to provide a means of cutting off the signal in order to check the dark current level. The detector port has a cylindrical collar that extends into the sphere. This collar, which is also coated with PTFE powder, restricts the field of view of the detector to prevent direct viewing of the sample and reference beam first reflections.

The exit slit optical system is illustrated in Figure 3. The exit slit of the monochromator is located in a light-tight diaphragm built into the partition between two rooms. The beam exiting the monochromator enters into a dark room. A 15° off-axis parabolic mirror near the exit slit collects and collimates the beam. This parabolic mirror is mounted on a mechanism designed to rotate the mirror 180° clockwise or counterclockwise about the beam axis. This is accomplished by the action of a small piston. When the mirror is in one position, the collimated beam is directed through the entrance port of the integrating sphere to the sample port. When the mirror is rotated to the second position, the same beam is directed at a different angle through the same entrance port to an area of the integrating sphere wall. This area of the wall is between the sample and detector ports. The sphere coating at this area of the wall is shaped as shown in Figure 11 of Appendix B, so that first reflections from the reference beam cannot be seen from the sample port. The measurement procedures will be described in Section II.D.1.

3. Specular-Reflectance Accessory

The specular reflectometer illustrated in Figure 4 is designed to measure the spectral reflectance of mirrors and other polished surfaces as a function of angle of incidence and polarization. This instrument is set up in a dark room adjacent to the room containing the reference spectrophotometer. The collimated beam formed by the exit slit optics of the reference spectrophotometer is directed horizontally to the specular reflectometer. The reflectometer has two stepper motor driven turntables, one for the sample and a second for the tracking mirror and detector averaging sphere. The two turntables operate independent of each other but share a common axis of rotation (see Fig. 4). Samples are mounted on a two position slider that moves them in and out of the beam. When the sample is out of the beam, the tracking mirror intercepts the beam and directs it into an integrating (signal averaging) sphere at the center of rotation of the detector turntable. This sphere rotates with the turntable but the detector is

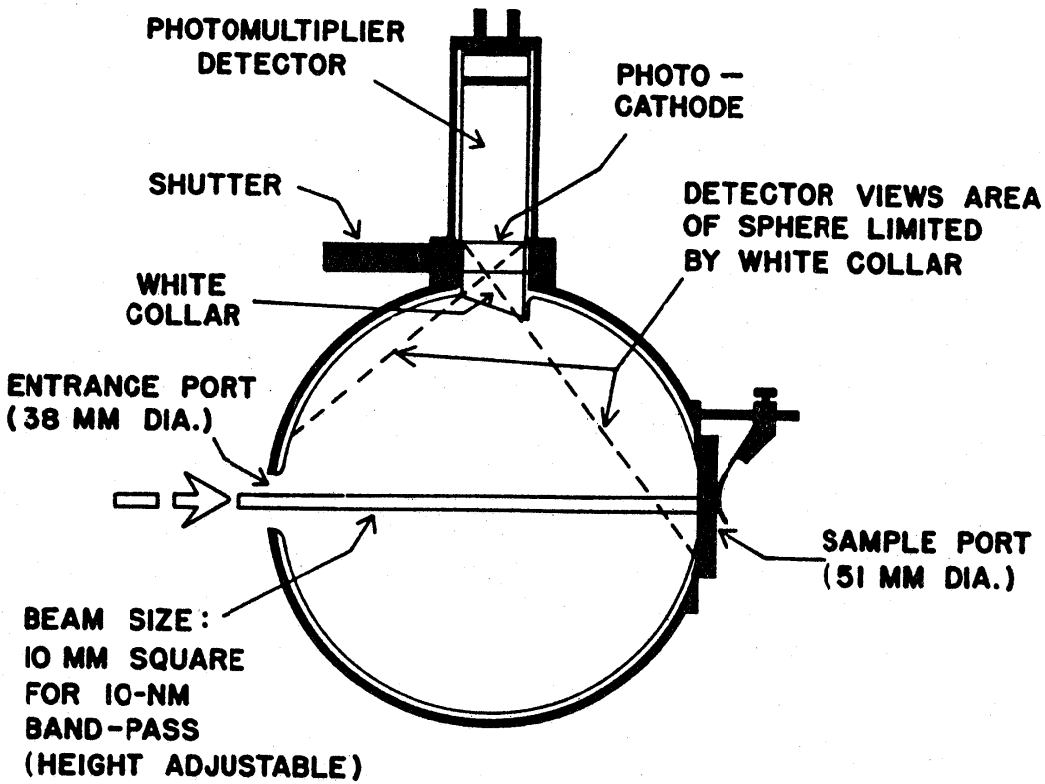

DIFFUSE REFLECTANCE INTEGRATING SPHERE (30 CM DIA.)

Figure 2. Diffuse reflectance integrating sphere showing detector position.

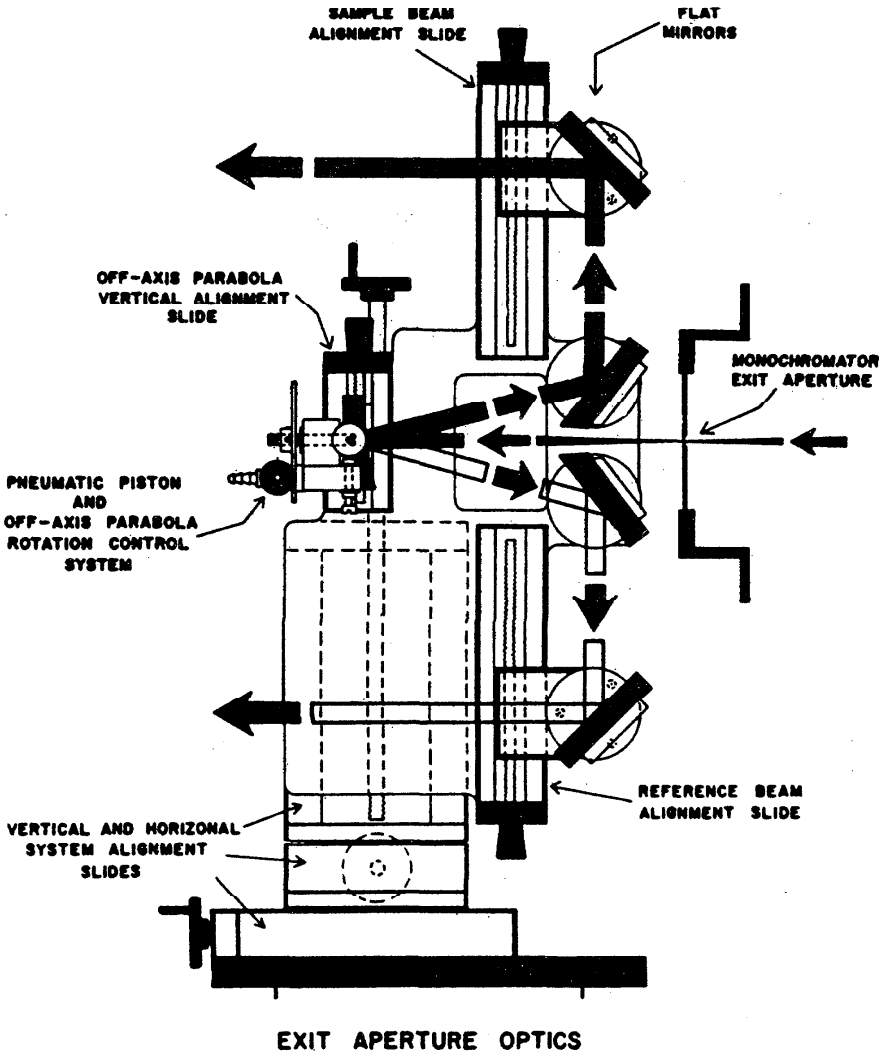

Figure 3. Exit aperture optics and beam switch.

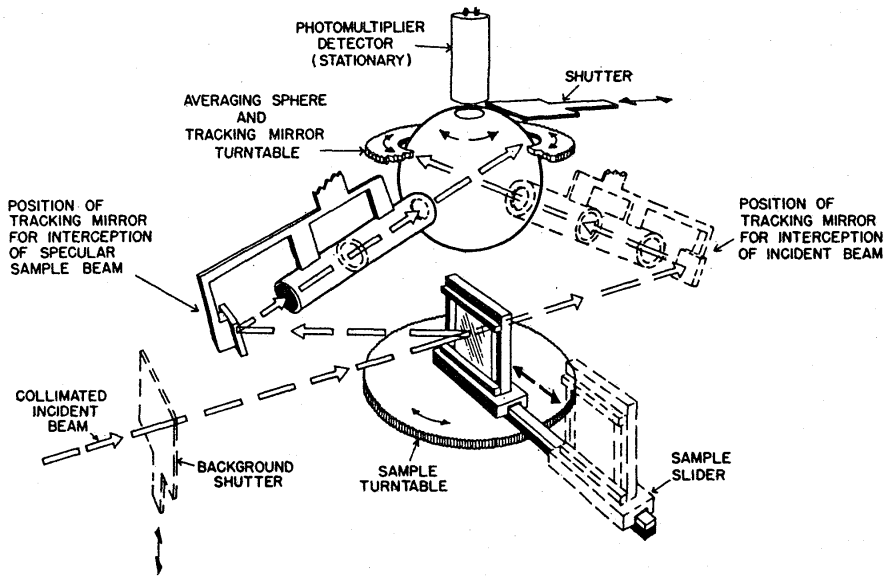

Fig. 1. General scheme of the NBS specular reflectometer showing the relationship of the sample turntable and beam-tracking turntable and detector systems.

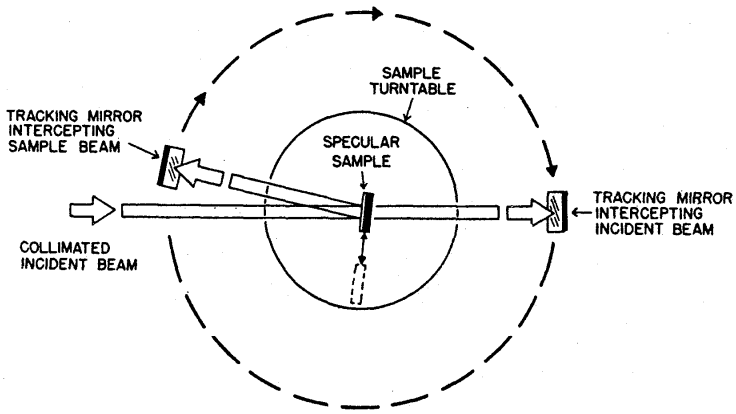

Fig. 2. Horizontal x section through the plane of the sample beam, specular sample, and the tracking mirror that orbits the sample.

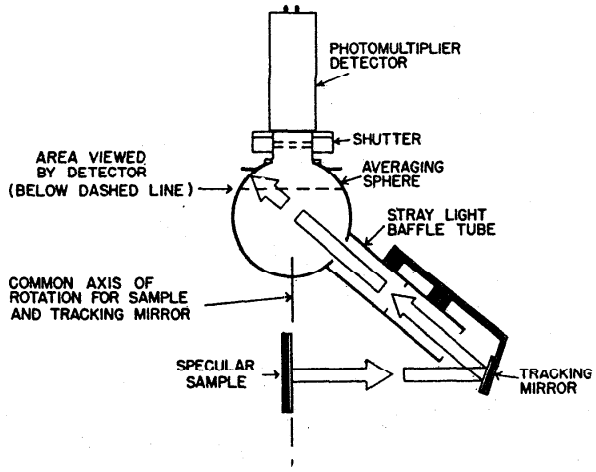

Figure 4 Specular Reflectance Accessory

designed to remain stationary over the axis of rotation because the respons of the photomulltiplier tube, even with magnetic shielding, may change if moved through local variations in ambient magnetic fields. The limiting aperture of the detector system is the entrance port in the averaging sphere A baffle tube extends from the limiting aperture to near the tracking mirro The system is programmed to measure the reflectance of a test mirror at required angles of incidence. The tracking mirror moves to the correct position to intercept and direct the beam into the averaging sphere below t detector. Before the specular reflectance of a sample can be measured, the alignment of the turntables and sample are checked by means of the sample beam and a laser to assure that the sample beam always passes through the center of the detector limiting aperture. The sample turntable is aligned that the sample beam reflects back on itself when normal to the sample plan The axis of rotation of the sample turntable is moved to the center of the sample beam. The tracking- mirror turntable axis of rotation is aligned to the same axis of rotation as the sample. The tracking mirror is adjusted t reflect the beam through the center of the limiting aperture. Measurements of specular reflectance are completely automated by means of the computer controlled stepper motors and the signal processing systems. The measurements are monitored by an operator to check the system alignment before and after each measurement at a given wavelength and polarization.

4. 45°/0°-Reflectance Factor Accessory

The 45°/0° reflectance factor accessory illustrated in Figure 5 is designed to measure the absolute reflectance factor for a sample illuminate at 45° incidence and viewed by a detector at normal incidence. The sample mounted on a two position slider on a turntable so that the sample plane is vertical and the axis of rotation is at the center of the collimated sample beam. The sample beam is diffusely reflected at the sample. The detector system consists of a limiting aperture and shutter attached to a signal averaging sphere, and a detector. Attached to this sphere at 90° from the optical axis (normal to the sample plane) is a second averaging sphere with photomultiplier detector. The reason for using two spheres is to have a uniform receiver system in order to measure a small light spot from a black glass and a larger light spot of a diffuser for the calibration of master standards (see II, C, 3). The measured reflectance signal depends on the size of the limiting aperture and its distance from the sample plane, and small compared to the intensity of the incident beam. The 45°/0° reflectan of a sample is compared to a white porcelain enamel plaque master standard mounted in the second position of the two position slider. Calibration of the standard is done by a step-down technique, requiring measurements of th ratio of two fluxes and some linear dimensions. The step-down technique al involves measuring the specular reflectance of a polished piece of black glass at 22.5° incidence. These absolute specular reflectance measurements are done on the reference specular reflectometer [4]. Additional details of the establishment of the scale and measurement procedures will be given in Sections II.C.3 and II.D.3.

B. Instrument Calibrations and Internal Quality Control

Since the best available standards may change over long periods of tim the instrument measuring reflectance must itself serve as a reference. For

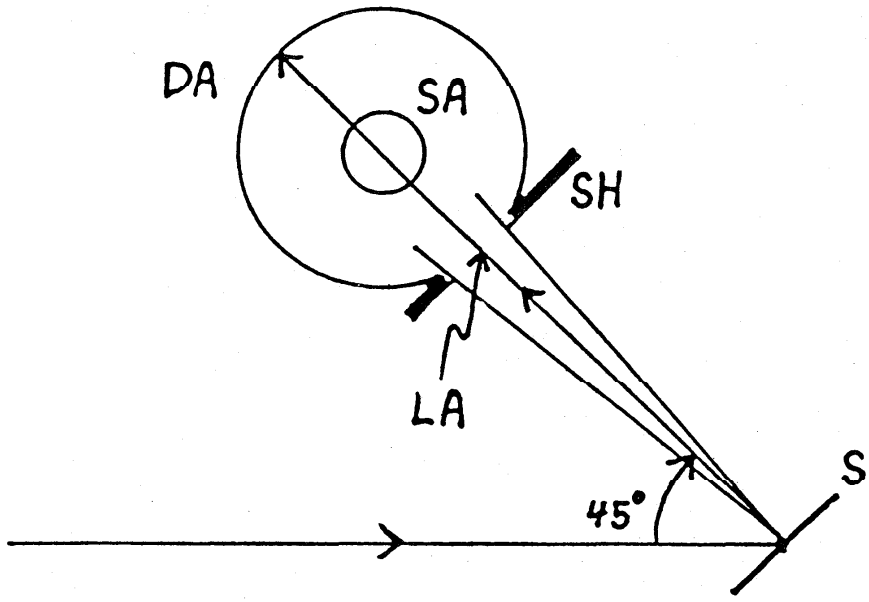

Figure 5a

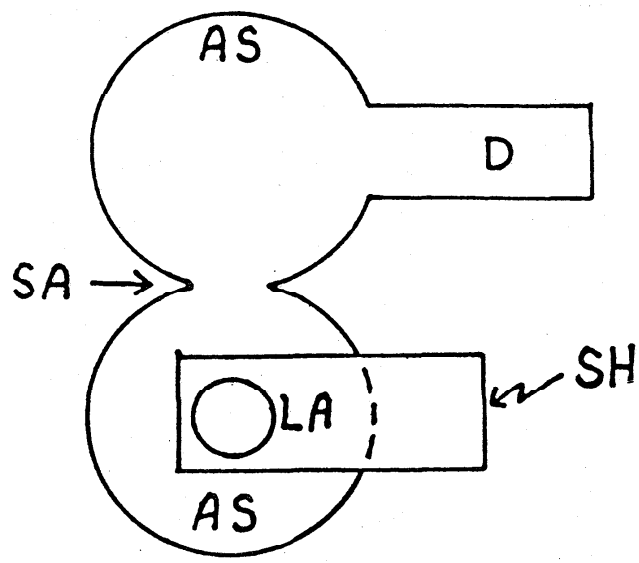

Figure 5b

Figure 5. Schematic of the 45°/0° Reflectometer.

Fig. 5a: Top view with top sphere not shown, for clarity.
S: Sample, LA: Limiting Aperture, DA: Detector assembly,
SA: Aperture between spheres.

Fig. 5b: Front view of two-sphere Receiver Assembly.
AS: Averaging Sphere, SH: Shutter, D: Detector,
LA: Limiting Aperture, SA: Aperture between spheres.

this purpose, the reference spectrophotometer must be monitored for change in performance. The five parameters which can affect the accuracy of measurement are wavelength calibration, linearity of the photometric scale, stray radiant power, instrument sensitivity function, and detector stability.

1. Wavelength Calibration

The wavelength scale error is determined by measuring the emissio lines [7] of spectral line sources and the absorption bands of some materials. These emission lines and absorption bands are listed in Table

The low-pressure arc-emission-line lamps are mounted at the source position of the reference spectrophotometer and imaged on the entrance sli of the predisperser. All the listed emission lines are relatively intense and isolated from other intense lines. The monochromator is scanned throu the wavelength region of the emission line and the signal is recorded at small wavelength intervals. These data are used to compute the centroid f the emission line. The natural bandwidth of the spectral line is much narrower than the instrument bandwidth. The spectrum of the emission line recorded as a triangular function with the peak representing the measured wavelength of the line. Using these techniques, the wavelength scale erro can be determined to an uncertainty of 0.2 nm for a 10-nm bandpass in the near ultraviolet and visible spectrum. Since the uncertainties are upper bounds, they may be regarded as having a 99.7% confidence level (3σ). All upper bounds in this publication will be of 3σ uncertainty. It is standar procedure to check the wavelength scale in the wavelength region of intere before using the instrument. This is usually done with the Hg source.

The near infrared wavelength scale is more difficult to check and the uncertainties in the wavelength scale are larger because of a lack of reliable emission lines. Hg emission lines, polystyrene absorption bands, and the absorption bands of 1,2,4-trichlorobenzene are used in the 1000 to 2500 nm wavelength range. The uncertainty of the wavelength scale in the near infrared is about 1 nm. Various factors can affect the wavelength calibration: temperature changes, problems with the wavelength drive mechanism, changing of gratings, and shifting of the optical table. Therefore, it is advisable to recalibrate the wavelength scale before each use of the instrument.

2. Linearity of the Photometric Scale

The non-linearity of the photometric scale is the deviation of the observed signal from a linear scale of signal attenuation ranging from 100 of the incident signal to the lowest level that can be measured. The non-linearity of the reference instrument photometric scale is determined through the use of a double aperture technique [8]. For reflectance measurements, the detector non-linearity needs to be considered only for signals between 100% and 1% since there are few requirements to measure materials having smaller reflectances. The non-linearity (3σ) of the photomultiplier detector is generally in the range of 1×10^{-5} to 9×10^{-5} the unattenuated incident beam. This magnitude is small compared to other

Table 2

Emission Lines and Absorption Bands Used to Calibrate the Reference Spectrophotometer Wavelength Scale.

Emission Lines:

Hg: 253.65 nm, 334.15 nm, 435.83 nm, 1014 nm, 1529.5 nm.
He: 587.56 nm, 667.81 nm.
Cd: 508.58 nm, 643.85 nm.

Absorption bands of Materials:

Polystyrene (0.6 mm): 2144 nm.
1,2,4-trichlorobenzene (0.5 mm): 1660.6 nm, 2152.6 nm, 2494 nm.
Didymium glass (6 mm): 1067 nm).

errors that affect measurements of reflectance, so that a non-linearity correction need not be applied if it remains in this range. The non-linearity of a lead sulfide infrared detector used on the reference instru ment was also tested by the double aperture technique. In this wavelength range the random noise is large enough to mask the magnitude of the non-linearity.

3. Stray Radiant Power

The level of stray radiation present within a selected 10 nm bandpass is checked by two tests.

The first test method uses glass filters. The transmittance of a sha cut-off selenium orange glass filter that passes about 90% at the wavelenc above 600 nm and nearly zero below 550 nm is measured below the cut-off. Then a second selenium orange glass filter is added and the transmittance the combined filters is measured. By comparing the transmittances measure with one and two filters, the amount of stray radiation from wavelengths above 600 nm can be determined. In this case the stray radiation at 400 a 500 nm is 5×10^{-6} and 3×10^{-4} respectively. A similar test is done with cobalt blue filters to check stray radiation at 600 nm, where the cobalt glass has a strong absorption band. The filter passes approximately 80% i the 350 to 450 nm range and 90% above 700 nm. By the filter addition tech nique, the stray radiation from wavelengths below and above 600 nm is four to be approximately 1×10^{-4} of the detector output for the total incident radiation.

A second stray radiation test is made with a 632.8 nm He-Ne laser. T test shows that the stray radiation drops off from 84.0×10^{-6} at 600 nm t 0.5×10^{-6} at 400 nm. A similar level of stray radiation is found on the long wavelength side of the laser line.

4. Instrument Sensitivity Function

The term "instrument sensitivity function" is used here to describe t relative signal output of the spectrophotometer without the test sample as function of wavelength. It is the resultant of the spectral distribution the source, the spectral response of the detector, and the spectral properties of the gratings, prisms, mirrors, and other optical components. The instrument sensitivity function introduces a shift in the wavelength a from the desired wavelength setting. This effect can exceed 1 nm if the slope of the instrument function curve is steep. The effect of a steep sl in the instrument function curve is a red shift if the slope is positive a a blue shift if it is negative.

Wavelength scale corrections are made by estimating the magnitude of shift using the following equation [9]:

$$d = aw^2/6,$$

where

d = wavelength shift,
a = slope of the curve normalized at the center of a triangle,
w = full width at half-height of the triangular passband.

5. Detector Stability

In all of the data taking procedures for the reference spectrophotometer, signal drift is monitored as a function of time. The 100% signal is measured before and after the samples are measured. The sample and background measurements are averaged to compensate for signal drift. If the standard deviation of three measurements is larger than 1×10^{-3} of the 100% signal, the measurements are repeated. The sudden appearance of a large standard deviation sometimes warns of a malfunction or equipment failure.

C. Establishment of Reflectance Scales, Calibration of Master Standards, and Uncertainties

1. 6°/Hemispherical Reflectance [6, 10]

The absolute NBS scale of 6°/hemispherical reflectance is established through the application of the double sphere system illustrated in Figure 6. This technique was first described by Van den Akker [11] and was also used by Goebel [12]. The term double sphere comes from the use of a sphere sample attached to the measuring integrating sphere of a spectrophotometer. The NBS system uses a 30 cm diameter integrating sphere illustrated in Figure 2. This same sphere is identified as the detector sphere in figure 6. The sample or "auxiliary sphere" is approximately 30 cm in diameter (a 20-cm diameter auxiliary sphere yielded the same reflectance scale within the measurement uncertainty). There is one port in this sphere. The spheres are attached to each other so that the sample beam can enter the auxiliary sphere. The auxiliary sphere is coated with a 10 mm thick pressed PTFE powder. Three flat specimens of the same coating are also prepared for direct measurement at the sample port of the detector sphere. From these measurements and measurements of the reflectance of the auxiliary sphere, and some measurements of the areas of the auxiliary sphere port and surface area of the sphere coating, the absolute reflectance of the coating material of the auxiliary sphere is computed. As the computations involve numerous equations and geometrical factors, the reader is referred to Appendix E for details.

Discussions of systematic and random errors associated with the measurements of diffuse reflectance are given in Appendices B and E. A representative estimation of uncertainties (3σ) are given in Table 3. The uncertainty due to the double-sphere measurement, which is for hemispherical incidence and hemispherical viewing h/h, is 0.0005. The uncertainty due to the conversion from h/h reflectance to 6°-incidence and hemispherical viewing reflectance (6°/h) is 0.0002. The uncertainty due to the retroflection correction is 0.0001. A typical noise level is 0.0015. The over- all uncertainty for the determination of absolute diffuse reflectance and the assigned values of

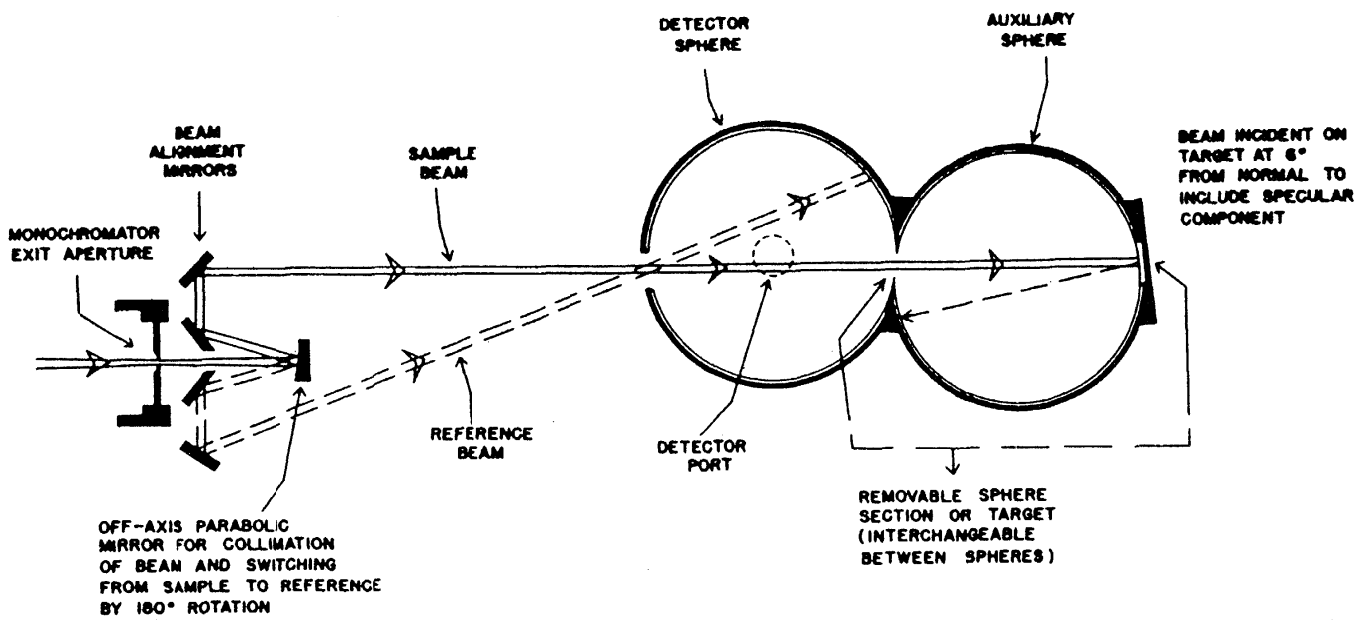

THE AUXILIARY SPHERE SYSTEM
FOR DETERMINATION OF THE

Table 3

Summary of Estimated Uncertainties of Spectral Reflectance Values for NBS Reference Spectrophotometer [A representative analysis in the visible Spectral region]

6^0/ Hemispherical Reflectance (6^0/h)	
Double Sphere (h/h)	5.0×10^{-4}
h/h -- 6^0/h	2.0×10^{-4}
Retroreflection Correction	1.0×10^{-4}
Random Noise	1.5×10^{-3}
Total Uncertainty* (3σ)	1.6×10^{-3}

Specular Reflectance	
Wavelength	5.0×10^{-4}
Stray radiation	3.0×10^{-4}
Linearity	1.0×10^{-4}
Detector response	1.0×10^{-4}
Random Noise	1.5×10^{-3}
Total Uncertainty* (3σ)	1.7×10^{-3}

45°/0° Reflectance Factor	
Wavelength	5.0×10^{-4}
Uniformity of the receiver system	5.0×10^{-4}
Stray radiation	3.0×10^{-4}
Scattering	1.5×10^{-3}
Black glass	1.7×10^{-3}
Angular setting	1.5×10^{-3}
Linearity	1.0×10^{-4}
View factor	5.0×10^{-4}
Random Noise	1.5×10^{-3}
Total Uncertainty* (3σ)	3.2×10^{-3}

*Square root of sum of squares

reflectance for the master standards are believed to be no greater than ±0.002 (3σ). The published results of an international inter- comparison of the absolute reflectance scale [13] support this finding. The smallest uncertainties are representative of measurements made in the visible spectrum. The uncertainties for the near ultraviolet and near infrared vary from ±0.0((3σ) to ±0.010 (3σ), depending on the wavelength range. They increase near the wavelength operating limits of the spectrophotometer due to limitations of the detectors, light sources, and optics.

The absolute reflectance of pressed PTFE powder was determined by the double-sphere technique for the ultraviolet, visible, and near infrared spectral ranges[10]. The absolute reflectance of this material is greater tha 96% from 200 to 2500 nm and greater than 99% from approximately 350 nm to 1800 nm.

Although the pressed PTFE powder serves as an absolute reflectance standard, it is desirable to have working standards of a more permanent nature. These are hard durable materials that remain stable and can be easily cleaned without affecting their spectral reflectance. Five master standards have been calibrated for 6°/hemispherical reflectance. These are: (1) Russian opal glass: (2) Vitrolite opal glass; (3) porcelain enamel on steel; (4) white ceramic (SRM 2019); and (5) black porcelain enamel on steel (SRM 2021). Each of these standards has been calibrated relative to a perfect diffuser by measuring them relative to the high purity PTFE at the time the double-sphere absolute technique is realized. Periodic comparison of their reflectance relative to the pressed PTFE standards indicate that they are stable to within an uncertainty better than ±0.005 (3σ).

2. Specular (Regular) Reflectance [4]

The absolute specular reflectance measurements are made in the followin sequence: background, incident flux, reflected flux, incident flux, background. The sequence is performed three times with the sample rotated clockwise to the desired angles of incidence and three times with the sample rotated counterclockwise to the same angles of incidence. For each clockwis and counterclockwise sequence, the background is first subtracted from the measured data of incident and reflected fluxes and the ratio of the reflecte flux to the incident-flux is computed. The ratios are averaged for the thre cycles and the standard error is computed.

After the measurements for both vertically and horizonally polarized incident beams for a given wavelength, the average of the two polarizations and the overall standard error are computed.

The components of the estimated uncertainty are as follows. The uncertainty due to the wavelength scale is 0.0005. The uncertainty due to the stray radiation is less than 0.0003. The uncertainty due to the non-linearity is less than 0.0001. The uncertainty due to the detector response at different tracking-mirror positions is 0.0001. And the uncertainty due to a typical random noise level is 0.0015. The overall uncertainty for specular reflectance measurements is less than ±0.002 (3σ) for the wavelength range 320 to 800 nm (see Table 3). Below 320 nm the

uncertainty increases to about ±0.005 (3σ) at 250 nm. The uncertainty in the near infrared is ±0.002 (3σ), except for wavelengths below 850 nm and above 2000 nm where it increases to about ±0.005 (3σ). Some brief discussions of the checks on the instrument performance are given in Appendix C.

The specular reflectance accessory of the reference spectrophotometer is used to calibrate master aluminum and gold mirrors for the wavelength range 250 to 2500 nm. These master mirrors are used to calibrate SRM mirrors on the transfer spectrophotometer. These mirrors are selected from an uncalibrated stock of SRM mirrors when a new batch is received from the manufacturer. A batch usually consists of about 30 mirrors that are coated at the same time. The new mirrors are aged under laboratory conditions in glass covered containers (Petri dishes) for about one year before being calibrated. New master mirrors are calibrated at approximately two year intervals because under the best of care the mirrors become contaminated and cannot be restored to their orignal reflectance by cleaning.

The master aluminum mirrors are calibrated at 25 nm intervals from 250 to 400 nm, 50 nm intervals from 400 to 1000 nm, 100 nm intervals from 1000 to 1300 nm, and at 250 nm intervals from 1500 to 2500 nm. They are also calibrated at the laser wavelengths of 632.8 and 1060 nm. The mirrors are measured at angles of incidence of 6°,30°, and 45°, for vertically and horizontally polarized incident beams. The master gold mirrors are calibrated in a similar way for wavelengths above 600 nm.

3. 45°/0° Reflectance Factor [5]

Because the detector accepts only a small solid angle of the total hemispherical reflection, the calibration of diffuse reflectance standards for 45°/0° reflectance factors involves comparing a very small reflected flux to a large incident flux. A step-down technique must be used to attenuate the incident beam by means of a calibrated polished black glass with an absolute specular reflectance of about 4% for a 22.5° angle of incidence. This black glass is mounted in the sample holder so that the light reflected by it enters the limiting aperture of the detection system. A white porcelain enamel plaque to be calibrated as a 45°/0° diffuse reflectance standard is also mounted in the sample holder. Alternate readings are taken with the collimated beam incident on the white plaque and the black glass. The reflectance of the white plaque is adjusted to the specular reflectance embodied in the black glass. The reflectance factor of the white plaque is obtained by dividing this adjusted reflectance by the geometrical factor [5] of the limiting aperture.

The overall uncertainty (3σ) in the measured 45°/0° reflectance factor is about 0.003. A representative analysis of estimated uncertainties are summarized in Table 3. The uncertainty due to the wavelength error is 0.0005. The uncertainty for the receiver system (uniformity) to receive the specularly and diffusely reflected radiation is less than 0.0005. The uncertainty due to the radiation scattering in the accessory is 0.0015. The uncertainty due to the black glass specular reflectance is 0.0017. The uncertainty due to the angular setting is 0.0015. The uncertainty due to the non-linearity is less than 0.0001. The uncertainty due to the view-factor

determination is less than 0.0005. And the uncertainty due to a typical random noise level is 0.0015. Appendix D provides some brief discussion of the instrument performance.

A Vitrolite opal glass is used as a check standard for monitoring the long term performance of the 45°/0° reflectometer. Any change in the measured ratio of the reflectance of the Vitrolite check standard to the master porcelain enamel plaque serves as a warning that the absolute scale has changed. Such a change could indicate that there is an alignment problem, or that one or both of the standards have aged.

D. Measurement Procedures for Test Samples

1. 6°/Hemispherical Reflectance

Measurements of 6°/Hemispherical reflectance are done with a ratio technique, switching the incident collimated beam back and forth between sphere wall and sample holder. Three measurements are necessary: backgroun signal with the beam blocked near the monochromator exit slit, reflectance the sample relative to the sphere wall, and reflectance of a master standar relative to the sphere wall.

Data are first recorded in the following order: background, sample, sphere wall, sample, background. This cycle is performed three times for each wavelength. To compensate for signal drift for each cycle, the two sample measurements are averaged and the two background measurements are averaged; the background is subtracted from the sample and sphere wall signals, and then the reflectance of the sample relative to the sphere wall is computed. The results of the three measurements are averaged, and a standard deviation of the averaged ratio is computed.

This procedure is repeated for the master standard, and then the relative reflectance of the sample is adjusted to the absolute scale embodie in the master standard. The reflectance of the sphere wall need not be know but must be stable throughout the measurements.

2. Specular (Regular) Reflectance

Calibration of samples requiring a high accuracy are performed on the reference spectrophotometer. The measurement procedures are the same as discussed in Section II.C.2.

3. 45°/0° Reflectance Factor

Data for measurements of 45°/0° reflectance factors are recorded in the sequence: background, white plaque master standard, test sample, white plaque master standards, background. This sequence is repeated two times fo each wavelength and polarization. The preliminary data reduction involves subtracting the background from the other measurements and computing the ratio of the test sample reflectance to the reflectance of the master white plaque. The 45°/0° absolute reflectance factor of the sample is obtained by multiplying this ratio by the 45°/0° absolute reflectance factor of the master white plaque.

E. Safety

The main hazards in the spectrophotometry laboratory are due to radiation from He-Ne lasers, xenon arcs, and spectral line sources. Laser signs are posted to alert personnel of possible hazards. The xenon arc is shielded to protect personnel from UV radiation, possible injury due to lamp explosion, or injury from high voltages. Ozone gas produced by the xenon arc is removed by an exhaust system. Similar precautions are taken with spectral line sources that produce UV radiation. Personnel wear protective goggles when working with light sources that emit harmful optical radiation.

There are also electrical hazards due to lamp power supplies and high voltage power supplies for detectors. Approved grounded cables are used on all electrical equipment.

III. Transfer Spectrophotometer for Spectral Reflectance

The transfer spectrophotometer is a commercial double beam instrument [14] with transmittance and reflectance capabilities. It is equipped with microprocessors with programmable features. It is also connected to an external computer with software to control the spectrophotometer and perform data reductions.

The wavelength range is from 200 to 2500 nm for diffuse reflectance measurements. The spectral bandwidth can be set to any fixed value between 0.1 and 3.6 nm for the wavelength range 200 to 900 nm when using the photomultiplier detector. The bandwidth, in the near infrared, may range from less than 1 nm to a maximum of 14.3 nm, depending on the available signal. The photometric scale can be recorded in percent reflectance or optical density ($= - \log_{10} \rho$, where ρ is a reflectance). The optical density scale ranges automatically to 4.5 and can be extended to about 6 in the ultraviolet and visible spectral ranges by attenuating the reference beam with photoetched nickel screens. In the near infrared the upper limit of the optical density scale is approximately 3.

A. Description of the Instrument

The wavelength range is divided into three operating ranges based on the selected source and detector combination. These are the ultraviolet (200 to 400 nm); visible (340 to 900 nm); and near infrared (700 to 2500 nm). The instrument has two gratings; one for the spectral range 200 to 900 nm and one for the 700 to 2500 nm near infrared. There is a deuterium lamp for the near ultraviolet wavelength range below 340 nm and a tungsten-halogen source for the spectral range 340 to 2500 nm. The deuterium lamp also serves as a wavelength calibration source with the instrument operated in the single beam mode. The gratings, sources, and order separating filters are automatically controlled so that continuous spectral scans can be made through the full wavelength range of the instrument. A number of instrument systems can be checked with computer routines stored in the microprocessor. A detailed description of all instrument controls and features is given in the operators manual supplied by the manufacturer. The measurement parameters are

continually displayed on the control panel monitor. Selected wavelength: bandwidth, scan speed, scale expansion, and other parameters are shown or monitor, and warning messages flash on the screen to alert the operator (problems or instrument parameters that are out of range.

The sample compartment is insulated and the temperature can be controlled within ±0.2^{0}C in the range 15°C to 40°C by circulating water fron control bath. The temperature of a sample can be monitored by means of a thermocouple probe in the sample compartment. The temperature is display on the control panel monitor and can be recorded on the thermal printer.

The spectrophotometer has a chart recorder and a thermal printer for recording digital spectral data and instrument parameters. There are fea tures for automatic repeat scans. The photometric scale baseline calibra can be stored in memory so that baseline corrections can be made continuc during a spectral scan.

The operation of the spectrophotometer can be controlled from the ex nal computer that controls all instrument parameters and records spectral data. Additional software is used to perform data averaging, conversion optical density to reflectance or vice versa, computing colorimetric term and other data manipulations.

The integrating sphere of the diffuse reflectance accessory is apprc mately 100 mm in diameter. The photomultiplier detector (PMT), a Hamamat tube, is mounted above the sphere and views the sphere interior through a elliptical aperture. The lead sulfide (PbS) detector port is adjacent tc PMT port. There are baffles attached to the top of the sphere interior t block first reflections from the sample to the detectors. The sphere interior and baffles are coated with pressed PTFE powder.

The reference beam enters the sphere through a port that is 22 mm hi and 12 mm wide and is located 90° from the sample port. The reference-be target is located about 33 mm inside the sphere.

The sample beam is nearly collimated and enters the sphere through a rectangular port of approximately 30 mm height and 20 mm width. The samp port is opposite this entrance port and is 22.5 mm in diameter.

An image of the exit slit of the monochromator is formed at the samp plane. The width of this image may vary, depending on the bandwidth sett The image height is about 15 mm when the exit slit height is set to full height. The image height can be reduced by reducing the exit slit to 1/3 full height.

The section of the sphere at the sample port can be turned in the pl of this sample port. In one position of this section the sample plane is tilted so that the sample beam is incident at 6° from the normal. This a allows the specular component of the reflected sample beam to be trapped the sphere. In the other position, this section is turned 180^0. The sam beam is normal to the sample plane and the specular component returns alo the axis of the sample beam and passes back out of the sphere through the

sample beam entrance port so that only the diffuse component of the reflected beam is measured. The solid angle subtended by the sample beam entrance port at a distance of 100 mm from the center of the sample extends approximately 15° in the vertical plane and 10° in the horizonal plane.

The integrating sphere described above is also used to make specular reflectance measurements of mirrors and other specular reflectors. Since measurements of specular reflectance on this device are not absolute, a master standard must be measured along with the test sample. The relative reflectance of the test sample is adjusted to the absolute scale embodied in the master standard. The master standard is either a first surface aluminum mirror, first surface gold mirror, or a second surface aluminum mirror that has been calibrated on the reference specular reflectometer [4]. The integrating sphere geometry allows only for 6° incidence for specular reflectance measurements on the transfer spectrophotometer.

B. Instrument Calibration

1. Wavelength

Emission lines [7] and absorption bands used to calibrate the transfer spectrophotometer wavelength scale are listed in Table 4. The wavelength scale uncertainty is ±0.1 nm (3σ) in the near ultraviolet and visible, and ±1.0 nm (3σ) in the near infrared. The deuterium lamp mounted in the spectrophotometer, is used to check the wavelength scale on a day-to-day basis at the wavelengths listed in Table 4.

2. Linearity

The linearity of photometric scales for the PMT and PbS detectors for diffuse reflectance measurements has been determined with a set of transmittance standards[15]. These transmittance standards have been calibrated on the NBS reference transmittance spectrophotometer at 770 nm. The results of linearity check for both detectors of the reflectance accessory are given in Table 5. The data in Table 5 are used to correct for non-linearity of measurements.

3. Stray Radiation

The presence of stray radiation in the transfer spectrophotometer sample beam was checked, using a number of solutions and glass filters that have sharp cut-off absorption features in different spectral regions. The techniques for measuring stray radiation are described in ASTM and other publications [16,17]. The level of stray radiation was checked for spectral bandwidths (SBW) of 1 nm and 3.6 nm. The results of these measurements are given in Table 6, and indicate that the level of stray radiation is not significant in this spectrophotometer.

C. Calibration of Standards

Many of the Standard Reference Materials (SRMs) listed at the beginning of this documentation are calibrated on the transfer spectrophotometer, using

Table 4

Emission Lines and Absorption Bands Used to Calibrate the Transfer Spectrophotometer Wavelength Scale.

Emission Lines:

Hg: 253.65 nm, 334.15 nm, 435.83 nm, 1014 nm, 1529.5 nm.

D_2: 486.0 nm, 656.10 nm, 1312.2 nm, 1968.3 nm, 2624.4 nm.

Note: the last 3 wavelengths for D_2 are 2nd, 3rd, and 4th order lines of the 656.1 nm line and are observed with the near infrared grating.

Ne: 703.24 nm.

Xe: 881.94 nm, 979.97 nm.

Kr: 1816.73 nm.

Absorption Bands of Materials:

1,2,4-trichlorobenzene (0.5 nm): 2152.6 nm.

Holmium oxide (SRM 2034): 241.0 nm, 249.8 nm, 278.1 nm, 287.0 nm 333.5 nm, 345.5 nm, 361.4 nm, 385.4 nm, 416.1 nm, 451.3 nm, 467.8 nm, 485.3 nm. 536.5 nm, 640.5 nm.

Rear-Earth Oxide (SRM 1920): 799.0 nm, 886.7 nm, 1132.4 nm 1260.8 nm, 1535.4 nm, 1682.2 nm, 1757.8 nm, 1847.0 1932.5 nm, 1970.8 nm.

Table 5

Linearity Check of the Photometric Scale of the Transfer Spectrophotometer at 770 nm for the PMT and PbS Detectors.

Reflectance Mode:

Filter No.	Reference Value	PMT	Difference	PbS	Difference
1-1	0.9185	0.9207	+0.0022	0.9208	+0.0023
1-2	.6644	.6651	+ .0007	.6659	+ .0015
1-3	.4787	.4789	+ .0002	.4795	+ .0008
1-4	.3289	.3284	- .0005	.3290	+ .0001
1-5	.1674	.1671	- .0003	.1669	- .0005
1-6	.0500	.0495	- .0005	.0489	- .0011
1-7	.01163	.01129	- .00034	.01041	- .00122

master standards as a means for transferring the absolute reflectance scale from the basic or fundamental measurements of these quantities on the reference spectrophotometer documented in Part II.

Pressed PTFE powder is preferred as a master standard for diffuse reflectance because the absolute reflectance of this material is well documented [10,18]. Other transfer standards used are: (1) a master white ceramic tile used for calibrating NBS SRM 2019 and a black porcelain enamel master tile used for calibrating SRM 2021; (2) master first surface aluminum and gold mirrors and second surface aluminum mirrors used for calibrating SRM's 2003, 2011, and 2023.

D. Operational Procedures and Uncertainties

The instrument parameters are set after a 30 minute warm-up period. The wavelength scale is checked at this time by running the instrument test procedure with the deuterium emission lines. The baseline is set before any measurements are recorded. In setting up the baseline calibration, a white diffuser is placed at the sample port of the reflectance attachment integrating sphere. The instrument scans the spectral region to be measured and stores the data required to correct the sample measurements for gross baseline fluctuations. As long as subsequent measurements are made for the same parameters, the recorded baseline information in the computer will be used. If the operator changes a critical parameter, a warning message will be displayed on the monitor screen and a new baseline must be established.

Data are recorded in the sequence: 100%, transfer standard, zero, test samples, zero, transfer standard, 100%. The zero measurements are made with a large black cavity at the sample port of the integrating sphere. The 100% and standard measurements are made at repeated intervals when many test samples have to be measured. Most samples are compared to a freshly prepared PTFE standard of known absolute reflectance, prepared as described in reference [18]. A black diffuse standard such as NBS SRM 2021 porcelain enamel standard is used as a transfer standard for dark samples. Similar sequences are measured when measuring specular reflectance except that the reference standard is a mirror.

Diffuse reflectance data are corrected to an absolute scale as follows:

(1) Test sample and standard data are corrected for linear drift by performing measurements in a time-symmetrical sequence and subsequent averaging.

(2) Any zero calibration error is subtracted.

(3) The ratio of the reference value of the transfer standard to the measured value of the transfer standard is multiplied by the measured value of the test sample to adjust the test sample data to an absolute scale.

The uncertainty (3σ) in the diffuse reflectance data obtained through these measurements and data reduction procedures is generally 0.005. A

Table 7

Summary of Estimated Uncertainties of Spectral Reflectance Values for NBS Transfer Spectrophotometer [A representative analysis in the visible region]

Wavelength	5.0×10^{-4}
Stray radiation	2.0×10^{-5}
Linearity	2.2×10^{-3}
Master Standard	1.5×10^{-3}
Random noise	2.5×10^{-3}
Stability (Drift)	1.5×10^{-3}
Total Uncertainty (3σ) (Square root of sum of squares)	4.1×10^{-3}

REFERENCES (cont'd)

[13] Budde, W., Erb, W., and Hsia, J.J., International intercomparison of absolute reflectance scale, Color Research and Application, 7, 24 (1982).

[14] Varian-Cary Model 2390 UV-VIS-NIR spectrophotometer.

[15] Eckerle, L., Weidner, V.R., Hsia, J.J., and Kafadar, K., Measurement assurance program transmittance standards for spectrophotometric linearity testing: Preparation and Calibration, J. Res. Nat. Bur. Stand. 88, 25 (January-February 1983).

[16] Mielenz, K.D., Weidner, V.R., and Burke, R.W., Heterochromatic stray light in UV absorption spectormetry: A new test method, Appl. Opt. 21, 3354 (1982).

[17] American Society for Testing and Materials, Standard Test Method for Estimating Stray Radiant Power Ratio of Spectrophotometers by the Opaque Filter Method, ASTM E387-84, Annual Book of ASTM Standards, Section 14.01, p. 469-4890, 1985.

*[18] Weidner, V.R., Hsia, J.J., and Adams, B., Laboratory intercomparison study of pressed polytetrafluoroethylene powder reflectance standards, Appl. Opt. 24, 2225 (1985). (Appendix G)

FORM NBS-443
(REV. 11-68)

APPENDIX A

U.S. DEPARTMENT OF COMMERCE
NATIONAL BUREAU OF STANDARDS
Gaithersburg, MD 20899

REPORT OF CALIBRATION

for
Spectral Reflectance
of
One Gold Mirror

Submitted by:

_____

_____

_____

_____

(Reference Purchase Order No. 55883 dated September 20, 1985.)

1. Purpose

The purpose of this test is to measure the spectral reflectance of one gold mirror over the spectral range 250 to 2500 nm.

2. Material

The gold mirror submitted for measurement by ___ Inc. is approximately 27 mm in diameter, identified by serial number 2007-9.

3. Measurements of Spectral Reflectance

Measurements of spectral reflectance of the gold test mirror, NBS Master Standard aluminum mirror #31 and NBS Master Standard gold mirror #16 were made by means of a Cary Model 2390 recording spectrophotometer. The Cary Model 2390 is equipped with an integrating sphere reflectance attachment with sample and reference beams. Measurements were made in the area approximately 8 mm by 12 mm at the center of each mirror.

The measurements of the test mirror and NBS Master Standard aluminum mirror #31 were made over the wavelength range 250 to 800 nm using a deuterium source and tungsten source in combination with a photomultiplier detector. The spectral band pass was 1-nm. The measurements of the test mirror and NBS Master Standard gold mirror #16 were made over the wavelength range 800 to 2500 nm using a tungsten source and lead sulfide detector. The spectral band pass varied from 2-nm to approximately 13-nm.

Spectral Reflectance, Gold Mirror - Serial Number 2007-9

TABLE 1

Wavelength (nm)	Reflectance
250	0.295
275	.341
300	.346
325	.342
350	.330
375	.348
400	.360
425	.363
450	.358
475	.354
500	.453
525	.671
550	.800
575	.868
600	.906
625	.931
650	.947
675	.958
700	.963
725	.968
750	.970
775	.972
800	.973
825	.973
850	.973
875	.974
900	.974
925	.974
950	.974
975	.974
1000	.974
1025	.975
1050	.975
1075	.975

NBS Test No.: 534/235956-85
Date: November 4, 1985

Spectral Reflectance, Gold Mirror - Serial Number 2007-9

TABLE 1 (continued)

Wavelength (nm)	Reflectance
2000	.976
2025	.976
2050	.976
2075	.976
2100	.976
2125	.976
2150	.976
2175	.976
2200	.976
2225	.976
2250	.976
2275	.976
2300	.976
2325	.976
2350	.976
2375	.976
2400	.976
2425	.976
2450	.977
2475	.977
2500	.977

Optical Radiation Measurements:

Development of an NBS Reference Spectrophotometer for Diffuse Transmittance and Reflectance

William H. Venable, Jr., Jack J. Hsia, and
Victor R. Weidner

Optical Physics Division
Institute for Basic Standards
National Bureau of Standards
Washington, D. C. 20234

U.S. DEPARTMENT OF COMMERCE, Elliot L. Richardson, *Secretary*

Edward O. Vetter, *Under Secretary*

Dr. Betsy Ancker-Johnson, *Assistant Secretary for Science and Technology*

NATIONAL BUREAU OF STANDARDS, Ernest Ambler, *Acting Director*

Issued October 1976

National Bureau of Standards Technical Note 594-11

Nat. Bur. Stand. (U.S.), Tech. Note 594-11, 47 pages (Oct. 1976)
CODEN: NBTNAE

U.S. GOVERNMENT PRINTING OFFICE
WASHINGTON: 1976

For sale by the Superintendent of Documents, U.S. Government Printing Office, Washington, D.C. 20402
(Order by SD Catalog No. C13.46:594-11). Stock No. 003-003- **Price $1.15**
(Add 25 percent additional for other than U.S. mailing).

PREFACE

This is the eleventh issue of a series of Technical Notes entitled OPTICAL RADIATION MEASUREMENTS. The series will consist primarily of reports of progress in, or details of, research conducted in radiometry, photometry and spectrophotometry in the Optical Radiation Section and the Radiometric Physics Section of the Optical Physics Division.

The level of presentation in OPTICAL RADIATION MEASUREMENTS will be directed at a general technical audience. The equivalent of an undergraduate degree in engineering or physics, plus familiarity with the basic concepts of radiometry and photometry [e.g., G. Bauer, Measurement of Optical Radiations (Focal Press, London, New York, 1965)], should be sufficient for understanding the vast majority of material in this series. Occasionally a more specialized background will be required. Even in such instances, however, a careful reading of the assumptions, approximations, and final conclusions should permit the non-specialist to understand the gist of the argument if not the details.

At times, certain commercial materials and equipment will be identified in this series in order to adequately specify the experimental procedure. In no case does such identification imply recommendation or endorsement by the National Bureau of Standards, nor does it imply that the material or equipment identified is necessarily the best available for the purpose.

Any suggestions readers may have to improve the utility of this series are welcome.

Henry J. Kostkowski, Chief
Optical Radiation Section
National Bureau of Standards

Jack L. Tech, Chief
Radiometric Physics Section
National Bureau of Standards

TABLE OF CONTENTS

Pa

I. INTRODUCTION 1

II. SPECTROPHOTOMETER DESIGN 3

A. Light Sources 3

B. Source Optics 3

C. Predisperser 3

D. Monochromator 5

1. Description 5

2. Calibrations and Tests 5

a. Wavelength calibration 5

b. Stray radiant energy 6

E. Exit Slit Optics 7

III. MEASUREMENT ACCESSORY SYSTEMS 7

A. General Purpose Integrating Spheres 9

1. Description 9

2. Definition of the Measurement 9

3. Reflectance Measurement Procedure 13

4. Evaluation 14

a. Detector linearity 14

b. Sample induced non-linearity 16

c. Polarization effects 16

d. Angular dependence of response 16

e. Sample plane to port plane displacement effect 17

B. Integrating Sphere for Measuring Relative Directional-Hemispherical Reflectance as a Function of Angle 17

1. Description 17

2. Measurement Procedure 19

3. The Entrance Port Correction 19

C. Auxiliary Spheres for Determination of the Absolute Reflectance Scale 20

D. Bidirectional Diffuse Reflectance Factor Accessory System 20

IV. SUMMARY 20

APPENDIX A: Sample-Induced Nonlinearity 23

1. Wall Retro-Reflectance Nonlinearity 23

2. Flat-Sample Nonlinearity 24

3. Baffle-Induced Nonlinearity 25

4. Combinations of Sample-Induced Nonlinearities 27

APPENDIX B: Method of Evaluating Sample-Induced Nonlinearity 28

APPENDIX C: Correcting for Scattered Radiation in Incident Beam 29

TABLE OF CONTENTS (continued) Page

APPENDIX D: Test for Polarization Effects 30
APPENDIX E: Estimation of Sample-Dependent Nonlinearity 31
1. Sphere Without Baffle 31
2. Sphere With Baffle 31
APPENDIX F: Estimating Error Due to Angular Dependence of Response 35
1. Surface Reflection 35
2. Body Reflection 36
APPENDIX G: Focusing the Exit Slit Optics 39

V. REFERENCES 41

DEVELOPMENT OF AN NBS REFERENCE SPECTROPHOTOMETER FOR DIFFUSE TRANSMITTANCE AND REFLECTANCE

William H. Venable, Jr., Jack J. Hsia and Victor R. Weidner

A new reference spectrophotometer, designed primarily for the analysis of diffuse transmittance and reflectance, has been developed in the Institute for Basic Standards at NBS. The spectrophotometer consists of a broadband monochromator with optional bandpasses of 2, 5, 10, and 20 nanometers. The exit aperture of the monochromator is provided with special mirror optics to collimate and switch the beam for optional use as a reference or sample beam. These collimated beams are directed into a dark room where a variety of sample mounts, light gathering devices, and detectors can be installed. Measurements for which provisions have been made or are being planned include directional-hemispherical reflectance as a function of angle of incidence, diffuse transmittance, haze, and bidirectional reflectance factor. This Technical Note describes the design of the instrument in detail, and gives the results of the performance tests and detailed error analyses which have been carried out to date.

Key Words: Bidirectional reflectance factor; diffuse reflectance, diffuse transmittance, reflectance; spectrophotometry.

I. INTRODUCTION

Improving the accuracy and usefulness of spectrophotometric measurements made throug out the scientific and industrial community is a fundamental purpose of the spectrophotom group of the Radiometric Physics Section of NBS. One type of spectrophotometric measurement in which a substantial improvement is needed is that of the interaction of light wit turbid media. The principal quantities which are to be measured are directional-hemisphe reflectance and transmittance, bidirectional reflectance factor, and bidirectional transm tance factor. However, in order to measure these accurately, one must determine the effe of a number of related parameters such as translucency and reflections at the sample boun aries.

A reference spectrophotometer for diffuse reflectance and transmittance measurements has been constructed at NBS utilizing a modular design and state of the art components. design allows flexibility in investigating the many aspects of the measurements and it ca be adapted to additional types of measurements in the future. The instrument consists of monochromatic source radiator which projects the radiation into an adjoining darkroom. T radiation source is described in part II of this Technical Note. A number of specialized sample mounts, light gathering devices, and detection systems can be installed in the dar room for performing specific measurements. For brevity, these will be called the "accessories". Several of them are described in part III. The experiments are controlled and data is gathered and analyzed by a mini-computer which is interfaced with the instrument using a modular interactive data acquisition system (MIDAS)[1][1] developed in part at NBS A block diagram showing the general arrangement of the experiment control and data gather system is shown in figure 1.

---

[1]Figures in brackets indicate the literature references at the end of this paper.

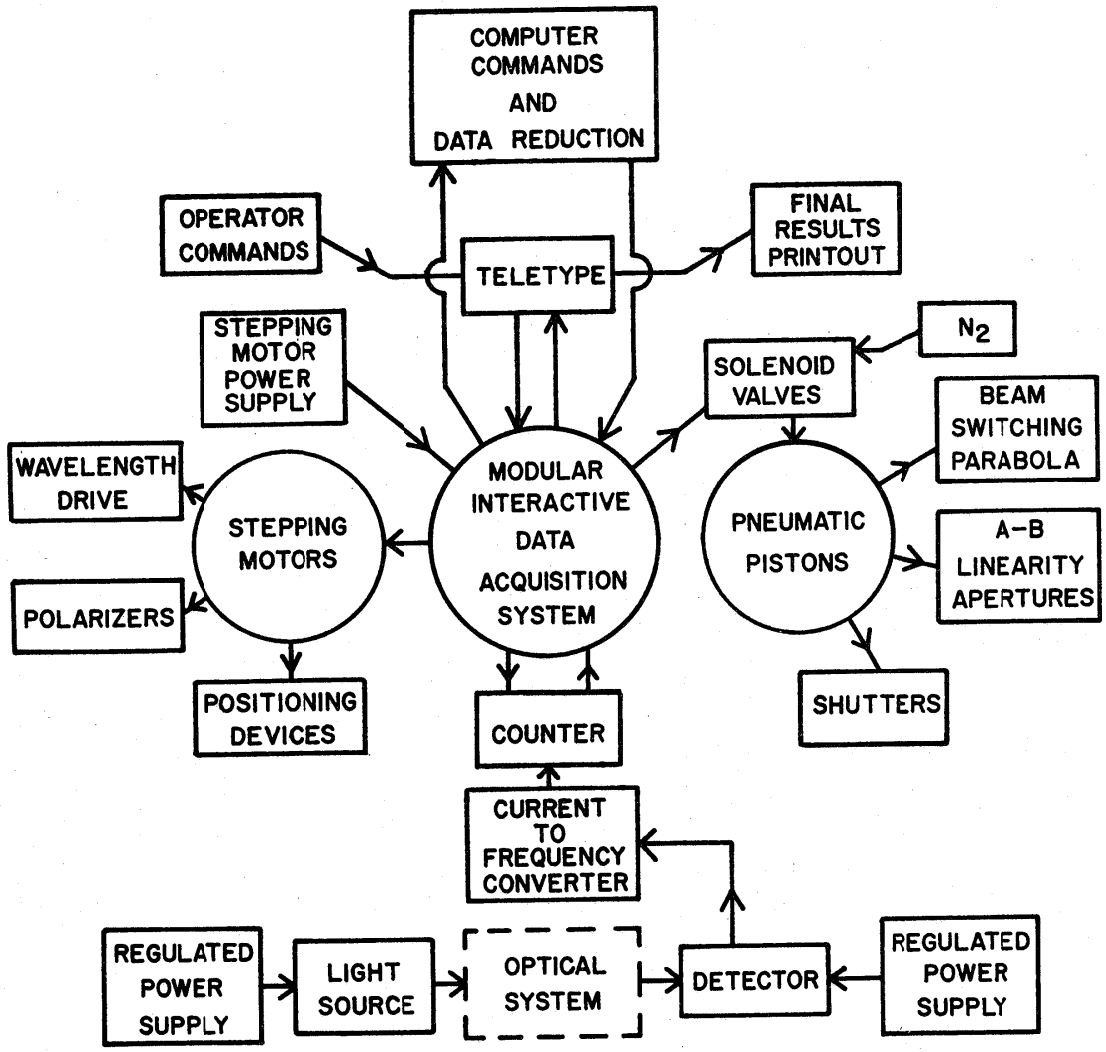

Figure 1. Block diagram for the spectrophotometer and its control system.

II. SPECTROPHOTOMETER DESIGN

The general layout of the optical system of the spectrophotometer is shown in figure 2 The source, alignment laser, and monochromator are mounted on a surface plate with their optic axes horizontal and parallel to the surface of the plate. The exit aperture of the monochromator is attached to a light tight diaphram in a partition that separates the room containing the monochromator and source optics from the dark chamber in which are located the exit aperture optics and the accessories. The accessory pictured in figure 2 is an integrating sphere for directional-hemispherical reflectance measurements. The electronics and control systems are located in the same room as the monochromator, leaving the dark chamber free of all sources of light except the beam from the monochromator. The dark chamber is lined with black felt to absorb stray radiation.

A. Light Sources

The light source ordinarily used with the instrument for the spectral range 400 to 800 nanometers is a tungsten lamp with a 14 mm long by 2 mm wide ribbon filament (GE Microscope Illuminator, T10 bulb, SR-8 filament, 6V, 18A [1]). The tungsten lamp is powered by a regulated supply operated in the constant voltage control mode. This lamp operates in the temperature range of 2100 K to 2900 K. Other sources such as deuterium lamps or xenon arcs can be substituted for operation in the ultraviolet and visible spectral ranges. A helium-neon laser is used to align the optical components in the system. The source and the optic system used to direct the radiation into the monochromator are enclosed in a cover to reduc air currents which can affect the stability of the source.

B. Source Optics

Associated with the light source is an optical bench on which are located mirrors for introducing the radiation into the predisperser and monochromator. The light from the tungsten source is collected and collimated by a 52 mm diameter, 15° off-axis parabolic mirror, having a focal length of 178 mm. The collimated beam of radiation is directed to a flat mirror near the end of the optical bench. The beam is directed by the flat mirror to a second 15° off-axis parabolic mirror which in turn focuses an image of the source on the entrance aperture of the predisperser. The use of mirrors rather than lenses in the system reduces interreflections, improves throughput of radiation in the UV and IR spectral ranges and eliminates wavelength dependent focusing. The mirrors have been coated with MgF_2 in order to maintain their reflectance to greater than 80% down to 180 nm wavelength. The off axis parabolic mirrors are mounted in micrometer controlled angular orientation devices whi are in turn mounted on micrometer cross fed slides for ease of alignment. Polarizers can b inserted into the collimated beam for controlling the intensity of the light or its plane o polarization. The polarizers are mounted in stepping motor driven rotators for independent programmable rotation of each polarizer in the beam.

The two off-axis parabolic mirrors used in the source optics along with a third off-axis parabolic mirror located at the exit slit of the monochromator were specially made for this instrument. They were tested [3] at 15° off-axis with a shearing interferometer at wavelength 577 nm. Collimated light with wavefront deviations no greater than 1/20 wavelength from a plane wave was incident on the parabolic mirror at an angle of 15° ± 0.25° with respect to the test system optical axis. This arrangement simulated the application for the mirror in which a light source at the mirror focus will produce a nearly collimated light. These mirrors were found to be within the diffraction limited performance desired. (In the strictest sense, off-axis parabolic mirrors cannot be diffraction limited because of their inherent astigmatism and coma.) The mirror focal lengths fell within the ±2 mm tolerances placed on them. The fringe pattern for these three mirrors and two additional mirrors that were prepared from the same parabolic mirror are the same to within 1/10 of a fringe when comparing the superpositioned interferogram negatives.

C. Predisperser

The predisperser is an Ebert prism instrument with a 2 mm entrance slit (McPherson 608M1 [1]). The purpose of the predisperser is to eliminate higher order wavelengths and reduce stray light in the monochromator. It has a range of 180 nm to 2600 nm. The focal length of the collimating and focusing mirrors is 15.2 cm with a horizontal aperture ratio

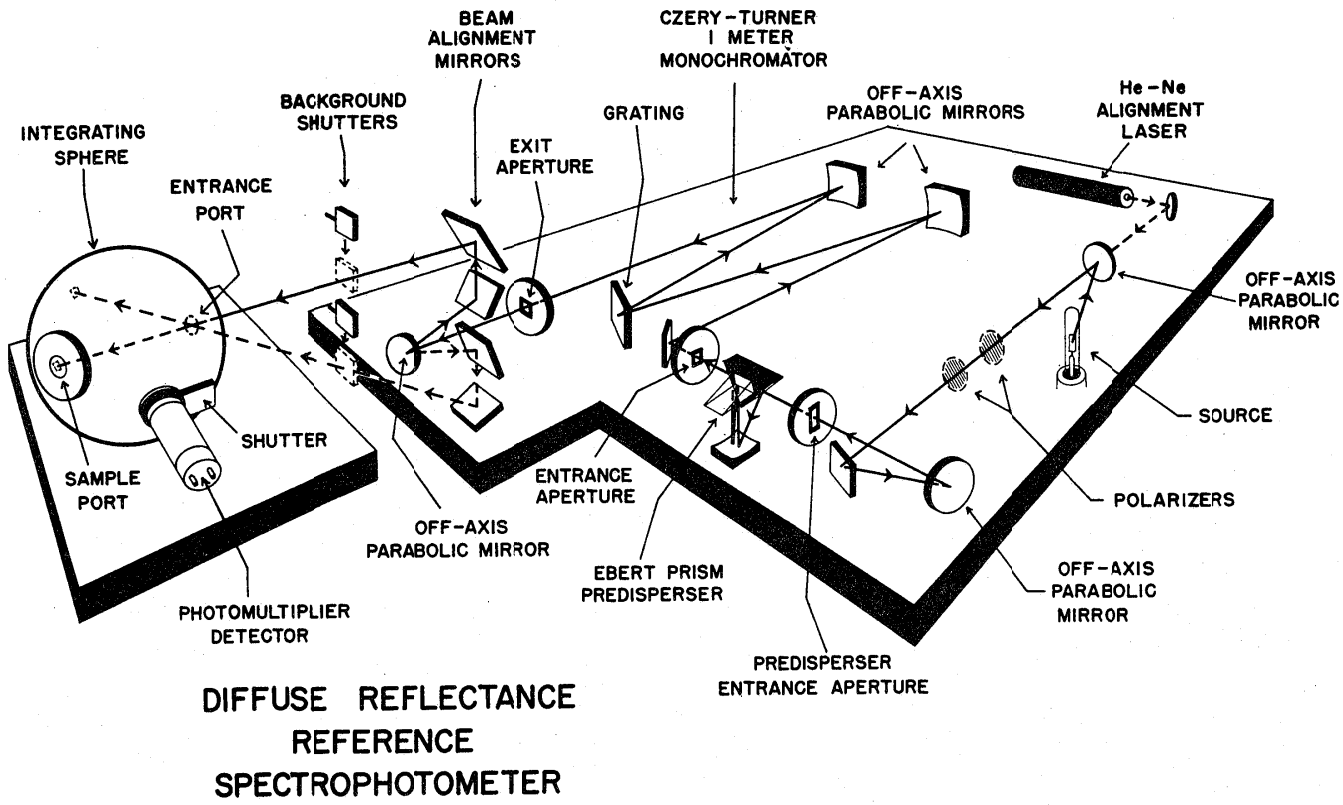

Figure 2. Pictorial diagram of spectrophotometer optical system.

of f/6. The predisperser wavelength drive is synchronized with the wavelength drive of the monochromator.

D. Monochromator

1. Description

The monochromator is a 1-meter Czerny-Turner system with an effective aperture of f/8.7 (McPherson 2051 [1]). Its useful wavelength range is from 200 nm to more than 30 μm with appropriate selection of gratings. The grating presently in use is a plane grating 102 mm by 102 mm having 150 grooves per mm and is blazed at 500 nm. With this grating, the monochromator has a linear dispersion of 6.66 nm/mm.

The monochromator utilizes off-axis parabolic mirrors to collimate the beam on the grating and to focus the dispersed beam on the exit aperture. The entrance and exit apertures of the monochromator are located on rotational devices with four stop positions to allow selection of apertures of 0.300 mm, 0.750 mm, 1.500 mm, and 3.000 mm straight slits corresponding to bandpasses of 2 nm, 5 nm, 10 nm, and 20 nm respectively. The height of the slit can be adjusted from zero to 10 mm. (A larger lamp filament or different source optics would be required for 20 nm band operation.)

The wavelength setting of the monochromator is precise to 0.01 nm. The initial setting of the wavelength scale in an experiment is accomplished by turning the wavelength drive by hand and observing a vernier dial. A stepping motor is used to change the wavelength settings during the experiment. The computer control program is designed to avoid errors due to backlash in the wavelength drive gear train, and at the end of each experiment the wavelength scale is returned to the initial position to allow a check for mechanical slippage.

2. Calibrations and Tests

a. Wavelength calibration -- For measurements in which wavelength is critical, such as the measurement of highly chromatic color samples, the wavelength calibration will be done using stable line emission sources. The general procedure, which has been employed in broadband measurements made with the IBS reference spectrophotometer for transmittance [4], is to scan the monochromator past a source line wavelength and, at regular wavelength intervals, to take readings proportional to the flux transmitted by the monochromator. From these readings, the centroid wavelength scale setting corresponding to the line wavelength can be determined. Since no wavelength-critical measurements have been performed to date with the instrument being described in this Technical Note, it has not been calibrated with line sources.

With the monochromator set at 10 nm bandpass, an NBS Standard didymium glass, calibrated with 10 nm spectral width [5], was employed to check the wavelength scale. The didymium glass was placed in a pneumatically driven slider which was mounted on the optical bench before the predisperser. The slider accommodates one didymium glass plus a clear space, so that the spectral transmittance of the didymium glass can be measured. The measured wavelength of minimum transmittance are listed below with the assigned wavelengths of minimum transmittance for the NBS Standard didymium glass.

Assigned Wavelength (nm)	Overall Uncertainty in Assigned Wavelength (nm)	Measured Wavelength (nm)
441.0	±1.0	440.6
475.5	±1.0	475.8
528.7	±1.0	529.1
585.0	±1.0	585.2
684.8	±1.0	685.0
743.5	±1.0	744.0

The differences between the measured and the assigned wavelengths of minimum transmittance are all within the uncertainty in the assigned values. Therefore it can be assumed from this test that the wavelength scale is accurate at least to within ±1.0 nm.

b. Stray radiant energy -- Stray radiant energy was checked by means of two test methods. The same apertures (1.5 × 1.5 mm) were used for these tests as are used for reflectance measurements with 10 nm bandpass.

The first method is to measure the transmittance of glass filters at the wavelengths for which their transmittance is low. When the value of transmittance does not change when an additional thickness of glass filter is palced in the light beam, then this apparent transmittance is due to the stray radiant energy passed by the filters at other wavelengths where their transmittance is high. The first filter check was made with two selenium orange glasses [6] measured at 400 and 500 nm. The results are as follows:

Wavelength (nm)	Transmittance of One Glass	Transmittance of Two Glasses
400	6.1×10^{-6}	4.1×10^{-6}
500	2.9×10^{-4}	2.4×10^{-4}

Since the transmittance of one filter is approximately 0.9 at wavelengths above 600 nm and nearly zero below 550 nm it follows that with the monochromator set at 400 nm the total stray radiant energy at wavelengths above 600 nm contributes 5×10^{-6} of the detector output due to the total incident radiation. With the wavelength set at 500 nm, the contribution to the detector output by radiation at wavelengths above 600 nm is 3×10^{-4}.

The second filter check was made with four cobalt blue filters [6]. The transmittance measured for three and four filters was found to be:

Wavelength (nm)	Transmittance of Three Glasses	Transmittance of Four Glasses
600	4.6×10^{-5}	4.6×10^{-5}

Each of these filters transmits approximately 0.8 in the wavelength region from 350 nm to 450 nm and approximately 0.9 above 700 nm. The total stray radiant energy in those wavelength ranges contributes approximately 1×10^{-4} of the detector output due to the total incident radiation.

The second type of stray radiation test made use of a helium-neon laser (632.8 nm) as the source of input radiation. Readings of the detector output were made at various wavelength settings of the monochromator. The normalized detector outputs were as follows:

Wavelength Setting (nm)	Normalized Detector Output
400	0.5×10^{-6}
500	3.0×10^{-6}
600	84.0×10^{-6}
632.8	1 (peak)
650	84.0×10^{-6}
700	16.0×10^{-6}
750	1.0×10^{-6}

If it is assumed that a similar performance would occur for incident monochromatic radiation at all other wavelengths, one can calculate that roughly 4×10^{-5} of the radiation passed by the monochromator will be at wavelengths outside the nominal passband. This is in order of magnitude agreement with the values observed with filter glasses.

E. Exit Slit Optics

The exit slit of the monochromator is attached to a light tight diaphragm in a wall so that the emerging radiation enters a 3 by 3 meter dark chamber. A unique feature of the instrument is an optical system located at the exit aperture of the monochromator which is designed to collimate the beam, switch the beam from one of two paths to the other, and provide for directing the beams to the positions required for the various experimental apparatus in the dark chamber. This system is located in the dark chamber, but is supported by a rigid extension of the frame supporting the monochromator surface plate so that its optical alignment remains stable with respect to the monochromator. It is illustrated in figures 2 and 3. (See also appendix G.)

The entire system can be positioned vertically and horizontally by three precision screw driven slides to facilitate its alignment with respect to the monochromator exit slit. The key optical component in this system is a 15° off-axis parabolic mirror 52 mm in diameter The exit aperture of the monochromator is located near the focal point of the parabola. The parabolis mirror is mounted on a pneumatic device which can rotate the mirror 180° clockwise or counterclockwise in approximately 1/4 second. This enables the collimated beam to be switched from one path to the other. This rotation assembly is mounted on a precision slide for independent vertical alignment. Located just above and below the exit aperture are sets of two flat mirrors that intercept the collimated beam from the parabolic mirror. Each flat mirror closest to the parabolic mirror is adjusted to direct the beam to a second flat mirror. located directly above it. The second flat mirror is mounted on precision slides which provide for up and down displacement of the beams. A rotation adjustment about a horizontal axis on each of these mirrors allows for setting the up and down angular direction of each beam. In addition, three spring washer loaded screws are provided for horizontal alignment of the beam. The emerging beam is approximately 10 mm wide for a 10-nm bandpass and the height is adjustable at the monochromator exit slit.

The accurate 180° rotation of the parabolic mirror is assured by means of a gravity dependent system in which a steel ball on the end of an arm attached to the mirror mounting disk is caused to fall against a stop when the pneumatic piston is triggered to rotate the mirror. When the steel ball is at rest on one stop the beam is directed to the upper mirror; when it is at rest on the second stop, the beam is directed to the lower mirrors. The piston intercepts an arm attached to the axis on which the mirror rotates and lifts the steel ball, flipping the ball over the center of gravity, at which point, gravity causes it to come to rest on the stop. The action of the piston is reversible and it is operated by the experiment control system.

All the mirrors in the exit aperture optics, including the off-axis parabolic mirror are made of Cer-Vit [1] glass having negligible thermal expansion. These mirrors are mounted on invar steel to further reduce mirror distortion due to variation in thermal expansion between the mirror and its mounting.

Also incorporated in the exit aperture system is a shutter consisting of two light traps, attached to the shaft of a pneumatic piston, which can be adjusted to intercept the beam as it leaves the exit aperture mirror system by either path. This shutter, which is used to trap the beam when making background signal measurements, can be moved in and out of the beam by actuating the piston through the experiment control system.

III. MEASUREMENT ACCESSORY SYSTEMS

Because of the modular design of the instrument, the optical system as it exists beyond the exit aperture optics depends upon the measurement being made. For each type of measurement, there is a measurement accessory system which may incorporate sample mounts, radiation gathering devices, and detectors. These are mounted on a platform which can be positioned

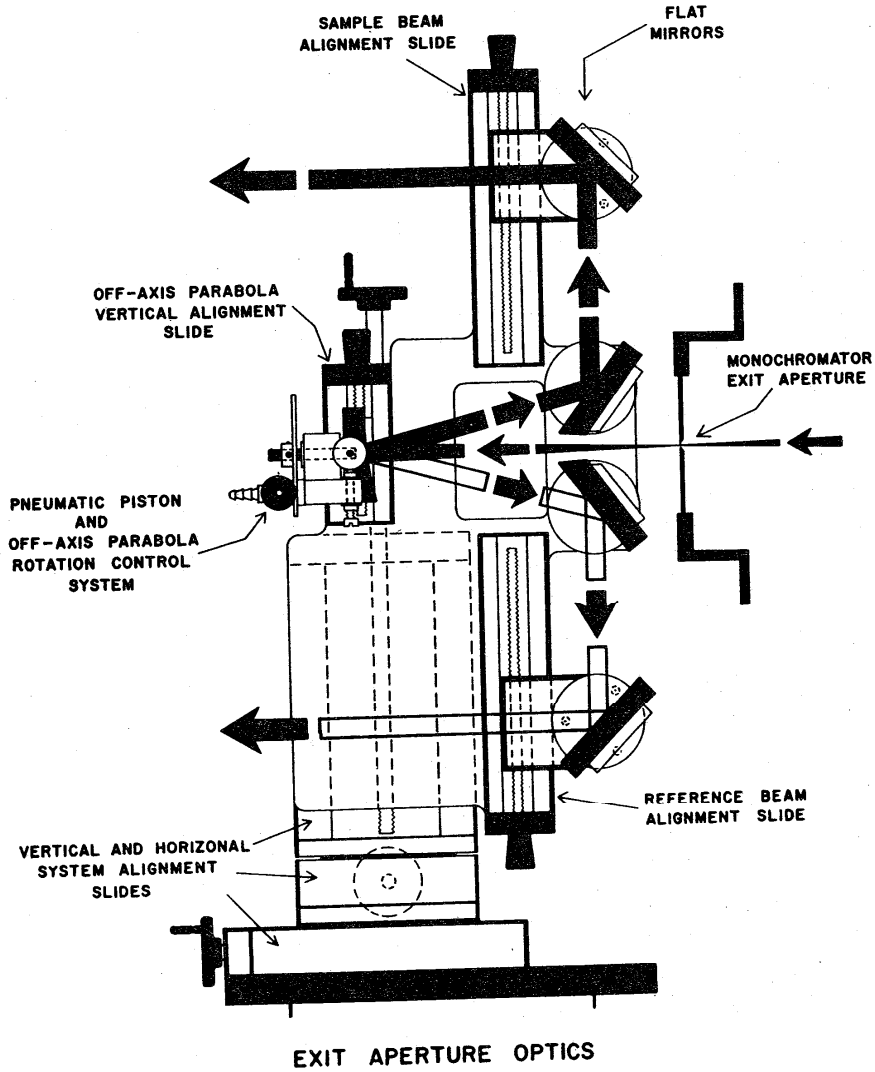

Figure 3. Exit aperture optics and beam switch.

vertically with a lift table and horizontally in both directions by means of ball bushing slides. Stepping motors can be attached to provide automated horizontal positioning as required. In the following sections, several of the measurement accessory systems are described as they now exist or as they are proposed.

A. General Purpose Integrating Spheres

1. Description

Two integrating spheres which are used for measuring directional-hemispherical reflectance are shown in figures 4 and 5. The two spheres are the same except for a variation in the angle at which the beam is incident upon the sample. In one sphere the beam is incident on the sample normal to its surface so that the surface reflection from a high gloss sample returns along the same path in which it entered the sphere and is excluded from the measurement. The other sphere includes most of the surface reflection because the beam is incident on the sample at 6° from normal.

The spheres are approximately 30 cm in diameter. The sample and reference beams enter through the same port, thus reducing the number of openings in the sphere to three: the entrance port, which is 38 mm in diameter; the sample port, which is 50.8 mm; and the detector port, which is approximately 48 mm. The spheres are constructed of two aluminum hemispheres with a white coating of a tetrafluroethylene powder [7,8] called Halon [1]. This coating is applied so as to completely eliminate the seam between the hemispheres, when they are assembled.

The two spheres are mounted together on a pier designed to allow measurements to be made with the specular component included or excluded by rotating either sphere into the position where the sample and reference beams are directed to enter the sphere. The support pier is designed with interchangeable sphere yokes that allow the system to measure samples by mounting them on the sample port in the vertical or horizontal plane. The provision for horizontal mounting of the specimen is to allow for measuring loose powders and liquids. An additional mirror is required to direct the sample and reference beams to the horizontally mounted samples.

The sample port is designed so that the sample surface to be measured is slightly inside the tangent to the curvature of the internal surface of the sphere. The edge of the sample port is only approximately 0.6 mm thick where the inside curvature of the sphere meets the plane of the sample to allow as much of the diffusely reflected radiation as possible to be included in the measurement. The sample beam illuminates an area of the sample approximately 10 mm by 18 mm in the center of the 50.8 mm diameter port. This allows for the complete return of the reflected signal from within most nearly opaque samples without losses caused by the port edge being too close to the area of illumination.

The relationship of the detector port to the entrance and sample ports is shown in figure 6. The detector port is located 90° from the other ports. Direct reflections from the sample port to the detector are prevented by a collar at the detector port. This collar is coated inside and out with the same white material as the sphere wall. A pneumatically operated shutter is located between the white lined collar and the photocathode surface to protect the detector when the room lights are turned on.

The reference beam strikes an area of the sphere near the sample port. The coating on this area is slightly built up so that direct reflection of radiation from this spot to the sample port is prevented. This is required to reduce a slight non-linearity as described in Appendix A.

2. Definition of the Measurement

These accessory spheres are used to determine the ratio of the spectral directional-hemispherical reflectances ρ_x and ρ_y of two flat diffusely reflecting samples x and y. The spectral directional-hemispherical reflectance can be defined generally as

$$\rho_x(\lambda) = \iint S_x(\vec{P},\vec{U};\vec{p},\vec{u},\lambda)\vec{u}\cdot d\vec{a}d\omega \qquad (1)$$

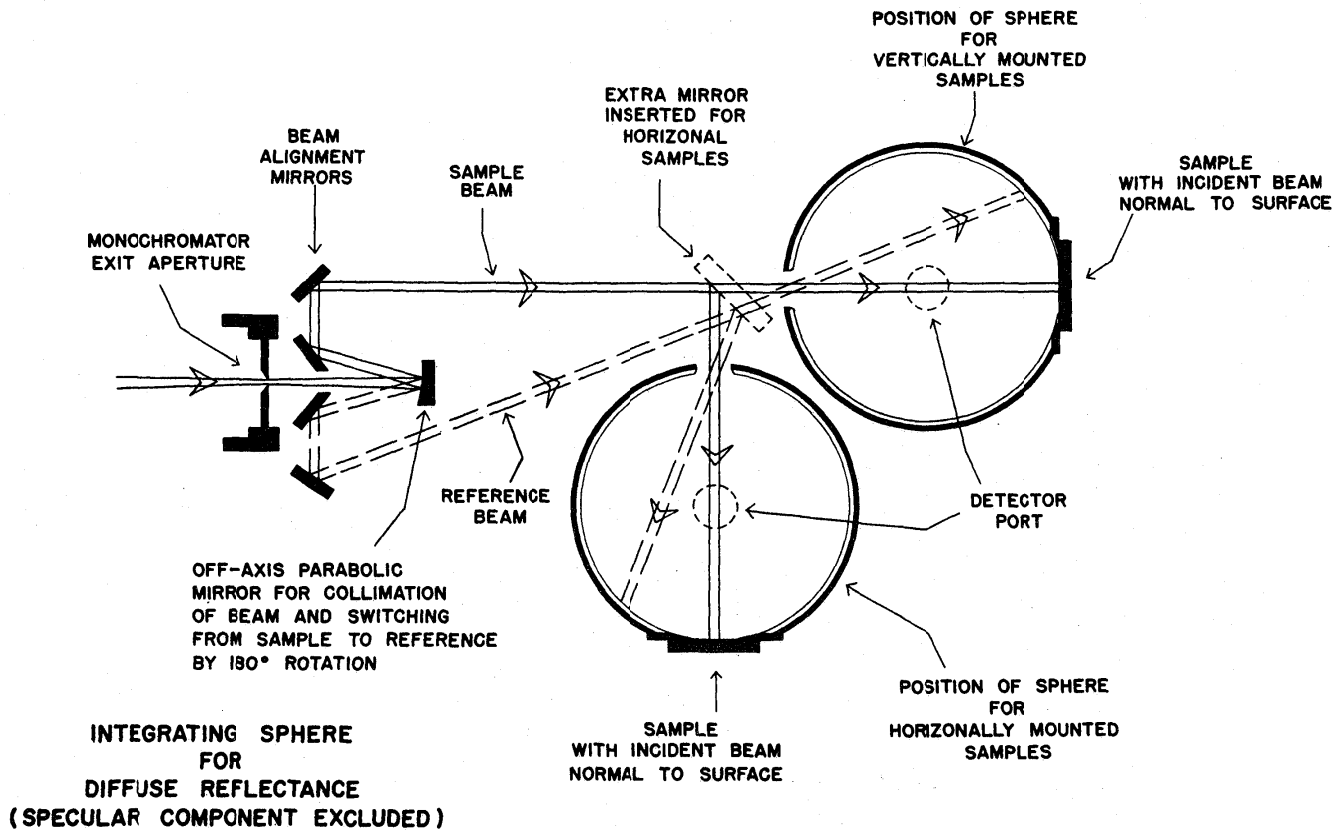

Figure 4. Integrating sphere for directional-hemispherical reflectance with specular component excluded.

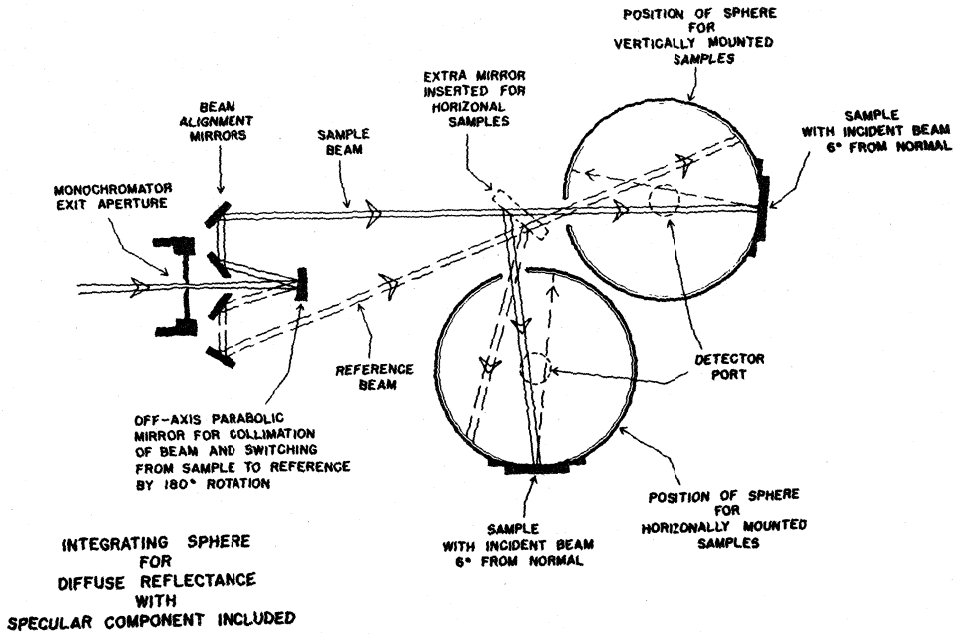

Figure 5. Integrating sphere for directional-hemispherical reflectance with specular component included.

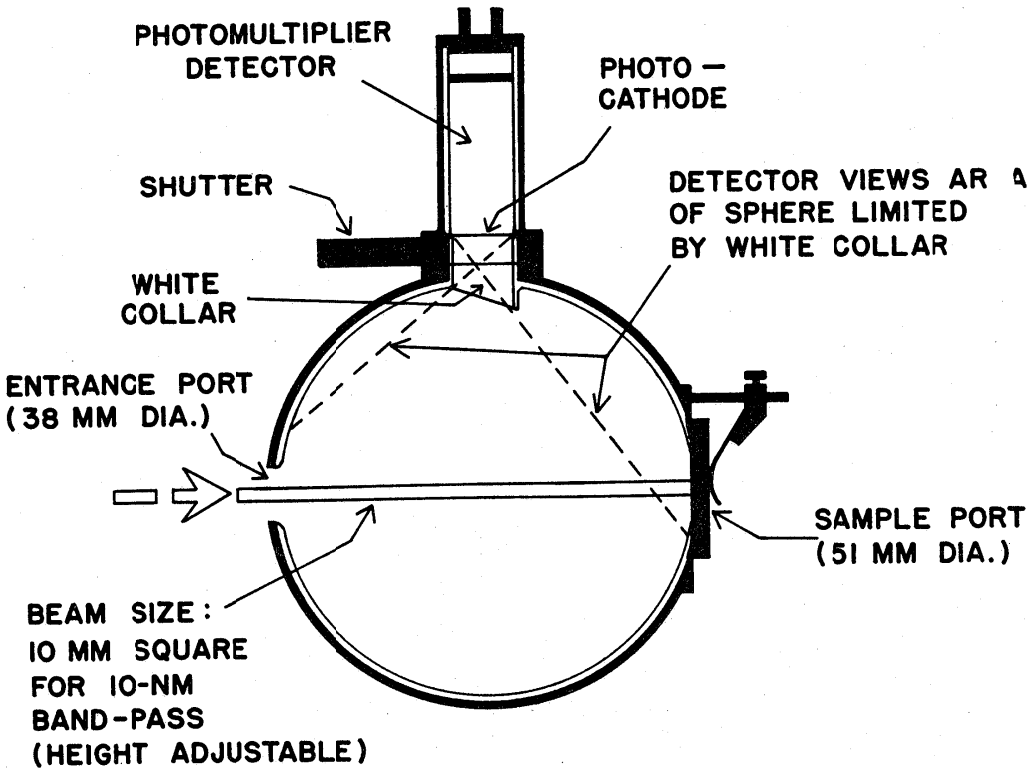

DIFFUSE REFLECTANCE INTEGRATING SPHERE (30 CM DIA.)

Figure 6. Diffuse reflectance integrating sphere showing detector position.

where $S_x(\vec{P},\vec{U};\vec{p},\vec{u},\lambda)$, the generalized scattering function for sample x, is the radiance emerging in a direction $\vec{u}$ from point $\vec{p}$ on the sample surface resulting from a unit flux incident in direction $\vec{U}$ at point $\vec{P}$ on the sample. These spheres are to be used only for non-fluorescing samples for which S_x is a function only of one wavelength λ. The integral of the reflected radiance is taken with respect to area a over the entire sample surface and with respect to solid angle ω over the entire hemisphere of directions of emergence. (A complete discussion of this approach to defining measurements appears in an earlier Technical Note.[9])

The measurement which is actually made involves the ratio Q_x of two signals, N_x which is obtained from the detector when the incident radiation falls on sample x, and N_w which is obtained when the incident radiation falls on the sphere wall.

$$Q_x = N_x/N_w \tag{2}$$

In terms of the defining notation of reference [9],

$$Q_x = \frac{\iiiint\!\!\int L_s S_x R_{sx} \vec{U}\cdot d\vec{A}d\Omega\vec{u}\cdot d\vec{a}d\omega d\lambda}{\iiiint\!\!\int L_w S_w R_{wx} \vec{U}\cdot d\vec{A}d\Omega\vec{u}\cdot d\vec{a}d\omega d\lambda} \tag{3}$$

where $L_s = L_s(U,P,\lambda)$ is the radiance in the sample beam at wavelength λ which strikes the sample at point $\vec{P}$ in direction $\vec{U}$, L_w is a similar expression for the radiance in the reference beam striking the sphere wall, $R_{sx}(\vec{p},\vec{u},\lambda)$ is a function describing the instrument's response to the radiation reflected from the sample, and R_{wx} is a similar expression for the instrument's response to reference beam radiation reflected from the sphere wall. Note that since the sample x is part of the sphere wall, both R_{sx} and R_{wx} depend upon the reflectance of the sample. The measurement assumption is that

$$\frac{\rho_y}{\rho_x} \simeq \frac{Q_y}{Q_x} \tag{4}$$

The extent to which the approximation in eq. (4) approaches true equality depends upon a number of factors, some of which will be discussed later in part III.A.4. In some cases, corrections for Q_y/Q_x can be determined which will cause the approximation in eq. (4) to be more reliably near equality. These corrected expressions are given in eqs. (8) and (9).

3. Reflectance Measurement Procedure

Measurements of spectral reflectance are made with these spheres by comparing first, the reflected signal from the sample to the reference beam signal, and then making the same comparison with a reflectance standard in place of the sample.

With the measuring sphere in position and sample x in the sample port, the relative directional-hemispherical reflectance of sample x to the sphere wall is ordinarily determined by the following procedure. The data are recorded for Z, N_x', N_w', N_x', Z and corresponding time t_1, t_2, t_3, t_4, t_5 where N_x' is the detector output signal when the sample beam strikes x; N_w' is the signal when the reference beam strikes the sphere wall; and Z is the dark current reading taken with the background shutters blocking both beams. The measurement sequence above is repeated two more times. Since the parabolic mirror and the shutter in the exit slit optical system are controlled remotely, this sequence of measurements is achieved easily. For each signal, the count from the current-to-frequency converter is integrated over a ten second interval. A waiting period of 10 seconds is allowed after changing the light level before the count is measured in order to allow any effects of electrical transients to subside. A computer program was written to reduce the data in the following manner. If the detection system is found to be non-linear as described in part III.A.4.a, the values of N_x' and N_w' are corrected accordingly. The signals of Z and N_x' are then linearly interpolated with respect to time to obtain a value for each at time t_3. The

relative reflectance Q_x of the sample x is then computed

$$Q_x = \frac{N'_x(t_3) - Z(t_3)}{N'_w(t_3) - Z(t_3)} \tag{5}$$

The same computing procedure is repeated for the other two measurements. The average of the three relative reflectance $\overline{Q}_x$, is computed and the standard error is determined.

$$\overline{Q}_x = (1/3)\ \Sigma Q_x \tag{6}$$

$$\sigma = [\frac{1}{(3)(2)}\ \Sigma(Q_x - \overline{Q}_x)]^{\frac{1}{2}} \tag{7}$$

For highly reflecting sample, a typical value for σ is found to be 2×10^{-4} and is less for a sample with low reflectance. This has been verified by repeated measurements. The values for $\overline{Q}_x$ are used in eq. (4) to calculate the measured ratio of reflectances ρ_y/ρ_x.

4. Evaluation

a. Detector linearity

The linearity of the detector and electronic system was determined by using the light-addition method with a double-aperture apparatus [4,10], that is, the output of the detector system when irradiated by two light beams simultaneously is compared to the sum of the outputs obtained when the detector is irradiated by each light beam separately. Measurements were also made of the signal as a function of time. Two typical cases are shown in figure 7. In both cases, the drift was approximately linear in time over a 30 minute time interval which is sufficient for the requirements of the linearity test. (The slope of the drift-in-time curve was not always negative.)

The non-linearity is less than 0.01 percent of the full-scale reading. The results are presented below together with the standard deviation of the non-linearity determination.

N_m	ΔN	$SD(\Delta N)$
0.1	6.5×10^{-5}	1.2×10^{-5}
0.2	9.3×10^{-5}	2.1×10^{-5}
0.3	9.4×10^{-5}	2.9×10^{-5}
0.4	7.5×10^{-5}	3.7×10^{-5}
0.5	4.5×10^{-5}	4.5×10^{-5}
0.6	1.1×10^{-5}	5.0×10^{-5}
0.7	1.9×10^{-5}	5.0×10^{-5}
0.8	3.6×10^{-5}	4.3×10^{-5}
0.9	3.2×10^{-5}	2.7×10^{-5}
1	0	0

N_m = the measured signal normalized to 1 at a photomultiplier current of 3×10^{-7} A. ΔN = the amount of the linearity correction on the same scale required to make N proportional to the flux striking the detector. $N = N_m + \Delta N$. $SD(\Delta N)$ = the standard deviation of ΔN.

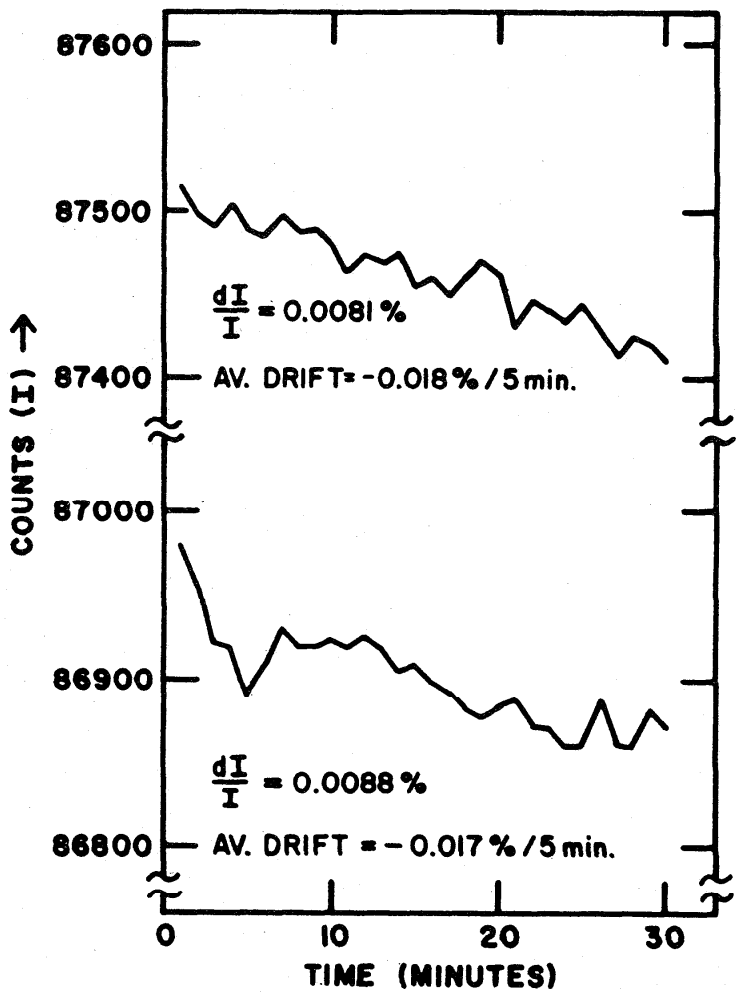

Figure 7. System drift as a function of time.

b. Sample-induced nonlinearity

The magnitude of the responses R_{sx} and R_{wx} in eq. (3) must have the same dependence on S_x if eq. (4) is to approach equality. The departure from this ideal condition will be called sample-induced nonlinearity, and some of its causes are discussed in appendix A. The general purpose measuring sphere with 6° incident angle (specular component included) was tested for sample-induced nonlinearity as described in appendix B. In this appendix, eq. (4) as modified to take sample-induced nonlinearity into account takes on the form:

$$\frac{\rho_y}{\rho_x} \simeq \frac{Q'_y}{Q'_x}\left(1 + \alpha(Q'_x - Q'_y)\right) \tag{8}$$

where Q'_x is the relative reflectance of the sample x as measured and α is a correction coefficient. (See final paragraph of appendix B.)

The initial measurements were made with no baffle between the sample port and the point at which the reference beam strikes the wall. In this case, the experimentally determined value of α was found to be -0.0076. In appendix E, it is shown that the value of the contribution to α caused by the sample's being flat is -0.0077. This suggests that the contribution to α due to other causes such as retroreflectance of the sphere wall was either negligible or not detected by the test. When a baffle was introduced between the sample and the incident point for the reference beam, the experimentally determined value of α was found to be 0.002. In this case, the nonlinearity caused by the sample's being flat should have been eliminated, but reflections from the baffle are estimated to contribute .001 to α. The difference between the estimated and measured values of α may be due to the approximate nature of the theory involved in estimating the nonlinearity caused by the baffle reflection or there may be another contributing factor to sample-induced nonlinearity which has not been taken into account. Since there is no reason at present to doubt the results of the nonlinearity test, and since independent tests of the wall retroreflectance have indicated that its contribution to α is an order of magnitude smaller than that of reflections from the baffle, the results of the test will be assumed correct and ratios of reflectance values will be determined using 0.002 for α in eq. (8).

c. Polarization effects

The detection system was tested for sensitivity to polarization of the reflected radiation and was found to be independent of polarization to within the measurement uncertainty of 0.05%. These tests are described in appendix D. The ratio of the signal for source radiation polarized with the electric vector parallel to the monochromator plane to the signal for the same amount of source radiation polarized perpendicular to the monochromator plane was 1.4 at 450 nm and 1.6 at 700 nm. This indicates that the monochromator partially polarizes the radiation it transmits, as would be expected in a grating instrument.

d. Angular dependence of response

The response R_{sx} depends upon the direction of emergence $\vec{u}$ of radiation reflected from the sample. The closer R_{sx} is to being constant, the more eq. (4) can be relied upon to approach equality. In the general purpose measuring spheres, there are two main departures from constant R_{sx}. The first of these is that R_{sx} is zero within the solid angle subtended at the sample by the entrance port. The second results from the structure of the sample port. In order to taper the sphere wall to the sample port, the portion of the sphere wall bounding the sample port is made of aluminum painted white, rather than being Halon.[1] Therefore, the response in the solid angle subtended by this ring is lower than the response of other directions by the ratio of the reflectance ρ_p of the paint to the reflectance ρ_H of the Halon, both reflectances being for grazing incidence.

If both S_x and S_y depend upon $\vec{u}$ in the same way, no error will be introduced by the nonuniformity of R_{sx}. However, if this is not the case, the detailed dependence of both S_x and S_y upon $\vec{u}$ must be used to calculate the error for a given pair of samples. In such a case, a more reliable approximation than eq. (4) to the reflectance ratio could be written as

$$\frac{\rho_y}{\rho_x} \simeq \frac{Q_y}{Q_x}(1 + \varepsilon_p + \varepsilon_r) \tag{9}$$

where

$$\varepsilon_p = \iint \left(\frac{S_y}{\rho_y} - \frac{S_x}{\rho_x}\right) \vec{u}\cdot d\vec{a}d\omega \tag{10}$$

where the integral with respect to solid angle ω is taken only over the solid angle subtended at the sample by the entrance port, and

$$\varepsilon_r = (1 - \frac{\rho_p}{\rho_H})\iint (\frac{S_y}{\rho_y} - \frac{S_x}{\rho_x})\ \vec{u}\cdot d\vec{a}d\omega \tag{11}$$

where the integral with respect to solid angle ω is taken over the solid angle subtended at the sample by the painted ring surrounding the sample port. The projected solid angle subtended at the sample by the entrance port is .013 sr, the projected solid angle subtended by the painted ring is .055 sr, and the ratio ρ_p/ρ_H is approximately .85 for these measuring spheres. A discussion of some common causes for measurement errors of this type is given in appendix F and ways to estimate values for ε_p and ε_r are given for each cause. The magnitude of ε_p and ε_r is usually quite small, except when samples of different surface textures are compared using the 0° incidence sphere, in which case ε_p can be quite large. For this reason the 6° incidence sphere will usually be used for directional-hemispherical measurements with this instrument.

e. Sample plane to port plane displacement effect

The general purpose measuring sphere with 6° incident angle (specular component included) was tested for sample plane to port plane distance effect on the relative reflectance measurement. A $BaSO_4$ sample was measured from 400 nm to 750 nm with four sample locations: the sample plane 0.9 mm into the measuring sphere from the normal location, at the normal location, and 0.9 mm and 1.8 mm out of the measuring sphere from its normal location. The differences of the relative reflectance from that in the normal position were 0.0009, 0, -0.0019, and -0.0054 respectively. Since the sample surface can be prepared and mounted within 0.1 mm to the port, the uncertainty in the relative reflectance measurement will be less than 0.0002.

B. Integrating Sphere for Measuring Relative Directional-Hemispherical Reflectance as a Function of Angle of Incidence

1. Description

The integrating sphere used in the measurement of relative directional-hemispherical reflectance as a function of angle of incidence is illustrated in figure 8. This 45 cm diameter sphere is mounted on a kinematic support system for ease of alignment when this device is to be used with the spectrophotometer system. The sphere is designed so that a sample can be suspended in the center of the sphere where it intercepts the sample beam. The sample surface is at the sphere center and the sample can be rotated 360° about the sphere center by means of a stepping motor controlled turntable at the top of the sphere. The turntable and the support rod on which the sample is mounted can be removed as a unit for changing samples. The beam goes through a cylindrical lens with its focal line at the center of the sphere and then enters the sphere through an aperture just large enough to allow its entry. A removable plug opposite the sample beam entry port, is opened to initially align the beam through the center of the sphere. To determine the correct position of the turntable for intercepting the beam at normal to the sample, a mirror is suspended in the center of the sphere and rotated until the beam reflects back out the entrance port. The mirror is then replaced with the sample to be measured. The stepping motor is programmed to turn the sample to any desired angle of incidence in the clockwise and counterclockwise direction.

The multiplier phototude detector is located in the bottom of the sphere. The diffuse radiation from the sphere must pass through the side of a transparent plastic rod projecting

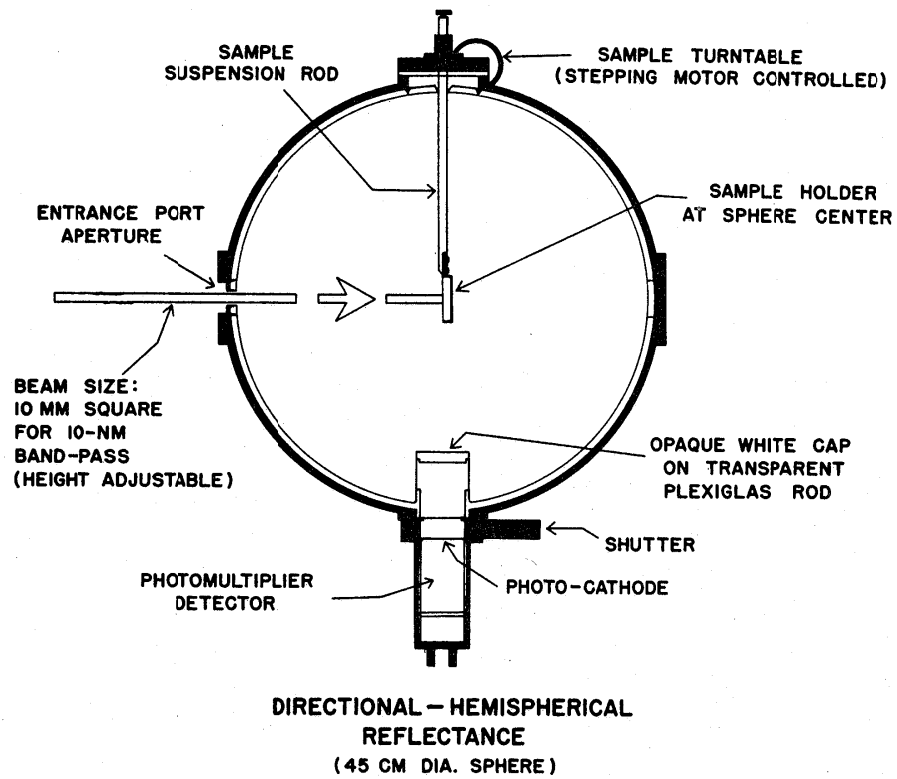

Figure 8. Integrating sphere for measuring relative directional-hemispherical reflectance as a function of angle of incidence.

into the sphere above the detector, in order to be measured. The top of this rod is capped by an opaque white coating and the lower portion of the rod is enclosed in the same white material as the sphere coating. These two coatings act as baffles to prevent direct reflections from the sample to the detector. The plastic rod acts as a light pipe in transmitting the signal to the detector and also acts as a rotationally symmetric support for the upper baffle. A shutter is provided to protect the detector when the room lights are turned on. The sphere coating is tetrafluorethylene powder, which completely seals the seam where the two hemispheres are joined during assembly.

2. Measurement Procedure

With the sample mounted in the center of the sphere and with only the sample beam in use the relative directional-hemispherical reflectance of the sample at angle of incidence of θ to that at normal incidence was determined using the following procedure. We choose to record data in the order of Z, N_0, $N_{+\theta}$, $N_{-\theta}$, $N_{-\theta}$, $N_{+\theta}$, N_0, Z and corresponding times t_1, t_2, t_3, t_4, t_6, t_7, t_8, t_9. The time which occurred about half way between two $N_{-\theta}$'s was also recorded as t_5. N_0 is the signal at normal incidence; $N_{+\theta}$ and $N_{-\theta}$ are signals with angle of incidence of θ at opposite sides of the normal; and Z is the dark current reading. A computer program was written to analyze the data in the following manner. The signals of Z, N_0, $N_{+\theta}$, and $N_{-\theta}$ are first linearly interpolated in time to obtain a value for each at time t_5. The ratio Q_θ of the uncorrected relative directional hemispherical reflectance of the sample at angle of incidence of θ to that at normal incidence is then computed as

$$Q_\theta = \frac{Q_{\theta/h}}{Q_{0/h}} = \frac{[N_{+\theta}(t_5) - Z(t_5)] + [N_{-\theta}(t_5) - Z(t_5)]}{2[N_0(t_5) - Z(t_5)]} \tag{12}$$

The procedure above is carried out for polarizations parallel and perpendicular to the plane of incidence and the results are averaged.

Computer programs for the control system have been written which scan the wavelength to obtain the spectral relative directional-hemispherical reflectance of the sample at one angle of incidence and which scan the angle of incidence at any desired interval at a fixed wavelength to obtain the goniometric relative directional-hemispherical reflectance of the sample at one wavelength.

3. The Entrance Port Correction

Some of the radiation reflected from the sample is lost out the entrance port. The amount of radiation lost depends upon the angle of incidence because of the cosine law and it may be affected further by non-Lambertian angular distribution of the reflected radiance. To make the principal correction for this, we assume that the sample is a Lambertian reflector. The fraction, f, of the reflected flux which escapes through the entrance port from the sample when it is at normal incidence is

$$f = \frac{A/R^2}{\pi} \tag{13}$$

where A is the effective non-reflecting area of the entrance port, R is the inner radius of the integrating sphere, and π is the projected solid angle of the entire hemisphere. For other angles of incidence θ, the fraction of the reflected flux which escapes through the entrance port from the sample is $f \cos\theta$.

The ratio Q_θ, can be expressed by the true directional-hemispherical reflectance $\rho_{\theta/h}$ at angle θ and $\rho_{0/h}$ at normal as

$$Q_\theta = \frac{Q_{\theta/h}}{Q_{0/h}} = \frac{\rho_{\theta/h}(1 - f\cos\theta)}{\rho_{0/h}(1 - f)} \tag{14}$$

Solving for the ratio q_θ of $\rho_{\theta/h}$ to $\rho_{0/h}$, we have

$$q_\theta = \frac{\rho_{\theta/h}}{\rho_{0/h}} = Q_\theta \frac{1 - f}{1 - f\cos\theta} \tag{15}$$

C. Auxiliary Spheres for Determination of the Absolute Reflectance Scale

The general purpose integrating sphere illustrated in figure 5, is equipped with a sample flange for mounting an auxiliary sphere as shown in figure 9. The theory of the use of this type of sphere to determine the absolute reflectance of a material has been described in earlier papers [10,11]. Three of these auxiliary spheres have been constructed having diameters of 30 cm, 20 cm, and 15 cm. The sphere illustrated in figure 9 is the 30 cm diameter auxiliary sphere, which is the same diameter as the detector sphere. These spheres are used to determine the absolute reflectance of white coatings applied to the auxiliary sphere. They have removable target plates that can be attached directly to the detector sphere. These spheres have entrance apertures 2.54 cm in diameter and the removable target is a section of the sphere of 5.08 cm diameter. The spheres are designed to allow the inside curvature of the white coating to meet the center of the entrance port. The edge of the entrance port is beveled about 30° on the side facing the detector sphere, thus providing a clean knife edge for the port. The sample beam enters the auxiliary sphere and is incident on the target at 6° from normal to allow any specular component to be included in the integration of the signal in this sphere. The coatings are applied to the two hemispheres which can be attached to each other so as to completely seal the seam between the hemispheres.

Details of the use of these auxiliary spheres to determine directional-hemispherical reflectance factor are to be given in a separate publication.

D. Bidirectional Diffuse Reflectance and Transmittance Factor Accessory System

A system has been constructed for utilizing the diffuse reflectance spectrophotometer in measuring bidirectional reflectance factor, particularly for 45°-0°. With this accessory set up for 45°-0° as shown in figure 10, the collimated sample beam from the spectrophotometer is incident on a sample at 45° from normal and the reflected signal at normal to the sample is collected and measured. The multiplier phototube detector is equipped with a signal averaging sphere. The detector and averaging sphere are attached to a stepping motor controlled vertical slide for alignment and scanning purposes. The averaging sphere has a limiting aperture facing the sample. The solid angle of collection is determined by the size of the limiting aperture and its distance from the sample. In this system the sample is mounted on a stepping motor controlled turntable, and the detector assembly is on an arm attached to another independently controlled turntable having the same axis of rotation as the sample turntable.

The sample is mounted on a two position slide that moves 12.5 cm between positions and is pneumatically driven. In one position the sample intercepts the beam, in the second position a polished black glass standard intercepts the beam. The polished black glass is mounted so that it intercepts the beam at 22.5° from its normal and the specular reflection, amounting to approximately 4%, is reflected into the detector averaging sphere. This black glass acts as a standard reflector. It has a specular signal level of about 40 times the magnitude of the diffuse signals that will be measured. Alignment is accomplished with the alignment laser built into the spectrophotometer. The stepping motors are controlled by computer to allow for scanning the detector position or changing the incident angle on the sample or viewing angle from the sample. This device has not been tested at the date of this publication.

IV. SUMMARY

Because of the modular nature of this instrument, it will probably never be completed in the sense that no more accessories will be constructed. Therefore it was decided to publish this technical note to document the development and testing of the NBS Reference Spectrophotometer for Diffuse Transmittance and Reflectance from its inception to the present (May 1976). The principal use of the instrument to date has been to investigate problems connected with realizing a scale of directional-hemispherical reflectance factor. The results of this investigation are to be published separately.

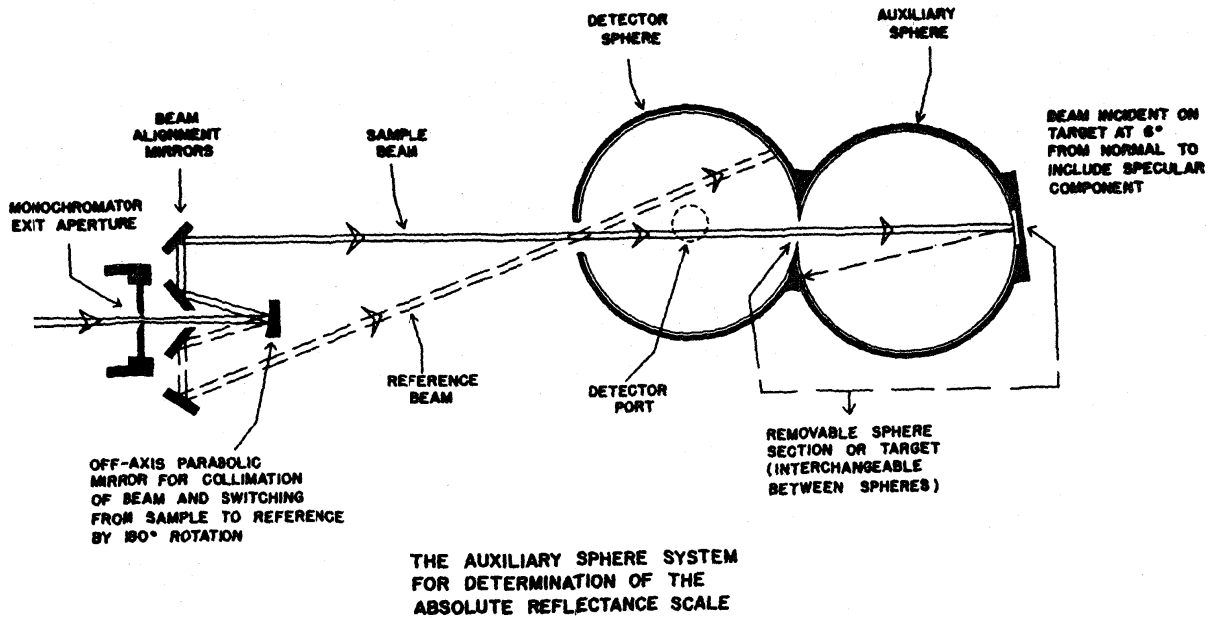

Figure 9. The auxiliary sphere system for determination of an *absolute reflectance scale*.

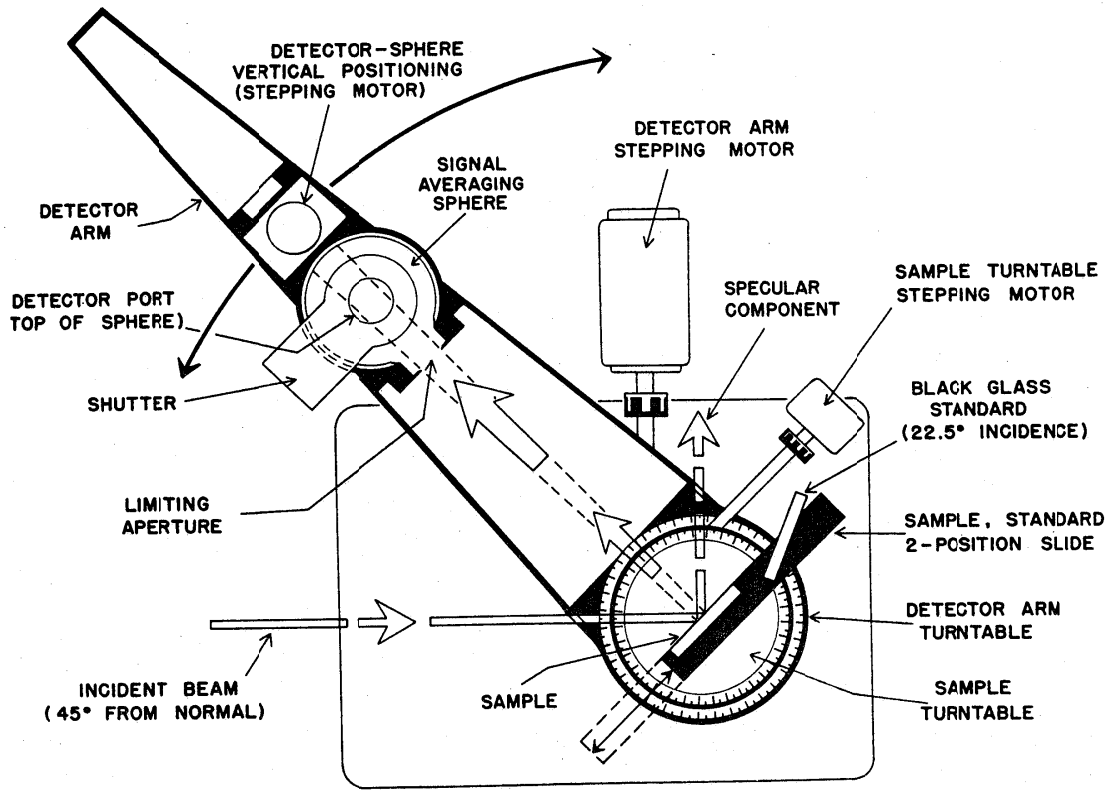

0°–45° DIFFUSE REFLECTANCE SYSTEM
(VERTICAL VIEWING)

Figure 10. Bidirectional reflectance factor system.

APPENDIX A

Sample-Induced Nonlinearity

The type of nonlinearity to be discussed here is not the result of detector or electronic nonlinearity, but is the result of slight differences in the efficiency with which the radiation reflected from the sample and the radiation from the reference beam, reflected from the wall, reaches the detector. Since the sample when presented at the sample port becomes part of the sphere wall, it affects the efficiency of the sphere in transmitting the radiation from the initial reflection of the sample beam or of the reference beam to the detector. In an ideal situation in which the sample is curved to fit the contour of the sphere wall and all reflections are Lambertian, the efficiency for transmitting radiation from the initial reflection from either beam will be the same, so that

$$Q_x = \frac{\phi_1 \rho_x}{\phi_2 \rho_w} \qquad \text{(A1)}$$

where Q_x is the relative reflectance as defined in eq. (2), ϕ_1 is the flux incident upon the sample, ρ_x is the directional-hemispherical reflectance of the sample x, ϕ_2 is the flux incident upon the sphere wall, and ρ_w is the directional-hemispherical reflectance of the sphere wall. However, real spheres seldom operate under such ideal conditions, so that a more complex and non-linear relationship exists between Q_x and ρ_x. Because this departure from linearity is small, it can usually be adequately represented by adding a small quadratic term in ρ_x to the right side of eq. (A1).

Three cases of such nonlinearity will be discussed in the remainder of this appendix. In each case, the following approach will be taken in the analysis. The reflected flux from the initial reflection of each beam will be described in terms of two or more parts. The principal part of each flux will be that part which can reasonably be expected to reach the detector with the same efficiency from both beams. The remaining parts of the flux will be transferred with different efficiencies and will be the cause of the non-linearity. Since the component which receives the same treatment will be by far the largest, the contribution of the detected flux from each reflection of the other fluxes can be written in terms of a rapidly converging geometric series. The sum of such a series can be evaluated and eventually written in an approximate simple quadratic form.

1. Wall Retro-Reflectance Nonlinearity

If the sphere wall coating retro-reflects, a simple model of the reflection from the sphere wall is one in which a fraction f_0 of the incident radiation is returned in precisely the opposite direction to the direction of incidence and the remaining fraction $(1-f_0)$ is reflected diffusely with a Lambertian distribution and will be transmitted to the detector through the sphere with an efficiency η_x. The retroreflected portion will be returned to the sample, where it will again be reflected with a reflectance ρ_x. (In discussing the reflectance from the sample, the sample will be treated as being non-retroreflecting, since the initial retroreflective component, if any, will be lost out the entrance port and the remaining contribution will produce only a small change in an already small correction term.) Thus, the signal* from the first reflection from the sphere wall will be:

$$N_{x1} = \phi_1 \rho_x (1 - f_0)\, \eta_x \qquad \text{(A2)}$$

where ϕ_1 is the flux in the beam of radiation incident on the sample. Let f' be the fraction of the reflected radiation which strikes the sphere wall as opposed, for example, to going out the ports. It is assumed here that the sphere contains a baffle which prevents radiation reflected from the sample from going directly to the detector. The retroreflected fraction

---

*In these appendices, the signal being discussed is the signal above background. In terms of the notation in section III.A.2, $N_x = N'_x - Z$ where N'_x is corrected for any detection system nonlinearity.

returns to the sample and is reflected again. Of the re-reflected radiation, a fraction $(1-f_0)$ makes a second contribution to the signal;

$$N_{x2} = \phi_1 \rho_x [f_0 \bar{\rho}_x f'](1 - f_0)\, \eta_x. \tag{A3}$$

where $\bar{\rho}_x$ is the reflectance of the sample for hemispherically incident radiation. Similar expressions can be written for the remaining contributions. The contributions form a geometric series in which the initial term is N_{x1} and the ratio of successive terms is the factor in brackets in eq. (A3). The entire signal is, then, the sum of the series, or:

$$N_x = \frac{\phi_1 \rho_x (1 - f_0)\, \eta_x}{1 - f_0 \bar{\rho}_x f'} \tag{A4}$$

When the signal from the reference beam is treated in the same way, a similar expression, in which ρ_x is replaced by ρ_w, ϕ_1 is replaced by ϕ_2, and $\bar{\rho}_x$ is replaced by $\bar{\rho}_w$ will result. The ratio of these two signals will be Q'_x, so that

$$Q'_x = \frac{\phi_1 \rho_x}{\phi_2 \rho_w} A_2 (1 + G_2 \bar{\rho}_x) \tag{A5}$$

where

$$A_2 = (1 - G_2 \bar{\rho}_w)$$

and

$$G_2 = f_0 f'$$

and terms in higher powers of $G_2 \bar{\rho}_x$ have been dropped. It can be seen that (A5) has the form of (A1) with a corrective term which depends upon the reflectance $\bar{\rho}_x$ of the sample. In reality, the retro-reflected radiation is not returned from the wall in exactly the direction it arrives, but is spread out typically in a distribution with a half-height width of a degree or two. However, in the usual case in which the initial radiation is reflected from the center of the sample, most of the retroreflected radiation is returned to some point on the sample, so that f_0 probably represents most of the radiation in the retroreflective peak along with a less easily defined contribution (either positive or negative) due to the fact that the level of the underlying diffuse radiation in the retro direction may be above or below the average of the distribution. Because of this difficulty in defining f_0 precisely, it is best evaluated using experiments such as are described in appendix B.

2. Flat-Sample Nonlinearity

As is indicated in the literature [12], if the sample is flat, the comparison between sample and reference may not be exact. The nonlinearity in this case arises because the sample does not reflect directly onto itself, whereas if the sphere design is such that the reference beam strikes the sphere at a point on the curved wall, some of the radiation from the first reflection does strike the sample. The signal due to the radiation reflected from the sample is given by

$$N_x = \phi_1 \rho_x \eta_x \tag{A6}$$

where η_x is the average efficiency of transfer to the detector for radiation striking the sphere wall anywhere outside the sample port. If the sample port receives a fraction f_1 of the radiation from the initial reflection of the reference beam, the signal from the reference beam is given approximately by

$$N_w = \phi_2 \rho_w [(1 - f_1) + f_1 \rho_x'] \eta_x \tag{A7}$$

where ρ_x' is the reflectance of the sample for radiation incident on it from the direction of the point of incidence of the reference beam. In this case, the ratio Q_x' becomes

$$Q_x' = \frac{\phi_1 \rho_x}{\phi_2 \rho_w} A_1 (1 + G_1 \rho_x') \tag{A8}$$

where

$$A_1 = 1/(1 - f_1)$$

and

$$G_1 = -f_1/(1 - f_1)$$

Note that in this case, the nonlinearity term is of the opposite sign from the retroreflective term so that the two contributions will tend to cancel.

3. Baffle-Induced Nonlinearity

In principle, the flat-sample nonlinearity just discussed can be avoided by placing the sample port and the surface struck by the reference beam in the same plane in the way that was done by Hardy [13]. However, this distorts the sphere considerably, so we chose to reduce the flat sample nonlinearity by introducing a small baffle between the sample port and the point of incidence of the reference beam. A sphere with baffle is shown in cross section in figure 11. Because of the presence of the baffle, the analysis becomes quite complex and depends upon the design of the baffle and the choice of the point of incidence of the reference beam. This analysis will be carried out in detail in appendix E to evaluate the specific sphere design we used. However, the procedure for carrying out the analysis and the nature of the results can be discussed in general. The reflecting areas in the sphere are divided up into six regions: region 1, the sample port; region 2, the portion of the sphere wall struck directly by the radiation reflected from the sample but not struck by the radiation reflected directly from the area irradiated by the reference beam; region 3, the side of the baffle toward the sample port; region 4, the side of the baffle away from the sample port; region 5, the portion of the sphere wall which is struck by the radiation from the initial reflection of the reference beam, but which is not struck by radiation reflected from the sample; and region 6, the remaining portion of the sphere. In a good sphere design of this type, region 6 is by far the largest region and it contains the detector port. In the analysis, once the radiation reaches region 6, it is assumed to be transferred to the detector with an efficiency η_x which is independent of the beam from which the radiation originated.

Although the solution of the problem of the transfer of the radiation from the point of incidence of the sample beam to region 6 is difficult, the form of the result can be anticipated.

$$N_x = \phi_1 \rho_x (a_x + b_x \rho_x') \eta_x \tag{A9}$$

where a_x and b_x are independent of the sample and depend only on the sphere geometry and the wall and baffle reflectances. The constant a_x is nearly 1 and represents the portion of the radiation which reaches region 6 without additional reflections from the sample, b_x represents the portion of the radiation which is reflected again by the sample before reaching region 6, and ρ_x' is the effective reflectance of the sample for irradiation from regions 2, 3 and 5. A similar expression can be written for the reference beam

$$N_w = \phi_2 \rho_w (a_w + b_w \rho_x') \eta_x \tag{A10}$$

where a_w, also nearly 1, represents the portion of the radiation transferred to region 6 without reflecting from the sample and b_w represents the portion reaching region 6 by reflecting from the sample. The signal ratio Q_x' takes the same form as in eq. (A8), except in this case

$$A_1 = \frac{a_x}{a_w}$$

and

$$G_1 = \left(\frac{b_x}{a_x} - \frac{b_w}{a_w}\right) \tag{A11}$$

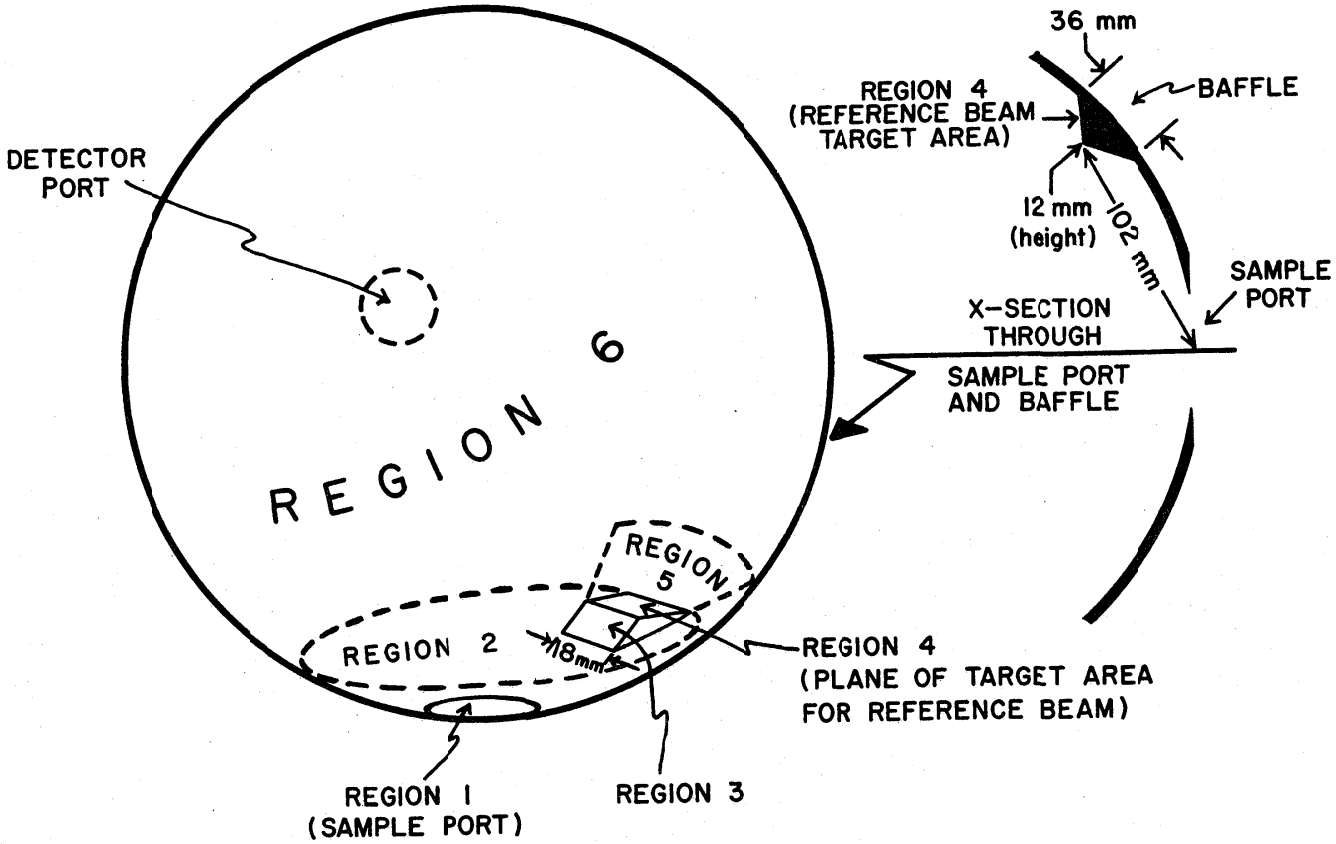

Figure 11. Pictorial representation of the sphere with baffle. The baffle is a triangular wedge built up with sphere wall material, and the reference beam is incident upon the wall of the baffle which is away from the sample port.

Because of the baffle's shielding effect, $b_x > b_w$ so that in this case G_1 is positive and the baffle-induced nonlinearity tends to be of the same sign as the wall retro-reflectance nonlinearity.

4. Combinations of Sample-Induced Nonlinearities

If the sample-induced nonlinearities are small, the wall retro-reflective nonlinearity term can simply be added to the appropriate geometrically-related nonlinearity term to yield an expression of the form:

$$Q'_x = \frac{\phi_1}{\phi_2} \frac{\rho_x}{\rho_w} A_1 A_2 (1 + G_1 \rho'_x + G_2 \bar{\rho}_x) \tag{A12}$$

where G_1 is given either by eq. (A8) or eq. (A11), depending upon the absence or presence of a baffle, and where G_2 is given by eq. (A5). Because of the sample-induced nonlinearities, it follows that the ratio of the actual reflectances of two samples y and x can be obtained from correcting the ratio of the corresponding measured values Q_y and Q_x. This correction can be determined from eq. (A12) to be:

$$\frac{\rho_y}{\rho_x} = \frac{Q'_y}{Q'_x} [1 + G_1(\rho'_x - \rho'_y) + G_2(\bar{\rho}_x - \bar{\rho}_y)] \quad . \tag{A13}$$

APPENDIX B

Method of Evaluating Sample-Induced Nonlinearity

The sample-induced nonlinearity can be evaluated by using two thin masks, each of which has a hole in it. The masks are identical in size, but one is painted black and the other is painted white. The hole in the mask is made smaller than the sample port, but larger than the irradiated area on the sample. Two measurements are made on a given sample, one with each mask in place between the sample and the sphere port. In both of these measurements, the relative reflectance must be corrected for scattered radiation surrounding the main incident beam as discussed in appendix C. For each measurement, the mask is aligned so that the incident beam passes through the hole. In this way, the average reflectance of what appears in the sample port can be changed without changing the surface which is initially struck by the incoming beam of radiation. Equation (A13) can be modified to give the measured relative reflectance with the white mask in place as:

$$Q'_{xA} = \frac{\phi_1 \rho_x}{\phi_2 \rho_w} A_1 A_2 \left\{ 1 + G_1[(1-F_1)\ \rho'_x + F_1 \rho'_A] + G_2[(1-F_2)\bar{\rho}_x + F_2 \bar{\rho}_A] \right\} \tag{B1}$$

where F_1 is the ratio of the area of the mask to the area of the sample port, F_2 represents the fraction of the retroreflected radiation which spills over from the irradiated area of the sample onto the mask, during the interreflections, ρ'_A is the reflectance of the white mask at the same angle of incidence at which ρ'_x is evaluated and $\bar{\rho}_A$ bears a similar relation to $\bar{\rho}_x$. (See discussion proceeding eq. (A8) and following eq. (A3) in appendix A.) It is expected that F_2 will be smaller than F_1.

A similar equation can be written for the black mask to obtain a relative reflectance Q'_{xB}. Taking the ratio Q'_{xB} to Q'_{xA} one obtains

$$1 - \frac{Q'_{xB}}{Q'_{xA}} = G_1 F_1 (\rho'_A - \rho'_B) + G_2 F_2 (\bar{\rho}_A - \bar{\rho}_B) \tag{B2}$$

where use is made of the assumption that $G_1 << 1$ and $G_2 << 1$. Since the correction coefficients G_1 and G_2 are small, there will be a large uncertainty in determining them. Therefore, the approximations used to determine the correction term in eq. (8) will be made conservatively, i.e., in such a way as to make the correction small in order to avoid overcorrection. The relative reflectance Q'_A and Q'_B of the mask materials can be measured. Since $\phi_1 \simeq \phi_2$ and $\rho_w \simeq 1$, these measured values can be used in place of ρ'_A and $\bar{\rho}_A$ in the first term of eq. (B2) and also in place of ρ'_B and $\bar{\rho}_B$ in the second term of eq. (B2). With this assumption, eq. (B2) can be written

$$\frac{1 - Q'_{xB}/Q'_{xA}}{F_1(Q'_A - Q'_B)} = G_1 + \frac{F_2}{F_1} G_2 \equiv \alpha \tag{B3}$$

Under the same assumption, eq. (A13) can be written as

$$\frac{\rho_y}{\rho_x} = \frac{Q'_y}{Q'_x} [1 + (G_1 + G_2)(Q'_x - Q'_y)] \tag{B4}$$

Since $F_2 < F_1$, it follows that

$$|\alpha| \leq |G_1 + G_2| \tag{B5}$$

when G_1 and G_2 have the same sign. Therefore, in the case of the sphere with baffle, eq. (8) provides a conservative correction when α is determined using eq. (B3).

APPENDIX C

Correcting for Scattered Radiation in Incident Beam

The beam of radiation incident on the sample can be considered to be made up of three fluxes: ϕ_1, which falls inside a given central circle and contains most of the incident radiation, ϕ_b which falls between the central circle and the boundary of the sample port, and ϕ_c which falls outside the boundary of the sample port. These three make up the total incident flux ϕ_{xmw}, i.e.

$$\phi_{xmw} = \phi_1 + \phi_b + \phi_c \tag{C1}$$

where $\phi_1 >> \phi_b$ and $\phi_1 >> \phi_c$ is the case in a good instrument. An expression for the uncorrected relative reflectance Q''_x as read from the instrument is

$$Q''_x = k\phi_1\rho_x\{1 + G_1[(1 - F_1)\ \rho'_x + F_1\rho'_m] + G_2[(1 - F_2)\ \rho_x + F_2\rho_m]\} + k\phi_b\rho_m + k\phi_c\rho_w \tag{C2}$$

where ρ_x is the reflectance of the sample in the central area, ρ_m is the reflectance of the sample in the area struck by ϕ_b, F_1 and F_2 are defined after eq. (B2) and, products of two small terms are neglected, and k is $A_1A_2/\phi_2\rho_w$. (See discussion in last paragraphs of appendix A.) One would like to correct Q''_x to obtain the contribution due just to the light reflected from the central area, i.e.

$$Q'_x = k\phi_1\rho_x\{1 + G_1[(1 - F_1)\ \rho'_x + F_1\rho'_m] + G_2[(1 - F_2)\ \rho_x + F_2\rho_m]\} \tag{C3}$$

To make this correction, four additional measurements are made. First a value of Q''_x is obtained with the sample port empty. This is called Q''_w and is given by:

$$Q''_w = k\phi_c\rho_w \tag{C4}$$

Second the value of Q''_x is obtained with a white card in the area struck by ϕ_b and the central area empty (a hole in the card). This is called Q''_{cw} and is given by:

$$Q''_{cw} = k(\phi_b\rho_c + \phi_c\rho_w) \tag{C5}$$

where ρ_c is the reflectance of the card. Third a value of Q''_x is obtained with a white card of the same material filling the entire port. This is called Q''_{ccw} and is given by:

$$Q''_{ccw} = k\phi_1\rho_c(1 + G_1\rho'_c + G_2\rho_c) + k\phi_b\rho_c + k\phi_c\rho_w \tag{C6}$$

For measurements in which the area struck by ϕ_b is to be occupied by a mask of reflectance ρ_m, a measurement of Q''_x with only the mask in place can be made. This is called Q''_{mw} and is given by:

$$Q''_{mw} = k(\phi_b\rho_m + \phi_c\rho_w) \tag{C7}$$

when a mask is used, a correction of the general measurement can be made as:

$$Q'_x = Q''_x - Q''_{mw} \tag{C8}$$

This expression is used to obtain Q'_{xA} and Q'_{xB} in appendix B. When the entire sample port is filled with the same material ($\rho_m = \rho_x$), one can correct Q''_x to give Q'_x as shown in eq. (C3) by using

$$Q'_x = (Q''_x - Q''_w)\ \frac{(Q''_{ccw} - Q''_{cw})}{(Q''_{ccw} - Q''_w)} \tag{C9}$$

This expression is used when comparing a sample without mask to a sample with mask for which eq. (C8) applies. This circumstance occurs in the use of the auxiliary sphere attachment described in III.C.

When two samples are to be compared, each of which fills the entire entrance port, a simpler correction is applicable. In this case, the mask area and, therefore ϕ_b, is considered to be zero and the corrected relative reflectance is:

$$Q'_x = k\phi_1\rho_x(1 + G_1\rho'_x + G_2\overline{\rho}_x) \tag{C10}$$

This can be obtained from the uncorrected values as:

$$Q'_x = Q''_x - Q''_w \tag{C11}$$

APPENDIX D

Test for Polarization Effects

The incident radiation can be polarized using a polarizer in the input optics as indicated in figure 2. The monochromator will not depolarize the radiation if the plane of polarization is either perpendicular to or parallel to the plane of the monochromator. For the polarization tests, the instrument is used in a single-beam mode, and the measurements are made in a time-symmetrical sequence to allow correction for linear drift of the source and detector in time.

To determine whether the reflectance measurement on a sample is polarization dependent, the ratio of the fluxes $\phi_{/\!/}$ and $\phi_{\perp}$ with the beam in the two polarizations is determined by using a second integrating sphere as a target. This sphere acts as a polarization insensitive target which effectively reflects depolarized radiation. The ratio q_a of the signals, equal to the ratio of the incident fluxes in this case, is

$$q_a = \frac{\phi_{/\!/}}{\phi_{\perp}} \tag{D1}$$

If a highly polarizing diffusing reflector is measured with $\phi_{/\!/}$ incident and then rotated 90° and measured with $\phi_{\perp}$ incident, the ratio q_b is determined.

$$q_b = \frac{\eta_{/\!/}\ \phi_{/\!/}}{\eta_{\perp}\ \phi_{\perp}} \tag{D2}$$

where $\eta_{/\!/}$ and $\eta_{\perp}$ are the sample beam efficiencies of the sphere for the given polarization. The polarizing diffuse reflector is made by cementing an absorbing polarizing film on a piece of white opal glass and using it in the orientation for maximum reflectance of the polarized light. If q_a and q_b are equal, the measuring sphere is polarization independent.

Finally, the polarization dependence of a sample can be evaluated by obtaining signals for each polarization to determine the ratio q_c.

$$q_c = \frac{\rho_{/\!/}\ \eta_{/\!/}\ \phi_{/\!/}}{\rho_{\perp}\ \eta_{\perp}\ \phi_{\perp}} \tag{D3}$$

where $\rho_{/\!/}$ and $\rho_{\perp}$ are the sample reflectances for the two polarizations with the given orientation of the sample. If $q_b = q_c$, the sample reflectance is polarization independent.

APPENDIX E

Estimation of Sample-Dependent Nonlinearity

In this appendix, an approximate evaluation of the constants G_1 defined in appendix A will be made for the general purpose integrating sphere. The measured dimensions of the spheres will be used as a basis for the estimation. The radius of the interior wall of the sphere is R = 14.6 cm and the sample port takes the form of a circle of radius r = 2.54 cm on this surface.

1. Sphere Without Baffle

From elementary geometry and the assumption of Lambertian reflection from the sphere wall, the fraction f_1 of the radiation reflected from the reference beam into the sample is

$$f_1 = 1/2\left[1 - \sqrt{1 - \frac{r^2}{R^2}}\right] \tag{E1}$$

Thus one can evaluate G_1 for this sphere from eq. (A8) as

$$G_1 = 0.0077$$

2. Sphere With Baffle

The treatment of a sphere with a baffle is considerably more complicated and a method of detailed flux balance will be used here to obtain an estimate of G_1 as given in eq. (A11). The flux ϕ_{nm} transferred from region n to region m can be obtained from evaluating an expression of the following form:

$$\phi_{nm} = \iint \frac{L_n \cos\theta_n \cos\theta_m \, dA_n \, dA_m}{D^2} \tag{E2}$$

where L_n is the radiance leaving dA_n, dA_i is an element of area on surface i, (i = m or n), D is the length of the line connecting dA_n to dA_m, and θ_i is the angle between the connecting line and the normal to dA_i. In the present estimate, this expression will be approximated as:

$$\phi_{nm} = L_n V_{nm} \tag{E3}$$

where the quantities V_{nm} are given by

$$V_{nm} = \iint \frac{\cos\theta_n \cos\theta_m \, dA_n \, dA_m}{D^2} \tag{E4}$$

The assumption here is that L_n is uniform at some average value over the entire region n. Except for the case when regions n and m are both on the sphere and in clear view of each other, it is difficult to evaluate V_{nm} exactly. For the general purpose integrating sphere described in section III and pictured in figure 11, rough estimates were made of the areas A_n of each region and the non-zero V_{nm}. (A V_{nm} would be zero if no part of region m is visible from region n.) The areas A_n were first determined, and then approximate V_{nm} not involving area 6 were obtained from the geometry of the sphere and baffle. The sum of all the V_{nm} involving region n must be

$$\sum_{m=1}^{6} V_{nm} = \pi A_n \tag{E5}$$

From which V_{n6} is calculated as

$$V_{n6} = \pi A_n - \sum_{m=1}^{5} V_{nm} \ . \qquad \text{(E6)}$$

This, with the fact that $V_{nm} = V_{mn}$, assures that the set of V_{nm} and A_n are consistent, even if only approximate. These values are presented below with the numbering of the regions the same as described in the first paragraph of part 3 in appendix A and as illustrated in figure 11.

A_n (cm^2)

$A_1 = 20.3$	$A_4 = 3.9$
$A_2 = 299$	$A_5 = 3.5$
$A_3 = 3.9$	$A_6 = 2350$

V_{nm} (cm^2 - steradian)

$V_{12} = 7.1$	$V_{26} = 821$
$V_{13} = 0.28$	$V_{36} = 6.7$
$V_{16} = 56$	$V_{45} = .55$
$V_{22} = 105$	$V_{46} = 12$
$V_{23} = 5.3$	$V_{55} = 0.014$
$V_{25} = 0.7$	$V_{56} = 9.6$

Figure 12 is a schematic illustration of the radiation transfer in the sphere. If the radiation is considered to be detected once it reaches the "common ground", region 6, then the fact that it is afterwards reflected and re-reflected need not be considered further and flux balancing equations can be set up which deal with only the photons which have never reached region 6. If L_{xn} is the radiance L_n leaving the surface of region n when the sample x is irradiated by the incoming beam, the following set of flux balance equations can be set up with the aid of figure 12.

$$\pi A_1 L_{x1} = \phi_1 \rho_x + (V_{12} L_{x2} + V_{13} L_{x3})\ \rho_x' \qquad \text{(E7)}$$

$$\pi A_2 L_{x2} = (V_{12} L_{x1} + V_{22} L_{x2} + V_{23} L_{x3} + V_{25} L_{x5})\ \rho_w \qquad \text{(E8)}$$

$$\pi A_3 L_{x3} = (V_{13} L_{x1} + V_{23} L_{x2})\ \rho_w \qquad \text{(E9)}$$

$$\pi A_4 L_{x4} = (V_{45} L_{x5})\ \rho_w \qquad \text{(E10)}$$

$$\pi A_5 L_{x5} = (V_{25} L_{x2} + V_{45} L_{x4} + V_{55} L_{x5})\ \rho_w \qquad \text{(E11)}$$

Using the A_n and the V_{nm} from the foregoing list, the radiances L_{xn} can be determined by simultaneous solution of these equations in terms of ϕ_1 ρ_x ρ_x' and ρ_w. From these, the signal N_x corresponding to the sample beam can be calculated as:

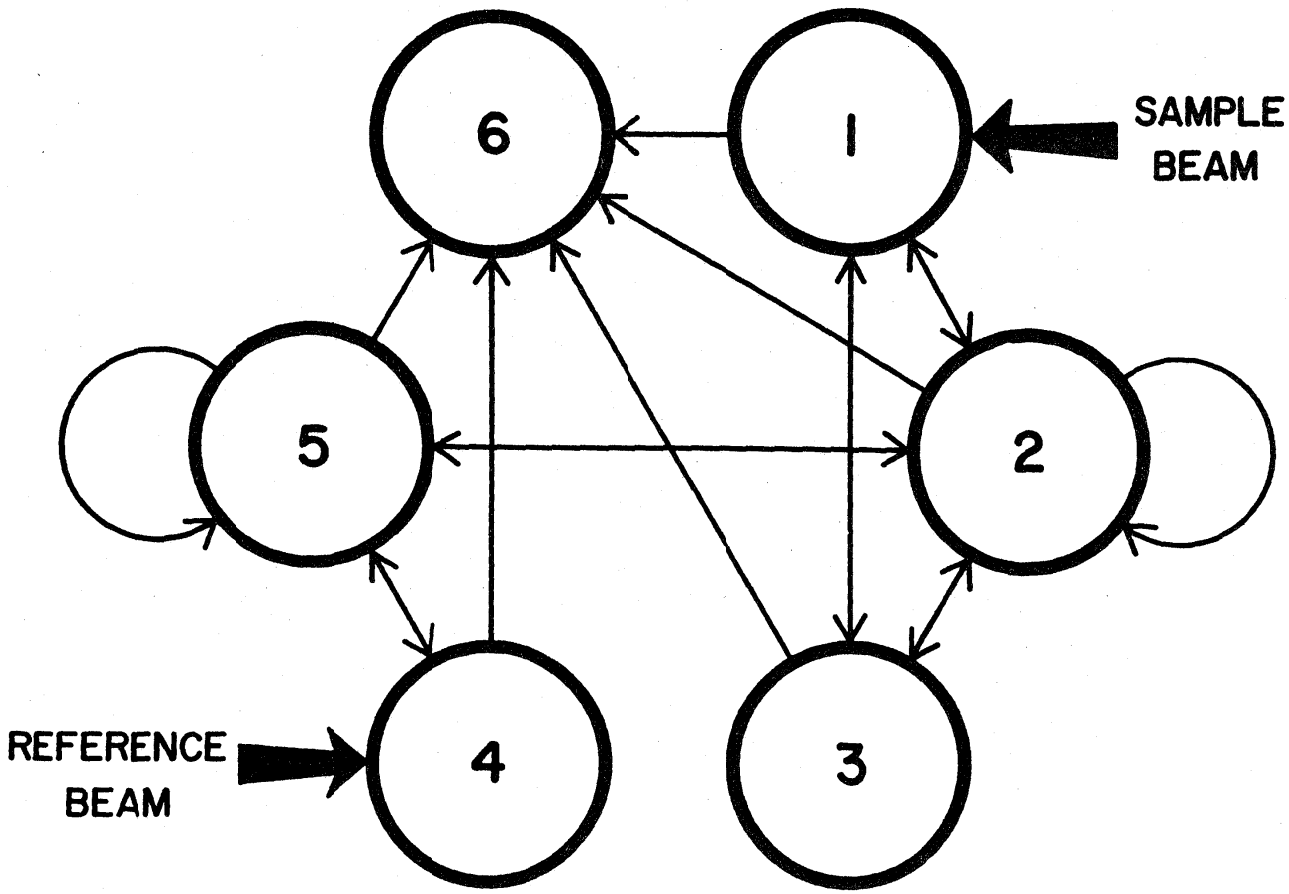

Figure 12. Schematic radiation transfer diagram for the sphere with baffle as shown in figure 11.

$$N_x = \eta_x \sum_{n=1}^{5} V_{n6} L_{xn} = \phi_1 \rho_x \eta_x (0.9989 + 0.0011\ \rho_x') \tag{E12}$$

where it has been assumed that $\rho_w = 1$. In a similar fashion the flux balance equations can be calculated for the case in which the incoming beam of radiation strikes region 4.

$$\pi A_1 L_{w1} = (V_{12} L_{w2} + V_{13} L_{w3})\ \rho_w' \tag{E13}$$

$$\pi A_2 L_{w2} = (V_{12} L_{w1} + V_{22} L_{w2} + V_{23} L_{w3} + V_{25} L_{w5})\ \rho_w \tag{E14}$$

$$\pi A_3 L_{w3} = (V_{13} L_{w1} + V_{23} L_{w2})\ \rho_w \tag{E15}$$

$$\pi A_4 L_{w4} = (\phi_2 + V_{45} L_{w5})\ \rho_w \tag{E16}$$

$$\pi A_5 L_{w5} = (V_{25} L_{w2} + V_{45} L_{w4} + V_{55} L_{w5})\ \rho_w \tag{E17}$$

From the L_{wn} determined by simultaneous solution of these equations, the signal N_w corresponding to the reference beam can be calculated as

$$N_w = \eta_x \sum_{n=1}^{5} V_{n6} L_{wn} = \phi_2 \rho_w \eta_x (0.99997 + 0.00003 \rho_x') \tag{E18}$$

where it has been assumed that after initial reflection $\rho_w = 1$. Comparing eqs. (E12) and (E18) with eqs. (A9) and (A10) respectively, it can be determined from eq. (A11) that

$$A_1 = .9989 \text{ and } G_1 = .0011 \tag{E19}$$

From the crudeness of the approximations used, this value for G_1 may be in error by as much as a factor of two.

APPENDIX F

Estimating Error Due to Angular Dependence of Response

The amount of error introduced by the entrance port and the painted ring around the sample port as discussed in section III.A.4.d depends upon the details of the specific scattering functions S_x and S_y of the samples x and y being compared. However, general cases can be treated in a way which will permit the magnitude of the errors introduced by the entrance port and the painted ring to be estimated. The scattering function S_x can be regarded as being the sum of two parts, S_{sx} which describes the Fresnel surface reflection and S_{bx} which describes the body reflection due to scattering which takes place beneath the surface. These two components are quite naturally distinguished in the case of polished surfaces, but the choice of the separate functions becomes more arbitrary in the case of samples with rough surfaces. However, even a rather arbitrary division can be useful, and no first order error will be introduced as long as

$$S_{bx} + S_{sx} = S_x \tag{F1}$$

1. Surface Reflection

The surface reflected component is not strongly chromatic but depends strongly on the texture of the surface. A function representative of the commonly occurring angular dependence of S_{sx} is:

$$S_{sx}(\vec{u}) = \rho_{sx} r(k) e^{-k\beta^2} \tag{F2}$$

where ρ_{sx} is the total surface reflectance at the given angle of incidence and β is the angle between the direction of emergence $\vec{u}$ and the direction of specular reflection which would occur if the sample were replaced by a plane mirror. The constant r(k) is a normalization constant which will be chosen so that

$$\int r(k) e^{-k\beta^2} \, d\omega = 1 \tag{F3}$$

when the integral is taken over the entire hemisphere. Since this is only a generalized model, since the angle of incidence is nearly normal, and since the response is polarization insensitive, it was felt to be unnecessary to include the details of polarization effects in the model for the purpose of estimating the measurement errors which are introduced by differences between S_{sx} for different samples. With this model for S_{sx}, the fraction of the total surface reflected radiation which is lost out the port can be calculated as

$$F_p(G_x) = \int_p S_{sx} \vec{u} \cdot a \, d\omega / \rho_{sx} \tag{F4}$$

where the integral is taken over the entrance port, and the fraction of the total surface reflected radiation which strikes the painted ring is

$$F_r(G_x) = \int_r S_{sx} \vec{u} \cdot a \, d\omega / \rho_{sx} \tag{F5}$$

where the integral is taken over the painted ring. The argument G is the percent of the total surface reflected flux which falls within a 11.7° by 4.4° rectangular solid angle centered on the specular direction. (The solid angle defining G is arbitrarily chosen the same as that in a glossmeter measuring ASTM 60° gloss [14]. Thus, for dark colored dielectric materials, G is approximately the ASTM 60° gloss [14].) $F_p(G)$ and $F_r(G)$ are

shown in figure 13. $F_r(G)$ is approximately the same for both of the spheres, but $F_p(G)$ differs markedly between the 0° and 6° incidence spheres. From the surface component of reflection, the contribution ε_{sp} to ε_p as defined in eq. (10) is

$$\varepsilon_{sp} = \frac{\rho_{sy}}{\rho_y} F_p(G_y) - \frac{\rho_{sx}}{\rho_x} F_p(G_x) \tag{F6}$$

From the surface component of reflection, the contribution ε_{sr} to ε_r as defined in eq. (11) is

$$\varepsilon_{sr} = 0.15 \left[\frac{\rho_{sy}}{\rho_y} F_r(G_y) - \frac{\rho_{sx}}{\rho_x} F_r(G_x) \right] \tag{F7}$$

To obtain an estimate of the magnitude of errors which can result, the case in which $\rho_y < \rho_x$ will be considered. With non-metallic materials for which $\rho_{sy} \simeq \rho_{sx} \simeq .05$, it follows that the maximum possible ε_{sr} is $1.3 \times 10^{-4}/\rho_y$, which would occur when y was perfectly diffuse ($G_y = 0.49$) and $G_x > 1$. For the 6° incidence sphere, the largest possible value of ε_{sp} is $2 \times 10^{-3}/\rho_y$ which would occur when a low gloss sample y for which $G_y \simeq 10$ is being compared to a higher gloss sample $x(G_x > 60)$. In either case, when ρ_y is reasonably large, a correction based on using measured gloss values for G_x and G_y would reduce the errors to insignificance. On the other hand, ε_{sp} can be as great as $5 \times 10^{-2}/\rho_y$ for the 0° incidence sphere, and the uncertainty in ε_{sp} per gloss unit is approximately $5 \times 10^{-4}/\rho_y$. For this reason the 0° incidence sphere will generally be restricted to use with samples with flat highly polished surfaces ($G > 95$). Since the F_p curves are almost the same for both the 0° and 6° incidence spheres only for $G < 2$, a very matte sample will be used to calibrate the 0° sphere measurements using a standard which has been evaluated on the 6° sphere, or a very high gloss standard ($G > 95$) for which the surface reflectance ρ_s is known will be used.

As a final observation on the effects of the distribution of the surface reflected flux upon measurements, a curve is shown in figure 13 giving the fractional error in measuring ρ_s using a 0°/45° bidirectional reflectometer. As long as $G > 5$, the fractional error in measuring ρ_s is -1, i.e. the surface component of reflection is effectively excluded from all measurements of samples having $G > 5$. Relative measurements of the reflectance of such samples can be made in this mode with negligible effects due to surface reflection. However, this mode of measurement will not be used with samples in the transition range $5 > G > 1$, and it should not be used for dark colored samples when $G < 5$.

2. Body Reflection

A second contribution to ε_p and ε_r is due to differences between the body component of the reflection of samples x and y. For normal incidence, the generalized scattering function S_{bx} can be described as:

$$S_{bx}(\gamma) = \sum_{i=0}^{\infty} a_{ix} Z_i(\gamma) \tag{F8}$$

where the $Z_i(\gamma)$ are a complete orthonormal set of functions such that

$$\int Z_j(\gamma)\, Z_i(\gamma) \cos\gamma \sin\gamma \, d\gamma = \begin{cases} 0; & i \neq j \\ 1; & i = j \end{cases} \tag{F9}$$

and γ is the angle of emergence measured from the normal to the sample surface. Such a set can be written in terms of functions resembling spherical harmonics in 2γ, and since most of the detailed structure of the total radiance distribution can be attributed to surface reflectance, the angular variation of the body reflection can be represented in most cases by the first three terms of eq. (F8) where

$$Z_0(\gamma) = \sqrt{1/\pi} \tag{F10}$$

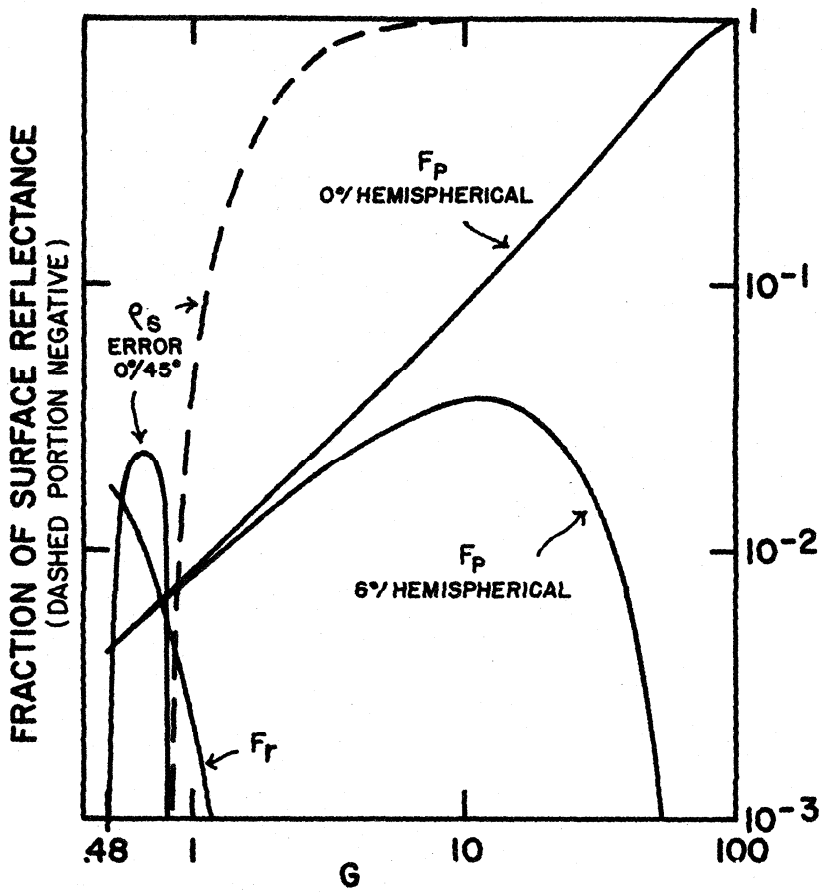

Figure 13. Data to be used in calculating errors due to differences in distributions of surface reflected radiation as described in appendix F.

$$Z_1(\gamma) = \sqrt{3/\pi}\,\cos 2\gamma \tag{F11}$$

$$Z_2(\gamma) = \sqrt{5/4\pi}\,(3\cos^2(2\gamma) - 1) \tag{F12}$$

With the entrance port subtending 0.013 sr at $\gamma \simeq 0$, one obtains ε_{bp}, the body reflection portion of ε_p, from eq. (10) as

$$\varepsilon_{bp} = 1.3 \times 10^{-2}\left[\sqrt{\frac{3}{\pi}}\left(\frac{a_{1y}}{\rho_y} - \frac{a_{1x}}{\rho_x}\right) + \sqrt{\frac{5}{\pi}}\left(\frac{a_{2y}}{\rho_y} - \frac{a_{2x}}{\rho_x}\right)\right]$$

with the painted ring of reflectance 0.85 subtending 0.055 sr at $\gamma \simeq \pi/2$, one obtains ε_{br}, the body reflection part of ε_r, from eq. (11) as

$$\varepsilon_{br} = -8.3 \times 10^{-3}\left[\sqrt{\frac{3}{\pi}}\left(\frac{a_{1y}}{\rho_y} - \frac{a_{1x}}{\rho_x}\right) - \sqrt{\frac{5}{\pi}}\left(\frac{a_{2y}}{\rho_y} - \frac{a_{2x}}{\rho_x}\right)\right]$$

The magnitude of these contributions depend upon a_{1x}, a_{2x}, a_{1y} and a_{2y}, which can be determined from bidirectional reflectance measurements made at the angles of viewing at which $Z_1(\gamma)$ and $Z_2(\gamma)$ go to zero. If reflecting surfaces x and y have the same goniometric distribution of reflected radiation,

$$\frac{a_{1x}}{\rho_x} = \frac{a_{1y}}{\rho_y} \quad \text{and} \quad \frac{a_{2x}}{\rho_x} = \frac{a_{2y}}{\rho_y}$$

and that both ε_{bp} and ε_{br} will be zero. One rather common occurrence in highly absorbing diffuse reflectors is for the body reflected radiation to be concentrated toward the surface normal, thereby resulting in a relatively large positive $Z_1(\gamma)$ component. Although ε_{bp} and ε_{br} tend to cancel under these circumstances, the cancellation is not complete and such measurements must be treated with special caution.

APPENDIX G

Focusing the Exit Slit Optics

Because the width (up to 3 mm) of the exit slit is significant compared to the focal length (178 mm) of the off-axis parabolic mirror in the exit slit optics, it is not practical to collimate the exit beam in the usual sense in which the exit slit is placed at the focus of the off-axis parabolic mirror. If this were done, the beam of radiation would diverge strongly, nearly doubling in its dimensions in going from the off-axis parabolic mirror to the experiment location. Instead, an image of the exit slit is formed at such a distance that the dimensions of the image and the dimensions of the illuminated area of the off-axis parabolic mirror are approximately the same. A simplified schematic optical diagram of this arrangement is shown in figure 14, where, for clarity the off-axis parabolic mirror is represented schematically as a lens and the beam-deflecting plane mirrors have been omitted. It can be seen from the figure that over the entire distance D, the radiation is confined to approximately a constant cross section, although the distribution of the radiation across the cross section differs at different locations along this path. With the instrument set for a 10 nm half-height bandpass (1.5 mm slit width) and adjusted for the conditions shown in figure 14, the distance D is approximately 1.4 meters and the distance d is approximately .4 meters.

The plane P in which the image of the monochromator exit mirror lies is of particular interest. At this location, the beam cross section is sharply defined and, in the ideal case of perfect optics, the spectral irradiance is independent of location within the cross section. At the location of the image of the exit slit, the spectral irradiance distribution is shifted by one half-height bandwidth from one side of the exit slit image to the other. For most of the experiments which are conducted with this instrument, it would be ideal if the sample could be located in plane P. However, because of the size of the accessory apparatus, in most of the measurements the sample is located at or just a little beyond the image of the exit slit. For this reason, when a sample is measured for which the uniformity of the spectral reflectance across the surface is suspect, the sample will be measured, rotated 180°, and remeasured in order to ascertain the effect of the coupling between the shift in spectral irradiance distribution across the beam and the non-uniformity in sample reflectance across the beam.

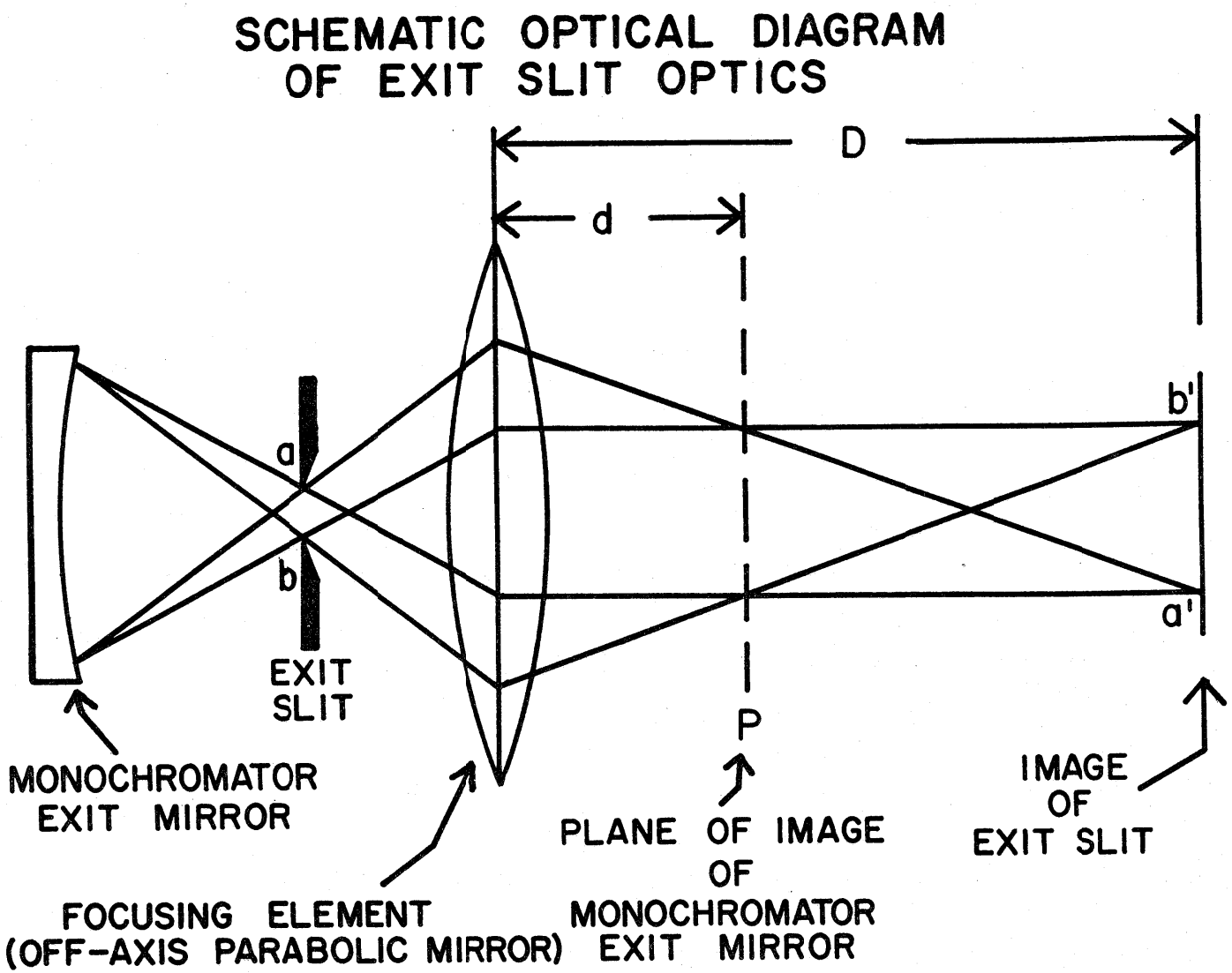

Figure 14. Schematic optical diagram of exit slit optics.

V. REFERENCES

1. Certain commercial materials are identified in this Technical Note in order to specify adequately the procedure. In no case does such identification imply endorsement or evaluation by the National Bureau of Standards.

2. Popenoe, C.H. and Campbell, M.C., "MIDAS Modular Interactive Data Acquisition System — Description and Specification", NBS Tech. Note No. 790 (August 1973).

3. Tests performed by Dr. John M. Jerke, Optics and Micrometrology Section, Optical Physics Division, National Bureau of Standards.

4. Mielenz, K.D. and Eckerle, K.L., "Design, Construction, and Testing of a New High Accuracy Spectrophotometer", NBS Tech. Note No. 729 (June 1972).

5. Keegan, H.J. and Gibson, K.S., "On the Use of Working Standards of Didymium and Vitrolite Glasses for Spectrophotometric Measurements", J. Opt. Soc. Am. 34 (12), 770 (1944).

6. Keegan, H.J., Schleter, J.C., and Judd, D.B., "Glass Filters for Checking Performance of Spectrophotometer — Integrator System of Color Measurement", J. Res. NBS. 66A (3), 203 (June 1962).

7. Eckerle, K.L., Venable, W.H., Jr., and Weidner, V.R., "Averaging Sphere for Ultraviolet, Visible, and Near Infrared Wavelengths: A Highly Effective Design:, Appl. Opt. 15 (3), 703 (March 1976).

8. Grum, F. and Saltzman, M., "New White Standard of Reflectance", presented at the 18th session of CIE, London, England in September 1975.

9. Venable, William H., Jr., and Hsia, Jack J., "Optical Radiation Measurements: Describing Spectrophotometric Measurements", NBS Tech. Note No. 594-9 (November 1974).

10. Mielenz, K.D. and Eckerle, K.L., "Spectrophotometer Linearity Testing Using the Double-Aperture Method", Appl. Opt. 11 (10), 2294 (1972).

11. Goebel, D.G., Caldwell, B.P., Hammond, H.K. III, "Use of an Auxiliary Sphere with a Spectroreflectometer to Obtain Absolute Reflectance", J. Opt. Soc. Am. 56 (6), 783 (June 1966).

12. Van den Akker, J.A., Dearth, L.R., and Shillcox, W.M., "Evaluation of Absolute Reflectance for Standardization Purposes", J. Opt. Soc. Am. 56 (2), 250 (February 1966).

13. Jacquez, J.A. and Kuppenheim, H.F., "Theory of the Integrating Sphere", J. Opt. Soc. Am. 45 (6), 460 (1955).

14. ASTM Designation: D523-67(1972), Standard Method of Test for Specular Gloss, Annual Book of ASTM Standards Part 27 (1974).

APPENDIX C

Reprinted from **Applied Optics,** Vol. 19, page 1268, April, 1980
Copyright © 1980 by the Optical Society of America and reprinted by permission of the copyright owner.

NBS specular reflectometer–spectrophotometer

Victor R. Weidner and Jack J. Hsia

A specular reflectometer has been constructed and tested for calibrating the reflectance of mirror standards over the 250–2500-nm spectral range. This instrument is a measurement accessory to a reference spectrophotometer, which is also used for diffuse hemispherical spectral reflectance and 45°/0° spectral reflectance. The specular reflectometer is designed to measure mirror reflectances at angles of incidence between 5 and 80° using both vertically and horizontally polarized radiation. Absolute reflectance measurements are obtained by an optical system, which provides for direct measurement of the incident beam and for the sample mirror reflectance using the same beam. This is accomplished by means of a beam tracking system through which the beam is directed into a signal averaging sphere. The sphere rotates with the beam tracking optics, and the stationary detector views the interior of the sphere. Control of the beam tracking optical system is accomplished by a computer-controlled stepping-motor-driven precision turntable. Uncertainties of the reflectance measurements obtained with this system are estimated to be ±0.2% of the measured value.

I. Introduction

The increasing requirements for standard specular reflectors, such as mirrors for reference measurements in activities associated with the solar energy utilization program, have also increased the need for instrumentation development to provide the required standard mirrors. The spectrophotometry group of the Radiometric Physics Division at NBS has developed a specular reflectometer for this purpose. It is designed to measure the specular reflectance of mirrors over the 250–2500-nm wavelength range. The instrument can be used to measure the specular reflectance of mirrors at angles of incidence between ~5 and 80°. The spectrophotometer provides a collimated beam, which can be polarized in either the vertical or horizontal plane. The spectral bandpass is usually set at 5 or 10 nm.

The specular reflectometer will be used primarily to calibrate mirrors for the NBS Standard Reference Materials program. Several types of mirrors will be available through the NBS Office of Standard Reference Materials when work is completed on the calibration of several master standards, and this reflectance scale can be transferred to the SRM mirrors. The mirrors being prepared for calibration include (a) glass substrates with either aluminum or rhodium front-surface coatings and (b) second-surface aluminum coatings sealed between quartz. A portion of this mirror preparation and calibration work is funded by the Department of Energy.

Calibrating a mirror for specular reflectance as a function of wavelength, polarization, and angle of incidence requires many individual measurements. These calibrations are impractical without automation. As an example, measurement of the specular reflectance of a single mirror at fifty wavelengths, for five angles of incidence and two polarizations requires 500 determinations. Moreover, this number is doubled if the angle of incidence is measured to both the left and right of the normal and then averaged. Since at each angle of incidence three measurements are made and other calibration data also have to be recorded, the total number of data may reach 13,000 individual numbers to be accumulated and processed. Even with automation it would be time-consuming and expensive to calibrate many mirrors at this many wavelengths and angles of incidence. For this reason most mirrors are calibrated at near normal incidence for 50- or 100-nm intervals and at only a few wavelengths for other angles of incidence.

II. NBS Reference Spectrophotometer

The specular reflectometer is an accessory to the NBS reference spectrophotometer for reflectance.[1] The monochromator, light source, and associated equipment are located in a system control room. The exit-slit housing of the monochromator is attached to a light-tight diaphragm in a wall, which allows the exit beam

The authors are with U.S. National Bureau of Standards, Washington, D.C. 20234.
Received 29 October 1979.

or sample beam to enter a second room where the various reflectance-measuring devices, such as integrating spheres or the specular reflectometer, are installed. The advantages of this arrangement are that the second room can be used as an experimental dark chamber, while the electronics, light sources, and control systems are isolated from the experimental area. The sample beam emerging from the exit slit of the monochromator can be controlled to provide a spectral bandpass of 2, 5, 10, or 20 nm. The beamwidth is determined by the selected bandpass. For a 10-nm bandpass, the beam is ~12 × 18 mm at the sample plane.

To measure spectral reflectance over the full wavelength range of the monochromator, the system employs a xenon source for measurements in the UV spectrum, a tungsten strip lamp for the visible spectrum, and a tungsten IR source for the IR spectrum. A photomultiplier detector is used for the UV and visible spectrum and a lead sulfide detector for the IR spectrum. A complete description of the spectrophotometer is given in an earlier publication,[1] with the exception of the IR detection and signal-processing system, which was completed at a later date.

III. Construction of the Specular Reflectometer

The concept around which the specular reflectometer is designed allows for detecting the incident beam either directly or after it is reflected from a mirror sample at some selected wavelength and angle of incidence. To accomplish this it is necessary to employ two turntables—one for positioning the sample mirror at a desired angle of incidence with respect to the sample beam and another for directing the reflected sample beam to reach the detector. The instrument is illustrated in Figs. 1–3. It is undesirable to irradiate the detector directly with the beam to be measured because the detector area lacks the necessary uniformity of sensitivity required for a system involving the movement of optical elements that direct the beam to the detector. Therefore, reproducibility of the measurements is not adequate for high-accuracy determinations. Since photomultiplier detectors tend to be affected by magnetic fields, which vary from one location to another, the instrument was designed with the detector located in a fixed position.

To overcome the problems of detector nonuniformity, the specular reflectometer is designed so that the sample beam enters a 15-cm diam averaging sphere; output variations caused by nonuniformity of the beam or by nonuniformity of the detector sensitivity to this beam are effectively reduced when the beam is first diffusely mixed by multiple reflections within the averaging sphere. The sphere coating is a fluorocarbon powder, which is a nearly perfect diffuser of very high reflectivity throughout the 250–2500-nm spectral range. The detector views the interior of the averaging sphere and is irradiated by the diffused flux. The incoming sample beam is incident on the sphere wall at a location outside the field of view of the detector to avoid direct viewing of this bright spot on first reflection.

The problem of magnetic fields affecting the detector performance required a design for the reflectometer that would keep the detector in a fixed position for all measurements regardless of the angle of incidence selected for the specular-reflectance measurements. To do this a mirror was attached to an arm suspended from a turntable located above the sample turntable. This mirror, referred to as the tracking mirror, can orbit the sample, intercepting the reflected sample beam at any angle of reflectance (= angle of incidence) between ~5 and 80°. The tracking mirror also intercepts the direct beam when the sample mirror is moved out of the beam by the slider on which it is mounted.

The tracking mirror is tilted upward at an angle of 20° with respect to the incident beam and reflects the beam up through a baffle tube and into the averaging sphere, which rotates with the tracking mirror and baffle tube. The axis of rotation of the averaging sphere is collinear with the axis of rotation of the sample turntable. The detector is mounted on a stationary platform above the averaging sphere and does not rotate with the sphere. A diaphragm allows the top of the sphere to rotate just below the detector aperture and maintains a radiation seal between the stationary and rotating parts. A 51-mm diam port on the top of the sphere allows the signal to pass into the detector. A shutter between the sphere and the detector can be opened or closed automatically or as required.

The baffle tube is attached to the averaging sphere and extends from the 32-mm diam entrance aperture of the sphere to near the 51-mm diam tracking mirror. The baffle tube limits the field of view of the averaging-sphere entrance aperture to the direction of the tracking mirror. The entrance aperture to the sphere is the limiting aperture in the optical system.

The tracking mirror orbits the sample at a radius of 25 cm. The axis of rotation of the sample and the axis of rotation of the tracking mirror must be collinear if the tracking mirror is to intercept accurately the reflected beam at all angles of incidence and reflection and redirect the beam into the averaging sphere.

The sample-mirror turntable and tracking-mirror turntable are driven by identical 240-tooth precision worm gears. Two hundred steps are required to turn the stepping-motor drive shaft through 360°. This translates through the worm gear into 48,000 steps to rotate the turntables 360°. The angular resolution for the turntable rotation is ~27 sec of arc/step of the stepping motor. The problem of backlash in the gear drive is avoided by always approaching the desired position from the same direction. This is done through the computer routines that control the direction of movement in approaching the desired angular settings for specular-reflectance measurements.

The IR measurements required the addition of a chopper at the light source, a preamplifier for the lead sulfide detector, and a lock-in amplifier that locks in the chopped signal and provides a suitable input to the data processing electronics. Figure 4 is a schematic diagram of the IR-system electronics and the signal-generation and detection system.

The signal processing of the output from the detector utilizes a current-to-frequency converter that can in-

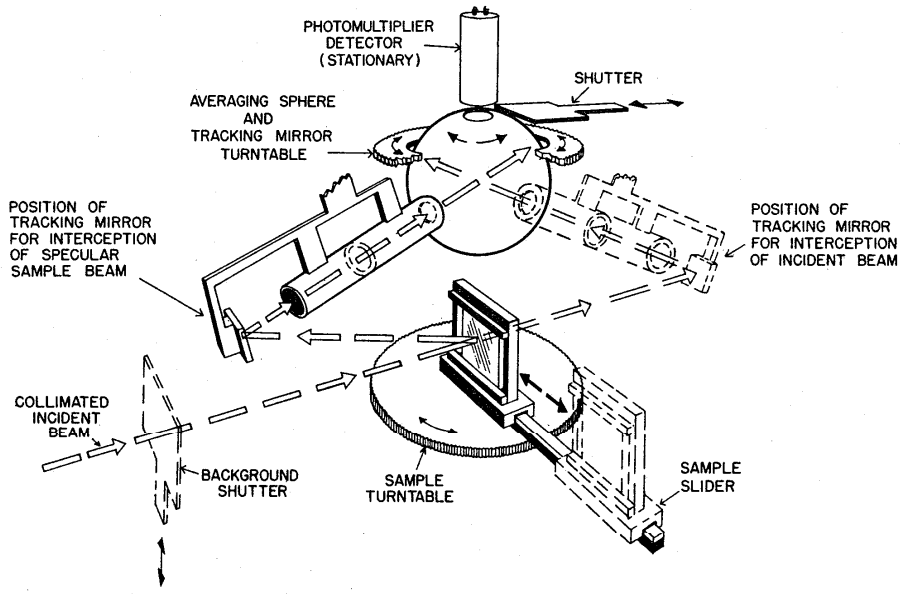

Fig. 1. General scheme of the NBS specular reflectometer showing the relationship of the sample turntable and beam-tracking turntable and detector systems.

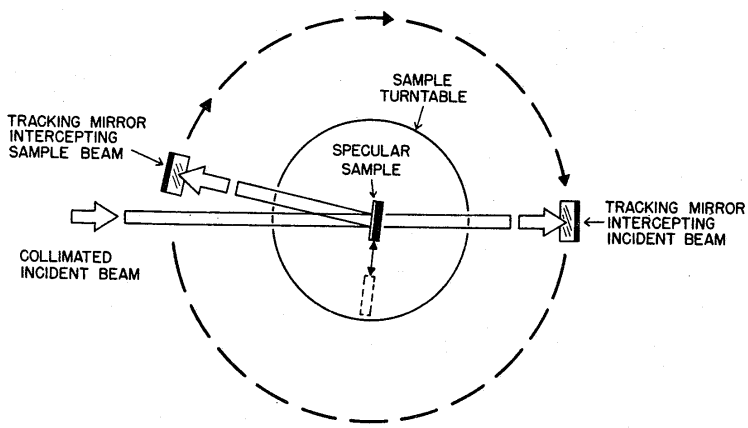

Fig. 2. Horizontal x section through the plane of the sample beam, specular sample, and the tracking mirror that orbits the sample.

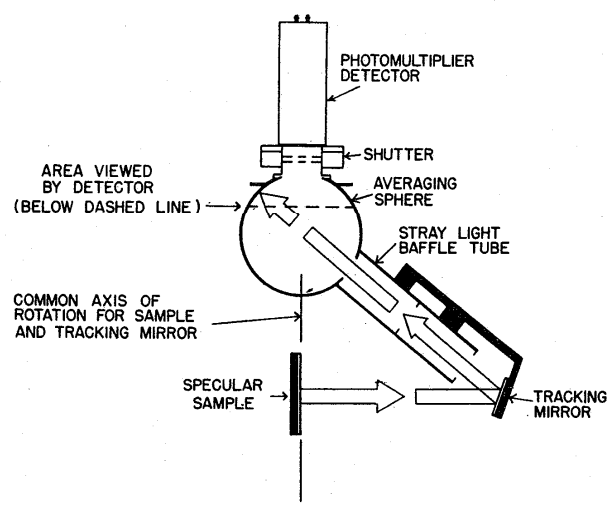

Fig. 3. A vertical x section through the plane of the sample beam, specular sample, tracking mirror, averaging sphere, and detector.

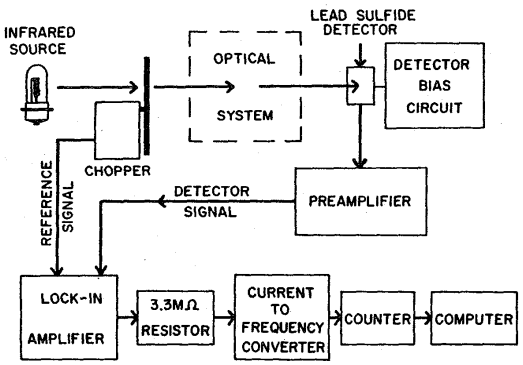

Fig. 4. Schematic of the IR signal processing system for the NBS specular reflectometer–spectrophotometer system.

tegrate the detector output over a selected time interval. The integration time may be as short as 1 sec or as long as 9 sec. This integrated signal is accumulated on a digital counter. The digital results in the counter are transferred to a computer for analysis. The results of the computer analysis are stored for future reference and printed out on a teletype printer.

IV. Alignment of the Reflectometer

Alignment of the specular reflectometer involves the spatial relationship of three basic elements in the system. These are the sample beam, the sample, and the tracking mirror. The sample beam is initially adjusted so that it is in a horizontal plane and passes over the sample turntable with the axis of rotation bisecting the beam. The reflectometer is mounted on a lift table for convenience in selecting the desired vertical position for the instrument. This lift table rides on bearings so that the instrument can be moved into or out of the sample beam at right angles to the beam. When these vertical and horizontal adjustments are correct for the relationship of the sample turntable with respect to the sample beam the system is locked to prevent further movement.

The upper portion of the specular reflectometer, consisting of the tracking-mirror turntable and the stationary detector platform, is independent of the sample turntable. This assembly is supported by three columns located at 120° intervals with respect to the axis of rotation of the turntables. Each of these columns is designed to provide a kinematic alignment of the detector and tracking-mirror assembly. The three legs of the tracking-mirror turntable assembly rest on the kinematic supports at the top of the three columns. The legs are fitted with steel-ball-tipped feet that fit into the kinematic supports consisting of a flat for one ball tip, a V-groove for the second ball tip, and a conical cavity for the third. The ball tips of the legs are on finely threaded bolts that screw into the legs and provide a means for adjusting the height and leveling the tracking mirror to the plane of the incident beam and sample mirror.

The alignment procedure involves a number of adjustments of the sample mirror and tracking mirror. These procedures involve a number of mechanical fixtures and optical techniques that will not be described in detail. As a final check of the overall alignment of the reflectometer system, the baffle tube is temporarily removed from the tracking mirror arm, and the sample turntable and tracking mirror turntable are programmed to move to several angles of incidence and interception, respectively. At these locations the sample beam must pass through the center of the entrance aperture to the averaging sphere. If this condition is not satisfactorily arrived at, the alignment procedures are rechecked and refined until they meet the required conditions.

A laser is used to monitor the system alignment for possible trouble during continued lengthy measurements in which the system is being driven by computer-controlled stepping motors. The laser is fixed to a stationary pier. The laser beam reflects off the sample mirror and strikes a target scale, which is used to initiate a measurement cycle. At the end of each measurement cycle the turntables return to this position if the stepping motors and computer have not malfunctioned and no mechanical misalignment has occurred. This laser alignment-checking procedure is especially useful when the measurements of specular reflectance are being made at wavelengths where the sample beam cannot be visually observed. However, the initial alignment is usually made with a sample-beam wavelength of 550 nm. Should a computer malfunction occur while working at IR or UV wavelengths, the laser is turned on, and the turntables are manually reset to the starting angles. Any large malfunction involving the positioning of the turntables is usually readily detected because the sample beam under these conditions ordinarily misses the detector system completely, a condition easily recognized in the data output. The laser alignment check alerts the operator to small misalignment problems that might not be apparent in the data output. The laser is used primarily to check the sample-turntable alignment. The tracking-mirror starting point can be accurately set by a scale mark on the 60-cm diam track and a similar scale mark on the tracking-mirror holder, which moves around this track. This initial sample-turntable position must be established by optical techniques to achieve the required accuracy in programming the angles of incidence for specular-reflectance measurements.

V. Measuring Specular Reflectance

Measurements of specular reflectance on the NBS specular reflectometer involve the following series of measurements repeated for each selected wavelength, polarization, and angle of incidence: B, S_1, S_2, S_1, B, S_1, S_2, S_1, B, S_1, S_2, S_1, B, where B is the background signal, S_1 is the measured signal of the incident beam, and S_2 is the measured signal of the beam after reflection from the sample mirror. The average B, average S_1, and average S_2 are used in the data reduction. The background is subtracted from S_1 and S_2. A correction

is also made for those effects associated with the rotation of the averaging sphere as determined in the β-light mapping procedure, which will be described in a later section.

The sample mirror reflectance R is calculated as $R = S_2/S_1$. The average value of specular reflectance for the vertically and horizontally polarized incident beam is usually reported. The usual practice is to determine the specular reflectance of a mirror at a specified angle of incidence by measuring the reflectance with the plane of the mirror rotated to the left with respect to the incident beam and again for the same angle of incidence with the mirror plane rotated to the right. These two determinations are then averaged. The specular reflectometer is programmed to perform these measurements, and the data are processed at the completion of each measurement cycle. A complete measurement cycle includes the specified wavelength and angles of incidence.

VI. Performance

It is beyond the intent of this paper to describe in detail the various checks that were made on the performance of the monochromator and other components of the spectrophotometer, except to mention briefly the magnitudes of errors associated with this portion of the system, since they do influence the accuracy of measurements of specular reflectance. Information regarding some of these investigations is presented in Ref. 1.

Involved in checking the performance of the instrument are wavelength scale uncertainties, stray light levels, detector linearity, and variations in detector response associated with movement of the specular reflectometer optical components.

The wavelength scale of the monochromator is periodically checked by measuring the emission lines of several line-source lamps, the transmission of a didymium glass wavelength standard, polystyrene absorption bands, and the absorption bands of 1-2-4 trichlorobenzene.[2] Uncertainty in the wavelength scale is 1 nm or less. Corrections for these errors are made by adjustment of the wavelength-scale setting to compensate for differences between the wavelength counter and the true wavelength.

The recent extension of the instrument to cover the IR spectral range to 2.5 μm involved checking for stray light in this spectral range. The amount of information on stray radiation in the IR range is limited somewhat by the lack of suitable filters for this purpose in the 2–2.5-μm wavelength range. Several IR cutoff selenium glass filters, silicon filters, and chloroform were used to check for stray radiation in the 0.8–1.7-μm wavelength range.[3] The selenium glass filters have sharp cutoffs between 0.7 and 0.9 μm, and the silicon filter cuts off at $\sim$1.0 μm. The filters block the UV and visible wavelengths and transmit the IR. The chloroform absorbs strongly[3] at 1.69 μm. The stray radiation levels for the wavelengths checked with these filters were found to be less than 0.1%. This is below the signal level for an optical density of 3, which is about as low a level as can be measured with a lead sulfide detector of the type used for these measurements.

The linearity of the lead sulfide detector was measured by the light addition method with a double aperture apparatus.[4] The results of these linearity measurements indicate that the detector is linear to better than $\pm$0.1% at all photometric levels between 10 and 100%, which is the photometric range of interest for most of the reflectance measurements of mirrors.

Radiation scattered off the optical components such as mirrors between the exit slit of the monochromator and the limiting aperture of the detector system is undesirable in a specular reflectometer. The room containing the reflectometer is lined with a black felt material to absorb scattered radiation. The level of scattered radiation in this room is low enough to be undetectable above the dark current signal of the detector with the sample beam trapped by the background shutter at the exit slit of the monochromator. Since the baffle tube limits the field of view of the limiting aperture to the area of the tracking mirror, very little scattered radiation can enter the averaging sphere. Most of the scattered radiation is associated with the scattering in the optical path of the sample beam. It is important that all the mirrors in this system be kept reasonably clean and free of dust.

One problem associated with a measurement of reflectance in which optical components are moved between the source and the detector to change the incidence and viewing angles is that of determining the magnitude of errors introduced by these movements. In this system the number of components that require movement has been reduced to the beam-tracking mirror and the averaging sphere. The detector remains stationary and views the interior of the sphere through a 51-mm diam port, which rotates with minimum translation in the field of view of the detector. The flux received by the detector is diffuse in nature since the interior of the sphere is a nearly perfect diffuser. To test the sensitivity of the detector response to changes in the angular positioning of the beam-tracking mirror, a β light was attached to the baffle tube entrance. The β light is radioactive tritium gas, which emits visible light when the β radiation excites a phosphorous target. This stable light source is also enclosed in a magnetic shield. Light from this source illuminates the averaging sphere at the other end of the baffle tube. Variations in the intensity of the signal from the β light as the tracking system turntable rotates may then be attributed to some change in the signal intensity at the detector, which is related to the turning of the averaging sphere and not to the instability of the light source. The maximum variation in signal intensity observed by this technique was $\sim\pm$0.2%. It was thought that this variation might be caused by the fact that the entrance port of the averaging sphere, which appears as a black spot in the detector field of view, is changing position as the averaging sphere rotates. However, when a white

baffle was installed in the sphere to prevent the detector from seeing this black spot, the variation in signal intensity for the β light test still existed and was actually larger than that observed without the baffle. The variation in signal intensity can be mapped as a function of the turntable position with respect to the incident beam, and corrections can be derived for this error. The β light mapping check is a regular part of the calibration procedure.

An analysis of the various sources of error that may be expected to affect the accuracy of specular reflectance measurements on the NBS specular reflectometer indicates that the final uncertainty in these measurements will be on the order of ±0.2% of the measured value.

VII. Summary

A specular reflectometer spectrophotometer was constructed for calibrating the reflectance of mirrors over the 250–2500-nm spectral range. The instrument is automated and computer controlled. The measurements are made as a function of wavelength and angle of incidence with a polarized light beam. The system performance was examined for such parameters as stray radiation levels, detector linearity, wavelength scale uncertainties, and spatial sensitivity of the detector system. Uncertainty in the measurements of specular reflectance will be on the order of ±0.2% of the measured value. The instrument will be used to provide calibrated mirrors, which will become available through the NBS Office of Standard Reference Materials.

The authors are indebted to William H. Venable, Jr., formerly of NBS and presently employed by Hunter Associates, Inc., for his contributions to the design and development of the specular reflectometer and reference spectrophotometer.

References

1. W. H. Venable, Jr., J. J. Hsia, and V. R. Weidner, Development of an NBS Reference Spectrophotometer for Diffuse Transmittance and Reflectance, Nat. Bur. Stand. Tech. Note U.S. 594-11 (October 1976).
2. E. K. Plyer and C. W. Peters, J. Res. Nat. Bur. Stand. **45**, 462 (December 1950).
3. W. Kaye, Appl. Opt. **14**, 1977 (1975).
4. K. D. Mielenz and K. L. Eckerle, Appl. Opt. **11**, 2294 (1972).

Metrologia 17, 97–102 (1981)

metrologia
© by Springer-Verlag 1981

NBS 45°/Normal Reflectometer for Absolute Reflectance Factors

Jack J. Hsia and Victor R. Weidner

National Bureau of Standards, Washington, DC 20234, USA

Received: March 25, 1981

Abstract

A 45°/normal reflectometer has been constructed and tested for calibrating the absolute reflectance factor of diffuse samples over the 380–770 nm spectral range using polarized radiation. The measurement equations have been derived for the method used. The method using a step-down technique and view factor calls for the measurements of the ratio of two fluxes and, in addition, some linear dimensions. The uniformity of the receiver system is achieved by means of a double-sphere signal averager. Uncertainties of the absolute-reflectance-factor measurements obtained with this system are estimated to be ±0.3% of the measured value. For all the samples that have been tested, the 45°/normal reflectance factor was found to be higher than the 6°/hemispherical reflectance factor. The higher reflectance values for 45°/normal geometry were confirmed by additional gonioreflectometer measurements.

1. Introduction

Measurements of the diffuse reflecting characteristics of materials are of basic importance in radiometry, photometry and colorimetry as well as many other fields of science, technology and industry.

The International Commission on Illumination (Commission Internationale de l'Eclairage – CIE) recommended that starting in 1969, in colorimetric measurements of opaque materials, the perfect diffuser was to be taken as the primary reference standard. There is no existing material having diffuse reflection properties corresponding to the perfect diffuser with sufficient approximation. Therefore, the characteristics of all physical standards actually employed in comparison measurements must be established by techniques through which their absolute reflectance factors can be determined. The measurements involve not only the determination of the ratio of radiometric quantities but also the determination of linear dimensions.

The four geometries recommended by the CIE are 45°/normal, normal/45°, diffuse/normal, and normal/diffuse. The method and instrumentation to realize the NBS scale of directional-hemispherical reflectance factor has been described in [1].

For the 45°/normal and normal/45° reflectance factor measurements, there exists a large ratio of the incident flux to the reflected flux contained in a small solid angle. Various step-down techniques have been used by several National Laboratories [2–8] to insure sufficient accuracy over this wide dynamic range.

The purpose of this paper is to describe the method and the instrumentation used to establish the NBS scale of absolute reflectance factor in the 45°/normal geometry.

2. Measurement Equations

An absolute reflectance factor is defined [9, 10] as the ratio of the radiant flux reflected in the directions bounded by a given cone with the apex at a point of the surface under test to that reflected in the same directions by a perfect reflecting diffuser identically irradiated. The term "perfect reflecting diffuser" means the ideal (lossless) lambertian (uniform in all directions) diffuser. If the solid angle of the cone approaches zero, or 2π steradians, the reflectance factor approaches radiance factor or reflectance, respectively.

The reflectance factor of sample x, R_x, can be expressed as

$$R_x = \frac{\int^S L(U,\lambda)\, S_x(U,u,\lambda)\, r(u,\lambda)\, U\cdot dA\, d\Omega u\cdot da\, d\omega\, d\lambda}{\int^S L(U,\lambda)\, S_{id}\, r(u,\lambda)\, U\cdot dA\, d\Omega\, u\cdot da\, d\omega\, d\lambda} \qquad (1)$$

where L is the incident radiance; S_x and S_{id} are the scattering functions of the sample and of the ideal surface, r is the relative responsivity of the receiver; U and u are the direction vectors of travel of the incident and emergent radiation; $d\Omega$ and $d\omega$ are elements of solid angle oriented in the direction U and u; dA and da are elements of area through which the energy passes on to the sample and emerges from the sample; $d\lambda$ is the element of wavelength; and the symbol $\int^n$ indicates inte-

0026-1394/81/0017/0097/$01.20

gration with respect to n variables. In general, the nomenclature (especially the symbols) used here is that of reference [11]. There it is more completely defined and discussed.

If there is no interaction between the wavelength dependence and the geometrical dependence of the incident radiance and of the responsivity, the functions are separable. For any source function $C(\lambda)$ and luminous efficiency function $V(\lambda)$, Eq. (1) can be written as

$$R_x = \frac{\int C(\lambda)\, V(\lambda)}{\int C(\lambda)\, V(\lambda)} \tag{2}$$

$$\frac{[\int^4 L(U)\, S_x(U,u,\lambda)\, r(u)\, U\cdot dA\, d\Omega\, u\cdot da\, d\omega]\, d\lambda}{[S_{id} \int^4 L(U)\, r(u)\, U\cdot dA\, d\Omega\, u\cdot da\, d\omega]\, d\lambda}$$

$$R_x = \frac{\int C(\lambda)\, V(\lambda)\, R_x(\lambda)\, d\lambda}{\int C(\lambda)\, V(\lambda)\, d\lambda} \tag{3}$$

The spectral reflectance factor $R_x(\lambda)$ is expressed as

$$R_x(\lambda) = \frac{\int^4 L(U)\, S_x(U,u,\lambda)\, r(u)\, U\cdot dA\, d\Omega\, u\cdot da\, d\omega}{S_{id} \int L(U)\, r(u)\, U\cdot dA\, d\Omega\, u\cdot da\, d\omega} \tag{4}$$

For a receiver system with uniform responsivity within the cone,

$$r(u) = r \text{ within } \omega \text{ and } r(u) = 0 \text{ outside of } \omega. \tag{5}$$

The scattering function of a perfect diffuser could be written as

$$S_{id} = \delta(P - p)/\pi \tag{6}$$

where P and p are position vectors on the testing surface for incident space and the emergent space, respectively.

Thus (4) can be expressed as

$$R_x(\lambda) = \frac{\pi}{\omega_p} \frac{\Phi_x(\lambda)}{\Phi_i(\lambda)} \tag{7}$$

where $\omega_p = \int^2 u\cdot da\, d\omega$ is the projected solid angle of the cone onto the surface to be measured.

$\Phi_x = \int^4 L(U)\, S_x(U,u,\lambda)\, U\cdot dA\, d\Omega\, u\cdot da\, d\omega$ is the reflected radiant flux for the sample that enters the limiting receiver aperture, and

$\Phi_i = \int^2 L(U)\, \delta(P - p)\, U\cdot dA\, d\Omega$ is the incident radiant flux.

In radiation heat transfer [12, 13], ω_p/π (or f_{1-2}) is named the view factor (alternatively designated as the form factor, configuration factor, geometrical factor, or angle factor) representing the fraction of the radiant flux leaving a diffuse surface that is entering the limiting aperture. In other words, f_{1-2} is the fraction of the incident flux reflected from (1) a perfect diffuser that is entering the (2) limiting aperture. The spectral reflectance factor can now be expressed as

$$R_x(\lambda) = \frac{1}{f_{1-2}} \frac{\Phi_x(\lambda)}{\Phi_i(\lambda)} \tag{8}$$

Equation (8) clearly indicates that the reflectance factor is the ratio of the reflected flux (into the limiting aperture) to that of a perfect diffuser. If another sample S with known reflectance is used to step down[1] the incident flux, the reflectance factor of sample x can be calculated as

$$R_x(\lambda) = \frac{1}{f_{1-2}} \frac{\Phi_x(\lambda)}{\Phi_S(\lambda)} \cdot \rho_S \tag{9}$$

where Φ_S and ρ_S are the flux and the reflectance of the step-down sample S, respectively. The view factor will be expressed in detail below.

For a circular limiting aperture (diameter D) which is parallel to the sample surface at a distance d, and for $\Delta A1$, a small portion of the illuminated area, and the distance between a point in $\Delta A1$ and the central normal (on the sample surface) to the circular area of the limiting aperture being c, (see Fig. 1) the view factor can be expressed [14] as:

$$f_{\Delta A1-A2} = [1 - J/K]/2, \tag{10}$$

where $J = 1 + G^2 - B^2$

$K = [G^4 + 2G^2(1 - B^2) + (1 + B^2)^2]^{1/2}$

$B = D/2d$

$G = c/d$

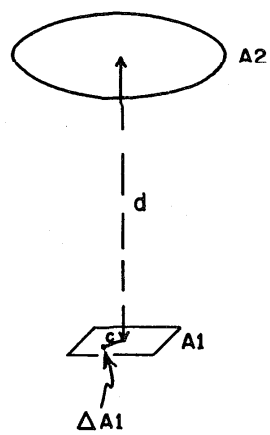

Fig. 1. Schematic for view factor (Eq. 10) Determination

When the illuminated area is very small and is at the central normal to the circular area of the limiting aperture, the view factor becomes

$$f_{1-2} = f_{\Delta A1-A2} = [1 + 4\, d^2/D^2]^{-1} \tag{11}$$

and when the illuminated area is finite, the view factor is

$$f_{1-2} = \frac{1}{A1} \int f_{\Delta A1-A2}\, dA1 \tag{12}$$

$$\text{or } f_{1-2} = \frac{\Delta A1}{A1} \sum_{A1} f_{\Delta A1-A2} \tag{13}$$

if $\Delta A1$ is selected to be sufficiently small.

[1] Procedure described in Sect. 5

3. NBS Reference Spectrophotometer

The 45°/normal reflectometer is an accessory to the NBS reference spectrophotometer for reflectance [15]. The light source, monochromator, electronics and other associated equipment are located in a system control room. The exit slit housing of the monochromator is attached to a light-tight diaphragm in a wall, which allows the exit light beam or sample beam to enter a second room where the various reflectance-measuring devices, such as the specular reflectometer or the 45°/normal reflectometer, are installed. The advantages of this arrangement are that the second room can be used as an experimental dark chamber, while the light source, electronics and control systems are isolated from the experimental area. The sample beam emerging from the exit slit of the monochromator can be controlled to provide a spectral bandpass of 2, 5, 10, or 20 nm. For a 10-nm bandpass, the light beam has a cross section 10 by 18 mm at the sample position.

To measure spectral reflectance factor over the visible wavelength range of the monochromator, the system employs a tungsten strip lamp and a photomultiplier detector. A complete description of the spectrophotometer is given in an earlier publication [15].

Data have been published [16, 17] on the large effect of polarization on the reflectance factor. Therefore, the NBS design includes a polarization-insensitive receiver system and the measurements are made with polarized incident light. The final result is the average of measurements made with light polarized perpendicular and parallel to the plane of incidence.

4. 45°/Normal Reflectometer

The light beam from the source system is incident on a sample at 45° from normal and the reflected flux at normal to the sample is collected and measured. The schematic of the instrument is shown in Fig. 2. The 45°/normal rather than the normal/45° geometry was chosen, because the distance between the limiting aperture and the sample surface and, in turn, the view factor could be determined more accurately.

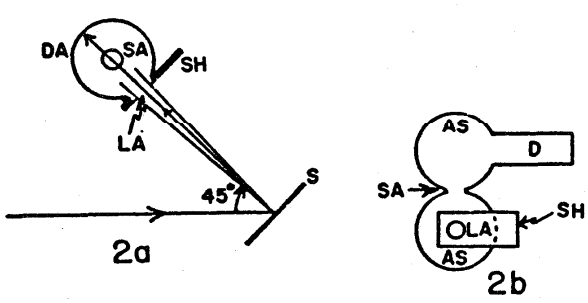

Fig. 2 a and b. Schematic of the 45°/normal Reflectometer. **a** Top view with top sphere not shown, for clarity. S: Sample, LA: Limiting Aperture, DA: Detector assembly, SA: Aperture between spheres; **b** Front view of the two-sphere Receiver Assembly, AS: Averaging Sphere, SH: Shutter, D: Detector, LA: Limiting Aperture, SA: Aperture between spheres

Because the step-down technique with a polished black glass is used to obtain the absolute reflectance factors of a diffuse sample, the instrument should be able to measure accurately both the specularly and the diffusely reflected light beams. This requires that the responsivity of the receiver system be uniform over its aperture area.

To fulfill the above requirement, the photomultiplier is equipped with a double-sphere signal averager. The spheres are approximately 15 cm in diameter. The sphere coating is a fluorocarbon powder, which is a nearly perfect diffuser of very high reflectivity. The two spheres are mounted together vertically and are designed to allow the inside curvature of the sphere coating to meet at the center of the port between the two spheres. The photomultiplier is mounted horizontally on the upper sphere. The spheres are attached to a stepping-motor-controlled vertical slide for alignment and scanning purposes. The lower sphere has a circular limiting aperture facing the sample. To prevent scattered radiation, other than that directly from the sample, reaching the limiting aperture, no component is placed between the surfaces of the sample and the limiting aperture. A black felt is placed on the top surface of the rotation arm to further reduce scattered radiation.

The sample holder, which can hold two samples, is mounted on a two-position slide that moves 12.5 cm between positions and is pneumatically driven. The slide is mounted on a stepping-motor-controlled turntable. The detector assembly is on an arm attached to another independently-controlled turntable having the same axis of rotation as that of the sample turntable.

The signal processing of the output from the photomultiplier utilizes a current-to-frequency converter that can integrate the detector output over a selected time interval, and a digital counter. The digital data from the counter are transferred to a computer for analysis.

5. Measurement Procedure

Before a measurement is performed, the instrument is first aligned. The sample holder can be adjusted normal to the incident light beam with the aid of a flat mirror in the sample position. The sample holder is then turned 22.5° from the normal position toward the limiting aperture. The limiting aperture is adjusted to center on the reflected light beam which is 45° from the incident light beam. A thin mirror, with the reflecting surface facing the limiting aperture, is held against the limiting aperture. The limiting aperture is aligned so that the light is reflected back to the exit slit of the monochromator. Thus the limiting aperture is aligned normal to the reflected light beam 45° from the incident beam.

The diameters of the limiting aperture were measured at eight places by using a shadow profile projector before the aperture was mounted on the lower sphere. The circularity has been checked by a deviation plotter. The average diameter is 38.238 mm. The distance be-

tween the surfaces of the limiting aperture and the sample is determined when the sample holder is turned 45° from the normal position. A thin glass plate is placed over the limiting aperture. The distance between this glass plate and a flat surface at the sample position is measured with an inside micrometer. The thickness of the glass plate is added to the micrometer measurement to give the total distance which in this case is 381.89 mm. The view factor can thus be calculated using (10) and (13).

The spectral 22.5° specular reflectances of a piece of polished black glass are first determined with the specular reflectometer [18] with light polarized perpendicular and parallel to the plane of incidence. This piece of black glass is then used to step down the incident flux to determine the 45°/0° reflectance factors of a sample. The flux of the sample in 45°/0° geometry is compared to the flux of the black glass in the 22.5°/22.5° geometry. The reflectance factor of the sample can thus be calculated using (9). The measurements are performed with polarized light, and the final result is the average of measurements made with light polarized perpendicular and parallel to the plane of incidence.

6. Performance

It is beyond the intent of this paper to describe in detail the various checks that were made on the performance of the monochromator, other components of the spectrophotometer, and the reflectometer, except to mention briefly the magnitudes of errors associated with this portion of the system, since they do influence the accuracy of measurements of reflectance factor. Information regarding some of these investigations is presented in [15].

Wavelength scale uncertainties, receiver linearity, receiver uniformity, scattered radiation, angular setting uncertainty, and view factor uncertainty are involved in checking the performance of the instrument.

The wavelength scale of the monochromator was checked by measuring the emission lines [18] of several line-source lamps and the instrument function, then determining the centroid wavelengths. Uncertainty in the wavelength scale is 1 nm or less for a 10 nm bandpass. Corrections for these errors are made by adjustment of the wavelength-scale setting to compensate for differences between the wavelength counter and the true wavelength.

The linearity of the receiver system was measured by the light addition method with a double aperture apparatus [20, 21]. The results indicate the receiver system is linear to better than ±0.1% and the nonlinearity is corrected for measured data.

Even though the receiver system utilizes double spheres as an averager device, there is still a slight nonuniformity causing 0.05% uncertainty in comparing the fluxes of specularly and diffusely reflected beams.

Radiation scattered off the components between the exit slit of the monochromator and the limiting aperture of the receiver system causes errors in a reflectometer. The room containing the reflectometer is lined with a black felt material to absorb scattered radiation. All mechanical components, including the sample holder and the limiting aperture, are black anodized to reduce the scattered radiation. Some interreflections between the limiting aperture and the sample and between the sphere coating and the sample are unavoidable. The scattered radiation caused by the interreflection is determined to be less than 0.05% of the reflected radiation.

The 0.05° uncertainty of the angular setting of the sample holder contributes to 0.15% uncertainty in determining the ratio of the reflected fluxes of the sample and the piece of black glass.

The uncertainties in determining the diameter of the limiting aperture, the distance between the sample surface and the limiting aperture, and the dimensions of the light image size on the sample surface result in an uncertainty of about 0.05% for the view factor.

An analysis of the various sources of error that may affect the accuracy of reflectance factor measurements on the NBS 45°/normal reflectometer indicates that the final uncertainty in these measurements will be of the order of ±0.3% of the measured value.

7. Ratio of R(45°/Normal) TO R(6°/Hemispherical) with Specular Component Excluded

The hemispherical reflectance factor R(0°/h) of a diffuser for normally incident light can be calculated from the angular variations of reflectance factors R(0°/θ) using the following expression:

$$R(0°/h) = \frac{\int_0^{\pi/2} R(0°/\theta)\cos\theta\sin\theta\, 2\pi d\theta}{\int_0^{\pi/2} \cos\theta\sin\theta\, 2\pi d\theta} \tag{14}$$

Divided by R(0°/45°), Eq. (14) can be written as:

$$\frac{R(0°/h)}{R(0°/45°)} = 2\int_0^{\pi/2} \frac{R(0°/\theta)}{R(0°/45°)}\sin\theta\cos\theta d\theta \tag{15}$$

In terms of measurable quantities, (15) can be rewritten as:

$$\frac{R(0°/h)}{R(0°/45°)} = 2\int_0^{\pi/2} B(0°/\theta)\sin\theta\cos\theta d\theta \tag{16}$$

where

$$B(0°/\theta) = \frac{\Phi(0°/\theta)/\cos\theta}{\Phi(0°/45°)/\cos 45°} \tag{17}$$

with Φ as the reflected flux from the sample.

The two working standards, vitrolite glass and porcelain enamel plate, one pressed $BaSO_4$ sample, and one pressed fluorocarbon sample were measured on the gonioreflectometer at 550 nm with 10 nm bandpass. The incident angle was 0° and the angles of viewing were from 5° to 85° at 10° intervals. Measurements were

made with light polarized parallel and perpendicular to the plane of incidence. $B(0°/\theta)$'s were calculated for each polarization and the averages obtained.

Average $B(0°/\theta)$'s at the discrete intervals were fitted by the least-squares method. Individual data did not deviate from the fitted curve by more than ±0.001 and were typically within 0.0005 of the fitted curve. The curve fittings were done by using a six-parameter equation:

$$B(0°/\theta) = \sum_{i=0}^{5} b_i \theta^i \tag{18}$$

Inserting (18) into (16), we have

$$\frac{R(0°/h)}{R(0°/45°)} = 2 \sum_{i=0}^{5} b_i I_i \tag{19}$$

where

$$I_i = \int_0^{\pi/2} \theta^i \sin\theta \cos\theta \, d\theta \tag{20}$$

The values [1] of the integrals I_i are (from i = 0 to 5): 0.50000, 0.39270, 0.36685, 0.37990, 0.42147, and 0.49129. With the values of I_i and b_i, $R(0°/h)/R(0°/45°)$ can be predicted using (19).

Six deg.-hemispherical reflectance factors, $R(6°/h)$, with specular component excluded and 45°/normal reflectance factors, $R(45°/0°)$, were also measured for the four samples. $R(6°/h)$ will not be different significantly from $R(0°/h)$, and $R(45°/0°)$ is equal to $R(0°/45°)$ according to the Helmholtz reciprocity principle.

The measured values of $R(45°/0°)$, $R(6°/h)$ and the ratio of the measured values and integrated ratios are given in Table 1. The measured and integrated values of the ratios agree to 0.005. These ratios are consistent with references [4, 22, 23] in that the values of 45°/normal reflectance factors are higher than the values of the 6°/h reflectance factors. And in the cases of vitrolite and enamel samples the ratios are about four percent higher than unity.

Table 1. Comparison of $R(45°/0°)$ and $R(6°/h)$* (at 550 nm)

Sample	Measured Value $R(45°/0°)$ (b)	$R(6°/h)$* (a)	$R(45°/0°)/R(6°/h)$ (b)/(a)	Integrated**
$BaSO_4$	0.987	0.982	1.005	1.002
Fluorocarbon	1.009	0.994	1.015	1.011
Vitrolite	0.922	0.884	1.043	1.044
Enamel	0.875	0.839	1.043	1.040

* Specular component excluded

** Integration using normalized gonioreflectance data

8. Summary

A 45°/normal reflectometer spectrophotometer was constructed for calibrating the absolute reflectance factor of diffuse samples over the 380–770 nm spectral range. The measurement equations were derived and the measurements were made as a function of wavelength with a polarized light beam. The system performance was examined for such parameters as wavelength scale uncertainties, receiver system linearity and uniformity, scattered radiation, angular setting and view factor uncertainties. Uncertainty in the measurements of reflectance factor will be of the order of ±0.3% of the measured value. Measured ratios of the 45°/normal reflectance factor to the hemispherical reflectance factor with specular component excluded were found to be greater than one for all the samples that have been tested. The higher reflectance values for 45°/normal geometry were confirmed by additional gonioreflectometer measurements.

References

1. W.H. Venable Jr, J.J. Hsia, V.R. Weidner: Establishing a scale of directional-hemispherical reflectance factor. I: The Van den Akker method. National Bureau of Standards (US). J. Res. 82, 29–55 (1977)
2. J.S. Preston, G.W. Gordon-Smith: A new determination of the luminance factor of magnesium oxide. Proc. Phys. Soc. B65, 76–80 (1952)
3. F.J.J. Clark, G.E.V. Lambert, J.M.B. Sparrock, F.A. Gargorth: Research on absolute reflectance standards at the National Physical Laboratory. Proc. Symp. Color Measur. Ind. 25–40, 1967 (The Color Group, London)
4. F.J.J. Clark, F.A. Garforth, D. Parry: Goniophotometric and polarization properties of the common white reflection standards. Nat. Phys. Lab. Rep. MOM 26 (1977)
5. W. Erb: Bestimmung des spektralen Leuchtdichte-Koeffizienten für die Messgeometrie 45°/Normal. Die Farbe 20, 179–186 (1971)
6. L. Morren: Mesure absolute des facteurs de luminance et de réflection. LUX No. 45, 448–453 (1967)
7. V.E. Kartahevskaya, S.P. Skachkova: New method of the luminance factors and total reflectances for the standard plates of the Institute of Metrology. Svetsteknika 1, 16–19 (1966); also available as translation NRC TT-1265
8. Commission internationale de l'éclairage: Absolute methods for reflection measurements. CIE Publication Nos. 44 and 46 (1979)
9. Commission internationale de l'éclairage: Colorimetry, official CIE recommendations. CIE Publication No 15 (1971)
10. F.E. Nicodemus, J.C. Richmond, J.J. Hsia, J.W. Ginsberg, T. Limperis: Geometrical considerations and nomenclature for reflectance. Nat. Bur. Stand. (US). Monogr. 160 (1977)
11. W.H. Venable, Jr, J.J. Hsia: Describing spectrophotometric measurements. Nat. Bur. Stand. (US). Tech. Note 594-9 (1976)

12. E.M. Sparrow, R.D. Cess: Radiation heat transfer (augmented edition) p. 121. New York: McGraw-Hill Book Company, 1978
13. F.E. Nicodemus (ed.): Self-study manual on optical radiation measurements: Part I – Concepts, Chap. 4 and 5 p. 97. Nat. Bur. Stand. (US). Tech. Note 910-2 (1978)
14. M. Jakob: Heat transfer. Vol. II p. 11. New York: John Wiley and Sons Inc., 1957
15. W.H. Venable, Jr, J.J. Hsia, V.R. Weidner: Development of an NBS reference spectrophotometer for diffuse transmittance and reflectance. Nat. Bur. Stand. (US). Tech. Note 594-11 (1976)
16. A.R. Robertson: Effect of polarization on reflectance factor measurements. Appl. Opt. **11**, 1936–1941 (1972)
17. D.C. Cramer, M.E. Bair: Some polarization characteristics of magnesium oxide and other diffuse reflectors. Appl. Opt. **8**, 1597–1605 (1969)
18. V.R. Weidner, J.J. Hsia: NBS specular reflectometer-spectrophotometer. Appl. Opt. **19**, 1268–1273 (1980)
19. C.E. Hodgman (ed.): Handbook of Chemistry and Physics, 44th. edn, pp. 2892, 2931, 2961. The Chemical Rubber Publishing Co. 1962–1963
20. K.D. Mielenz, K.L. Eckerle: Design, construction, and testing of a new high accuracy spectrophotometer. Nat. Bur. Stand. (US). Tech. Note 729 (1972)
21. K.D. Mielenz, K.L. Eckerle: Spectrophotometer linearity testing using the double-aperture method. Appl. Opt. **11** 2294 (1972)
22. V.E. Kartachevskaya, H. Korte, A.R. Robertson: International comparison of measurements of luminance factor and reflectance of white diffusing samples. Appl. Opt. **14**, 2694–2702 (1975)
23. A.R. Robertson, W.D. Wright: International comparison of working standards for colorimetry. J. Opt. Soc. Am. **55**, 694–706 (1965)

APPENDIX E

JOURNAL OF RESEARCH of the National Bureau of Standards
Volume 82, No. 1, July–August 1977

Establishing a Scale of Directional-Hemispherical Reflectance Factor I: The Van den Akker Method

William H. Venable, Jr., Jack J. Hsia, and Victor R. Weidner

Institute for Basic Standards, National Bureau of Standards, Washington, D.C. 20234

(May 22, 1977)

A thorough study and error analysis was made of the Van den Akker or "auxiliary sphere" method of determining a scale of directional-hemispherical reflectance factor. The effects of a non-Lambertian distribution of the reflected radiation, including retroreflection, were included in this study. Three working standards were measured to an uncertainty in reflectance of less than ±0.0015 and these will be used as a basis for a new, more accurate NBS scale of 6°-hemispherical reflectance factor. The new scale and the NBS scale established in 1965 are in agreement to within the uncertainty of ±0.005 assigned to the 1965 scale.

Key words: Absolute reflectance; diffuse reflectance; error analysis; reflectance; reflectance factor; spectrophotometry.

Foreword

We have arranged this paper in a way which should accomodate readers who have an interest in this work from three quite different points of view:

1. Those who must make decisions based upon the results of the measurements are addressed principally in the Summary which directly follows this foreword. The material in parts I. and V.B. would also be of interest to such readers.

2. Those who wish to use the Van den Akker auxiliary sphere method for determining absolute reflectance should find the material in parts II, III, and V.A. to be of particular interest, and part IV can be read superficially, if at all, in order to glean a few technological ideas.

3. Those who are interested in a detailed understanding of the way in which these measurements are carried out at NBS and in a detailed discussion of the error analysis should, after a careful reading of parts II and III, place their emphasis on part IV.

Summary

Of the light or other optical radiation incident upon a surface in a given direction and at a given wavelength, a fraction is reflected from the surface. This fraction is called the spectral directional-hemispherical reflectance of the surface, and measuring it accurately is important in two different classes of applications:

1. Applications in which the value of the reflectance is of direct importance. Such applications include radiative energy transfer as in solar energy devices, lighting system engineering, calibrating radiometers in remote sensing satellites, and formulating the pigmentation in paints and other finishes.

2. Applications in which the actual value of the reflectance is of secondary importance, but for which the basis of measurement must be extremely stable in time. These applications include quality control in automated production and specifications involving color or appearance of finished products. For such applications, the instruments which are used are calibrated with material standards, and the laboratories supplying these standards must be able to measure reflectance directly in order to measure the standards and verify their stability.

The economic benefits derived from having this portion of the measurement system under control are very large, coming in the form of an accumulation of modest benefits over a very large base of application [1].[1] In order to realize these advantages, it is important that the uncertainty in the measurements be commensurate with the uniformity and stability of the reflectance of the surfaces encountered in practice.

For a number of applications, it is important to measure directional-hemispherical reflectance factors near 1 with an uncertainty in the neighborhood of ±0.001. The present extensive work on spectral directional-hemispherical reflectance was undertaken at NBS for two reasons. First, the stated uncertainty of ±0.005 for the NBS reflectance factor scale established in 1965 [2][1] was too large for many of the applications for which we were called upon to standardize the measurements. Second, and even more disturbing, intercomparisons between the scales of national standardizing laboratories in connection with the work of the International Standardization Organization (ISO) revealed differences as great as 0.015 between the measured value of reflectance of the same samples. Such a large difference can have serious economic consequences in international trade in finished goods such as paper.

As a first step in this work, we have investigated in great detail the Van den Akker auxiliary sphere method of determining spectral directional-hemispherical reflectance which

[1] Figures in brackets indicate the literature references on page 49.

has been used in the past at NBS, improving upon the techniques and providing the necessary corrections to make the measurements precise and accurate to within ±0.0015 to the best of our knowledge. This step has been completed and is reported in this paper. The new and former NBS scales of measurement agree to well within the combined measurement uncertainties.

As a second step, we plan to investigate the techniques used by the other major national laboratories and to work with our colleagues in these laboratories to determine the cause of the discrepencies which have been encountered internationally. As part of this step, we have already completed a set of measurements using a second method of determination, the Sharp-Little method. The results obtained with that method are in good agreement with those reported in this paper and are to be published soon in another paper in this same series. We have visited the National Research Council Laboratories in Canada (NRC) for detailed discussions of these results. We also plan to conduct experiments with the Korte method currently used by the Physikalisch-Technische Bundesanstaldt (PTB) in Germany and possibly with one or two other approaches less commonly used.

The scale of directional-hemispherical reflectance as currently established will be disseminated through standards supplied through the NBS Office of Standard Reference Materials and through commercial secondary standards laboratories in the United States. The improvements in techniques which have been developed as a result of this work will be submitted to the appropriate committees of ASTM, ANSI, and TAPPI for possible incorporation in standard procedures. When the international discrepancies have been eliminated, we will be working with NRC, PTB, and possibly other laboratories as standardizing laboratories for ISO reflectance measurements.

I. Introduction

Directional-hemispherical (d/h) reflectance factor measurements are important in a wide variety of applications. If the results of these measurements are to be a useful tool for technical communication, the measurements must be made accurately. Most reflectometers are not capable of measuring d/h reflectance factor directly, but can only compare the reflectance factors of two objects. The calibration of such instruments is accomplished by measuring a standard object which has a known reflectance factor. To see that accurately measured reflectance standards are available to the measurement community is one of the primary responsibilities of the spectrophotometry group of the Radiometric Physics Section of the Institute for Basic Standards.

In the development and production quality control of finished products in which appearance is an important factor, the measurement of reflectance should be accurate to within ±0.002. This level of accuracy or better is also important to rapidly evaluating the stability of reflecting materials under weathering and ageing. These two types of applications are the ones which commonly call for the lowest measurement uncertainty. It is difficult to produce highly reflecting surfaces for which the reflectance is reproduced to better than ±0.001 and the reflectance of most surfaces is not even uniform to this degree. Therefore, a reflectance measuring capability for which the uncertainty is less than ±0.001 is both necessary and sufficient for a national standardizing laboratory. The work described in this technical note is part of an effort to reduce the uncertainty in diffuse reflectance factor measurements at NBS from an estimated ±0.005, which it has been in the recent past, to ±0.001.

The National Bureau of Standards (NBS) has established its scale of d/h reflectance factor in 1965 through an extensive series of measurements by Goebel, Caldwell, and Hammond [2]. At that time, Vitrolite [3] glass standards [4] to calibrate the General Electric Recording Spectrophotometer (GERS) [5] (Cat. 5962004 G28 No. 732986) were measured. Until recently, that instrument has been used for most reflectance measurements made at NBS. The reflectance of the Vitrolite standards has been shown to be very stable by measurements made over a period of thirty years relative to freshly prepared MgO surfaces [6]. In 1974, the scale of measurement was rechecked using the same apparatus used in the 1965 experiments and the agreement was within the experimental error associated with the measurements.

In April of 1974 and through the following year, it was determined from measurements made on a number of samples that there was a systematic difference between the scales of measurement being used by NBS and the National Research Council Laboratories of Canada (NRC). This difference was approximately 0.015 at the short wavelength end of the visible spectrum and decreased more or less regularly to approximately 0.01 at the long wavelength end of the spectrum (table I). A similar intercomparison between NRC and Physikalisch-Technische Bundesanstalt of Germany (PTB) [7] revealed only slight differences between the measurements being made by these laboratories (table II). Since the NBS uncertainty at that time is conservatively estimated to be ±0.005 and the NRC uncertainty is conservatively estimated to be ±0.003, the difference is clearly significant.

TABLE I

Data from an intercomparison between NRC and NBS of reflectance measurements on a sprayed $BaSO_4$ coating*. (June 1975) (Spectral directional (6°)-hemispherical reflectance).

Wavelength	Reflectance		
	NRC	NBS†	Difference (NRC-NBS)
400	0.961	0.975	0.014
420	.963	.975	.012
440	.966	.978	.012
460	.970	.980	.010
480	.970	.981	.011
500	.972	.981	.012
520	.972	.985	.013
540	.972	.985	.013
560	.974	.984	.010
580	.975	.985	.010
600	.975	.985	.010
620	.976	.982	.006
640	.975	.986	.011
660	.976	.985	.009
680	.976	.985	.009
700	.977	.985	.008
720	.978	.985	.008
740	.979	.985	.007

* Samples prepared at NRC.
† Data from NBS test 232.14/49D.

The methods used by NBS, NRC, and PTB are all different. In any such case of disagreement between measurements, all measurements and methods are logically suspect

TABLE II

Data from an intercomparison between NRC and PTB of reflectance measurements on a pressed $BaSO_4$ tablet [7] (Spectral Hemispherical-directional (0°) reflectance factor).

Wavelength	Reflectance		
	NRC	PTB	Difference (PTB-NRC)
370	0.961	0.965	0.004
380	.969	.971	.002
390	.974	.976	.002
400	.977	.979	.002
420	.982	.983	.001
440	.985	.984	−0.001
460	.986	.985	−0.001
480	.987	.986	−0.001
500	.987	.987	0
550	.988	.988	0
600	.988	.988	0
650	.987	.988	0.001
700	.987	.989	.002
750	.987	.988	.001

until the cause of the difference is located. However, since the NRC and PTB measurements were in close agreement, it seemed reasonable to investigate the method used by NBS first. A Diffuse Transmittance and Reflectance Reference Spectrophotometer [8], which will be referred to by the acronym DRS for convenience, was completed at NBS in October 1975. This has been used to make detailed measurements of all aspects of the Van den Akker auxiliary sphere method for realizing an absolute scale of d/h reflectance factor [9], which was the method used to establish the NBS scale. The results of this investigation are reported in this paper.

As a result of this investigation a new NBS scale of diffuse reflectance factor measurements for 6° incidence and hemispherical collection has been established which is believed to be accurate to within ±0.0015. The new scale of reflectance factor differs by less than 0.002 from the scale formerly used by NBS. Since this investigation revealed no cause for the discrepancy between national laboratories, we are undertaking a thorough examination of the methods used by the other laboratories. The results of that work are to be reported in future papers.

II. Definitions

A. Directional-Hemispherical Reflectance

One quantity to be measured is the spectral d/h reflectance, ρ (**U**, **P**, λ) at a point on a plane surface. Using the notation described in NBS Technical Note 594-9 [10], this quantity can be expressed in terms of a generalized scattering function S as:

$$\rho\,(\mathbf{U}, \mathbf{P}, \lambda) = \iint S\,(\mathbf{U}, \mathbf{P}; \mathbf{u}, \mathbf{p}, \lambda)\,\mathbf{u}\cdot d\mathbf{a}\,d\omega \qquad (1)$$

where $S(\mathbf{U}, \mathbf{P}; \mathbf{u}, \mathbf{p}, \lambda)$ is the radiance emerging from the sample surface at point **p** in direction **u** due to a unit flux striking the sample at point **P** in direction **U**. It is assumed that the sample is non-fluorescent so that all of the radiation can be confined to a very narrow band at wavelength λ. The integral with respect to the solid angle, ω, in which the radiation emerges is taken over the entire hemisphere of directions and the integral with respect to the area a from which the radiance emerges is taken over the entire area from which the flux emerges. For the uniform, isotropic samples to be discussed in this paper, the d/h reflectance can be represented by $\rho(\Gamma, \lambda)$, where Γ is the angle between the direction of incidence **u** and the surface normal.

B. Directional-Hemispherical Reflectance Factor

A typical d/h reflectometer has an entrance port which subtends at the sample a circularly shaped solid angle ω' which in magnitude is on the order of 10^{-3} steradians. None of the flux falling into ω' reaches the detector, and therefore the instrument does not compare d/h reflectances of the samples as just defined but rather compares "directional-hemispherical" reflectance factors [11] $F(\Gamma, \lambda)$ for collection over the entire solid angle except for ω'. That is to say, the retroreflected flux is excluded from the measurement. To a very good approximation,

$$F(\Gamma, \lambda) = \frac{\iint' S(\mathbf{U}, \mathbf{P}; \mathbf{u}, \mathbf{p}, \lambda)\mathbf{u}\cdot d\mathbf{a}d\omega}{\iint'[\delta(\mathbf{P} - \mathbf{p})/\pi]\mathbf{u}\cdot d\mathbf{a}d\omega} \qquad (2)$$

where the prime on the integral indicates integration over the entire hemisphere except for ω' and $\delta(\mathbf{P} - \mathbf{p})/\pi$ is the idealized scattering function S for an ideal diffuse reflector.

It is the quantity $F(\Gamma, \lambda)$ in which we are most interested when calibrating a reflectometer, and determining this quantity for several working standards is the object of the work reported in this paper.

III. An Overview of the Method

The method to be described for determining d/h reflectance factor is more complex than the method for measuring d/h reflectance originally proposed by Van den Akker. In the original method, it was assumed that d/h reflectance is independent of the direction of incidence. Since this is not sufficiently correct for many surfaces, additional measurements are needed in order to accurately determine the d/h reflectance using this approach. Also, the relationship between d/h reflectance and the reflectance factor as measured by an instrument must be determined. However, for simplicity, we will continue to call the entire process the Van den Akker method.

Although this method is simple in principle and is potentially one of the most accurate methods, the descriptions of it in the literature are usually given in terms of involved summations of infinite series. These descriptions tend to cloud the simplicity of the method and to lead to a misunderstanding of it. Therefore, before describing the details of the measurements as performed at NBS, we will first provide a brief overview of the method in terms of four main steps. The first and last steps were used in the original Van den Akker method, and we have added the additional steps to take into account the variation of $\rho(\Gamma, \lambda)$ with Γ and the difference between $\rho(\Gamma, \lambda)$ and $F(\Gamma, \lambda)$.

The primary measurement in the Van den Akker method is a measurement of the reflectance of the wall of an integrating sphere (fig 1) under the irradiation it receives in the sphere. We will call this reflectance the Van den Akker reflectance $\rho_v(\lambda)$. A flux is introduced into the sphere by reflecting a collimated beam of radiation from the back of the sphere.

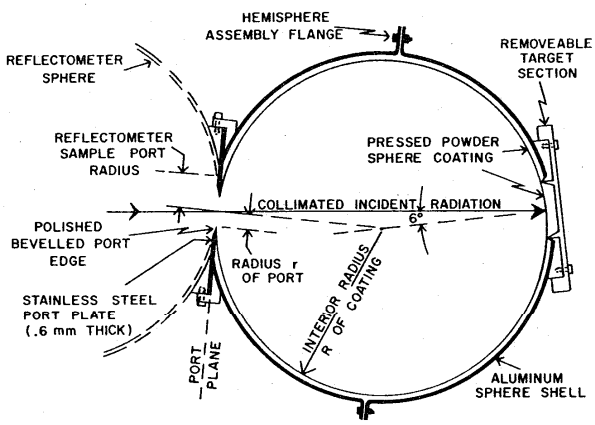

FIGURE 1. *Sphere used for measuring Van den Akker reflectance.*

Most of the radiation which strikes a given area of the sphere wall has undergone many reflections. In a sphere of this type, the average number of times a photon will have passed into the sphere wall and been reflected before it is absorbed or escapes would be between fifty and one-hundred. Because the reflection from the sphere wall is very diffuse, any asymmetry in the way the photons are introduced is dispelled in one or two reflections and the distribution of radiance, L_s, striking the wall has two characteristics properties. First, the irradiance is very nearly uniform over the sphere wall. This follows from the fact that a perfectly Lambertian (radiance constant with respect to direction) reflected flux would produce a uniform irradiance over the sphere wall. Since the distribution of the reflected flux is very nearly Lambertian, the distributon over the sphere wall of incident photons which have been reflected more than two or three times is for all practical purposes uniform. This phenomenon is well-known and forms the basis for the many applications of integrating spheres in which the sphere is used as a flux averaging device. Another property of the spherical geometry which is less often noticed is that a photon which leaves the sphere wall at an angle θ will next strike the sphere wall at the same angle. Thus, after one or two reflections, an angular distribution of radiance L_s (Γ), will be set up which represents, to within a proportionality constant, the incident and emerging radiance at any point on the sphere wall. Unlike the distribution of irradiance over the wall area, the distribution of the radiance with respect to the angle *does not become uniform with angle* but takes on a distribution determined by the bidirectional reflectance properties of the wall coating.

The remaining steps in the method relate the Van den Akker reflectance to the d/h reflectance factor and provide a method of using this reflectance data to calibrate an instrument. The four steps in the Van den Akker method can be outlined as follows:

A. Determining the Van den Akker Reflectance $\rho_v(\lambda)$

A sphere with a single port (see fig. 1) is lined with a highly reflecting white coating, radiation is introduced into the port in a collimated beam, and, from measurements made of the flux re-emerging from the port and of the flux reflected from the target area, the Van den Akker reflectance ρ_v[2] is determined. A flux ϕ_0 (λ) is introduced into the sphere in a collimated beam which strikes the target area of reflectance ρ_t (Γ, λ), providing a nearly Lambertian source of radiation which emits a flux $\phi_0\rho_t$. A fraction f of this flux passes out through the port as a nearly collimated beam, and the remaining portion falls on the sphere wall and is reflected with reflectance ρ'_v, the average reflectance of the sphere wall, excluding the port. This flux, the strength of which is given by $\phi_0\rho_t(1-f)\rho'_v$, acts as a radiation source which is uniformly distributed over the sphere wall. This flux is the source of radiant energy for the total flux $\phi_i(\lambda)$ striking the sphere boundary. A fraction f of λ_i passes out through the port, and a fraction $(1-\rho'_v)$ of the remaining $(1-f)$ is absorbed in the sphere wall or otherwise lost and is not returned to the sphere. In equilibrium, the flux lost from ϕ_i out the port and into the walls is replaced by the uniformly distributed source, from which an equilibrium flux balance equation can be obtained:

$$\phi_0\rho_t(1-f)\rho'_v = \phi_i[f + (1-f)(1-\rho'_v)]. \tag{3}$$

If the flux ϕ_0 is the sample beam flux from a dual beam reflectometer, a signal $Q_s(\lambda)$ is obtained with the sphere in the sample position:

$$Q_s = k[\phi_i f(1-f') + \phi_0\rho_t f(1-f'')] \tag{4}$$

where f' is the fraction of the lambertian flux which escapes from the ports of the reflectometer sphere and f'' is the corresponding fraction of the nearly collimated beam which emerges from the sphere as a result of the first reflection from the back of the Van den Akker sphere. With the target area from the back of the sphere placed directly on the reflectometer sample port as a sample, a signal $Q_t(\lambda)$ is obtained:

$$Q_t = k\phi_0\rho_t(1-f'). \tag{5}$$

It is arranged that the angle of incidence Γ at which ϕ_0 strikes the target when Q_t is measured is the same as when Q_s is measured. Equations (3), (4), and (5) can be solved to obtain an expression for ρ'_v in terms of Q_t, Q_s, f, f' and f''.

$$\rho'_v = \frac{1-(fQ_t/Q_s)(1/(1-\alpha))}{1-f} \tag{6}$$

where

$$\alpha = \frac{f(f'-f'')}{(1-f')}\frac{Q_t}{Q_s}. \tag{6a}$$

If α were 0, this would be the usual form cited for the Van den Akker reflectance. The factor $1/(1-\alpha)$ takes into account that the first reflection of the incident beam from the target in the sphere emerges nearly collimated whereas the remaining flux emerging from the sphere is nearly Lambertian. If the reflectometer handled both fluxes in the same way, i.e., if f' and f'' were equal, this term would be zero. However, it is usually the cause that f'' is very much larger than f' and this contribution must be included.

[2] To keep the writing uncluttered, the functional dependence of each quantity is shown only when it is introduced and at key points in the development.

An additional modification must be made in the original Van den Akker equation to take into account the effect on ρ_v' of the retroreflectance of the sphere wall. This modification, which results in only a small adjustment ρ_v' but which greatly complicates the form of eq (6), is discussed in detail in appendix A.

Since $(1 - f)(1 - \rho_v')$ in eq (3) represents the portion of ϕ_i which is lost everywhere but out of the port, it follows that the reflectance ρ_v' is the average reflectance over the sphere area excluding the port. To relate ρ_v' to a property of the sphere coating, it is important that the sphere coating be uniform and completely cover all of the sphere area except for the entrance port. If it is necessary to have cracks or other gross imperfections in the coating, the losses in such imperfections must be estimated and ρ_v' must be suitably corrected in order to obtain the Van den Akker reflectance ρ_v of the sphere coating.

B. Adjustment from Van den Akker Reflectance $\rho_v(\lambda)$ to d/h Reflectance $\rho(\Gamma, \lambda)$

In order that the need for the next steps be more readily understood, ρ_v will be interpreted in terms of the directional-hemispherical reflectance, ρ, as defined in eq (1).

$$\rho_v = \frac{2\pi \int_0^{\pi/2} L_s(\Gamma)\, \rho(\Gamma) \cos(\Gamma) \sin(\Gamma)\, d\Gamma}{2\pi \int_0^{\pi/2} L_s(\Gamma) \cos(\Gamma) \sin(\Gamma)\, d\Gamma} \tag{7}$$

where $L_s(\Gamma)$ is the radiance associated with ϕ_i at the incident angle Γ and explicit indication of the dependence on wavelength has been omitted for clarity. As we have indicated, ρ_v is just the weighted average over all directions of incidence Γ of the d/h reflectance. The weighting function $L_s(\Gamma) \cos\Gamma \sin\Gamma$ is proportional to the irradiance of the sphere wall per unit angle at the angle Γ. If the d/h reflectance were independent of angle of incidence, one can see from equation (7) that ρ_v and $\rho(\Gamma)$ would be identical. However, in any real sphere coating, $\rho(\Gamma)$ is not quite constant and this variation must be taken into account if d/h reflectance is to be determined from ρ_v.

The flux, ϕ_i, striking the sphere wall is composed of radiation most of which has undergone many reflections. As has already indicated, the radiance $L_s(\Gamma)$ striking the wall in one location emerged from the wall at the same angle at some other location. When the irradiance of the wall is uniform and if the generalized scattering function S of the coating were known, the function L_s could be determined by solving the integral equation

$$\rho_v L_s(\gamma) = 2\pi \int_0^{\pi/2} L_s(\Gamma)\, S(\Gamma, \gamma) \cos\Gamma \sin\Gamma\, d\Gamma. \tag{8}$$

Because the irradiance of the sphere wall is uniform, the self radiance distribution, L_s, can be determined to within a constant by measuring the radiance, $L_s(\gamma)$, emerging from the sphere coating through the port with an uncalibrated gonioreflectometer. The relative signal N_g from the gonioreflectometer as a function of the angle of observation γ can be related to $L_s(\gamma)$ as

$$L_s(\gamma, \lambda) = k_1(\lambda)\, N_g(\gamma, \lambda) / \cos(\gamma) \tag{9}$$

where k_1 is a constant of proportionality.

To complete the adjustment, information about the form of $\rho(\Gamma, \lambda)$ is obtained. A flat sample of the sphere wall coating is prepared in the same way as the sphere wall coating and its relative d/h reflectance is measured. The corrected reflectometer signal [12] N_G is proportional to the d/h reflectance.

$$\rho(\Gamma, \lambda) = k_2(\lambda)\, N_G(\Gamma, \lambda). \tag{10}$$

The constant k_2 can be expressed in terms of measured quantities by simultaneous solution of eqs (7), (9), and (10).

$$k_2(\lambda) = \frac{\rho_v(\lambda) \int N_g(\Gamma, \lambda) \sin\Gamma\, d\Gamma}{\int N_G(\Gamma, \lambda)\, N_g(\Gamma, \lambda) \sin\Gamma\, d\Gamma} \equiv \frac{\rho_v(\lambda)}{\bar{N}_G(\lambda)} \tag{11}$$

where $\bar{N}_G$ is the weighted average of $N_G(\Gamma, \lambda)$ with weighting function $N_g(\Gamma, \lambda) \sin\Gamma$. With the value of k_2 determined, the d/h reflectance for any wavelength and angle of incidence can be calculated from the relative d/h reflectance data by using eq (10). However, we prefer to use an expression for $\rho(\Gamma, \lambda)$ which takes the form of a small adjustment of the Van den Akker reflectance. By substituting the expression for k_2 from eq (11) into eq (10) and using some algebraic manipulation, one can put eq (10) into the form

$$\rho(\Gamma, \lambda) = \rho_v(\lambda)\, [1 + C(\Gamma, \lambda)] \tag{12}$$

where

$$C(\Gamma, \lambda) = \frac{N_G(\Gamma, \lambda)}{\bar{N}_G(\lambda)} - 1.$$

C. From d/h Reflectance $\rho(\Gamma, \lambda)$ to d/h Reflectance Factor $F(\Gamma, \lambda)$

If the generalized scattering function S for directions of incidence and reflectance both falling within the reflectometer entrance port (retroreflectance at entrance angle Γ) were equal to the average of S over all directions of viewing, then the reflectance $\rho(\Gamma, \lambda)$ and the reflectance factor $F(\Gamma, \lambda)$ will be equal. However, for the usual type of sphere coating, S in the retroreflective direction has been observed to be as much as 50 percent above the average at small angles of observation [13]. Therefore, the bidirectional reflectance factor $F(\mathbf{U}, \mathbf{u}\, \lambda)$ must be determined over the extent of the solid angle ω' surrounding the incident direction $\mathbf{U}$ and the relationship between $F(\Gamma, \lambda)$ and $\rho(\Gamma, \lambda)$ determined from eqs (1) and (2) as

$$F(\Gamma, \lambda) = \frac{\rho(\Gamma, \lambda) - \frac{1}{\pi} \int \mathbf{F}(\mathbf{U}, \mathbf{u}) \cos\gamma\, d\omega}{\left(1 - \frac{1}{\pi}\, \omega' \cos\gamma\right)} \tag{13}$$

where the integral in ω is taken over ω'. (Note that $F(\mathbf{U}, \mathbf{u}) = \pi \int S\, (\mathbf{U}, \mathbf{u})\, da$.)

D. Determining the Directional-Hemispherical Reflectance Factor of Standards and Other Samples

The d/h reflectance factor $F(\Gamma, \lambda)$ as determined in the preceding four steps is the d/h reflectance factor of the sphere wall coating. The final step is to use this information to measure a stable standard reflector which can then be used to calibrate a d/h reflectometer. One of the methods used by Van den Akker [9] was to compare the standard directly with sections of the sphere wall which were hoped to be representative. Another method is to prepare a large number of samples using the same materials and preparation techniques that were used in coating the sphere itself and comparing these to the standard. In either case, the d/h reflectance factor $F_c(\Gamma, \lambda)$ of the standard is calculated from the previously determined d/h reflectance factor $F(\Gamma, \lambda)$ of the sphere wall as

$$F_c(\Gamma, \lambda) = F(\Gamma, \lambda) \frac{n\, Q_c(\Gamma, \lambda)}{\sum_{i=1}^{n} Q_i(\Gamma, \lambda)} \tag{14}$$

where Q_c is the reflectometer signal for the standard and Q_i is the reflectometer signal for the ith one of the n samples which are taken to represent the sphere wall. In day-to-day use, the d/h reflectance factor $F_x(\Gamma, \lambda)$ of a sample can be measured by comparison to the stable standard.

$$F_x(\Gamma, \lambda) = F_c(\Gamma, \lambda) \frac{Q_x(\Gamma, \lambda)}{Q_c(\Gamma, \lambda)} \tag{15}$$

where the reflectometer readings Q_x and Q_c are taken close together in time in order to minimize the effects of instrument drift.

IV. The Measurements as Currently Made at NBS

The overview in the preceding section describes in general the way that d/h reflectance can be determined by the Van den Akker method. Three determinations of the d/h reflectance of a set of standards has been made using the DRS. Through the experience gained in these determinations, a procedure for making the measurements with this instrument has been worked out. That procedure is described in this section to give a documented starting point for future improvements in the method and the data from these three determinations provide the basis for the current NBS scale of 5°/h reflectance factor.

Three different materials were used as sphere coatings for the determinations. In the first determination, the sphere was coated with $BaSO_4$ powder [3, 14] from a stock which had been on our laboratory shelf for some time and had been opened on previous occasions. This was used to obtain experience with the method and to obtain an idea of some of the difficulties which might be encountered with a material which was slightly contaminated and which had a slightly lower reflectance than the best quality coatings. In the second determination, the sphere was coated with Halon [3, 15] powder, and in the third determination a fresh lot of reagent grade $BaSO_4$ powder [3, 16] was used. The advantages and disadvantages of each coating will be brought out in the discussion of the measurement errors in the description of each of the three main measurement steps.

A. Determining the Van den Akker Reflectance $\rho_v(\lambda)$

The design of the spheres used to determine the Van den Akker reflectance of the sphere coating material is shown in figure 1. In some of his earlier work using this method, Van den Akker used a sphere with many removable sections in order to sample at many points the actual sphere coating being measured. However, the presence of many removable sections provides an uneven substructure for the sphere coating, creating a potential for dark rings and even cracks in the coating at the border of each removable section. Therefore, we decided to have only the target area removable and to rely on reproducing the coating for a representative sampling.

The sphere coating is made by packing the powder into the aluminum sphere shell with an electrically driven hammer which has a Teflon [3] head (fig. 2). The hammer is mounted on a stand and each hemisphere of the sphere is mounted in turn on a gimbal which allows it to be rotated about a point a fixed distance behind the hammer. In this way, a hemisphere of constant interior radius R is packed uniformly in a mechanical way. A plastic ring attached to the flange of each hemisphere as it is being packed allows the packing jig to be aligned the same for both hemispheres and allows the coating to be built up to full thickness at the edge of the hemisphere. In this way, when the plastic ring is removed and the sphere is joined, a uniform sphere coating of interior radius R results which has no crack at the plane where the hemispheres join.

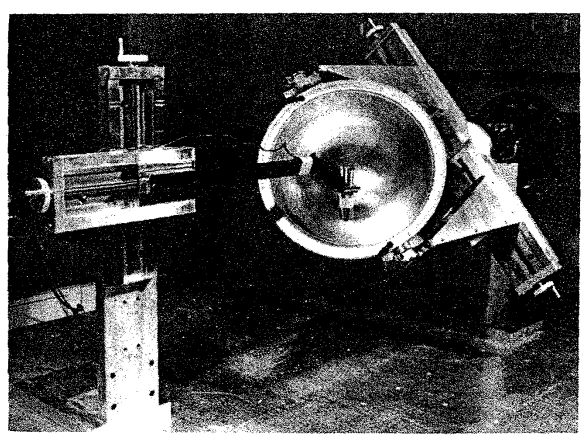

FIGURE 2. *Apparatus used to produce the sphere coating.*

1. Determining the Uncorrected Van den Akker Reflectance ρ_v'

The fraction f introduced in eq (6) is taken as that portion of the area of the sphere of radius R which is occupied by the port of radius r, i.e.,

$$f = (1 - (1 - (r/R)^2)^{1/2})/2. \tag{16}$$

Associated with each determinaton of f there is an estimated random error, as defined in appendix B. A random error δR arises from our inability to pack the sphere to the same radius

R from one determination of reflectance to the next and from the inability to measure the average R exactly. This gives rise to a random error δf which is given by:

$$\delta f = \frac{(r^2/R^3)}{2(1 - (r/R)^2)^{1/2}} \delta R. \tag{17}$$

A systematic error arises from any error in measuring r and from assuming that the measured r is the effective r. Both of these can be taken into account in terms of an uncertainty Δr in the effective port radius. The estimated systematic error Δf is given by

$$\Delta f = \frac{(r/R^2)}{2(1 - (r/R)^2)^{1/2}} \Delta r. \tag{18}$$

The reflectance of the sphere was measured using the DRS with the $6°/h$ (specular included) general purpose integrating sphere [17]. In this mode of operation, the instrument is a dual beam reflectometer with a capability of highly accurate measurements of relative $6°/h$ reflectance factor, i.e., the instrument measures a quantity Q which is proportional to the $6°/h$ reflectance factor of the sample appearing in the plane of its sample port. With the sphere in place as a sample, a reflectance value which will be called Q'_s is measured. As is described in detail in the Technical Note on the DRS [18], a correction must be made for the small amount of radiation which does not enter the sphere port but instead is reflected from that portion of the sphere port plate which shows in the reflectometer sample port or is reflected from the sphere wall of the reflectometer itself. In order to correct for this scattered radiation, a second reflectance measurement is made with the auxiliary sphere port plate in place without the sphere behind it, i.e., with most of the sample beam of the reflectometer passing out into the room and being lost. The reflectance value Q_p obtained in this manner must be subtracted from Q'_s in order to obtain a reflectance value proportional to the radiation being returned from inside the sphere. Most of the radiation emerging from the sphere passes freely back through the port into the reflectometer sphere. A small fraction of it, however, will strike the polished beveled edge of the auxiliary sphere port and will, thereby, suffer a slight loss as it returns to the reflectometer sphere. To correct for this loss, we measured the relative reflectance Q_f of a flat plate of the same stainless steel from which the auxiliary sphere port plate was made. Since Q_f in the reflectometer is approximately the reflectance of the sample relative to the sphere wall which in turn has a reflectance nearly 1, Q_f was approximately the reflectance of the stainless steel plate for 6° incidence. The radiation coming from the sphere which strikes the beveled edge strikes it at near grazing incidence. Since the reflectance from a metal surface near grazing incidence is higher than the near-normal reflectance, we chose to represent the reflectance from the beveled edge by $(1 + 2Q_f)/3$. This estimate is based on the general shape of the reflectance curves for metals [19] and on the port dimensions (fig. 3) [20]. Under this assumption, if the projected solid angle subtended by the beveled edge of the port averaged over the port area is ω_e, an expression for the corrected sphere reflectance Q_s can be written as

$$Q_s = (Q'_s - Q_p)\Big/\left[1 - \frac{\omega_e}{\pi}\frac{2(1 - Q_f)}{3}\right]. \tag{19}$$

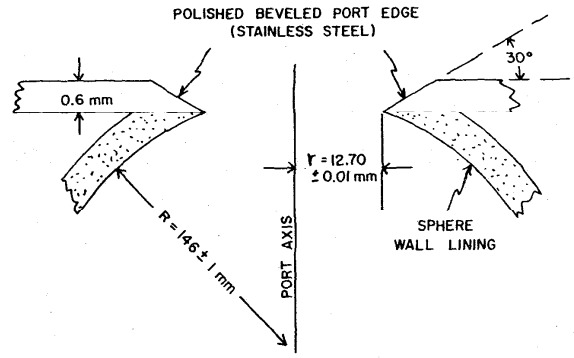

FIGURE 3. *Cross section detail of polished beveled port edge.*

Associated with this determination of Q_s, there is a random error δQ_s arising from the random errors in measuring Q'_s, Q_p, and Q_f. Because of the smallness of ω_e, the denominator in eq (19) is approximately 1 and the small random error in Q_f has little effect on the total random error. Therefore

$$\delta Q_s \simeq (\delta Q'^2_s + \delta Q^2_p)^{1/2}. \tag{20}$$

Also associated with the determination of Q_s is a systematic error ΔQ_s which arises from the uncertainty in ω_e and from the approximation used in estimating the effective reflectance of the beveled edge of the port. The systematic uncertainty in the beveled edge correction is estimated to be one-half as large as the correction itself, so that

$$\Delta Q_s \simeq Q_s \frac{2(1 - Q_f)}{3\pi}\left(\Delta\omega_e^2 + \left(\frac{\omega_e}{2}\right)^2\right)^{1/2} \tag{21}$$

The reflectance of the removable target was measured using the same instrument. In this case a value Q'_t was obtained which also included a small contribution due to stray radiation from the sample beam which is reflected from the reflectometer sphere wall and from that portion of the target which is outside the region occupied by the auxiliary sphere port. A correction for this contribution was obtained by measuring Q_e with a sample in the port made of the same material as the target but which has a hole in it the size of the port in the auxiliary sphere. Note that in this measurement, the beveled edge is not present, since the stainless steel port structure depicted in figure 3 is part of the auxiliary sphere. The corrected relative reflectance of the target Q_t is obtained as

$$Q_t = Q'_t - Q_e. \tag{22}$$

An expression for the random error associated with this determination of Q_t is determined in a straightforward fashion and resembles eq (20).

$$\delta Q_t = [\delta Q'^2_t + \delta Q^2_e]^{1/2}. \tag{23}$$

The values of f, Q_s, and Q_t obtained above were used in eq (6) (more specifically, eq (A7)) to calculate values of $\rho'_v(\lambda)$,

the Van den Akker reflectance of the sphere wall in its entirety. The random error in ρ_v' is obtained from eq (6) as

$$\delta\rho_v' = [((1 - Q_d/Q_s)/(1 - f)^2)^2\delta f^2 + ((f/Q_s)/(1 - f))^2\ \delta Q_t^2 + ((fQ_d/Q_s^2)/(1 - f))^2\ \delta Q_s^2]^{1/2}. \quad (24)$$

The systematic error in ρ_v' is given similarly by:

$$\Delta\rho_v' = [((1 - Q_d/Q_s)/(1 - f)^2)^2\Delta f^2 + ((fQ_d/Q_s^2)/(1 - f))^2\Delta Q_s^2]^{1/2} \quad (25)$$

where ΔQ_s is only that portion of the systematic uncertainty in Q_s given by eq (21). Note that the contribution to the systematic error in Q_s and Q_t due to systematic errors in the DRS are omitted because these errors are very small [21] and because they tend to cancel when the ratio Q_d/Q_s is taken in determining ρ_v' from eq (6). Therefore there is no ΔQ_t term in eq (25).

2. From Uncorrected Van den Akker Reflectance ρ_v' to Corrected Van den Akker Reflectance ρ_v

The quantity ρ_v' as determined in the preceding section is the average Van den Akker reflectance of the sphere wall. In order to obtain the Van den Akker reflectance of a thick coating of the sphere wall material, it is necessary to correct ρ_v' for the effect of the crack around the removable target section and for translucency in the sphere wall coating.

a. The Gap Around the Target

Since the target portion of the sphere is removable, there is a narrow gap in the sphere wall around the target. The gap acts as a light pipe between two aluminum surfaces, so that the effective reflectance of the gap is essentially zero. Therefore, in order to relate the measured Van den Akker reflectance ρ_v' to the Van den Akker reflectance ρ_v of the wall coating, the loss in the gap must be accounted for:

$$\rho_v = \frac{\rho_v'}{k_t\,[1 - 2r_tW/(4R^2 - r^2)]} \quad (26)$$

where r_t is the radius of the target, W is the width of the gap, r is the radius of the entrance port, and k_t is a transluency correction factor as determined in section IV. A.2.b. below. The systematic error associated with the crack correction is estimated to be one-half the magnitude of the correction. The total systematic error in ρ_v is given by

$$\Delta\rho_v = \rho_v\left[\left(\frac{\Delta\rho_v'}{\rho_v'}\right)^2 + \left(\frac{\Delta k_t}{k_t}\right)^2 + \left(\frac{r_tW}{4R^2 - r^2}\right)^2\right]^{1/2}. \quad (27)$$

b. Translucency of the Wall Coating

The relative reflectance as a function of thickness was measured at each of three wavelengths on samples of each type of coating material. The results of these measurements are depicted in figure 4. The coating in the sphere is, on the average, about 4 mm thick, so that the reflectance of a barium sulfate sphere wall is equal to the reflectance in the limit of a very thick wall, ρ_∞ [22]. Therefore, for these coatings $k_t = 1$. However, in the case of Halon, the wall is not thick enough and a correction was made based on the data in figure 4. In this correction, the thickness of the coating at any point was taken to be the distance from the surface to the aluminum substrate at that point, and a translucence correction factor k_t was obtained by a calculation having the following form:

$$k_t = \frac{\int \frac{\rho_x}{\rho_{10}}\,dA}{\int dA} \quad (28)$$

where ρ_x is the relative reflectance for the coating thickness at a given point,

ρ_{10} is the relative reflectance for a 10 mm thick coating (assumed equal to ρ_∞),

dA is an element of the sphere wall area,

and the integral is taken over the entire area of the sphere wall.

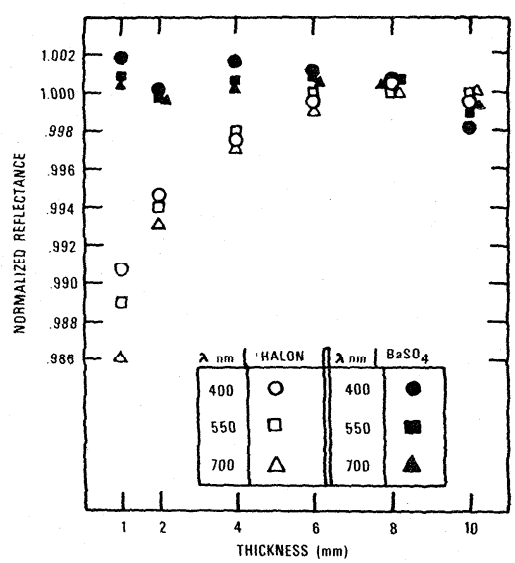

FIGURE 4. *Reflectance of wall coatings as function of thickness.*
(Normalized to give a reflectance of approximately 1 for thick samples.)

It is estimated that the coating thickness measurements might have been in error by as much as 1/2 mm for the 4 mm thickness. Therefore the calculation of eq (28) was redone using 3.5 and 4.5 mm for the average coating thickness over the main sphere wall in order to obtain an estimate of the random uncertainty δk_t of this correction. An expression for

the random error in ρ_v as given by eq (26) is

$$\delta\rho_v = \rho_v\left[\left(\frac{\delta\rho_v'}{\rho_v'}\right)^2 + \left(\frac{\delta k_t}{k_t}\right)^2\right]^{1/2} \tag{29}$$

Since using the distance from the coating surface to the aluminum substrate as its thickness is only a rough approximation in the regions of the port and of the target boundary, a systematic error will be introduced by that approximation. An estimation of this uncertainty was obtained by calculating $k_t' = \rho_4/\rho_{10}$, and estimating the systematic error as $(k_t' - k_t)/2$. We assumed the translucency correction to be approximately independent of wavelength. The data in figure 4, for 1 mm thickness indicates that this may not be exactly correct. Therefore, there may be a wavelength dependent systematic error of approximately ± 0.0005 in k_t, with the positive error associated with short wavelengths and the negative error with long wavelengths.

The Halon coatings used in our apparatus had a density of 0.8 g cm^{-3}. Grum [23] refers to a coating of Halon which is opaque at 2 mm thickness. However, from the description of the pressure under which the coating was formed, his coatings are probably much denser than ours.

3. Sample Curvature and Sphere Size

Questions have been raised concerning the effect of the size of the sphere upon the Van den Akker reflectance. Possible errors may arise due to the inability of the measuring instrument to properly compare the reflectance of curved and flat surfaces, either due to the difference in the relative areas of the port and the remainder of the sphere wall or due to a change in the reflectance of the wall coating with curvature. This question has been addressed experimentally in two different ways. The relative $6°/h$ reflectance of curved and flat samples was measured directly. The average relative reflectance at 550 nm of four concave $BaSO_4$[14] samples from the first determination was 0.9826 ± 0.0027 and the average reflectance of two flat samples of the same material was found to be 0.9834, and the uncertainty is probably of the same order of magnitude. The difference of 0.0008 is probably not significant.

In the second test, the Van den Akker reflectance was determined using two different sized spheres, one with a 95 mm interior radius and the other with a 146 mm interior radius. Both spheres were coated with the type of $BaSO_4$ [6] used in the third determination. The Van den Akker reflectances for these two determinations are given in table III. It can be seen that there is no significant difference between the results from the two spheres.

4. Results and Error Analysis

The Van den Akker reflectances ρ_v determined for each coating at twenty-five nanometer intervals over the wavelength range 400 nm to 750 nm are given in tables IV, V and VI, and are pictured in figure 5. A listing of typical values used in the calculations for the Van den Akker reflectance is shown in table VII, and representative calculations of the random and systematic uncertainties in ρ_v are presented in tables VIII and IX respectively. The only known wavelength dependency of these uncertainties is in the random errors.

TABLE III

Comparison of the Van den Akker reflectance of ρ_v of the walls of two different size spheres coated with $BaSO_4$ [16].

Wavelength (nm)	Sphere radius R		Difference in ρ_v
	14.6 cm	9.5 cm	
400	0.9744	0.9744	0
425	.9771	.9769	0.0002
450	.9789	.9788	.0001
475	.9802	.9801	.0001
500	.9813	.9812	.0001
525	.9823	.9821	.0002
550	.9829*	.9828	.0001
575	.9834	.9832	.0002
600	.9836	.9835	.0001
625	.9838	.9836	.0002
650	.9838	.9836	.0002
675	.9837	.9836	.0001
700	.9836	.9835	.0001
725	.9835	.9833	.0002
750	.9832	.9831	.0001

* For this value, $\epsilon\rho_v = 2.1 \times 10^{-4}$.

TABLE IV

First Determination $BaSO_4$ [14]

Wavelength (nm)	Van den Akker Reflectance ρ_v	$\rho(6°, \lambda)$	$F(6°, \lambda)$
400	0.9661	0.9606	0.9599
425	.9688	.9638	.9631
450	.9721	.9675	.9668
475	.9744	.9703	.9696
500	.9767	.9728	.9721
525	.9788	.9752	.9745
550	.9806†	.9774*	.9767@
575	.9823	.9793	.9786
600	.9835	.9807	.9800
625	.9845	.9818	.9811
650	.9852	.9826	.9819
675	.9858	.9834	.9827
700	.9864	.9840	.9833
725	.9869	.9846	.9839
750	.9873	.9850	.9843

† $\epsilon\rho_v$ is 2.3×10^{-4} ($\delta\rho_v = 2.1 \times 10^{-4}$ and $\Delta\rho_v = 1.1 \times 10^{-4}$).
* $\epsilon\rho$ is 9.8×10^{-4} ($\delta\rho = 9.5 \times 10^{-4}$ and $\Delta\rho = 2.3 \times 10^{-4}$).
@ $\epsilon\delta$ is 1.01×10^{-3} ($\delta F = 9.5 \times 10^{-4}$ and $\Delta F = 3.3 \times 10^{-4}$).

TABLE V

Second Determination Halon [15]

Wavelength (nm)	Van den Akker Reflectance ρ_v	$\rho(6°, \lambda)$	$F(6°, \lambda)$
400	0.9961	0.9930	0.9927
425	.9961	.9932	.9929
450	.9961	.9933	.9930
475	.9960	.9934	.9931
500	.9959	.9935	.9932
525	.9958	.9935	.9932
550	.9957†	.9935*	.9932@
575	.9956	.9935	.9932
600	.9955	.9935	.9932
625	.9954	.9935	.9932
650	.9952	.9934	.9931
675	.9951	.9934	.9931
700	.9950	.9933	.9930
725	.9949	.9932	.9929
750	.9948	.9931	.9928

† $\epsilon\rho_v$ is 9.0×10^{-4} ($\delta\rho_v = 7.3 \times 10^{-4}$ and $\Delta\rho_v = 5.1 \times 10^{-4}$).
* $\epsilon\rho$ is 9.6×10^{-4} ($\delta\rho = 7.9 \times 10^{-4}$ and $\Delta\rho = 5.5 \times 10^{-4}$).
@ ϵF is 9.7×10^{-4} ($\delta F = 7.9 \times 10^{-4}$ and $\Delta F = 5.6 \times 10^{-4}$).

TABLE VI

Third Determination $BaSO_4$ [16]

Wavelength (nm)	Van den Akker Reflectance ρ_v	$\rho(6°, \lambda)$	$F(6°, \lambda)$
400	0.9744	0.9695	0.9688
425	.9771	.9732	.9725
450	.9789	.9757	.9750
475	.9802	.9775	.9768
500	.9813	.9791	.9784
525	.9823	.9804	.9797
550	.9829†	.9813*	.9806@
575	.9834	.9819	.9812
600	.9836	.9822	.9815
625	.9838	.9824	.9817
650	.9838	.9824	.9817
675	.9837	.9822	.9815
700	.9836	.9819	.9812
725	.9835	.9815	.9808
750	.9832	.9808	.9801

† $\epsilon\rho_v$ is 2.3×10^{-4} ($\delta\rho_v = 2.1 \times 10^{-4}$ and $\Delta\rho_v = 1.1 \times 10^{-4}$).
* $\epsilon\rho_v$ is 2.1×10^{-3} ($\delta\rho = 2.1 \times 10^{-3}$ and $\Delta\rho = 2.3 \times 10^{-4}$).
@ϵF is 2.1×10^{-3} ($\delta F = 2.1 \times 10^{-3}$ and $\Delta F = 3.3 \times 10^{-4}$).

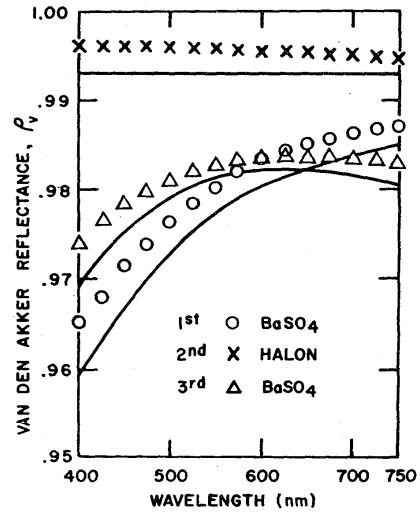

FIGURE 5. *Van den Akker reflectance of three coatings.*
(The height of the symbols × represent the total uncertainty. Height of the symbols 0 and Δ represents approximately 4 times the total uncertainty.) The associated solid curves show $\rho(6°, \lambda)$ for each coating.

The smallest random error is in the central region of the spectrum, where the product of the source intensity and the receiver sensitivity is maximum. At the short wavelength end of the spectrum, there is an increase in uncertainty in Q_t and Q_s associated with a decrease in source intensity, while at the long wavelength end of the spectrum there is an increase in uncertainty associated with a decrease in receiver sensitivity. However, because the random error associated with f dominates the overall uncertainty, we will cite only error figures at 550 nm for ρ_v as representing the entire spectrum.

The total uncertainty in determining the Van den Akker reflectance is obtained by adding the random and systematic uncertainties in quadrature. The total uncertainty in the Van den Akker reflectance is 0.0002 for the $BaSO_4$ coating. It can be seen that this uncertainty is very small, confirming the results of the error analysis by Goebel, et al., [2]. The larger uncertainty for the Halon coating is due to the transluscence of the coating and is introduced in the extrapolation to the reflectance of a thick enough layer rather than being caused by an uncertainty in the measurement. This additional uncertainty would not exist if the Halon coating were twice as thick.

B. Adjustment from Van den Akker Reflectance $\rho_v(\lambda)$ to 6°/h Reflectance $\rho(6°, \lambda)$

The second main step is the transition from $\rho_v(\lambda)$ to $\rho(6°, \lambda)$. As was pointed out in section III, this step is an intrinsic part of the determination which is needed because the sphere coating is a real material and not an ideal Lambertian reflector. For this reason it is not proper to regard this step as a correction. However, for the type of sphere coatings being examined, the departure from Lambertian reflection is small and the difference between ρ_v and ρ is small. For this reason, we will refer to the transition step from ρ_v to ρ as an adjustment in order to emphasize the small size of the change with respect to the quantity being changed.

TABLE VII

Typical Values Used in Calculating the Van den Akker Reflectance ρ_v (λ = 550 nm) for $BaSO_4$ [14].

Symbol	Reference Equation	Value	Comments
(a) r	(16)	12.70 mm	measured with inside caliper and micrometer.
(b) R	(16)	146 mm	measured with steel rule.
(c) f	(16)	1.90×10^{-3}	calculated using r and R above.
(d) Q'_s	(19)	8.731×10^{-2}	measured reflectance of auxiliary sphere.
(e) Q_p	(19)	1.24×10^{-3}	measured with stainless port open to dark room.
(f) Q_f	(19)	7.0×10^{-1}	measured reflectance of stainless steel port plate.
(g) ω_e	(19)	3.78×10^{-2} radians	calculated from dimensions of port structure [17].
(h) Q_s	(19)	8.630×10^{-2}	calculated using Q'_s, Q_p, Q_f, and ω_e above.
(i) Q'_t	(21)	9.832×10^{-1}	measured reflectance of target.
(j) Q_e	(21)	1.36×10^{-4}	measured with reflectometer port open into dark room.
(k) Q_t	(21)	9.831×10^{-1}	calculated using Q'_t and Q_e above.
(l) ρ_v	(6) and (A7)	9.805×10^{-1}	calculated using f, Q_s and Q_t from lines (c), (h) and (k) above respectively.
(m) r_t	(26)	25.4 mm	measured with micrometer caliper.
(n) W	(26)	0.17 mm	measured with traveling microscope.
(o) k_t	(26)	1 (0.9974)	$BaSO_4$ (Halon determination only).
(p) ρ_v	(26)	9.806×10^{-1}	calculated using ρ'_v, r_t, W, and k_t above.

TABLE VIII

Calculation of the Random Error in the Van den Akker Reflectance

Symbol	Reference Equation	Value	Comments
(a) δR	(17)	.8 mm	Uncertainty in packing sphere coating to constant radius.
(b) δf	(17)	2×10^{-5}	Calculated from δR above.
(c) $\delta Q'_s$	(20)	7×10^{-5}	Uncertainty from 3 measurements.
(d) δQ_p	(20)	7×10^{-5}	Roundoff uncertainty.
(e) δQ_s	(20)	1×10^{-4}	Calculated from $\delta Q'_s$ and δQ_p as given above.
(f) $\delta Q'_t$	(23)	2×10^{-4}	See comment on (d) above.
(g) δQ_e	(23)	7×10^{-5}	See comment on (d) above.
(h) δQ_t	(23)	2.1×10^{-4}	Calculated from $\delta Q'_t$ and δQ_e above.
(i) $\delta \rho'_v$	(25)	2.1×10^{-4}	Calculated from δf, δQ_s, and ΔQ_t from (c), (g) and (j) above.
(j) δk_t	(27)	(7×10^{-4})*	Corresponds to an uncertainty in coating thickness of 0.5 mm.
(k) $\delta \rho_v$	(27)	2.1×10^{-4} (7.3×10^{-4})*	Calculated from $\delta \rho'_v$ and δk_t above.

* Halon coating only.

TABLE IX

Calculation of the Systematic Error in the Van den Akker Reflectance

Symbol	Applicable Equation	Value	Comments
(a) Δr	(18)	0.03 mm	Uncertainty in measuring port ±.01 mm. Another contribution is uncertainty in amount scattered back from port lip, which is estimated.
(b) Δf	(18)	9×10^{-6}	Calculated from Δr above.
(c) $\Delta \omega_e$	(21)	2×10^{-3} rad	
(d) ΔQ_s	(21)	1.1×10^{-4}	Calculated from $\Delta \omega_e$ above and from Q_f, ω_e, and Q_s from entries (f), (g) and (h) in table VII.
(e) $\Delta \rho'_v$	(25)	9.7×10^{-5}	Calculated from Δf and ΔQ_s from (b) and (d) above.
(f) Δk_t	(27)	(5×10^{-4})*	Wavelength dependent error ±.0005 estimated from fig. 4; uncertainty due to tapered edges of coating ±0.0001.
(g) $\frac{r_t W}{(R^2 + r^2)}$	(27)	5×10^{-5}	Calculated using R, r, r_t, W from (a), (b), (m), and (n) in table VII.
(h) $\Delta \rho_v$	(27)	1.1×10^{-4} (5.1×10^{-4})*	Calculated using $\Delta \rho'_v$, Δk_t, and the gap uncertainty as given in (e), (f) and (g) above respectively.

* Halon coating only.

1. Determining the Relative Self-Radiance $N_g(\gamma)/\cos\gamma$

For each type of sphere coating, the relative self-radiance $N_g(\gamma)/\cos\gamma$ was determined as a function of angle of emergence. A 75 mm radius sphere was coated using the same procedure as was used when coating the spheres for the Van den Akker reflectance determinations. This sphere was irradiated through its single port and the flux emitted from the port past a knife-edge was observed at a number of angles. The geometry of this measurement is illustrated in figure 6. The instrument used was the NBS-Gaertner goniophotometer illustrated in figure 7. The source aperture permitted collimation to within 0.25° of the optical axis, and the receiver was collimated to within 0.6° of the optic axis. All three coatings were measured with a V_λ-illuminant C [24] spectral weighting, the centroid of which falls at approximately 550 nm. In addition, the coatings from the second and third determinations were measured using a 550 nm low pass interference filter, which resulted in a centroid of spectral weighting at 450 nm, and using a 600 nm high pass filter which resulted in a centroid spectral weighting at approxi-

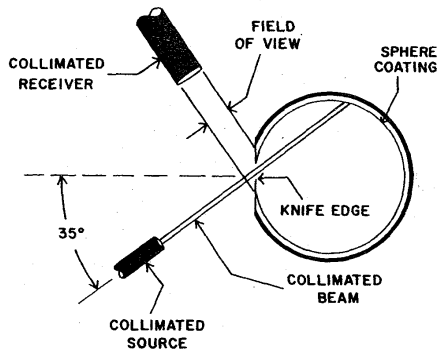

FIGURE 6. *Arrangement of knife-edge apparatus for measuring $N_g(\gamma)$.*

mately 700 nm. No distinction between the measurements under different spectral weightings were observed, indicating that $L_s(\gamma)$ depends principally on the geometrical nature of the surface. The relative magnitude of the observed flux divided by the cosine of the observation angle is shown in figure 8. Also shown in figure 8 are measurements made by scanning, with a telescopic detector, the interior of a 20 cm radius sphere coated with Halon. These latter measurements, believed to be much more accurate (± 0.001) than the knife-edge measurements, extend only to 45°. Because of the method used to produce the coating by hammering, there is reason to expect an increase in $N_g(\gamma)/\cos(\gamma)$ as γ approaches 90° because of a slight glossiness in the surface. However, it appears that this effect is not nearly as great as the measurements using the knife-edge indicate. Two possible sources for the difficulties at large γ are reflections from the corner of the knife-edge and scattered light from the receiver optics. At large γ, the flux to be measured is small, so that small amounts of stray radiation can cause large errors. Fortunately, this uncertainty in $N_g(\gamma)/\cos\gamma$ results in only a small uncertainty in determining $C(\Gamma, \lambda)$. A discussion of our

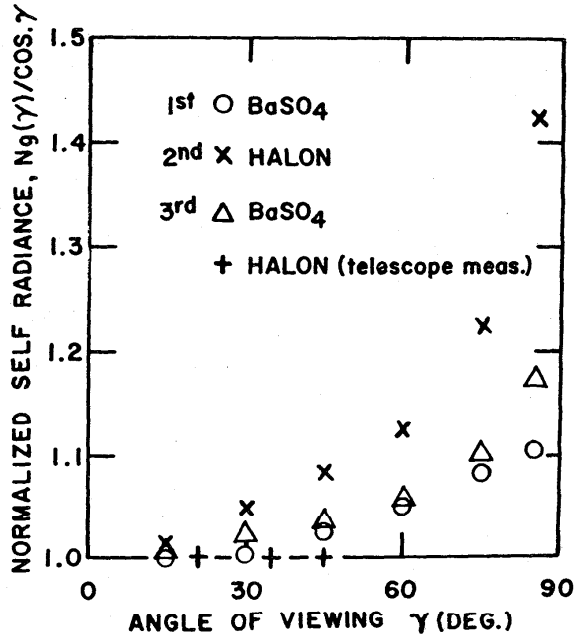

FIGURE 8. *Normalized self-radiance at 550 nm for each of three coating materials.*

choice of function to represent $N_g(\gamma)$ will be deferred to part IV.B.3 in which $C(\Gamma, \lambda)$ is calculated.

2. Determining the Relative Directional-Hemispherical Reflectance $N_G(\Gamma)$

The relative directional-hemispherical reflectance of a sample of each of the three coatings was measured with the

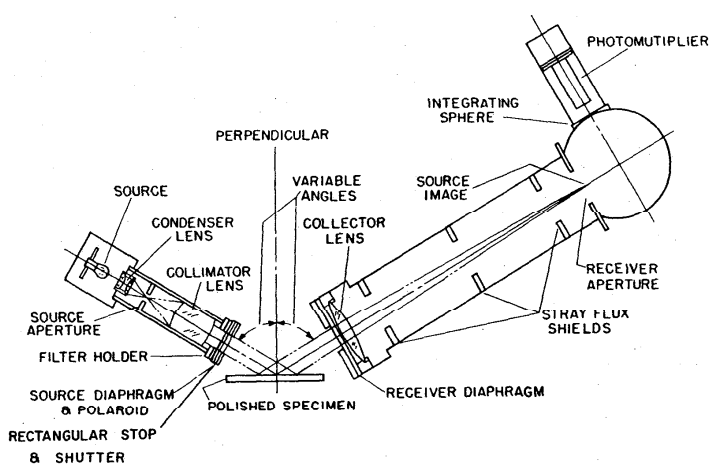

FIGURE 7. *NBS-Gaertner goniophotometer.*

DRS using the special measurement accessory apparatus for this purpose [12]. A diagram of this measurement accessory is reproduced from that reference in figure 9. The reflectance values were measured for radiation polarized with the electric vector in the plane of incidence and perpendicular to the plane of incidence. The average of the relative reflectance for the two polarizations was determined as a function of angle of incidence for each material for each of three wavelengths, 450 nm, 550 nm, and 750 nm. The data were fitted with a quadratic function, using a least-squares fitting program, to obtain the $N_G(\Gamma, \lambda)$ shown in figure 10. These curves were used to determine the adjustment function $C(\Gamma, \lambda)$ of eq (12). The general trend is for the reflectance to increase as the angle of incidence approaches grazing. The amount of the increase is greater for the materials with lower reflectance.

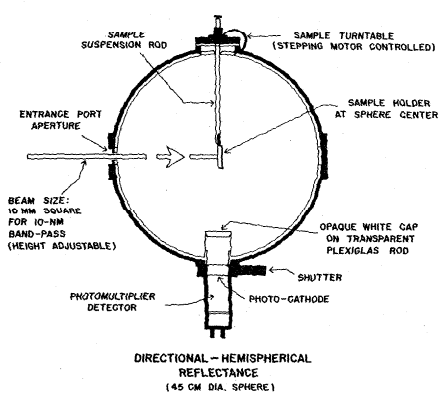

FIGURE 9. *Integrating sphere for measuring relative directional-hemispherical reflectance as a function of angle of incidence.*

3. Determining $C(\Gamma, \lambda)$

For each type of coating, the function C was evaluated using in eq (13) the $N_g(\gamma)$ and $N_G(\Gamma, \lambda)$ data from parts 1. and 2. above for each of the three wavelengths 450, 550, and 750 nm. Actually three sets of C were calculated for each of three interpretations of the highly uncertain data for $N_g(\gamma)$ in figure 8 above in order to evaluate the effect of that uncertainty. We wish to distinguish between the data taken from measurements of the radiance from the sphere wall and the interpretations of this data which are used as incident radiance values in calculating $C(\Gamma, \lambda)$. We will do this by using a lower case γ in $N_g(\gamma)/\cos\gamma$ to indicate the data obtained directly from the measurements and by using an uppercase Γ in $N_g(\Gamma)/\cos\Gamma$ to indicate the processed data used as the relative radiance distribution incident on the sphere wall when we calculate $C(\Gamma, \lambda)$. The first set of $C(\Gamma, \lambda)$ was calculated assuming that

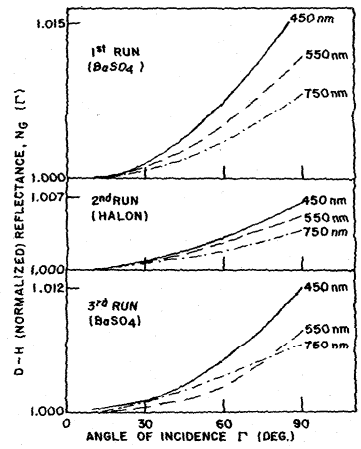

FIGURE 10. *Relative directional-hemispherical reflectance $N_g(\Gamma, \lambda)$ as a function of angle of incidence Γ for each of three coatings at three wavelengths.*

$N_g(\gamma)/\cos\gamma$ is independent of γ. This provides a lower limit on C. The second was calculated by using 1 for $N_g(\gamma)/\cos\gamma$ between 0 and 45°. To obtain the $N_g(\gamma)/\cos\gamma$ above 45° in this approximation, a straight line was drawn through the knife-edge experiment data from 0 to 45° and the amount by which the experimental data for greater than 45° fell above this line was added to 1 to obtain $N_g(\gamma)$. (See fig. 11 for a diagram illustrating this procedure for the Halon data in fig. 8.) The set of $N_g(\gamma)$ obtained in this way were consistent with the more accurate data from the telescopic detector scan and the $C(\Gamma, \lambda)$ calculated with these $N_g(\gamma)$ are used as the accepted values. Finally, as an upper limit, C's are calculated using the unmodified knife-edge experiment data given in figure 8. The functions $C(\Gamma, \lambda)$ corresponding to the accepted values, are plotted against Γ for each of the three materials at each of three wavelengths in figure 12. (See appendix C for details of the calculations leading to this figure.)

Since the goal of this section is to determine $\rho(6°, \lambda)$ at 25 nm intervals over the wavelength range 400 nm $\leq \lambda \leq$ 750 nm, we need values of $C(6°, \lambda)$ at these wavelengths. Since the large amount of data required would make impractical determining all of these values of $C(6°, \lambda)$ in the way described above, we choose to determine $C(6°, \lambda)$ from the data at the three wavelengths 450, 550, and 750 nm by interpolation and extrapolation. This determination is based on the definition of $C(6°, \lambda)$ which comes from eq (12)

$$C(6°, \lambda) = \frac{N_G(6°, \lambda)}{\bar{N}_G} - 1. \tag{30}$$

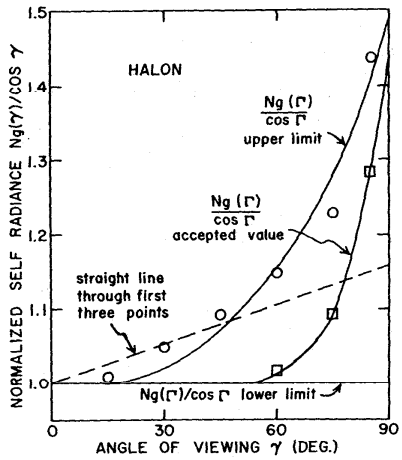

FIGURE 11. *An illustration of the three assumptions used in interpreting the $N_g(\gamma)$ data from the knife-edge determinations.*

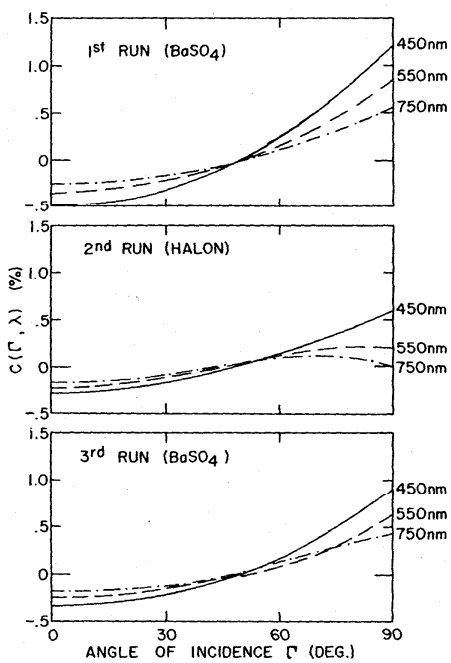

FIGURE 12. *$C(\Gamma, \lambda)$ as a function of Γ at three wavelengths for each of three coatings.*

Since the weighing to determine $\bar{N}_G(\lambda)$ is heaviest at 45°, it follows that

$$\bar{N}_G(\lambda) \simeq N_G(45°, \lambda). \tag{31}$$

Making use of this, we can write a correction factor $C'(6°, \lambda)$ which is a rough approximation to $C(6°, \lambda)$ as:

$$C'(6°, \lambda) = \frac{N_G(6°, \lambda)}{N_G(45°, \lambda)} - 1. \tag{32}$$

Since C and C' are approximately equal, their ratio is a smoothly varying function of wavelength. Therefore, we determined $J(\lambda)$ as

$$J(\lambda) = d_0 + d_1\lambda + d_2\lambda^2 \tag{33}$$

such that

$$J(\lambda) = \frac{C(6°, \lambda)}{C'(6°, \lambda)} \tag{34}$$

at the wavelengths 450 nm, 550 nm and 750 nm. We then determined $C(6°, \lambda)$ at other wavelengths as

$$C(6°, \lambda) = J(\lambda)C'(6°, \lambda) \tag{35}$$

where $C'(6°, \lambda)$ is calculated from expression (32) using values of $N_G(6°, \lambda)$ and $N_G(45°, \lambda)$ measured with the relative d/h reflectance instrument [12]. The values of $C(6°, \lambda)$ so determined are plotted in fig. 13.

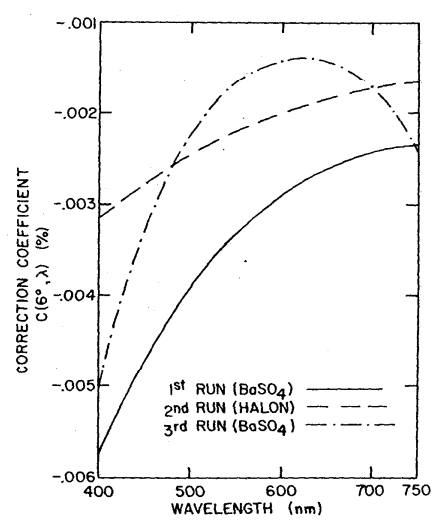

FIGURE 13. *$C(6°, \lambda)$ as a function of wavelength for each of three coatings.*

4. Results and Error Analysis

The three sets of values for $C(6°, \lambda)$ determined above were used in eq (12) to calculate $\rho(6°, \lambda)$ for the three wall materials. The results of this calculation are shown in the third columns of tables IV, V and VI and by the line curves in fig. 5.

From eq (12) one can determine a propagation of error formula for the random error $\delta\rho(6°, \lambda)$ as:

$$\delta\rho(6°, \lambda) = [\delta\rho_v(\lambda)^2 + \delta N_G(6°, \lambda)^2 + \delta\bar{N}_G(\lambda)^2]^{1/2}. \quad (36)$$

In this form ρ_v, N_G and $\bar{N}_G$ are each assumed to be 1, and errors common to N_G and $\bar{N}_G$ are ignored, since these will effectively cancel when the ratio is taken. Therefore the only errors to be included in eq (36) are the independent errors in the various quantities. The principal independent uncertainty in $\bar{N}_G$ is that due to the uncertainty in the self-radiance measurements as shown in appendix C. The principal random uncertainty in N_G is due to the noise in the d/h data. Since the value of $N_G(6°, \lambda)$ was obtained through a rather indirect procedure involving curve fitting, it is difficult to establish a good theoretical basis for the error estimate. Therefore, we sought a reproducible way of estimating the error which depended as little as possible on arbitrary judgment. Since most of the curves involved fitting through ten to fifteen points with a quadratic function with two independent parameters, there is almost no likelihood that a point taken from the curve will depart from the most probable value by more than the root mean square deviation of the individual points with respect to the curve. Therefore, we will use this deviation as the estimated random uncertainty. In determining N_G, two such fittings are involved, one to the original data as a function of angle and one to the $C(\lambda)$ data used in the interpolation. A summary of the random error analysis for the $\rho_v(\lambda)$ to $\rho(6°, \lambda)$ adjustment is given in table X.

The only source of systematic error which we have identified for this adjustment step is an uncertainty in the measurement of N_G due to the correction which is made for the entrance port of the reflectometer. This results in an uncertainty in $C(\Gamma, \lambda)$ of 2×10^{-4} independent of wavelength.

The total uncertainty in $\rho(6°, \lambda)$ for a given determination is obtained by adding $\delta\rho(6°, \lambda)$ and $\Delta\rho(6°, \lambda)$ in quadrature. The additional uncertainty introduced in making the adjustment from $\rho_v(\lambda)$ to $\rho(6°, \lambda)$ is of the same order of magnitude as the uncertainty in $\rho_v(\lambda)$ itself. Particularly noteworthy is the large increase in uncertainty in the third determination. The barium sulfate used in this determination had a rather "sticky" consistency which made it difficult to pack it into a uniform smooth surface, and this may have had an effect upon the noise in the $N_G(\Gamma, \lambda)$ data from this surface.

C. Adjustment from d/h Reflectance $\rho(6°, \lambda)$ to d/h Reflectance Factor $F(6°, \lambda)$

In order to determine the bidirectional reflectance factor in the retroreflective direction, apparatus was set up as customarily used for measuring the coefficient of luminous intensity of retroreflective sheeting (See fig. 14). Since the retroreflectance of the sphere coatings is essentially spectrally nonselective over the visible wavelength range [13] we measured the luminous reflectance factor for CIE illuminant A as being representative of the entire spectrum to within the uncertainty of the retroreflectance measurements.

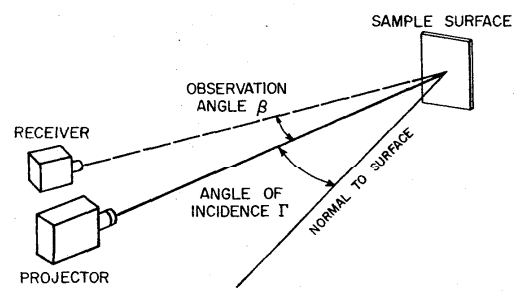

FIGURE 14. *Diagram of apparatus used in retroreflectance measurements.*

TABLE X

Calculation of the errors in the $\rho_v(\lambda)$ to $\rho(6°, \lambda)$ adjustment (See equation (36) and the accompanying discussion).

Symbol	$BaSO_4$ [14]	Halon [15]	$BaSO_4$ [16]	Comments
(a) $\delta\rho_v$	2.1×10^{-4}	7.3×10^{-4}	2.1×10^{-4}	See Table VIII.
(b) $\delta\bar{N}_G(\lambda)$	0.5×10^{-4}	0.5×10^{-4}	0.5×10^{-4}	See Appendix C.
(c) $\delta N_g(6°, \lambda)$	7×10^{-4}	3×10^{-4}	20×10^{-4}	Component due to fitting angular data for $N_G(\Gamma, \lambda)$.
(d) $\delta N_g(6°, \lambda)$	6×10^{-4}	3×10^{-4}	5×10^{-4}	Component due to fitting wavelength data to $C'(\lambda)$.
(e) $\delta N_g(6°, \lambda)$	9.2×10^{-4}	4.3×10^{-4}	21×10^{-4}	Quadrature combination of (c) and (d) above.
(f) $\delta\rho(6°, \lambda)$	9.5×10^{-4}	7.9×10^{-4}	21×10^{-4}	Quadrature combination of (a), (b) and (c) above.
(g) $\Delta\rho_v$	1.1×10^{-4}	5.1×10^{-4}	1.1×10^{-4}	See Table IX.
(h) ΔC	2×10^{-4}	2×10^{-4}	2×10^{-4}	Associated with d-h reflectometer port correction.
(i) $\Delta\rho(6°, \lambda)$	2.3×10^{-4}	5.5×10^{-4}	2.3×10^{-4}	Quadrature combination of (g) and (h) above.

To make the measurements, the receiver was placed in the sample position and a signal N_R proportional to the normal illuminance I_R on the sample was measured.

$$N_R = k_R I_R. \tag{37}$$

The receiver was then moved to a position a distance d away from the sample and, on the same scale of measurement and using the same receiver aperture, signals $N_r(\beta)$, which is in the same way proportional to the illuminance $I(\beta)$ on the receiver due to the radiation reflected from the sample, was measured with the entire sample area A in view. From the basic definition for reflectance factor, it follows that the reflectance factor $F_\Gamma(\beta)$ can be determined from

$$F_\Gamma(\beta) = \frac{N_r(\beta)}{N_R} \frac{A}{d^2 \cos(\Gamma) \cos(\Gamma + \beta)}. \tag{38}$$

The value of $F_{6°}(\beta)$ so determined as a function of observation angle β is given for $BaSO_4$ and for Halon in fig 15. (See appendix A, sec. A.2 for further discussion of these data and the evaluation of the integrals.) The retroreflectance factor $F_{6°}(\beta)$ was found to be essentially independent of the angle which the plane of observation makes with respect to the plane of incidence. Therefore, the integral in eq (13) becomes

$$\int^{\omega'} F(\mathbf{U}, \mathbf{u}) \cos\gamma \, d\omega = 2\pi \cos 6° \int_0^{r/d'} F_{6°}(\beta)\beta \, d\beta \tag{39}$$

and ω' in (13) becomes

$$\omega' = 2\pi \int_0^{r/d'} \beta \, d\beta \tag{40}$$

where r is the radius of the reflectometer entrance port and d' is the distance in the reflectometer sphere from the sample to the plane of the entrance port. The $\rho(6°, \lambda)$ data were adjusted to $F(6°, \lambda)$ using eq (13). In general, the difference $\rho(6°, \lambda) - F(6°, \lambda)$ is 0.0007 for $BaSO_4$ and 0.0003 for Halon. The estimated systematic uncertainty in this adjustment is approximately one-third of its value in each case. These uncertainties, added in quadrature with the uncertainties in $\rho(6°, \lambda)$ yield the total systematic uncertainty in $F(6°, \lambda)$. The values of $F(6°, \lambda)$ for the three coatings are given in the third columns of tables IV, V, and VI.

D. Determining the d/h Reflectance Factor of Working Standards

The d/h reflectance factor $F(6°, \lambda)$ determined in IV.C. above is the average for the wall coating used in the Van den Akker sphere. Since this coating is neither permanent nor readily accessible, the reflectance factor $F_c(6°, \lambda)$ is determined for working standards made of glass, ceramic, or some other permanent material. The value of F_c is assigned as indicated in eq (14) and the accompanying text. Specifically, we will denote by $F_{c,j}(6°, \lambda)$ the reflectance factor for standard c as obtained from the jth determination. Equation (14) takes the form:

$$F_{c,j} = \frac{Q_c}{\bar{Q}_j} F_j \tag{41}$$

where

$F_j \equiv F_j(6°, \lambda)$ is the reflectance factor for the jth wall coating,

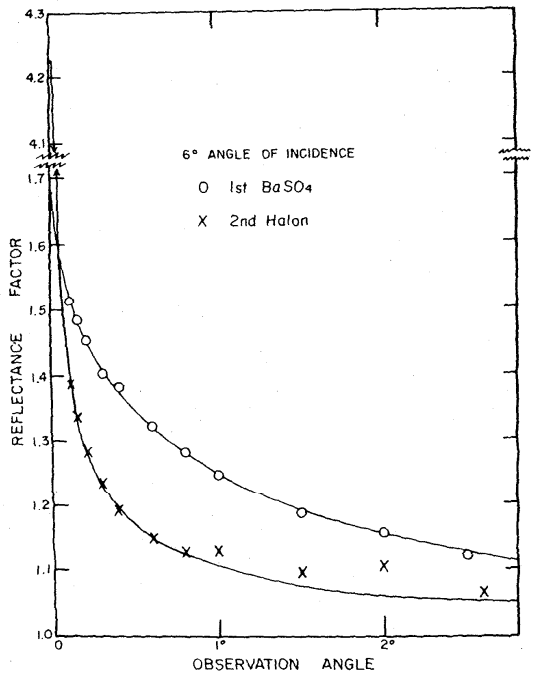

FIGURE 15. *Retroreflective bidirectional reflectance factor for 6° incidence as a function of observation angle.*

Q_c is the measured relative reflectance of working standard c, and

$\bar{Q}_j$ is the average of the measured relative reflectance for several representative samples of the jth wall coating.

The relative reflectances Q_c and $\bar{Q}_j$ were found by experiment to be independent of the polarization of the incident radiation for the working standards and sphere coatings used. It follows that the random error in $F_{c,j}$ is given by:

$$\delta F_{c,j} = F_{c,j}\left[\left(\frac{\delta Q_c}{Q_c}\right)^2 + \left(\frac{\delta \bar{Q}_j}{\bar{Q}_j}\right)^2 + \left(\frac{\delta F_j}{F_j}\right)^2\right]^{1/2}. \tag{42}$$

The largest new contribution to the uncertainty which is introduced in this step is $\delta\bar{Q}_j$. This is due to the variability between the representative samples and the resulting uncertainty in whether these samples properly represent the sphere coating. If the values of Q_c and $\bar{Q}_j$ differ significantly a small correction for instrument non-linearity must be made in the ratio $Q_c/\bar{Q}_j$. With this non-linearity is associated a small contribution to the systematic uncertainty.

$$\Delta F_{c,j} = F_{c,j}\left[\left(\frac{\Delta(Q_c/\bar{Q}_j)}{(Q_c/\bar{Q}_j)}\right)^2 + \left(\frac{\Delta F_j}{F_j}\right)^2\right]^{1/2}. \tag{43}$$

Three different working standards are currently used. These are identified and described in appendix D. The values of $F_{c,j}$ for each of these standards for each of three determinations are given in tables XI, XII and XIII, and sample calculations for the uncertainties appear in table XIV.

TABLE XI

Reflectance Factor of Working Standard 1
(Russian Opal Glass, Polished)

Wavelength (nm)	$F_{1,1}$	$F_{1,2}$	$F_{1,3}$	$\bar{F}_{1,2}$	$\bar{F}_{1,3}$
400	0.9793	0.9734	0.9738	0.9759	0.9753
425	0.9781	0.9739	0.9743	0.9756	0.9753
450	0.9803	0.9765	0.9779	0.9781	0.9781
475	0.9841	0.9807	0.9812	0.9822	0.9819
500	0.9854	0.9823	0.9846	0.9836	0.9838
525	0.9856	0.9821	0.9845	0.9836	0.9838
550	0.9837	0.9813	0.9830	0.9823	0.9835
575	0.9810	0.9785	0.9805	0.9796	0.9798
600	0.9792	0.9761	0.9785	0.9775	0.9777
625	0.9777	0.9742	0.9769	0.9757	0.9760
650	0.9770	0.9745	0.9774	0.9756	0.9761
675	0.9771	0.9751	0.9772	0.9759	0.9763
700	0.9761	0.9736	0.9761	0.9747	0.9750
725	0.9742	0.9718	0.9741	0.9728	0.9732
750	0.9716	0.9687	0.9711	0.9699	0.9702
δ	2.2×10^{-3}	1.6×10^{-3}	2.7×10^{-3}	1.3×10^{-3}	1.2×10^{-3}
Δ	3.3×10^{-4}	5.5×10^{-4}	3.3×10^{-4}	5.5×10^{-4}	5.5×10^{-4}
ϵ	2.2×10^{-3}	1.7×10^{-3}	2.7×10^{-3}	1.4×10^{-3}	1.3×10^{-3}
w	4.5	6.0	3.7	—	—
W	—	—	—	10.5	14.2

TABLE XII

Reflectance Factor of Working Standard 2
(Vitrolite)

Wavelength (nm)	$F_{2,1}$	$F_{2,2}$	$F_{2,3}$	$\bar{F}_{2,2}$	$\bar{F}_{2,3}$
400	0.9100	0.9049	0.9049	0.9071	0.9065
425	.8944	.8901	.8907	.8920	.8916
450	.9006	.8977	.8981	.8990	.8987
475	.9140	.9116	.9083	.9126	.9114
500	.9192	.9169	.9178	.9179	.9179
525	.9242	.9204	.9226	.9221	.9222
550	.9245	.9222	.9243	.9232	.9235
575	.9215	.9190	.9213	.9201	.9204
600	.9160	.9125	.9155	.9140	.9145
625	.9099	.9066	.9085	.9080	.9082
650	.9050	.9027	.9043	.9037	.9039
675	.9035	.9013	.9040	.9023	.9028
700	.9010	.8991	.8999	.8999	.8999
725	.8959	.8939	.8953	.8948	.8949
750	.8893	.8867	.8882	.8878	.8879
δ	2.2×10^{-3}	1.6×10^{-3}	2.3×10^{-3}	1.3×10^{-3}	9.8×10^{-4}
Δ	3.2×10^{-4}	5.3×10^{-4}	3.2×10^{-4}	5.3×10^{-4}	5.3×10^{-4}
ϵ	2.2×10^{-3}	1.7×10^{-3}	2.4×10^{-3}	1.4×10^{-3}	1.1×10^{-3}
w	4.5	5.9	4.2	—	—
W	—	—	—	10.4	14.6

The systematic uncertainty associated with the F_c for a particular standard is, by definition, independent of the number of determinations which are made. However, the random uncertainty associated with a given F_c can be reduced by taking the average of the F_c's from a number of determinations. We maintain a running weighted average $\bar{F}_{c,j}$ of the results of all determinations from 1 through j by means of the calculation

$$\bar{F}_{c,j} = \frac{W_{c,j-1}\bar{F}_{c,j-1} + w_{c,j}F_{c,j}}{W_{c,j}} \tag{44}$$

where the weighting factor $w_{c,j}$ for the jth determination of F_c is

$$w_{c,j} = 1/100\ \epsilon F_{c,j} \tag{45}$$

where $\epsilon F_{c,j}$ is the total uncertainty in $F_{c,j}$ as is given in appendix B. The weighting factor $W_{c,j}$ for the average of the j determinations is

$$W_{c,j} = \sum_{i=1}^{j} w_{c,i}\,. \tag{46}$$

TABLE XIII

Reflectance Factor of Working Standard 3
(Porcelain Enamel 80-1)

Wavelength (nm)	$F_{3.1}$	$F_{3.2}$	$F_{3.3}$	$\bar{F}_{3.2}$	$\bar{F}_{3.3}$
400	0.7615	0.7573	0.7571	0.7591	0.7585
425	.7936	.7911	.7915	.7922	.7920
450	.8042	.8019	.8034	.8029	.8030
475	.8093	.8072	.8073	.8081	.8079
500	.8105	.8078	.8101	.8090	.8093
525	.8104	.8091	.8096	.8096	.8096
550	.8090	.8083	.8094	.8086	.8088
575	.8063	.8045	.8071	.8053	.8058
600	.8030	.8017	.8032	.8022	.8025
625	.7990	.7969	.7994	.7978	.7983
650	.7949	.7937	.7960	.7942	.7947
675	.7926	.7911	.7925	.7917	.7919
700	.7909	.7900	.7927	.7904	.7910
725	.7885	.7869	.7886	.7875	.7878
750	.7855	.7839	.7860	.7846	.7850
δ	2.1×10^{-3}	1.5×10^{-3}	2.3×10^{-3}	1.3×10^{-3}	1.1×10^{-3}
Δ	3.0×10^{-4}	4.7×10^{-4}	3.0×10^{-4}	4.7×10^{-4}	4.7×10^{-4}
ϵ	2.2×10^{-3}	1.6×10^{-3}	2.3×10^{-3}	1.4×10^{-3}	1.2×10^{-3}
w	4.6	6.2	4.2	—	—
W	—	—	—	10.8	15.0

TABLE XIV

Calculation of the Uncertainties in the $\rho(6°,\lambda)$ to $F(6°,\lambda)$ and $F(6°,\lambda)$ to $F_{c,j}(6°, \lambda)$ steps as determined for Working Standard No. 2.

	Symbol	Value			Comments
		$BaSO_4$ [14]	Halon [15]	$BaSO_4$ [16]	
(a)	$\delta F(6°, \lambda)$ $(=\delta\rho(6°, \lambda))$	9.5×10^{-4}	7.9×10^{-4}	2.1×10^{-3}	See table X, entry (f).
(b)	F_j	0.9767	0.9932	0.9806	See tables IV, V, and VI.
(c)	δQ_c	2.7×10^{-4}	8.7×10^{-4}	3×10^{-4}	From three measurements in each determination.
(d)	Q_c	0.929833	0.931036	0.92922	Measured.
(e)	$\delta\bar{Q}_j$	2×10^{-3}	1.2×10^{-3}	1.2×10^{-3}	From measurements on a number of samples.
(f)	$\bar{Q}_j$	0.985022	1.00283	0.985982	Measured.
(g)	$\bar{F}_{2,j}$	.9245	0.9222	0.9243	Calculated from (b), (d) and (f) above in equation (41).
(h)	$\delta F_{2,j}$	2.2×10^{-3}	1.6×10^{-3}	2.3×10^{-3}	Calculated from equation (42) and (a) through (g) above.
(i)	$\Delta(Q_c/\bar{Q}_j)$ $(\simeq -\Delta\bar{Q}_j)$	-1×10^{-4}	-1×10^{-4}	-1×10^{-4}	From reference [17].
(j)	ΔF_j	3.3×10^{-4}	5.6×10^{-4}	3.3×10^{-4}	From tables IV, V, and VI.
(k)	$\Delta F_{2,j}$	3.2×10^{-4}	5.3×10^{-4}	3.2×10^{-4}	Calculate from equation (43) and (b), (d), (f), (i) and (j) above.
(l)	$\epsilon F_{2,j}$	2.2×10^{-3}	1.7×10^{-3}	2.4×10^{-3}	Quadrature combination of (i) and (k) above.
(m)	$w_{c,j}$	4.5	5.9	4.2	Calculate from equation (45) using (l) above.
(n)	$W_{c,j-1}$	—	10.4	14.6	Calculate from equation (46) using (m) above.
(o)	$\bar{F}_{c,j}$	—	0.9232	0.9235	Calculate from equation (44) using (g) and (m) above.
(p)	$\delta\bar{F}_{c,j}$	—	1.3×10^{-3}	9.8×10^{-4}	Calculate from equation (47) using (g), (m), (n), and (o) above.
(q)	$\Delta\bar{F}_{c,j}$	—	5.3×10^{-4}	5.3×10^{-4}	Largest entry from (k) above.
(r)	$\epsilon\bar{F}_{c,j}$	—	1.4×10^{-3}	1.1×10^{-3}	Quadrature combination of (p) and (q) above.

The random uncertainty in the $\bar{F}_{c,j}$ is given by

$$\delta\bar{F}_{c,j} = \frac{[(W_{c,j-1}\delta\bar{F}_{c,j-1})^2 + (w_{c,j}\delta F_{c,j})^2]^{1/2}}{W_{c,j}} \tag{47}$$

The values of $\bar{F}_{c,2}$ and $\bar{F}_{c,3}$ appear in tables XI, XII, and XIII along with the $F_{c,j}$. The results of these three determinations are also displayed by way of summary in figure 16.

V. Conclusions

A. Precautions and Pertinent Parameters

In the work reported in this paper, a large number of potential sources of error in determining reflectance factor using the Van den Akker method were investigated in order to evaluate the magnitude of their importance. Many of these sources of uncertainty were of little importance in themselves and even cumulatively were of importance only to a laboratory seeking the highest accuracy possible. For a laboratory for which a total uncertainty on the order of ±0.005 is tolerable, a number of the detailed steps described in section IV are not necessary. In this section we will briefly describe precautions which should still be taken in the case of such truncated measurement procedures and make suggestions for possible improvements in the overall procedure.

1. Determining the Van den Akker Reflectance $\rho_v(\lambda)$

In an experiment designed and carried out with reasonable care, the Van den Akker reflectance ρ_v can be determined very accurately. The principal strong point in this method is the insensitivity of the basic measurement accuracy to uncertainties in any of the measured parameters such as the port diameter, the sphere diameter, or the ratio of the reflectance of the sphere to the reflectance of the wall sample. The sensitivity to such parameters is kept lowest by using a large sphere with a small port (low f) and by using a highly reflecting coating in the sphere so that the sphere reflectance is still reasonably high.

Considerable care should be taken however to make the sphere coating in such a way that the Van den Akker reflectance can be related meaningfully to the reflectance of a sample of the coating. This means that a coating should be chosen the reflectance of which is uniform and very reproducible. It is especially important that no cracks appear in the finished coatings and that the coating should be thick enough to be opaque. In this regard, it is probably best not to incorporate a removable port in the Van den Akker sphere at all, but rather to rely upon the reproducibility of the coating and use the average Q from several separate samples of coating for Q_t in eq (6).

2. Adjustment from the Van den Akker Reflectance ρ_v to the d/h Reflectance $\rho(6°, \lambda)$

As can be seen from figure 13, the magnitude of this adjustment was in no case greater than −0.006. Since $\rho(\Gamma, \lambda)$ can never be greater than 1, it follows that this adjustment will be smaller for samples for which ρ_v closer to 1. It also is clear that the need for this adjustment comes about from the rise in reflectance at near-grazing incidence. This rise is due to the specular reflectance of the slightly glossy surface which is produced in pressing. For this reason, a coating technique which produces a rougher or more matted coating is to be preferred if no adjustment is to be made. It is probably the roughness of the coating that Goebel, et al., [2] produced by scraping which led to the rather remarkably good agreement between their results, which are the basis of the earlier NBS scale of $F(6°, \lambda)$, and the present adjusted results. (See fig. 17 and the discussion in section V.C. which follows.) An error of as much as 0.01 in the upward direction can result from assuming ρ_v and ρ to be equal, and an adjustment based on relative d/h reflectance measurements $N_G(\Gamma, \lambda)$ should be made if an uncertainty of less than ±.01 is desired. In all but the highest accuracy work, it is safe to assume the self-radiance is Lambertian, i.e., $N_g(\gamma, \lambda)/\cos\gamma$ is constant.

It should be pointed out that in every case ρ_v and $\rho_{45°/h}$ are very nearly equal, as can be determined from the $C(\Gamma, \lambda)$ curves in figure 12. Therefore the Van den Akker method is especially well adapted for calibrating measurements of directional-hemispherical reflectance at 45° incidence.

3. Adjustment from d/h Reflectance $\rho(6°, \lambda)$ to d/h Reflectance Factor $F(6°, \lambda)$

Since most reflectometers compare reflectance factor $F(6°, \lambda)$ rather than reflectance $\rho(6°, \lambda)$, it is in principle necessary to make an adjustment. However, since the solid angle subtended at the sample is small compared to the total hemisphere, any departure from Lambertian reflectance by the sphere coating would have to be large if the difference between ρ and F is to be significant. In the sphere coating materials ordinarily in use, the reflectance factor departs greatly from 1 only for small solid angles of collection at very small observation angles β (fig. 14). Therefore in general ρ is less than 0.001 higher than F and this adjustment can be ignored or estimated from data in the literature [13].

Note that if the object of the measurement is to determine the radiative transfer properties of the sphere coating itself, then ρ is the quantity of interest and the adjustment to F should not be made. This would be the case, for example, if the coating were being studied in order to determine the radiative heat transfer to the coating material.

4. Determining the d/h Reflectance Factor $F(6°, \lambda)$ of Working Standards

Next to the adjustment from ρ_v to ρ, it is this step which contains the highest potential for error. These measurements are meaningful only to the extent that the samples of coating with which the working standards are compared are representative of the sphere wall coating. It is for this reason that the sphere coating and the samples should be prepared in precisely the same way and that reproducibility of reflectance is an important requirement of the coating. It is also this reason that favors Van den Akker's original technique of having many removable sections in the sphere wall itself, provided that the presence of such removable sections does not give rise to irregularities in the sphere coating.

B. The Present NBS Scale of d/h Reflectance Factor $F(6°, \lambda)$

The present NBS scale of spectral d/h reflectance factor is maintained by means of three carefully preserved working standards which have been evaluated at 25 nm intervals. The reflectance factor data for the first three determinations are given in tables XI, XII and XIII. Figure 16 provides a

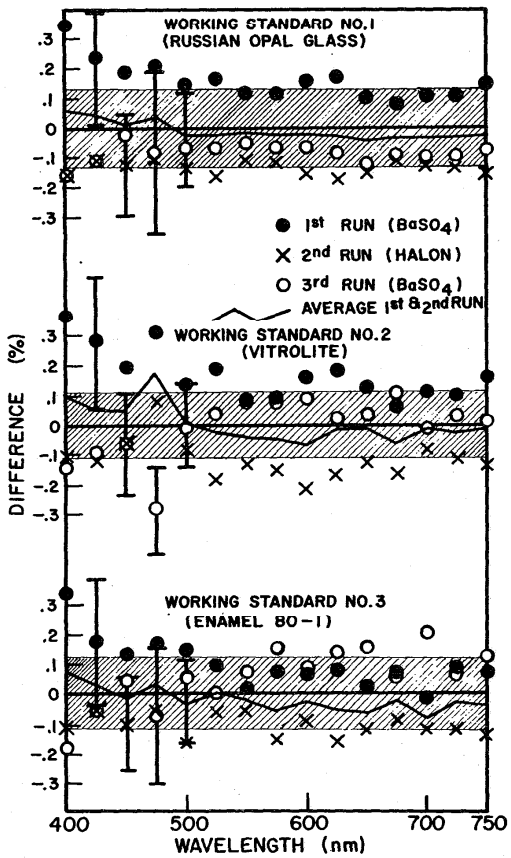

FIGURE 16. *Reflectance factor differences for the measurement of three working standards in three reflectance scale determinations.*

graphical record of the establishment of the average value for the three determinations. The representative error bars given to the left of the diagram actually were derived for 550 nm, but are fairly representative of the entire spectral range. The zero line in each case represents the average for the three determinations, and the shaded area represents the range of the total uncertainty of that average. Although the distribution of the points in general is consistent with the uncertainty levels which have been assigned, there is a lack of consistency from standard to standard between the relative values from pairs of determinations. For example, for working standard No. 1 (Russian opal glass), the third determination reflectance values are consistently lower than those of the first determination, whereas, for the other two working standards the first and third determinations yielded values which were more nearly equal (fig. 16). This difference in general behavior is too large to be explained by the uncertainties in the measured values of Q_c in expression (41). The most straightforward explanation for this difference is a slight drop in the reflectance of the working standard No. 1 during the interval between the second and third determinations. A better knowledge of the stability of the working standards will be obtained as more data are gathered from additional determinations.

The results of the work reported in this paper document the establishment of a scale of d/h reflectance factor at 25 nm intervals over the wavelength range 400 to 750 nm. The error analysis indicates that for high quality, uniform samples with reflectance greater than 0.5 there is only a very small probability that our measured reflectance factor values will be in error by more than 0.0015.

C. Relationship to Other Scales

In order to determine the relationship between the newly established NBS scale of d/h reflectance factor and the former one, we measured the three working standards on the NBS scale established in 1965. The results of this comparison are summarized in figure 17. In this figure, the data points indicate the departure of the old scale from the new for each working standard. The departure of the average value of the spectral $6°/h$ reflectance factors for the three standards on the 1965 scale from the same average on the new scale is shown by the light continuous line (GE average). The shaded area in the figure represents the uncertainty of the new scale, and the error bar on a central point indicates the uncertainty attributed to the 1965 scale. On the average, the old scale appears to depart from the new by about 0.002 at the short wavelength end of the range with the magnitude of the departure diminishing as the wavelength increases.

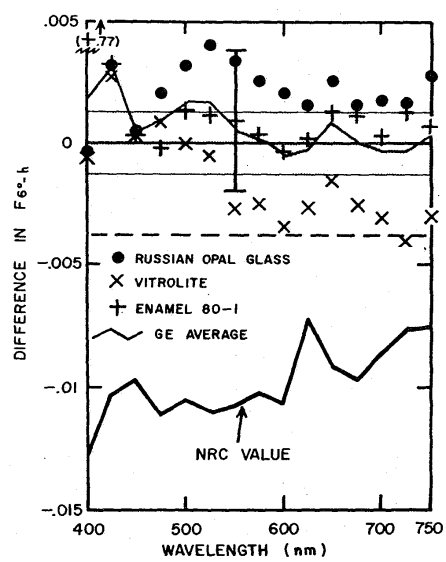

FIGURE 17. *Comparison of present NBS scale of $F_{6°-h}$ (taken as zero line) to previous NBS scale and to Results of an intercomparison with NRC.*

In 1974, measurements were made of several samples of pressed $BaSO_4$ and matte ground Russian opal glass at the National Research Council Laboratories (NRC) in Canada and at NBS on the 1965 NBS scale. The heavy line in figure 17 (NRC value) departs from the light line (GE average) by the difference between the averages of the reflectance values determined in the intercomparison. In this way, the present NBS scale and the NRC scale of 1974 are compared indirectly. The rather noisy appearance of the difference can very

probably be attributed to the imprecision of the NBS GE spectrophotometer.

The dashed line at approximately −0.004 indicates the combined error for this comparison. Since the NRC value differs from the present NBS value by over twice that amount, it is clear that at least one of these scales is in error by an amount greater than that claimed for it. At the time of this writing, work is under way on a new direct intercomparison between the present NRC and NBS scales of directional-hemispherical reflectance factor and on joint efforts to determine the cause of any differences.

D. Looking Ahead

We have already begun work on a determination of d/h reflectance factor by the Sharp-Little method [25, 26]. Most of the data have been obtained, and detailed analysis will be begun soon. Preliminary results indicate that the reflectance factors of the three working standards obtained by that method agree with those obtained by the Van den Akker method to well within the uncertainty of 0.0015. Therefore, it appears that the present NBS scale is accurate to within the uncertainty reported in this paper.

Mainly because of the slight instability and non-uniformity of the working standards, it is doubtful that an uncertainty in $F(6°, \lambda)$ of less than 0.1 percent of its value can be achieved on a practical, routine basis by any technique which relies on such standards. However, these working standards are more stable and more uniform than most samples encountered in practice. For this reason, we believe the newly established NBS scale of d/h reflectance factor to be sufficiently accurate and precise to serve the current needs for such measurements in science and industry.

VI. References

[1] Venable, William H. Jr., The National Measurement System for Spectrophotometry (Part of NBS Special Publication series 445, currently being prepared for publication.)

[2] Goebel, David C., Caldwell, B. Patrick, Hammond, Harry K., III, Use of an auxiliary sphere with a spectrophotometer to obtain absolute reflectance, J. Opt. Soc. Amer. **56**, 783 (1966).

[3] Certain products are mentioned in this paper by brand name or manufacturer for purposes of identification. This in no way implies recommendation or endorsement by the National Bureau of Standards.

[4] Keegan, Harry J., and Gibson, Kasson S., On the use of working standards of didymium and Vitrolite glasses for spectrophotometric measurements. J. Opt. Soc. Amer. **34**, 770 (Dec. 1944). (abstract).

[5] J. Opt. Soc. Amer. **28** (Oct. 1938). (Issue devoted to early development of recording spectrophotometer).

[6] NBS Letter Circular 1050 (June 1970). Preparation and Colorimetric Properties of a Magnesium-Oxide Relectance Standard.

[7] Private communication from W. Erb., Physikalisch-Technische Bundesanstalt.

[8] Venable, William H. Jr., Hsia, Jack J., and Weidner, Victor R., Development of an NBS reference spectrophotometer for diffuse reflectance and transmitance, Nat. Bur. Stand. (U.S.), Tech. Note 594-11, 47 pages (Oct. 1976).

[9] Van den Akker, J. A., Dearth, L. R., and Shillcox, W. M., Evaluation of absolute reflectance for standardization purposes, J. Opt. Soc. Am. **56**, 250 (1966).

[10] Venable, William H. Jr., and Hsia, Jack J., Describing spectrophotometric measurements, Nat. Bur. Stand. (U.S.), Tech. Note 594-9, 50 pages (Nov. 1974).

[11] International Lighting Vocabulary, Publication CIE No. 17 (E-1.1) 1970, section 45-20-201.

[12] Section III.B. of reference [8] above.

[13] Egan, W. G., and Hilgeman, T., Retroreflectance measurements of photometric standards and coatings, Applied Optics **15**, 1845 (1976).

[14] $BaSO_4$ manufactured by Mallincrodt Chemical Works (Reagent powder for X-ray diagnosis) #3808. [3]

[15] Halon tetrafluoroethylene powder manufactured by Allied Chemical Co. Type G-80, Lot 463169 Drum 31. [3]

[16] $BaSO_4$ manufactured by J. T. Baker Chemical Co. #5-1030 (553-1011) (analytical Reagent) [3].

[17] See section III. A. of reference [8] above.

[18] See Appendix C of Reference [8] above.

[19] Jenkins, F. A., and White, H. E., Fundamentals of Optics, 3rd edition (McGraw-Hill, N. Y., 1957) pg. 521, figure 25M.

[20] Jakob, Max, Heat Transfer, Volume II, p. 14 (John Wiley and Sons, N. Y., 1963), ($\omega_e/\pi = 1 - f_{12}$).

[21] See section III.A.4 of reference [8] above.

[22] Kubelka, Paul, New contributions to the Optics of Intensely Light-Scattering Materials. Part I, J. Opt. Soc. Amer. **38**, 448 (1948).

[23] Grum, F. and Saltzman, M.; P-75-77 New White Standard of Reflectance. Compte Rendu 18e Session, Londres 1975, CIE Publication No. 36, 91 (1976).

[24] Colorimetry, Publication CIE No. 15 (E13.1) 1971, pages 81 and 93.

[25] Sharp, C. H. and Little, W. F., Measurement of Reflection Factors, Transactions I.E.S. **15**, 802 (1920).

[26] Budde, Wolfgang, and Dodd, C. X., Absolute reflectance measurements in the $D/0°$ Geometry, Die Farbe **19**, 94 (1970).

[27] Hapke, Bruce W., A theoretical photometric function for the lunar surface, Journal of Geophysical Research **68**, 4571 (1963).

[28] Born, M., and Wolf, E., Principles of Optics, 3rd Edition, (Pergamon Press, New York, 1964), p. 399.

VII. Appendix A. Accounting for Retroreflectance

Retroreflectance refers to the tendency of objects to preferentially reflect radiation back in the direction from which it is incident. This can arise from several causes. If a focussing element such as a small dielectric sphere directs radiation onto a reflecting surface at or near its focal point, the reflected radiation will be returned back into the direction from which it came. This type of retroreflectance can be very directional, i.e., most of the radiation returns within a few tenths of a degree of the angle from which it came. A second, much less directional retroreflectance effect, results from the fact that shadows are not visible from the direction of incidence. This mechanism is important only for surfaces which are not highly reflecting, so that the radiation is not re-reflected out of the shadows. In the case of the highly reflecting coatings being used in the spheres in this experiment, the highly directional retroreflectance dominates.

1. The Effect of Retroreflectance

In order to obtain an estimate of how the presence of retroreflectance will affect a determination of the Van den Akker reflectance ρ_v, we will use a simple model in which most of the radiation is reflected in a Lambertian distribution but a small retroreflected fraction f_r appears above the Lambertain background. The effect which the retroreflectance has upon the flux $\phi_i(\lambda)$ (see III.A.) striking the sphere boundary can be seen by going one step backwards in determining the source of ϕ_i. The flux ϕ_i comes from the walls by reflection, and the incident radiation for this reflection is from the sphere walls, but *not from the port*. Therefore, in the presence of retroreflection the irradiance on the sphere boundary is higher on the wall coating than in the port. The makeup of ϕ_i can be determined by noting that, in this model, the flux incident upon the walls (which also comes from the walls) is *either absorbed or reflected. The total reflected flux, which is* ϕ_i, is made up of two parts

$$\phi_i = \phi_r + \phi_i \tag{A1}$$

where ϕ_r is the retroreflected fraction of the reflected flux

$$\phi_r = f_r \phi_i \tag{A2}$$

and ϕ_i' is the diffusely reflected fraction

$$\phi_i' = (1 - f_r)\phi_i. \tag{A3}$$

With this model, the power balance equation, equation (3) of part III.A., takes on the following form.

$$\rho_v'(1 + f_r\rho_v')(1 - f)\rho_t\phi_0 = \phi_i' f + [(1 - f)\phi_i' + \phi_r](1 - \rho_v') \tag{A4}$$

where ρ_t is reflectance of the target exclusive of the augmented reflection in the retro direction, which is lost through the port of the measuring instrument in every case. The relative reflectance Q_s of the sphere is

$$Q_s = k[\phi_i' f(1 - f') + \phi_0(1 + f_r\rho_v')\rho_t f(1 - f'')] \tag{A5}$$

and the relative reflectance of the target is, as before

$$Q_t = k\phi_0\rho_t(1 - f'). \tag{A6}$$

Equations (A2), (A3), (A4), (A5), and (A6) can be solved to obtain an expression for ρ_v' in the following form:

$$\rho_v' = \frac{1 - f(1 - f_r)\dfrac{Q_t}{Q_s}}{1 - f(1 - f_r)} \quad \frac{1}{1 - \alpha} \tag{A7}$$

where

$$\alpha = \left\{\frac{f(1 + \rho_v' f_r)[f' - f'']}{(1 - f')} + \frac{ff_r(1 - f_r\rho_v'^2)}{1 - \rho_v'[1 - f(1 - f_r)]}\right\}\frac{Q_t}{Q_s} \tag{A7a}$$

Comparing (A7) with (6), it is seen that f in the dominant first term is replaced by $f(1 - f_r)$. This in essence states that the fraction the flux escaping from the port hás been reduced relative to the flux lost to the walls by an amount proportional to the retroreflected fraction. The correction term α for the singular treatment of the first target reflection when the target is in the auxiliary sphere is also modified by the retroreflectance, making the form of this term so complicated that a closed solution in terms of the measurement parameters is not practical. We solve the equation iteratively, using as a first approximation for ρ_v' the value obtained from (A7) with $\alpha = 0$. Taking the retroreflectance into account has a very small effect on the calculated value of ρ_v'. For example, if $f_r = 0.001$, the effect of not ignoring this in the case of a sample for which $\rho_v' \simeq 0.98$ is to reduce the calculated ρ_v' by approximately 10^{-6}. Note that ρ_v' must be the total reflectance, including retroreflectance, since $1 - \rho_v'$ represents loss of radiation by absorption.

2. *Models for Retroreflective Mechanisms*

Our measurements of retroreflective bidirectional reflectance factor, the data for which are shown in figure 15, were limited to observation angles greater than 0.1°. Therefore we sought a model which could be used to interpolate our data to 0° observation angle so that we could evaluate the integral in eq (39).

A model based on shadowing was developed by Hapke [27] to explain the retroreflective phenomena observed from the lunar surface. This model, which was quite successful in Hapke's application, was used by Egan and Hilgeman [13] in an effort to quantitatively evaluate the retroreflectance which they observed from barium sulfate paint and other highly reflective white coatings. Other possible mechanisms for producing retroreflectance include cube corner reflectors formed from broken cubic crystals and retroreflectance by focussing, as occurs in glass beaded retroreflecting sheeting. In the following paragraphs we will treat special cases of each mechanism.

a. Shadowing

The Hapke model includes as one of its basic assumptions that the absorbance of the scattering particles is very high. In this way, there will be a considerable contrast between the radiance coming from shadowed areas in which the radiation undergoes several reflections and the radiance reflected from an unshadowed area. Although there is relatively little loss in highly reflecting materials such as barium sulfate or Halon, it is still possible for an initial first surface reflection to add to the background of multiply reflected radiation in a preferential manner. In order to estimate the order of magnitude of the non-diffuse reflection, one can use layers of close-packed spheres as a model for the many randomly oriented particles in the coating. Referring to one such sphere as shown in figure 18a, one can calculate the reflectance factor for such an array as follows. The bidirectional reflectance factor is given by

$$F(\mathbf{U}, \mathbf{u}) = \frac{\pi L(\mathbf{u})}{E(\mathbf{U})} \tag{A8}$$

where $E(\mathbf{U})$ is collimated irradiance incident in the direction $\mathbf{U}$ and $L(\mathbf{u})$ is the reflected radiance in the direction $\mathbf{u}$, both averaged over a sufficiently large area of the sample. In the case of retroreflectance, we set the unit vectors $\mathbf{U}$ and $\mathbf{u}$ equal. The average reflected radiance is given by definition as

$$L(\mathbf{u}) = \frac{\Phi(\omega, A)}{\omega(\mathbf{u})A\cos\gamma}. \tag{A9}$$

where $\omega(\mathbf{u})$ is an element of solid angle oriented in the direction $(\mathbf{u})$, A is the area of the surface over which the average is being taken, and $\Phi(\omega, A)$ is the flux reflected from area S into solid angle ω. Collimated incident radiation will come to a virtual focus at a point I which is $r/2$ from the outer surface of the sphere. The solid angle ω is defined in terms of a small arbitrary area a on the sphere

$$\omega = \frac{4a}{r^2}. \tag{A10}$$

The flux reflected from this area into ω is given by

$$\Phi = \rho E a/\cos\gamma \tag{A11}$$

where ρ is the reflectance of the sphere surface. (Note that since we are treating retroreflectance, a is chosen so that it is centered on a radius in the direction of E, and therefore the direction of incidence is normal to a.) The area A occupied by this sphere in a hexagonal close-packed array is

$$A = \frac{6r^2}{\sqrt{3}}. \tag{A12}$$

Using expressions (A9), (A10), (A11), and (A12) above in (A8) one obtains under conditions of retroreflectance:

$$F\ (\bar{\mathbf{U}}, \mathbf{u}) = \frac{\pi\sqrt{3}}{24}\rho/\cos^2\gamma = 0.227\rho/\cos^2\gamma. \tag{A13}$$

This would be roughly the maximum amount of additional bidirectional reflectance factor which might occur in the retro-direction under ideal conditions of shading by surrounding particles. The $\cos^2\gamma$ term in the denominator is an artifact of the "array of spheres" model we are using. In the continuous surface being represented by the array of spheres model, the projected surface area goes as $\cos^2\gamma$ so that the $\cos^2\gamma$ term should be omitted.

b. Cube corners

In the ideal case, the bidirectional reflectance factor for a cube corner reflector would be infinite at zero observation angle and zero at all other observation angles. However, imperfections in the cube corners and diffraction tend to spread the reflected radiation out so that bidirectional reflectance factor has meaning in describing reflection by cube corners. For the model for maximum reflectance, we will assume that the cubes are perfect and that diffraction is the limiting factor. For near normal incidence the total retroreflectance from a close-packed array of cube corner reflectors is

$$\rho_t = \rho_1^3(1 - \rho_2)^2 \tag{A14}$$

where ρ_1 is the reflectance of the cube faces and ρ_2 is the reflectance of the entrance surface. For a perfect internal corner ρ_1 is 1 and ρ_2 is roughly 0.05, so that ρ_t is roughly 0.9. For an external corner (cube corner "hole"), $\rho_2 = 0$ and ρ_1 is roughly 0.05 so that ρ_t is roughly 1.25×10^{-4} in that case. The reflected radiance is distributed in the diffraction pattern associated with the reflecting faces treated as apertures. For this order of magnitude calculation, we will assume the pattern to be that of a circular aperture of effective radius $r = \sqrt{\frac{A}{\pi}}$ where A is the area of the entrance surface. The radiance in such a pattern would be given by [28].

$$L(\beta) = \frac{EA}{\lambda^2}\left[\frac{2J_1(x)}{x}\right]^2 \tag{A15}$$

where

$$x = 2\pi r \sin(\beta)/\lambda,$$

from which it follows that the reflectance factor is given by

$$F(\beta) = \frac{\pi A}{\lambda^2}\left[\frac{2J_1(x)}{x}\right]^2\rho_t. \tag{A16}$$

The data in figure 15 suggest that the particle sizes are such that the central bright spot would subtend an angle of about 1° for $BaSO_4$. The edge of the central bright spot falls at $x = 3.8$. For an effective wavelength of approximately 550 nm, it follows that the particle size would have to be such that $r \simeq 20\ \mu$m. Thus, the reflectance factor at $\beta \ll 1°$ would be roughly

$$F(\beta) \simeq 10^4\rho_t. \tag{A17}$$

c. Focussing retroreflectors

If the index of refraction of a bead is such that the radiation passing through it comes to a focus behind it, a suitable reflector may be placed at the focal point (I in fig. 18c.) and the radiation will be reflected back through the bead into a collimated retroreflected beam. Here, the spreading of the reflected radiance can be brought about either by diffraction, poor focussing, or both. The diffraction limiting case in the previous paragraph can be applied to the Halon data in figure 15. In this case, the central bright spot appears to subtend an angle of about 0.5° which corresponds to an effective lens radius of $r \simeq 40\ \mu$m. If one assumes a refractive index of 1.5 so that the radiation will come to a focus on the back of the bead and from experience with cheap cameras assumes that

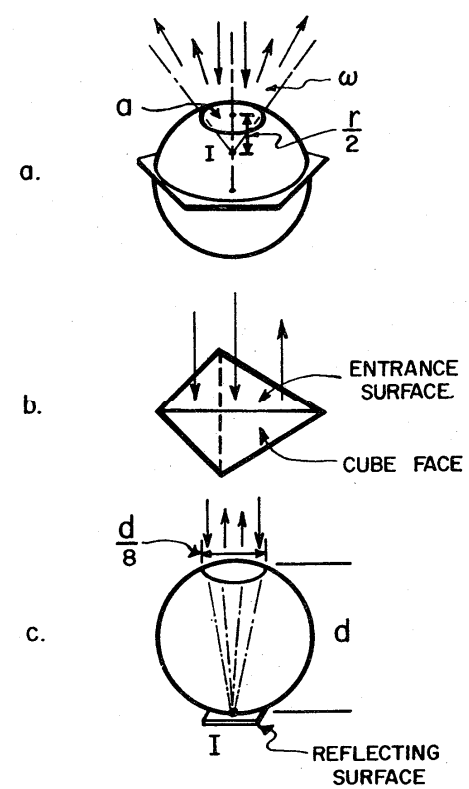

FIGURE 18. *Diagrams for estimating magnitude of retroreflectance by various means.*

the diameter of the effective lens area is roughly one-eighth of the diameter of the bead, it follows from expressions (A12) and (A16) that a closely packed array of such spheres would have a reflectance factor for $\beta \ll 1$ of

$$F(\beta) \simeq 6 \times 10^2 \rho_t \tag{A18}$$

for a specular reflector of reflectance ρ_t located at I and

$$F(\beta) \simeq 10 \rho_t \tag{A19}$$

for a diffuse reflector of reflectance ρ_t at I.

3. Interpolating the retroreflectance data

From the foregoing analysis, one can make the following deductions, assuming that the 0.5 excess reflectance factor is caused by only one mechanism:

a. Shadowing cannot by itself account for the observed retroreflectance.
b. At least 6×10^{-5} of the area is effectively taken up with inside corner cube retroreflectors.
c. At least 0.4 of the area is effectively taken up with outside corner cube retroreflectors.
d. At least 1.6×10^{-2} of the area is effectively taken up with focusing sphere retroreflectors backed by specular reflectors of reflectance 0.05.
e. At least 5×10^{-2} of the area is effectively taken up with sphere retroreflectors backed by diffuse reflectors of reflectance 1.

Since the mechanisms are not mutually exclusive, it is expected that all will operate to some extent in pressed powder samples. However it is highly unlikely that cube corner reflectors will be formed in Halon, so it would be expected that the mechanism in d. or e. above would predominate. Even though the cleavage of a crystal in such a way that it forms an inside corner cube reflector is not very likely, mechanism b. probably predominates in the $BaSO_4$ powder. Shadowing will contribute some effective retroreflectance in both cases.

The predominate mechanisms appear to depend on the sum of the diffraction patterns associated with a number of reflectors, each with a different effective aperture, and the statistical distribution of the aperture sizes is unknown. Therefore we chose to use an emperical fitting function. The function

$$F(\beta) = 1 + \exp(a + b\beta^c) \tag{A20}$$

was found to fit the data adequately. Fitting all $BaSO_4$ data, we obtained

a = −0.393
b = −0.966
c = 0.57

and fitting the first seven points of the Halon data we obtained

a = 1.18
b = −3.41
c = 0.21

These fitting functions are shown as solid curves in figure 15. The average of the function $F(\beta)$ for $BaSO_4$ over the range $0 \leq \beta \leq 0.5°$ is 1.42 which is in good agreement with the data of Egan and Hilgeman [13]. The difference values for $\rho(6°, \lambda) - F(6°, \lambda)$ were obtained by using the fitted functions in eqs (39) and (40) with $r = 1.9$ cm and $d' = 29.4$ cm. In each case, the contribution from the region of extrapolation ($|\beta| < 0.1°$) was only a small part of the total flux in the retroreflected component, so the choice of fitting functions was not critical. A crude measurement of $BaSO_4$ using a beam splitter yielded $\rho(6°, \lambda) - F(6°, \lambda) = 0.0006$ which is in good agreement with the value of 0.0007 obtained from the data in figure 15.

VIII. Appendix B. Interpretation of Error Statements

The error analysis in this paper involves three distinct classes of errors. The first class of error is the measured random error. This type of error appears as noise in the measurements and is evaluated by making each measurement several times and performing the usual error analysis on the results. For this type of error, we will cite three times the standard deviation of the mean.

The second class of error is the estimated random error. This class of error contributes to the outcome in the same way as the measured random error, but, either because of the inconsequential effects of the error or because of experimental difficulties which would be involved in evaluating it, we choose to estimate the size of the error instead of determining it by making several measurements. In making such an estimate, we choose to estimate the smallest range of uncertainty within which the correct value will fall with a very high probability, i.e., an intuitive ninety-five times out of a hundred. For this type of error, we will cite the size of the estimated error itself. The estimation process is carried out in such a way that the sign of the error is indeterminant. If it is known that a particular cause of error will result in an error which is always of one sign, we will correct the measured value to a most probable value and reduce the magnitude of the estimated random error appropriately. The estimated random error is combined in quadrature with the measured random error to obtain the total random error. All random errors, whether measured or estimated, will be denoted by the symbol δ.

The third type of error is the estimated systematic error, indicated by the symbol Δ. This error is like the estimated random error in all respectes except one, namely it is not independent from determination to determination, i.e., it will affect all determinations in the same way. It should be pointed out that this does not mean that the sign of the measurement is known, but only that the sign of the effect is known to be fixed from determination to determination. For example, in correcting for the reflection of radiation from the beveled lip of the sphere, we estimate that the radiation will be reflected with an average reflectance intermediate between one and the normal reflectance of the stainless steel. (See discussion preceding (19).) If the actual reflectance is less than our estimated value, determinations of reflectance made using this estimate will result in ρ_v values which are all slightly higher than if the estimates were correctly made. In the course of many determinations, the total random error will be reduced, but the systematic error will remain. Since the

sign of the systematic errors is not known, systematic errors from independent causes will be added in quadrature, and at each point in the analysis at which it is desirable to estimate a total uncertainty, the systematic error and the total random error will be added in quadrature. However, when proceeding to combine the results of several determinations, we will first combine the random errors in the ordinary way and add the largest systematic error in quadrature at the end. In this way, the calculated systematic error is not reduced by repeating the measurements. The total uncertainties so calculated are to be regarded as determining a range within which we expect the correct value to fall with a probability of approximately 0.95. This total uncertainty will be indicated by the symbol ϵ.

IX. Appendix C. Calculating $C(\Gamma, \lambda)$

The integrals in (11) are evaluated in closed form after fitting the experimental data for N_g and N_G.

1. *Fitting $N_G(\Gamma, \lambda)$*

The data for N_G were fitted by an expression of the form:

$$N_G(\Gamma, \lambda) = a_0(\lambda) + a_1(\lambda)\Gamma^2 + a_2(\lambda)\Gamma^4. \qquad \text{(C1)}$$

An even function of Γ was used, since we have assumed the directional-hemispherical reflectance of the coatings does not depend on the angle of azimuth of the incident direction, but depends only on the angle of elevation. The coefficients in (C1), as determined by a least squares fitting of the experimental data are given in table C1.

2. *Fitting $N_g(\Gamma, \lambda)$*

Since the experimental data for $N_g(\gamma, \lambda)/\cos(\gamma)$ were found to be nearly independent of wavelength, only one function $N_g(\Gamma)$ is needed for each type of coating. However, since there was such a large uncertainty in the $N_g(\Gamma)$ data, three sets of $N_g(\Gamma)$ were fitted as described in part IV.B.3. in the main text. The form used for the fitting the data was:

$$N_g(\Gamma)/\cos\Gamma = \sum_{i=0}^{4} b_i\Gamma^i. \qquad \text{(C2)}$$

TABLE CI

Coefficients for the expansion of $N_G(\Gamma, \lambda)$ in even powers of the angle of incidence Γ in radians at three different wavelengths for three sphere wall coatings.

Coating	Wave-length	a_0	a_1* $\times 10^3$	a_2* $\times 10^3$
$BaSO_4$ [14]	450	0.999942	5.99	0.438
	550	.99978	4.40	0.159
	750	1.00011	3.27	0.00014
Halon [15]	450	0.999875	3.97	−0.172
	550	1.00004	4.17	−0.985
	750	1.00027	3.68	−1.20
$BaSO_4$ [16]	450	0.999829	4.08	0.405
	550	1.00047	1.43	0.741
	750	1.00012	3.91	−0.471

* The second and third digits are not significant but are kept to avoid round-off error in further calculations.

In the case of the original knife-edge data, the values of the coefficients, as obtained by least squares fitting, are given in table CII as describing the "upper limit" curve. In the original data, the least uncertainty was associated with the $\Gamma = 0$ reading. Therefore, all data were normalized to the $\Gamma = 0$ reading and b_0 was taken to be 1 when the data were fitted. Because of the symmetry in azimuth, b_1 and b_3 are taken to be zero.

In the accepted data, $N_g(\Gamma)/\cos\Gamma$ was taken as 1 up to $\Gamma = \pi/4$. To obtain the remaining part of this curve we obtained $N_g(\gamma)$ according to the expression

$$N_g'(\gamma)/\cos\gamma = 1 + C_1\gamma. \qquad \text{(C3)}$$

The difference data $N_g(\gamma) - N_g'(\gamma)$ using the data for the angles $\pi/3$ (60°), $5\pi/12$(75°) and $17\pi/36$(85°) were fitted using the form

$$N_g(\gamma)/(\cos\gamma) = 1 + b_1'(\Gamma - \frac{\pi}{4})^2 + b_2'(\Gamma - \frac{\pi}{4})^4. \qquad \text{(C4)}$$

After b_1' and b_2' were determined, these were used to obtain the b_i in the expression (C2).

3. *Calculating $C(\Gamma, \lambda)$*

With the expressions (C1) for $N_G(\Gamma, \lambda)$ and (C2) for $N_g(\Gamma, \lambda)$ substituted into eq (11), the integrals in that equation can be evaluated in closed form in terms of integrals of the form

$$I_i = \int_0^{\pi/2} \Gamma^i \cos\Gamma \sin\Gamma d\Gamma \qquad \text{(C5)}$$

for the upper and lower limit functions, and

$$I_i' = \int_0^{\pi/4} \Gamma^i \cos\Gamma \sin\Gamma d\Gamma \qquad \text{(C6)}$$

and

$$I_i'' = \int_{\pi/4}^{\pi/2} \Gamma^i \cos\Gamma \sin\Gamma d\Gamma \qquad \text{(C7)}$$

for the accepted value functions. The values of these integrals are given in table CIII, and the resulting values of $\bar{N}_G(\lambda)$ are given in table CIV. It can be seen from table CIV that the difference between the various assumptions concerning the self-radiance has a very small effect on the value of $\bar{N}_G$ in all cases. Therefore only the accepted value of $\bar{N}_G$ will be used in each case to calculate $C(\Gamma, \lambda)$. The results of the scanning which has been done to date with the telescopic detector indicate that the real value probably lies toward the lower limit from the accepted value. On this belief, we will assign the largest difference between an accepted value and a lower limit value, 0.00005, as the magnitude of the uncertainty in $\bar{N}_G$ due to the uncertainty in evaluating the self-radiance by measuring N_g.

X. Appendix D. The Three Working Standards

The properties which standards for reflectance factor measurements should have is a subject over which there is much diversity of opinion. By definition, reflectance factor is reflectance relative to the reflectance of a totally reflecting Lambertian reflector, both measured on the same instrument. Based on this definition, the best standard for calibrating an

TABLE CII

Coefficient for the expansion of $N_g(\Gamma)/\cos\Gamma$ in powers of the angle of incidence Γ in radians for three different sphere coatings and three different assumptions concerning the self-radiance distribution.

Coating	Curve Type	b_0	$b_1 \times 100$	$b_2 \times 100$	$b_3 \times 100$	$b_4 \times 100$
	upper limit	1	0	7.0	0	1.1
$BaSO_4$ [14]	accepted; $\Gamma \leq \pi/4$	1	0	0	0	0
	$\Gamma > \pi/4$	1.03	−1.240	−12.4	16.7	−5.33
	lower limit	1	0	0	0	0
	upper limit	1	0	5.3	0	6.1
Halon [15]	accepted; $\Gamma \leq \pi/4$	1	0	0	0	0
	$\Gamma > \pi/4$	1.45	−219	405	−339	107
	lower limit	1	0	0	0	0
	upper limit	1	0	3.8	0	1.6
$BaSO_4$ [16]	accepted; $\Gamma \leq \pi/4$	1	0	0	0	0
	$\Gamma > \pi/4$	1.17	−120	271	−248	79
	lower limit	1	0	0	0	0

TABLE CIII

Values of the integrals in equations (C5), (C6), and (C7) for nine values of i.

i	I_i	I_i'	I_i''
0	0.50000	0.25000	0.25000
1	.39270	.12500	.26770
2	.36685	.07135	.29550
3	.37990	.04382	.33608
4	.42147	.02819	.39328
5	.49129	.01872	.47257
6	.59443	.01273	.58170
7	.74046	.00882	.73164
8	.94416	.00614	.93802

TABLE CIV

Values of the weighted averages $\bar{N}_G(\lambda)$ for each of three coatings for three wavelengths and three different assumptions concerning the self-radiance distribution.

Determination number	Wave-length λ	Upper limit	Accepted value	Lower limit
$BaSO_4$ [14]	450	1.00486	1.00479	1.00476
	550	1.00343	1.00338	1.00336
	750	1.00244	1.00240	1.00239
Halon [15]	450	1.00294	1.00282	1.00277
	550	1.00233	1.00225	1.00223
	750	1.00175	1.00170	1.00169
$BaSO_4$ [16]	450	1.00343	1.00335	1.00333
	550	1.00173	1.00168	1.00167
	750	1.00253	1.00247	1.00247

instrument to measure reflectance factor would be a totally reflecting Lambertian reflector, or the closest thing to it which could be obtained. The Halon and barium sulfate sphere linings which were used in the work described in this paper were very close to this ideal.

However, if reflectance factor measurements are going to be of use in practical applications, the instrument must be defined as part of the specification of the measurement. It is for this reason that we have defined the measurements as carefully as possible in terms of integrals describing the incident radiation and the instrument response. We believe the properties of our reference reflectometer are very close to those specified in the definition for directional-hemispherical reflectance factor which we have used, and furthermore, we believe the geometrical properties of that instrument to be stable in time. In order to confirm this, however, we feel that it is important to have several working standards representing the gamut of the highly reflecting materials which we would be measuring with this instrument. It is also important that several different types of working standards be used in order to be able to detect changes in the optical properties of any one of them. As a means of retaining our scale of measurement in day-to-day measurements and as a means of comparing one determination with another, we are using the following working Standards:

Working Standard No. 1—This standard is a piece of MC-20 opal glass purchased in September 1970 from

Mashpriborintorg
Smolenskaja pl., 32/34
121200, Moscow, G-200
U.S.S.R.

The piece used is 99 mm by 99 mm and is 20 mm thick. It is marked MC-20-2 for identification and is usually referred to as the Russian Opal Glass. The side which is measured has a very flat, highly polished surface.

Working Standard No. 2—This standard is a piece of Vitrolite glass which was manufactured by

Libbey Owens Ford
1701 E. Broadway
Toledo, Ohio 43605

The exact date of manufacture of this particular piece of glass is unknown, but it has been at least twenty years since any glass of this type has been manufactured. The piece used is

100 mm by 100 mm and is 11 mm thick. It is marked V6-D1 for identification. The side which is measured is flat and highly polished.

Working Standard No. 3—This standard is a porcelain enamel on steel plaque which was made around 1946 by

The Harshaw Chemical Co.
Division of Kewanee Oil Company
1933 E. 97th St.
Cleveland, Ohio 44106

The plaque used is 108 mm by 108 mm and is marked 80-1 for identification. The surface which is measured is smooth and non-porous, but it has a slight ripple or "orange peel" texture.

These three working standards cover the range of reflectance factor from nearly 1 to approximately 0.8, which is the range generally used for standards to calibrate the gain setting of reflectometers. In addition, the Vitrolite standard is slightly translucent. Recent tests have shown our instrument to be insensitive to this amount of translucence, but if this should change the difference will be noticeable in the measurements obtained using this standard as compared to the others. Because of the rippled surface in the porcelain enamel standard, the surface reflection from this standard is spread out more than that from the other two standards which have flat surfaces. Therefore, differences in the way the instrument handles specular reflection may show up in the relative measurements of this standard with respect to the others. (The most sensitive test of the way the instrument treats specular reflectance is made by measuring a specular mirror. We intend to use this procedure as soon as we have the capability to measure the reflectance of a mirror with the necessary accuracy.)

The cleaning procedure used is an important part of maintaining working standards of reflectance. Our present approach is to use a procedure which will disturb as little as possible the layers of oxides and other surface films characteristic of the materials. Therefore, we store the standards in dessicators and before each measurement we wash them with a mild nonfluorescing soap, rinse them thoroughly with hot water, rinse them with distilled water, and blot them dry with soft tissue paper. Any lint which remains on the surface is removed by gently brushing with a soft brush.

APPENDIX F

Reflection properties of pressed polytetrafluoroethylene powder

Victor R. Weidner and Jack J. Hsia

Radiometric Physics Division, National Bureau of Standards, Washington, D.C.

Received December 18, 1980; revised manuscript received February 12, 1981

The reflection properties of pressed polytetrafluoroethylene powder have been under investigation by the Radiometric Physics Division at the National Bureau of Standards for the past five years. This material has a great potential use, both as a standard of diffuse reflectance and as a coating for integrating spheres for applications in reflectance spectrophotometry and other signal-averaging devices. It possesses certain physical and optical properties that make it ideal for use in these applications. Techniques are given for preparing reflection standards and coating integrating spheres with the pressed powder. The effects of powder density and thickness on its reflectance are reported, and observations of possible problems with fluorescence that are due to the presence of contaminants in the powder are discussed. The absolute reflectance (6°/hemispherical reflectance factor relative to a perfect diffuser) is reported for the spectral range of 200–2500 nm. The directional/hemispherical reflectance factor relative to 6°/hemispherical reflectance is given for several wavelengths in the ultraviolet and visible spectrum and for angles of incidence between 5 and 75°. The bidirectional reflectance factor is reported for 300, 600, and 1500 nm at angles of incidence of −10, −30, −50, and −70° and at viewing angles at 10° intervals from −80 to +80°.

INTRODUCTION

The reflection properties of pressed polytetrafluoroethylene (PTFE) powder[1] in the ultraviolet, visible, and near-infrared spectral regions, combined with certain desirable physical characteristics, make this material exceptionally useful when there is a need for a good white diffuser or a standard of diffuse reflectance. The diffuse reflectance of pressed PTFE powder is remarkably high over the spectral range of 200–2500 nm and is probably higher than that of any other known material, its reflectance being 99% or higher over the spectral range of 350–1800 nm. It is particularly useful as a coating for integrating spheres commonly used in diffuse reflectance spectrophotometry. Historically, the most commonly used materials for this purpose have been magnesium oxide and barium sulfate powders or barium sulfate paint.[2] Much has been written on the optical properties of these materials, and the advantages and disadvantages of their use in spectrophotometric applications have been experienced by nearly everyone involved with reflectance spectrophotometry. Certainly, there is no longer any advantage in coating integrating spheres by the old method of burning magnesium and collecting the magnesium oxide smoke. The standards that still specify that reflectance measurements be reported on a photometric scale relative to smoked magnesium oxide should be rewritten to specify that reflectance measurements be reported on an absolute reflectance scale (relative to a perfect diffuser[3]). A review of publications on properties and reflection values of material reflection standards is given in Ref. 2.

The purpose of this paper is to make available the technical findings of several years of research on the optical properties of pressed PTFE powder. Other authors[4] have reported on the potential usefulness of this material as a reflection standard. The spectrophotometry group of the Radiometric Physics Division at the National Bureau of Standards (NBS) began studies of the reflection properties of pressed PTFE powder in 1975. At that time, this group was engaged in constructing a new reference spectrophotometer for diffuse reflectance[5] along with a number of accessory devices for measuring diffuse reflectance. These accessory devices include integrating spheres for measuring 6°/hemispherical reflectance factor, 45°/0° reflectance factor, and directional/hemispherical reflectance factor and a specular reflectometer.[6] At the same time, a more accurate absolute diffuse reflectance scale was being established by the auxiliary sphere or Van den Akker method.[7] A technique was developed for coating integrating spheres with the PTFE powder, and extensive measurements of the optical properties of this material were carried out over a five-year period. The results of these studies are reported here along with some descriptive details of the techniques used in preparing reflection standards from PTFE powder and its application to integrating spheres.

PREPARATION

The PTFE powder is somewhat lumpy as it comes in a shipping drum. It can be prepared for optical-coating purposes by reducing it to a uniform low-density powder. This can be accomplished with a blender or other chopping device, preferably one with stainless-steel blades and a glass container. The powder should be kept in glass containers and handled with tools made of materials such as stainless steel that are less likely to contaminate the material. The powder will adhere to itself on pressing, but it does not adhere well to metal, glass, or plastic. One technique for making it adhere to metal (or other materials) is first to coat the metal with a thin film of high-vacuum silicone grease. Once this is done, the powder can be pressed into place in thicknesses varying from 1 to 10 mm without much difficulty. The silicone grease has a low volatility and does not affect the reflection properties of the

Reprinted from **Journal of the Optical Society of America,** Vol. 71, page 856, July 1981

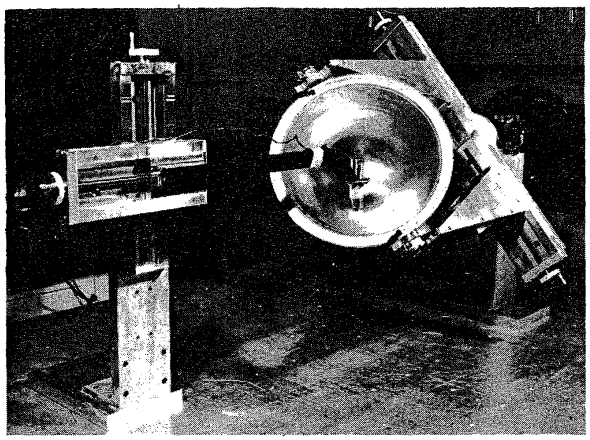

Fig. 1. The NBS integrating-sphere-coating apparatus showing the hemisphere manipulator with the electronically controlled tamping head used to press the PTFE powder into the hemisphere with a uniform radius.

PTFE powder because it contacts only a thin layer at the powder–metal interface.

PTFE powder has been successfully applied to integrating spheres ranging in diameter from a few centimeters to 45 cm and to large, flat surfaces used as reflection standards. The coatings are not affected by conditions of high humidity because the pressed powder repels water. Exposure to high-intensity ultraviolet radiation,[4] such as that encountered near a xenon arc, will slightly degrade the reflection properties of the coatings in the ultraviolet spectral region. The reflectance will be degraded as a result of contamination from smoke, dust, or other contaminants that may be present.

The time required for coating an integrating sphere of 20-cm diameter with a 6-mm-thick coating is typically about 4 h. This includes preparing the PTFE powder with a blender, trimming up the finished coating around the ports, and assembly of the usual two hemispheres. At NBS, spheres up to 45-cm diameter are coated with the aid of a special hemisphere manipulator (Fig. 1) that enables the technician to rotate and pivot the hemisphere about the center point of the sphere and pack the PTFE powder into the curvature of the hemisphere with a light pressure, using hand tools such as a stainless steel spoon or a round-bottom glass flask. In some special applications, such as in the preparation of an auxiliary sphere for determining the absolute reflectance of the sphere coating, the radius of curvature of the coating surface is carefully controlled by tamping the PTFE powder under an electronic tamping head before it is rolled to a final finish. A retainer ring is attached to the hemisphere flange during the coating procedure to retain the powder at the open edge of the hemisphere. When the coating is completed, this retaining ring is removed, and the two completed hemispheres are attached to each other by means of the flanges. The PTFE coating expands slightly at the hemisphere edge when the retaining ring is removed. This is an advantage because it results in the formation of a tight fit when the two hemispheres are combined to form the sphere.

As with any sphere-coating material, PTFE powder has its advantages and disadvantages. Some practice is required in order to master the coating techniques. The powder should be packed in lightly at first, to a depth of approximately 2–3 times the desired final thickness before it is pressed to a finish. The application of added powder to an already hard-pressed coating may result in a peeling and separation of the material into layers. The best results are obtained with a sand-blasted or ground-glass pressing tool, such as a round-bottom flask of small diameter. The coating should be done in a relatively clean, dust-free environment because the PTFE coating usually becomes electrostatically charged during the pressing and will hold small specks of dirt or lint. These can be picked up or removed with a small, clean artist's brush.

PTFE powder is very fine and easily mixes in the air about the working area. Although the powder is believed to be nontoxic, it is a good practice to use a dust mask to avoid unnecessary breathing of the material.

PTFE may form toxic gases at thermal decomposition temperatures above 400°C. These toxic products may be produced inadvertently by contact of the fine powder with a flame or other high-temperature source. For further information on the safe handling of fluorocarbon resins, refer to Ref. 8.

It should be noted that there are U.S. patents dealing with the use of fluorocarbons as coatings for integrating spheres. These U.S. patents are given in Ref. 9.

DENSITY

The reflectance of PTFE powder is influenced by the density to which the powder is pressed. This relationship is illustrated in Fig. 2, in which the results of a number of measurements of reflectance versus powder density are plotted. The reflectance scale in this illustration is a relative one with the data normalized at a density of 1.0 g/cm^3, because this is the density at which the powder reflectance is the highest. There seem to be no noticeable wavelength-related effects for wavelengths less than 2000 nm. The vertical bars in Fig. 2 show the spread in reflectance values at the 10 selected

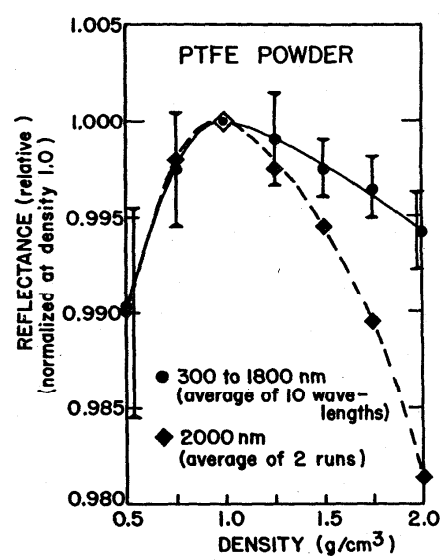

Fig. 2. Pressed PTFE powder reflectance as a function of powder density (10-mm thickness).

Table 1. Reflectance of Pressed PTFE Powder (0.8 g/cm³) Relative to That of a 10-mm-Thick Layer at Each Wavelength

Thickness (mm)	Relative Reflectance 400 nm	550 nm	700 nm
1	0.991	0.989	0.986
2	0.995	0.994	0.993
4	0.998	0.998	0.997
6	1.000	1.000	0.999
8	1.000	1.000	1.000
10	1.000	1.000	1.000

wavelengths. The maximum reflectance is obtained by compressing the powder to a density of from 0.8 to 1.2 g/cm³. The loose powder has a density of approximately 0.5 g/cm³. A sample of the pressed powder having the maximum reflectance can easily be prepared by compressing 2–2.5 volumes of loose powder into 1 volume. This results in a pressed sample that is rather soft. A sample compressed to a density of 2 g/cm³ will have a much harder surface and slightly lower reflectance. Higher densities require higher pressures, and a mechanical press must be used. As is shown in Fig. 2, the reflectance does not vary much with change in powder density for the density range of 0.8–1.2 g/cm³. Repeated preparation of pressed samples having reflectances that are the same to within a few tenths of a percent can easily be achieved, and a fresh sample can be prepared in minutes. At wavelengths greater than 2000 nm the reflectance drops more rapidly with increasing powder density.

THICKNESS

The diffuse reflectance of pressed PTFE powder is influenced by the thickness of the powder layer. Its translucency is such that at least a 6-mm thickness at a density of approximately 1 g/cm³ is required to obtain maximum reflectance. Table 1 shows the influence of thickness on the reflectance of PTFE powder at 400, 550, and 700 nm. These measurements were made with an aluminum backing having a reflectance of approximately 60%. Later measurements in the infrared out to 2500 nm indicate that 6- to 8-mm thicknesses and a density of 1 g/cm³ are adequate in order to achieve maximum diffuse reflectance values for the pressed powder. Coatings this thick are not required in applications where the coating is used in a signal-averaging sphere. However, when the PTFE powder is used as a reflection standard, a 10-mm thickness will be certain to give the maximum reflectance at all wavelengths.

FLUORESCENCE

There has been no clear evidence to show that the PTFE powder itself fluoresces. However, coatings made from PTFE powder show a very weak fluorescence. This fluorescence may be associated with a slight contamination from the plastic bag used to contain the PTFE powder in its shipping drum. As a test of the contribution of fluorescence to the reflectance of PTFE powder, a specimen was first measured on a double-beam reflectance spectrophotometer with the use of monochromatic illumination of the PTFE powder and then with polychromatic illumination. In Table 2 the normalized difference D between the reflectances obtained by these two modes of illumination is given as $D = (R_m - R_p)/R_p$, where R_m is proportional to the reflectance of the PTFE powder sample relative to that of an aluminum mirror with monochromatic irradiation and R_p is the same relative reflectance with polychromatic irradiation. There appeared to be a slight amount of fluorescence with excitation at wavelengths less than 290 nm and emission in the wavelength range of 310–350 nm. Subsequent measurements with a spectrofluorometer[10] confirmed these conclusions.

The levels of fluorescence observed may be negligible for most radiometric and spectrophotometric applications. However, in applications in which a small amount of fluorescence can cause a significant error, it would be wise not to use any kind of pressed-powder coating without first checking for the presence of fluorescence that is due to contaminants, especially when ultraviolet radiation below 300 nm is involved.[11]

REFLECTION PROPERTIES

The 6°/hemispherical reflectance factor of a diffuse reflectance standard is probably the most important calibration. The term 6°/hemispherical reflectance refers to a measurement geometry in which the sample is illuminated by a collimated source incident upon the sample at 6° from the normal

Table 2. Data from Fluorescence Check

Wavelength (nm)	D	Wavelength (nm)	D
250	0.019	500	0.000
260	0.016	510	−0.002
270	0.022	520	0.000
280	0.018	530	0.000
290	0.005	540	0.002
300	−0.004	550	0.000
310	−0.018	560	0.000
320	−0.011	570	0.000
330	−0.021	580	0.005
340	−0.015	590	0.001
350	−0.009	600	0.006
360	−0.007	610	0.004
370	−0.006	620	0.001
380	−0.003	630	0.001
390	−0.002	640	0.000
400	−0.006	650	−0.002
410	−0.002	660	0.000
420	−0.002	670	−0.002
430	0.002	680	−0.002
440	0.002	690	−0.006
450	0.000	700	−0.003
460	0.002	710	−0.004
470	−0.002	720	−0.003
480	0.002	730	0.002
490	0.002	740	−0.008
		750	−0.007

Table 3. 6°/Hemispherical Reflectance Factor of a 10-mm-Thick Pressed PTFE Powder Relative to a Perfect Diffuser

λ (nm)	ρ	λ (nm)	ρ	λ (nm)	ρ
200	0.962[a]	950	0.994	2140	0.964
210	0.964[a]	1000	0.994	2150	0.965
220	0.967	1050	0.994	2160	0.967
225	0.968	1100	0.994	2170	0.970
230	0.969	1150	0.994	2180	0.973
240	0.971	1200	0.993	2190	0.975
250	0.973	1250	0.993	2200	0.977
260	0.976	1300	0.992	2210	0.977
270	0.978	1350	0.991	2220	0.978
275	0.979	1400	0.991	2230	0.978
280	0.980	1450	0.992	2240	0.977
290	0.982	1500	0.992	2250	0.977
300	0.984	1550	0.992	2260	0.976
310	0.985	1600	0.992	2270	0.976
320	0.987	1650	0.991	2280	0.975
325	0.988	1700	0.990	2290	0.974
330	0.988	1750	0.990	2300	0.972
340	0.989	1800	0.990	2310	0.971
350	0.990	1850	0.986	2320	0.970
360	0.990	1900	0.985	2330	0.968
370	0.991	1950	0.984	2340	0.966
375	0.991	2000	0.981	2350	0.965
380	0.991	2010	0.979	2360	0.964
390	0.992	2020	0.978	2370	0.963
400	0.993	2030	0.976	2380	0.963
450	0.993	2040	0.975	2390	0.962
500	0.994	2050	0.973	2400	0.962
550	0.994	2060	0.972	2450	0.961
600	0.994	2070	0.971	2500	0.960
650	0.994	2080	0.970		
700	0.994	2090	0.969		
750	0.994	2100	0.968		
800	0.994	2110	0.967		
850	0.994	2120	0.966		
900	0.994	2130	0.964		

[a] Extrapolated.

and in which the reflected flux is averaged by an integrating sphere-detector system. An angle of 6° off the normal is commonly used to allow for including the specular component in the measurement.

The 6°/hemispherical reflectance factor of samples of PTFE powder pressed to a thickness of 6 mm or more with a density of 0.8–1.2 g/cm^3 is very reproducible. For a set of samples made at different times from different lots of PTFE powder, a standard deviation of less than 0.001 in measured reflectance was found for the wavelength range of 400–750 nm. Further measurements will have to be made in order to establish what this deviation will be in the ultraviolet and infrared regions. The 6°/hemispherical reflectance factor of pressed PTFE powder is given in Table 3 for a PTFE coating 10 mm in thickness and having a density in the range of 0.8–1.2 g/cm^3. The data listed in Table 3 are plotted in Fig. 3. These data are reported on an absolute reflectance scale (relative to a perfect diffuser) and were obtained by the auxiliary sphere

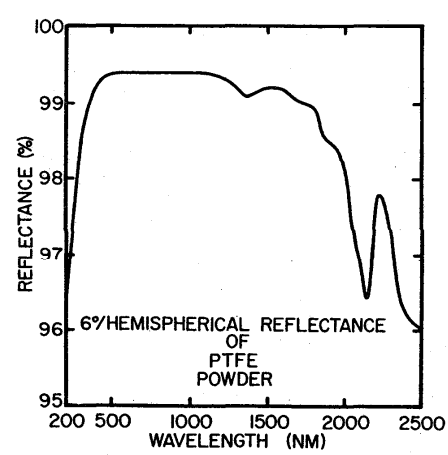

Fig. 3. The 6°/hemispherical reflectance factor (relative to a perfect diffuser) of 10-mm-thick, 1-g/cm^3-density pressed PTFE powder.

Table 4. Directional/Hemispherical Reflectance Factor of Pressed PTFE Powder for a 10-mm-Thick Coating (Relative to Hemispherical Reflectance at 6° Incidence)

Angle of Incidence	Reflectance					
	250 nm	300 nm	350 nm	450 nm	600 nm	750 nm
6°	1.0000	1.0000	1.0000	1.0000	1.0000	1.0000
10°	1.0003	1.0002	1.0001	1.0001	1.0001	1.0001
15°	1.0009	1.0005	1.0004	1.0002	1.0002	1.0002
20°	1.0017	1.0010	1.0007	1.0004	1.0004	1.0004
25°	1.0026	1.0015	1.0011	1.0007	1.0006	1.0006
30°	1.0038	1.0022	1.0015	1.0010	1.0008	1.0008
35°	1.0052	1.0030	1.0021	1.0013	1.0011	1.0011
40°	1.0066	1.0038	1.0026	1.0016	1.0014	1.0014
45°	1.0082	1.0047	1.0032	1.0020	1.0017	1.0017
50°	1.0099	1.0056	1.0038	1.0023	1.0020	1.0020
55°	1.0117	1.0065	1.0044	1.0026	1.0023	1.0023
60°	1.0134	1.0074	1.0049	1.0029	1.0025	1.0025
65°	1.0153	1.0083	1.0054	1.0031	1.0027	1.0027
70°	1.0170	1.0090	1.0058	1.0032	1.0028	1.0029
75°	1.0186	1.0097	1.0061	1.0032	1.0029	1.0029

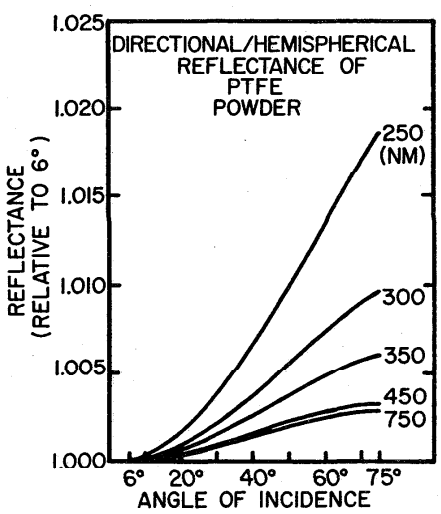

Fig. 4. The directional/hemispherical reflectance factor of pressed PTFE powder as a function of angle of incidence and wavelength.

method.[7] These absolute reflectance data are believed to be accurate to within ±0.002 on the basis of the analysis of the known sources of error as discussed in Ref. 7.

The directional/hemispherical reflectance factor of pressed PTFE powder given in Table 4 shows how the hemispherical reflectance of the material varies as a function of the angle of incidence. These measurements were made by means of an integrating sphere accessory to the NBS reference spectrophotometer for diffuse reflectance. This accessory consisted of a 45-cm-diameter sphere designed so that the sample can be mounted in the center of the sphere where it can be rotated to control the angle of incidence. The measurements were made at several wavelengths in the ultraviolet and visible spectra for both vertically and horizontally polarized sample beams. The results listed in Table 4 and illustrated in Fig. 4 are an average of the two polarizations. The values for either polarization did not vary by more than ±0.5% from the average. The most noticeable changes in reflectance as a function of angle of incidence occur in the ultraviolet spectral region. The data are relative to the 6°/hemispherical reflectance factor values.

The bidirectional reflectance factor of pressed PTFE powder listed in Table 5 shows how the reflectance varies over a wide range of viewing angles for four different angles of incidence. These measurements were made by means of the NBS specular reflectometer.[6] This instrument is ordinarily used for specular reflectance measurements as a function of angle of incidence. It can be used to measure the bidirectional reflectance of a diffuse sample in the plane of the incident sample beam. Measurements were made at 300, 600, and 1500 nm for angles of incidence of −10, −30, −50, and −70°. The angles of viewing were selected at 10° intervals from −80 to +80°. The bidirectional reflectance data reported in Table 5 are an average of the vertical and horizontal polarizations. The values for either polarization varied from this average by as little as ±0.2% to as much as ±20% depending on the combination of beam incidence and viewing angle. These data are relative to the reflectance values obtained at 0° (normal) viewing. The results listed in Table 5 are representative of the bidirectional reflectance of a "rough" surface prepared by pressing the PTFE powder with a coarsely ground glass plate. Samples pressed with a polished glass plate exhibit slightly higher values of reflectance, particularly at viewing angles greater than 75°. Figure 5 illustrates the bidirectional reflectance properties of pressed PTFE powder at 600 nm. Similar results are shown for barium sulfate powder in Fig. 6.

Further studies of the reflection properties of pressed PTFE powder are being made at NBS. Among these properties are the 45°/0° or 0°/45° reflectance factors for the visible spectral region. The results of these studies will be published at a future date.

Table 5. Directional/Directional Reflectance Factor (Bidirectional Reflectance) of 10-mm-Thick Pressed PTFE Powder

Angle of Viewing	Angle of Incidence 300 nm −10°	300 nm −30°	300 nm −50°	300 nm −70°	600 nm −10°	600 nm −30°	600 nm −50°	600 nm −70°	1500 nm −10° gnhr	1500 nm −30°	1500 nm −50°	1500 nm −70°
−80°	0.763	0.792	0.872	1.148	0.743	0.761	0.827	1.048	0.702	0.830	0.820	1.045
−70°	0.836	0.867	0.937	–	0.822	0.840	0.898	–	0.760	0.882	0.855	–
−60°	0.882	0.914	0.980	1.074	0.872	0.891	0.946	1.019	0.819	0.918	0.886	1.000
−50°	0.919	0.949	–	1.022	0.909	0.931	–	0.987	0.875	0.952	–	0.992
−40°	0.946	0.979	1.000	0.996	0.939	0.967	0.982	0.974	0.920	0.974	0.936	0.980
−30°	0.967	–	0.993	0.982	0.963	–	0.980	0.971	0.959	–	0.945	0.980
−20°	0.988	1.005	0.991	0.981	0.986	0.998	0.984	0.974	0.978	0.980	0.966	0.985
−10°	–	1.000	0.994	0.988	–	0.998	0.991	0.983	–	0.990	0.982	0.995
0°	1.000	1.000	1.000	1.000	1.000	1.000	1.000	1.000	1.000	1.000	1.000	1.000
10°	0.991	1.001	1.008	1.021	0.991	1.002	1.012	1.027	0.998	1.005	1.010	1.010
20°	0.982	1.001	1.022	1.052	0.983	1.003	1.027	1.067	0.986	1.012	1.018	1.060
30°	0.970	0.999	1.036	1.098	0.971	1.004	1.048	1.125	0.971	1.015	1.040	1.155
40°	0.960	0.997	1.056	1.163	0.957	1.004	1.076	1.212	0.942	1.018	1.066	1.270
50°	0.943	0.996	1.085	1.265	0.938	1.002	1.114	1.343	0.895	1.022	1.100	1.440
60°	0.921	0.992	1.125	1.426	0.914	1.000	1.168	1.549	0.832	1.030	1.155	1.695
70°	0.882	0.974	1.167	1.691	0.872	0.985	1.227	1.897	0.754	1.035	1.235	2.075
80°	0.817	0.937	1.214	2.190	0.802	0.946	1.291	2.551	0.660	1.040	1.340	3.090

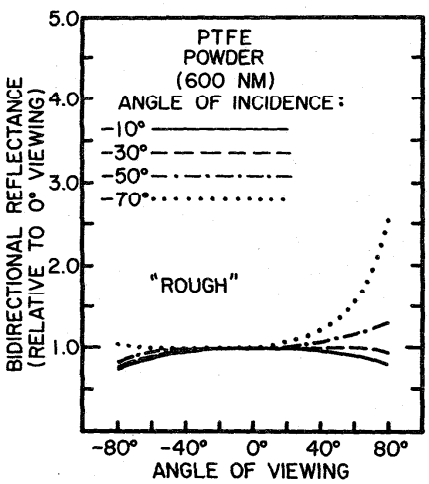

Fig. 5. The bidirectional reflectance factor at 600 nm of pressed PTFE powder having a rough surface finish.

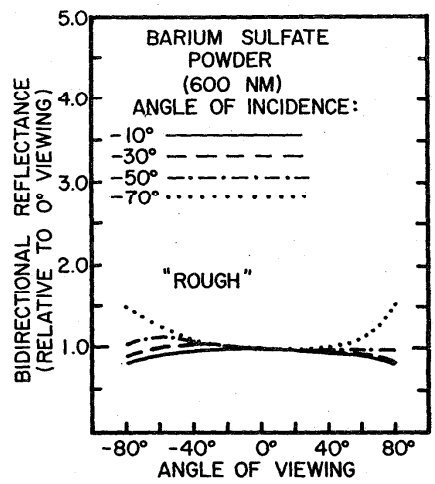

Fig. 6. The bidirectional reflectance factor at 600 nm of pressed barium sulfate powder having a rough surface finish.

REFERENCES

1. The polytetrafluoroethylene powder used in these investigations is manufactured by Allied Chemical Company. The material is commonly referred to by the trade name Halon and is further identified as type G-80 tetrafluoroethylene resin. The commercial name of this material is given here for purposes of identification only and in no way implies endorsement by the National Bureau of Standards.
2. Bureau Central de la Commission Internationale de l'Eclairage, *Review of Publications on Properties and Reflection Values of Material Reflection Standards* (Paris, 1979), CIE Publication 46 (TC-2.3), pp. 15–72.
3. The term "perfect diffuser" is defined in Bureau Central de la Commission Internationale de l'Eclairage, *International Lighting Vocabulary* (Paris, 1970), CIE Publication 17 (E-1.1), p. 95.
4. F. Grum and M. Saltzman, *P-75-77 New White Standard of Reflectance* (Paris, 1976), CIE Publication 36, 91.
5. W. H. Venable, J. J. Hsia, and V. R. Weidner, "Development of an NBS reference spectrophotometer for diffuse reflectance and transmittance," Nat. Bur. Stand. U.S. Tech. Note **594-11**, 47 pp. (1976).
6. V. R. Weidner and J. J. Hsia, "NBS specular reflectometer–spectrophotometer," Appl. Opt. **19**, 1268–1273 (1980).
7. W. H. Venable, J. J. Hsia, and V. R. Weidner, "Establishing a scale of directional–hemispherical reflectance factor I: the Van den Akker method," J. Res. Nat. Bur. Stand. **82**, 29–55, (1977).
8. E. I. Du Pont de Nemours and Company, Inc., Fluorocarbons Division, *Teflon Fluorocarbon Resins—Safety in Handling and Use* (Wilmington, Del., 1970), pp. 1–10. This publication references technical papers dealing with the thermal decomposition of fluorocarbons and associated safety problems.
9. The following U.S. patents are assigned to J. A. Seiner of PPG Industries, Inc., Pittsburgh, Pa.: U.S. Patent No. 3,956,201, May 11, 1976, and U.S. Patent No. 3,764,364, October 9, 1973.
10. From uncorrected emission spectra supplied by K. Mielenz and R. Velapoldi using the reference spectrofluorimeter in the NBS Center for Analytical Chemistry.
11. R. D. Saunders and W. R. Ott, "Spectral irradiance measurements: effect of UV produced fluorescence in integrating spheres," Appl. Opt. **15**, 827–828 (1976).

APPENDIX G

Laboratory intercomparison study of pressed polytetrafluoroethylene powder reflectance standards

V. R. Weidner, J. J. Hsia, and B. Adams

The object of this paper is to present results of several experiments relating to the preparation and use of pressed polytetrafluoroethylene (PTFE) powder as a diffuse reflectance standard for the 200–2500-nm spectral range. These experiments include two round-robin intercomparisons involving nine laboratories. These round-robin experiments provided data on the variability of the reflectance of pressed PTFE reflectance standards prepared in different laboratories. Results of these measurements provided insight into the problems associated with the PTFE standards and helped to establish what practices needed to be standardized to improve interlaboratory agreement for diffuse reflectance measurements.

I. Introduction

The object of this paper is to present the results of several experiments relating to preparation and use of pressed polytetrafluoroethylene (PTFE) powder as a diffuse reflectance standard for the 200–2500-nm spectral range. The usefulness of this material as a reflectance standard was first reported by Grum and Saltzman.[1] Further investigations into the reflection properties of pressed PTFE powder were reported by the authors.[2] As a result of the growing need for improved diffuse reflectance standards for the UV, visible, and near IR, and the interest shown in this material, the Inter Society Color Council (ISCC, Subcommittee 22) has suggested that a laboratory intercomparison be conducted to study the methods of preparation and uniformity of reflectance of pressed PTFE powder. In addition to these round-robin experiments, the results of some closely related PTFE investigations at the National Bureau of Standards (NBS) are also included.

II. Round-Robin Intercomparisons

Two round-robin experiments were conducted in spring 1984. The first experiment yielded results that established a need for further control over the experiment. Therefore, a second round robin was initiated. The design of the two experiments and the resulting data provided some insight into the problems associated with the use of PTFE reflectance standards and also helped to establish what practices needed to be standardized to improve the interlaboratory agreement for reflectance measurements.

A. Round-Robin Experiment 1

Six laboratories participated in this experiment. A quantity of PTFE powder sufficient to prepare two pressed plaques was sent to each laboratory. The PTFE powder was provided by NBS. It was mixed thoroughly by means of a glass blender and shipped in sealed glass jars. NBS also provided 50-mm diam by 10-mm depth holders with covers for the participating laboratories to use in preparation of the pressed PTFE specimens. The instructions requested that the laboratories weigh the powder holders before and after pressing the powder to be used in the pressing because the object was to determine what variations in reflectance would result if this part of the experiment were uncontrolled.

The participating laboratories were accustomed to using commercial powder presses and encountered some difficulty in using the holders provided by NBS. Because of this, some laboratories submitted additional pressed specimens in their own holders. As a result, more specimens were returned to NBS for analysis than had originally been planned on. However, this turned out to be useful because it provided a larger sampling for comparison.

Measurements of the spectral reflectance of the returned PTFE specimens were made at NBS and are reported in Table I. A white ceramic tile of known spectral reflectance was used to compare the PTFE specimens and place the measurements on an absolute scale for the 400–2500-nm wavelength range. For the

The authors are with U.S. National Bureau of Standards, Radiometric Physics Division, Gaithersburg, Maryland 20899.

Received 18 January 1985.

Table I. Round-Robin 1; Spectral Reflectance of Pressed PTFE Powder

Wavelength (nm)	Laboratory 1	1	2	2	2	2	2	3	3
250	0.973	0.973	0.931	0.935	0.962	0.967	0.922	0.983	0.984
300	0.984	0.984	0.963	0.963	0.974	0.975	0.956	0.988	0.988
350	0.990	0.990	0.984	0.984	0.983	0.983	0.977	0.992	0.992
400	0.993	0.993	0.991	0.991	0.985	0.986	0.984	0.993	0.993
500	0.992	0.992	0.992	0.991	0.988	0.987	0.989	0.993	0.993
600	0.993	0.993	0.993	0.993	0.990	0.990	0.992	0.994	0.994
700	0.993	0.993	0.993	0.993	0.987	0.988	0.991	0.993	0.993
800	0.993	0.993	0.993	0.993	0.988	0.988	0.992	0.993	0.993
1000	0.992	0.992	0.992	0.992	0.986	0.987	0.991	0.993	0.993
1200	0.989	0.989	0.989	0.989	0.983	0.984	0.988	0.991	0.991
1500	0.987	0.987	0.987	0.987	0.979	0.983	0.987	0.987	0.987
2000	0.978	0.978	0.978	0.978	0.960	0.962	0.976	0.979	0.980
2100	0.962	0.963	0.962	0.962	0.933	0.935	0.960	0.964	0.965
2200	0.967	0.967	0.965	0.966	0.946	0.948	0.963	0.967	0.967
2300	0.965	0.966	0.965	0.964	0.940	0.943	0.963	0.966	0.968
2400	0.960	0.960	0.959	0.959	0.923	0.926	0.956	0.961	0.960
2500	0.960	0.960	0.960	0.960	0.922	0.924	0.958	0.960	0.960
Density (g/cm^3)	(1.05)	(0.94)	(1.16)	(1.15)	(1.65)	(1.64)	(1.04)	(0.87)	(0.81)

Wavelength (nm)	Laboratory 3	3	4	4	5	5	6	Average of 16	Standard dev.
250	0.978	0.977	0.947	0.955	0.960	0.960	0.983	0.9619	0.0195
300	0.984	0.984	0.964	0.976	0.968	0.967	0.987	0.9753	0.0106
350	0.990	0.990	0.976	0.982	0.977	0.976	0.990	0.9847	0.0059
400	0.990	0.990	0.978	0.983	0.982	0.978	0.993	0.9877	0.0054
500	0.992	0.992	0.978	0.983	0.983	0.980	0.992	0.9886	0.0049
600	0.992	0.992	0.981	0.986	0.983	0.981	0.993	0.9900	0.0046
700	0.992	0.992	0.976	0.983	0.980	0.977	0.993	0.9886	0.0061
800	0.992	0.992	0.975	0.982	0.977	0.975	0.990	0.9881	0.0068
1000	0.990	0.990	0.974	0.981	0.974	0.971	0.988	0.9866	0.0075
1200	0.987	0.987	0.972	0.980	0.967	0.964	0.988	0.9836	0.0085
1500	0.985	0.985	0.966	0.976	0.957	0.954	0.986	0.9800	0.0111
2000	0.976	0.976	0.934	0.962	0.905	0.900	0.977	0.9824	0.0262
2100	0.960	0.960	0.893	0.937	0.845	0.832	0.962	0.9372	0.0430
2200	0.964	0.965	0.913	0.945	0.879	0.873	0.965	0.9475	0.0313
2300	0.964	0.964	0.903	0.945	0.860	0.848	0.964	0.9430	0.0386
2400	0.958	0.958	0.872	0.928	0.814	0.796	0.956	0.9279	0.0536
2500	0.957	0.957	0.862	0.923	0.795	0.781	0.948	0.9242	0.0592
Density (g/cm^2)	(1.18)	(1.23)	(1.77)	(1.67)	(2.05)	2.10	(1.15)	—	—

measurements at wavelengths of <400 nm the data were adjusted to an absolute scale by comparison of the specimens to a freshly prepared PTFE specimen. The absolute reflectance of this specimen was assumed to be that of the published data for the 6°/hemispherical reflectance of pressed PTFE powder (see Ref. 2). The average reflectance of the sixteen specimens and the standard deviations are listed in the last two columns of Table I. The approximate densities of the specimens are listed at the bottom of the table.

The densities of the pressed PTFE specimens listed in Table I varied from ~0.8 to 2 g/cm^3. The data indicate that the reflectances are less for the higher density specimens. Two specimens submitted by laboratories 2, 4, and 5 have densities that exceed 1.5 g/cm^3. At these higher densities the reflectance decreases at longer wavelengths in the 2000–2500-nm range. Similar effects have been reported for other compacted powders.[3] These specimens also have slightly lower reflectances at shorter wavelengths.

There are some larger variations in specimen reflectances at wavelengths <300 nm in the UV. These differences do not correlate with variations in specimen densities. This is a wavelength range in which the specimen reflectance may be easily altered by contamination. Since all the PTFE powder originated from the same source, it is assumed that these variations in the UV reflectance are the result of some change in the sample purity that took place during the round robin.

The variation in reflectance for the visible spectral range, shown in Table I, is small for all the specimens having densities of <1.5 g/cm^3. Because the PTFE reflectance is so reproducible in the visible spectrum, it is clear that the material can be used as a diffuse reflectance standard in this range. To improve the reproducibility of spectral reflectance measurements for pressed PTFE powder in the UV and near IR, the density of the pressed specimens must be controlled, and care must be taken to maintain material purity.

Table II. Round Robin 2; Spectral Reflectance of Pressed PTFE Powder

Wavelength (nm)	Laboratory 1	1	2	2	2	3	3	4	5	5
200	0.959	0.963	0.948	0.946	0.947	0.959	0.960	0.888	0.963	0.961
250	0.972	0.974	0.966	0.967	0.968	0.972	0.972	0.923	0.969	0.967
300	0.984	0.984	0.982	0.976	0.977	0.984	0.984	0.962	0.983	0.982
350	0.989	0.990	0.988	0.989	0.990	0.989	0.991	0.983	0.989	0.988
400	0.992	0.992	0.992	0.992	0.993	0.991	0.993	0.987	0.991	0.990
500	0.993	0.993	0.993	0.993	0.993	0.993	0.993	0.987	0.992	0.991
600	0.993	0.993	0.993	0.993	0.993	0.991	0.993	0.986	0.991	0.991
700	0.993	0.993	0.993	0.993	0.993	0.991	0.992	0.986	0.991	0.991
800	0.993	0.993	0.993	0.993	0.993	0.991	0.993	0.985	0.991	0.990
1000	0.994	0.993	0.993	0.993	0.993	0.990	0.991	0.986	0.991	0.988
1500	0.992	0.991	0.991	0.991	0.991	0.989	0.989	0.983	0.987	0.986
2000	0.981	0.981	0.981	0.980	0.980	0.980	0.979	0.974	0.978	0.975
2100	0.970	0.965	0.970	0.967	0.971	0.969	0.969	0.963	0.967	0.963
2200	0.976	0.973	0.981	0.976	0.982	0.974	0.977	0.968	0.971	0.976
2300	0.970	0.973	0.971	0.967	0.970	0.967	0.967	0.961	0.967	0.968
2400	0.968	0.962	0.962	0.964	0.964	0.962	0.960	0.953	0.952	0.951
2500	0.964	0.960	0.960	0.960	0.960	0.962	0.961	0.946	0.954	0.955
Density (g/cm^3)	(0.905)	(0.990)	(0.835)	(0.920)	(0.800)	(1.025)	(1.025)	(0.920)	(1.085)	(1.08)

Wavelength (mm)	Laboratory 6	7	7	8	8	9	9	Average of 17	Standard Dev.
200	0.898	0.823	0.905	0.905	0.911	0.954	0.949	0.9317	0.0382
250	0.968	0.920	0.950	0.921	0.929	0.971	0.970	0.9576	0.0204
300	0.985	0.968	0.975	0.977	0.979	0.983	0.982	0.9792	0.0063
350	0.990	0.984	0.986	0.988	0.989	0.989	0.989	0.9883	0.0021
400	0.993	0.988	0.988	0.991	0.992	0.992	0.992	0.9911	0.0018
500	0.993	0.988	0.989	0.992	0.993	0.993	0.993	0.9919	0.0020
600	0.993	0.987	0.988	0.992	0.993	0.993	0.993	0.9915	0.0023
700	0.992	0.987	0.988	0.992	0.993	0.993	0.993	0.9914	0.0023
800	0.992	0.987	0.988	0.991	0.993	0.992	0.993	0.9912	0.0024
1000	0.992	0.987	0.988	0.991	0.991	0.991	0.993	0.9910	0.0024
1500	0.989	0.985	0.984	0.988	0.988	0.990	0.990	0.9885	0.0027
2000	0.980	0.976	0.975	0.979	0.980	0.979	0.980	0.9787	0.0023
2100	0.965	0.962	0.962	0.972	0.973	0.972	0.971	0.9677	0.0038
2200	0.979	0.961	0.971	0.974	0.979	0.980	0.982	0.9753	0.0055
2300	0.965	0.967	0.974	0.965	0.972	0.967	0.968	0.9682	0.0032
2400	0.966	0.957	0.956	0.964	0.965	0.957	0.952	0.9597	0.0055
2500	0.959	0.948	0.953	0.957	0.962	0.961	0.962	0.9579	0.0051
Density (g/cm^3)	(0.900)	(0.845)	(0.830)	(0.900)	(0.890)	(0.900)	(0.895)	—	—

B. Round-Robin Experiment 2.

It was decided at the ISCC meeting in Apr. 1984 that a second round-robin experiment should be undertaken and that each participant would try to submit pressed PTFE specimens of 0.9 ± 0.05-g/cm^3 density in their own holders. All the participants received a new supply of PTFE powder from NBS. The six laboratories that participated in the first round robin also took part in the second, and three more laboratories joined in the experiment.

The returned specimens were measured relative to a freshly prepared PTFE specimen. The data were then adjusted to an absolute reflectance scale based on the 6°/hemispherical reflectance of PTFE previously published.[2] It was necessary to place all the measurements on an equal scale for comparison. The white ceramic tile used in round robin 1 to establish the absolute scale was not used since the same scale could be established with a fresh PTFE specimen. The freshly prepared PTFE specimen served to accomplish that purpose. Results of the spectral analysis of the pressed PTFE specimens for round-robin experiment 2 are shown in Table II.

The PTFE specimens ranged in density from ~0.80 to 1.08 g/cm^3 for the second round robin indicating that the density can be controlled at or near 0.9 ± 0.1 g/cm^3. This is a small spread in density, considering that most of the powder presses used to prepare these specimens are not well designed for controlling the density of the finished specimen.

Controlling the density of the specimens resulted in a smaller spread in the reflectance values than those reported in the first round robin. This is especially true for reflectance values in the wavelength range between 2000 and 2500 nm. The reflectance data at 250 nm show less variation than reported in the first round robin. However, the variation in the UV is still large and cannot be reduced by controlling the PTFE density.

Some of the variation in reflectance for the PTFE specimens listed in Tables I and II can be attributed to random noise. At wavelengths below 250 nm the noise level is approximately ±0.003. In the near-IR range of 2000 to 2500 nm, the noise is as high as ±0.010.

The data submitted by laboratories 4 and 7 for the second round robin show lower reflectances by ~0.5% than the other specimens. The reason for this is not clear. However, these specimen holders have a 0.2-mm raised metal ridge that causes a gap between the surface of the PTFE and the plane of the sample port of the reflectometer integrating sphere. This condition may contribute toward this observed lowering of the measured reflectance of the three PTFE specimens. However, 0.5% is a larger difference than would be expected for an 0.2-mm gap. Data will be presented in a later part of this paper that show how the reflectance of PTFE appears to decrease as the gap between the measured surface and port increases.

C. Conclusion of the Round-Robin Experiments

The round-robin experiments emphasize the need for some degree of standardization in the techniques used to prepare reflectance standards from PTFE powder. They also indicate that this material can be a useful and convenient diffuse reflectance standard if these techniques are followed.

NBS has found through experiment that pressed PTFE powder of ~1 g/cm^3 produces a reflectance standard with reflectance values that are reproducible to ±0.01 in the 200–300-nm wavelength range, ±0.005 for the 300–2000-nm wavelength range, and ±0.01 for the 2000–2500-nm wavelength range. Larger variations in the reflectance are possible, however, if the material is contaminated or if the specimen holders are not filled so that the measured surface is in contact with the plane of the sample port of the reflectometer. The data from these round-robin experiments confirm these findings.

III. Additional Experiments Relating the PTFE Reflectance

A. Influence of Specimen Positioning at the Reflectometer Sample Port

The influence of specimen positioning at the reflectometer sample port is demonstrated by the experimental results shown in Fig. 1. The data show how the diffuse reflectance of a specimen of pressed PTFE powder is influenced by controlling the spacing between the specimen plane and the plane of the sample port. The data are shown for measurements at 300, 550, and 1800 nm. Measurements with no spacing between the specimen and sample port are set equal to 100%, and measurements at increasing distance between the specimen and port are plotted relative to the zero spacing data. The sample beam illuminated an area of ~1-cm diameter in the center of a port of 2.3-cm diameter. The results plotted in Fig. 1 show that the effects are about the same at different wavelengths. The measured reflectance is ~1% lower if the spacing were

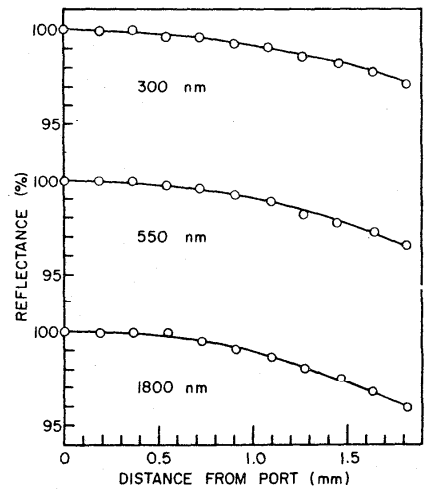

Figure 1. Measured diffuse reflectance of a pressed PTFE powder specimen is influenced by varying the spacing between the plane of the specimen and the plane of the integrating sphere port. The effect is shown for measurements at 300, 550, and 1800 nm.

1 mm. A spacing of 0.1 or 0.2 mm seems to have little effect on measured reflectance. However, an error of 0.5% could be introduced by a spacing as small as 0.7 mm. The results may vary for different instruments because the effect can be influenced by the ratio of the beam diameter to the port diameter and thickness of the port rim. One problem when the PTFE specimen is in contact with the sample port is of course that of damaging the standard. This occurs if the standard slips across the port during mounting and can only be avoided by allowing a small spacing between the specimen and port. The other solution is to prepare fresh samples when required and always allowing contact between the specimen and port.

B. Comparison of PTFE from Two Manufacturers

A comparison of the diffuse reflectance of pressed PTFE powder from two manufacturers was made to see if significant differences existed between them. The relative differences in the spectral reflectance of the two types of PTFE are shown in Table III. The differences reported are not significant since they fall within the random uncertainties associated with sample preparation and measurement.

C. Reproducibility of the Absolute Reflectance of Pressed PTFE Powder using the Double-Sphere Method

The best values of spectral reflectance of pressed PTFE powder as determined at NBS are reported in Ref. 2. The values are reported for the 6°/hemispherical reflectance factor (relative to a perfect diffuser). The reproducibility of the reflectance values for pressed PTFE powder as determined by the double-sphere technique was tested by repeating the experiment three times and computing the standard deviation for the three trials. Details of the double-sphere technique are reported in Refs. 2, 4, and 5. The standard deviations for three trial runs using this technique are reported in

Table III. Differences in Spectral Reflectance of PTFE Obtained from Manufacturers A and B

Wavelength (nm)	Reflectance differences	Measurement uncertainty
300	+0.004	±0.005
400	+0.003	±0.005
500	+0.002	±0.005
600	+0.002	±0.005
700	+0.001	±0.005
800	+0.001	±0.005
900	+0.001	±0.005
1000	0.000	±0.005
1100	0.000	±0.005
1200	+0.001	±0.005
1300	−0.002	±0.005
1400	+0.001	±0.005
1500	−0.002	±0.005
1600	−0.001	±0.005
1700	−0.001	±0.005
1800	−0.002	±0.005
1900	0.000	±0.005
2000	−0.003	±0.005
2100	−0.002	0.010
2200	−0.001	0.010
2300	−0.012	0.010
2400	−0.003	0.010
2500	−0.002	0.010

Table IV. Standard Deviation for Three Independent Determinations of the 6°/Hemispherical Reflectance Factor of Pressed PTFE Powder by the Double-Sphere Technique for Measuring Absolute Reflectance

Wavelength (nm)	Standard deviation of three determinations
200	0.0014
210	0.0014
220	0.0012
230	0.0008
240	0.0008
250	0.0011
300	0.0007
350	0.0003
400	0.0002
500	0.0003
600	0.0004
700	0.0005
800	0.0006
900	0.0006
1000	0.0006
1100	0.0006
1200	0.0006
1300	0.0006
1400	0.0008
1500	0.0007
1600	0.0007
1700	0.0008
1800	0.0007
1900	0.0006
2000	0.0004
2100	0.0005
2200	0.0005
2300	0.0007
2400	0.0007
2500	0.0006

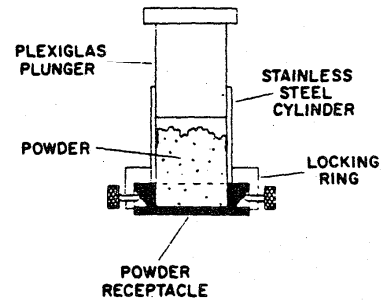

Fig. 2. Powder press is designed to provide a means for controlling the density of pressed PTFE diffuse reflectance standards. The preferred density is 1 g/cm^3.

Table IV. Each of the three trials represents independent determinations in which the auxiliary sphere was recoated with the pressed PTFE powder for each determination. The PTFE powder for two of the trial runs came from a drum of the powder that was the source of supply for the round-robin experiments described earlier. A third trial run was made with PTFE powder from a newer drum that had never been opened before. The resulting data indicated no differences in reflectance for the PTFE powder from these two drums.

IV. Recommended Procedures for Preparing and Using Pressed PTFE Powder as a Reflectance Standard

It is suggested that the following procedures and precautions be followed to improve the reproducibility of diffuse reflectance measurements and increase agreement among laboratories using pressed PTFE powder as a reflectance standard:

(1) Store the powder in sealed glass containers.

(2) Prepare the powder for use by pulverizing it into a uniform consistency in a glass blender with stainless steel blades.

(3) Use stainless steel spoons to transfer the powder.

(4) Press the powder into holders that have a depth of 10 mm.

(5) Press the powder to a density of ~1 ± 0.1 g/cm^3. A 1-g/cm^3 density results in a firmer and less fragile specimen than lower densities. This can be done very conveniently with a powder press of the design shown in Fig. 2. This press is designed with a metal cavity of 10-mm depth. The diameter of this cavity will depend on the diameter of the sample port of the reflectometer integrating sphere. It should be made slightly larger than the diameter of the port. A stainless steel cylinder of the same inside diameter as the PTFE cavity is press fitted into a locking ring that can be locked onto this cavity with three thumbscrews. The PTFE powder is introduced into the stainless steel cylinder after it is locked onto the receiving cavity. To obtain a pressed PTFE reflectance standard of 1 g/cm^3, the volume of the receiving cavity must be determined in cubic centimeters. The pressing operation is done with a Plexiglas

plunger made for a sliding fit into the stainless steel cylinder. The plunger is designed so that when fully inserted into the cylinder, it just reaches the plane of the cavity opening. The plunger surface can be roughened by sandblasting if a coarser surface on the pressed PTFE is desired. However, this will not significantly affect the reflectance of the specimen. The pressure required to produce a standard of 1 g/cm^3 can easily be achieved by force of hand. A protective cover can be provided for storing the standard. This powder press and powder receptacle are not available commercially but can be made easily in a small machine shop.

(6) When measuring the PTFE reflectance standard, make sure it is pressed against the sample port of the integrating sphere so that no gap exists between the standard and port.

(7) Prepare fresh standards every day if necessary to avoid using soiled or damaged reflectance standards.

(8) Prepare at least three fresh standards when making reflectance measurement in the UV and use an average value of reflectance for these standards.

V. Remarks

The results of the round-robin experiments reported in Tables I and II should not be used as reference data for the absolute reflectance of pressed PTFE powder. Even the reported averages appearing in these tables are not considered good for reference purposes because some of the submitted specimens had significantly lower reflectances. Refer to the 6°/hemispherical reflectance data published in Ref. 2 for the absolute reflectance of PTFE powder.

The following laboratories participated in the round-robin experiments described in this paper: Burlington Industries, Corp. Research & Development, Greenboro, N.C.; E. I. Dupont Co., Troy, Mich.; Hunter Associates, Reston, Va.; Macbeth Division, Kollmorgen Corp., Newburgh, N.Y.; Munsell Color Science Laboratory, College of Graphic Arts and Photography, Rochester Institute of Technology, Rochester, N.Y.; National Research Council of Canada, Ottawa, Canada; Pacific Scientific, Gardner/Neotec, Silver Spring, Md.; The Sherwin-Williams Co., Chicago, Il., National Bureau of Standards, Radiometric Physics Division, Gaithersburg, Md.

References

1. F. Grum and M. Saltzman, P-75-77 New White Standard of Reflectance, CIE Publication 36, (Paris, 1976), p. 91.
2. V. R. Weidner and J. J. Hsia, "Reflection Properties of Pressed Polytetrafluoroethylene Powder," J. Opt. Soc. Am. **71**, 856 (1981).
3. E. Schatz, "Effects of Pressure on the Reflectance of Compacted Powders," J. Opt. Soc. Am. **56**, 389 (1966).
4. W. H. Venable, J. J. Hsia, and V. R. Weidner, "Establishing a Scale of Directional-Hemispherical Reflectance Factor I: The Van den Akker Method," J. Res. Natl. Bur. Stand. **82**, 29 (1977).
5. D. G. Goebel, B. P. Caldwell, and H. K. Hammond III, "Use of an Auxiliary Sphere with a Spectroreflectometer to Obtain Absolute Reflectance," J. Opt. Soc. Am. **56**, 783 (1966).